NUREG/CR-3428
UCRL-53483
RD & RM

Application of the SSMRP Methodology to the Seismic Risk at the Zion Nuclear Power Plant

Manuscript Completed: May 1983
Date Published: November 1983

Prepared by
M. P. Bohn, L. C. Shieh, J. E. Wells, L. C. Cover, D. L. Bernreuter, J. C. Chen, J. J. Johnson, S. E. Bumpus, R. W. Mensing, W. J. O'Connell, and D. A. Lappa

Lawrence Livermore National Laboratory
7000 East Avenue
Livermore, CA 94550

Prepared for
Office of Nuclear Regulatory Research
U.S. Nuclear Regulatory Commission
Washington, D.C. 20555
NRC FIN No. A0126

ABSTRACT

The Seismic Safety Margins Research Program (SSMRP) is a U.S. NRC-funded multiyear program conducted by Lawrence Livermore National Laboratory (LLNL). Its goal is to develop a complete, fully coupled analysis procedure (including methods and computer codes) for estimating the risk of an earthquake-induced radioactive release from a commercial nuclear power plant. The analysis procedure is based upon a state-of-the-art evaluation of the current seismic analysis and design process and explicitly accounts for uncertainties inherent in such a process.

The SSMRP is the first effort to trace seismically induced failure modes in a reactor system down to the individual component level, and to take into account common-cause earthquake-induced failures at the component level. This report presents the results of our seismic risk analysis of the Zion nuclear power plant using the SSMRP methodology.

The risk analysis included a detailed seismological evaluation of the region around Zion, Illinois, which provided the earthquake-hazard function and an appropriately randomized set of 180 time histories (having peak ground acceleration (PGA) values up to 1.8 g). These time histories were used as input for dynamic structural response calculations for four different Zion buildings. Detailed finite-element models of the buildings were used. Calculated time histories at piping support points were then used to determine moments throughout critical piping systems. Twenty separate piping models were analyzed. Finally, the responses of piping and safety system components within the buildings were combined with probabilistic failure criteria and event-tree/fault-tree models of the plant safety systems to produce an estimate of the frequency of core melt and radioactive release due to earthquakes.

The base case is our best estimate of the configuration of the Zion plant and its current operating procedures, normal and emergency. Some important assumptions as to the consequences of certain localized structural failures were made. For this base case, the median frequency of core melt was computed to be 3E-5 per year, with upper (90%) and lower (10%) bounds of 8E-4 and 6E-7 per year.

Three additional cases were analyzed to test the effects of fundamental assumptions made for the base case. The frequency of core melt and radioactive release in the base case was due primarily to (1) failure of pipes between the reactor building and the auxiliary building caused by relative motion between the two buildings and soil failure and uplift of the containment basemat, and (2) loss of on-site emergency AC power caused by failure of the roof slab of the service-water pump enclosure, and the assumption that all six service-water pumps would be damaged by the falling slab. Without these assumptions of adverse consequences, the frequency of core melt and release are reduced by a factor of 2.

The base case analysis assumed that the operator could perform a "feed-and-bleed" operation to provide core cooling in the event that the auxiliary feedwater system failed. If this assumption is not made, the core melt

frequency increases by a factor of 3. The radioactive release (expressed in terms of man-rem/yr) increases by only 13%, however, because the additional accident scenarios lead to release via basemat melt-through rather than overpressure failure of the containment.

Other analyzed cases showed that the effect on risk of local site conditions at the plant were important, while the effects of structure-to-structure interaction were not significant and the assumption of rigid foundations was reasonable.

Finally, several analyses investigated the effect of correlation of responses of plant components and correlation of fragilities of components. Correlation was found to have a significant effect on risk, where the dominant risk contributors are pairs of component failures, such as electrical components.

CONTENTS

LIST OF FIGURES

Page

Figures in Appendices

LIST OF TABLES

Page

Tables in Appendices

ACKNOWLEDGMENTS

This report is the final product of the Zion Risk Analysis project of the Seismic Safety Margins Research Program (SSMRP). It represents the Phase II work of the SSMRP.

A team approach accomplished the objectives of this project in an efficient manner and provided the best technical product possible within the time available. The team consisted of a core group of Lawrence Livermore National Laboratory (LLNL) personnel and selected consultants. This group, primarily drawn from the Engineering Mechanics section of the Nuclear Test Engineering Division of the Mechanical Engineering Department, the Computation Department, the Engineering Research Division of the Electronics Engineering Department, and selected subcontractors, included

L. C. Shieh - Project Manager
D. L. Bernreuter - Seismic Input Group Leader
S. E. Bumpus - SMACS Code Programmer and Analyst
J. C. Chen - Soil Structure Interaction Leader
L. C. Cover - Fragility Development Leader
L. L. George - Systems Analyst
J. J. Johnson - Affiliated with Structural Mechanics Associate in charge of Major Structural Analysis
D. A. Lappa - Systems Analyst
R. W. Mensing - Senior Statistical Consultant
W. J. O'Connell - General Consultant
J. E. Wells - System Analysis Group Leader

A special debt of gratitude is owed to M. P. Bohn, the Program Manager of the SSMRP, for his continuous encouragement, interest, and consultation.

We would like to thank L. L. Cleland, Program Leader of the Nuclear Systems Safety Program of LLNL, G. E. Cummings, Deputy Program Leader of the Nuclear Systems Safety Program of LLNL, and P. D. Smith, Associate Program Leader of the Seismic and Structural Safety Program at LLNL for their helpful, critical review of this report.

We are grateful to S. M. Pratuch for his assistance in developing auxiliary feedwater piping models and generating most of the response plots, and to M. W. Eli for his assistance in data analysis of the local site conditions and for generating all the plots related to the local site conditions. We would also like to thank Mrs. E. Carpenter for her efforts in maintaining the SEISIM code.

In Phase I, we developed the overall seismic risk assessment methodologies, which are embodied in three computer codes, HAZARD, SMACS and SEISIM. The Program Manager of the Phase I SSMRP was P. D. Smith. Under his leadership the Phase I methodology developments were completed. R. G. Dong, the Deputy Program Manager, coordinated all the projects of the Phase I program. G. E. Cummings, who was the System Analysis project manager, successfully developed the SEISIM code. T. Y. Chuang was the Subsystem Analysis project manager. The SAPPAC code, which later was assimilated as part of the SMACS code, was also developed as part of the Phase I effort. We would like to express our

appreciation to the above for their contribution to the Phase I work and their continued consultation on Phase II.

The manuscript of this report was prepared and edited by T. L. Patters, C. S. Aubuchon, and D. P. Hendry. Their ongoing diligence, patience and dedication are deeply appreciated.

The Project Manager of the Completion of Zion Risk Analysis Project of the SSMRP, L. C. Shieh, would like to express his thanks to the project staff and LLNL's subcontractors. Finally, we wish to thank the NRC Project Manager, D. J. Guzy for his support and guidance.

This work was supported by the United States Nuclear Regulatory Commission under a Memorandum of Understanding with the Department of Energy of the United States.

EXECUTIVE SUMMARY

To assist the NRC in its licensing and evaluation role, the NRC funded the Seismic Safety Margins Research Program (SSMRP) at LLNL with the goal of developing tools and data bases to evaluate the risk of earthquake-caused radioactive release from a commercial nuclear power plant. This program began late in 1978, and the methodology was finalized in 1982. A complete seismic risk assessment for the Zion plant was finished in October 1982. This report describes the SSMRP risk assessment methodology and the results of the Zion analysis.

Scope of the SSMRP

A nuclear power plant is designed to ensure the survival of safety-related systems, buildings, and equipment in a worst-case, safe shutdown earthquake (SSE). The assumptions underlying this design process are deterministic. In practice, however, these assumptions are subject to uncertainty. It is not possible, for example, to accurately predict the "worst" earthquake that will occur at a given site. Soil properties and dynamic characteristics of structures and subsystems are subject to uncertainty in their definition. To model and analyze the coupled phenomena that contribute to the total risk of radioactive release it is therefore necessary to consider all significant sources of uncertainty. Total risk is then obtained by considering the entire spectrum of possible earthquakes and rationally combining the associated consequences.

There are five steps in the SSMRP methodology for calculating the seismic risk at a nuclear power plant:

1. Characterize the seismic hazard.
2. Determine response of structures and subsystems to seismic excitation.
3. Determine fragility functions.
4. Identify accident scenarios.
5. Calculate probability of failure and frequency of radioactive release.

A brief discussion of each of these steps is given below.

Step 1: Characterize the Seismic Hazard

The earthquake hazard at a given power plant site is characterized by a hazard function which gives the probability of exceedence (per year) of a ground motion parameter, such as peak ground acceleration. Figure 1 shows this so-called hazard curve for the Zion Nuclear Power Plant, located at Zion, Illinois, approximately 40 miles north of Chicago. This curve is derived from a combination of recorded earthquake data, estimated earthquake magnitudes of known events for which no data are available, review of local geological investigations, and use of expert opinion based on a survey of seismologists and geologists familiar with the region in question.

The frequency characteristics of the earthquakes are required, as well as their likelihoods. We use response spectra or time histories to define their frequency characteristics. We used the computer program HAZARD to generate response spectra. From these response spectra, artificial acceleration time

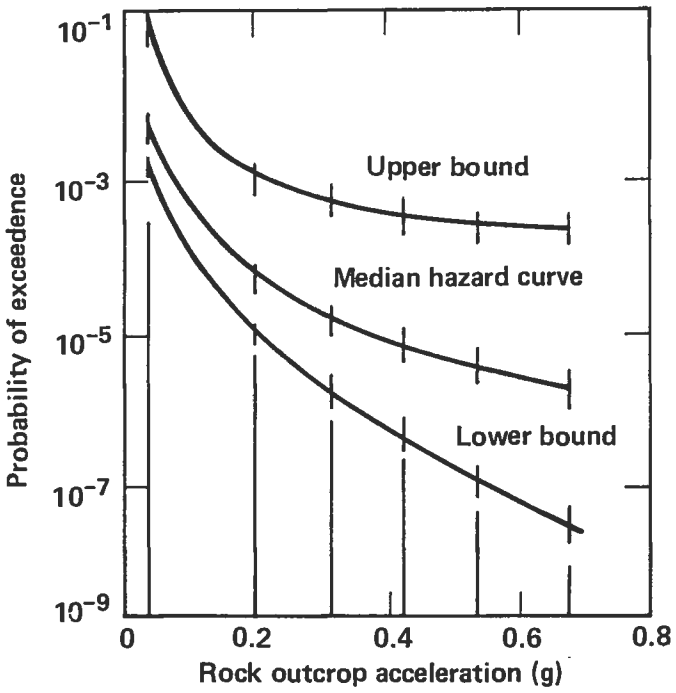

Fig. 1. Seismic hazard curve for the Zion site.

histories were generated. Three orthogonal components (two horizontal and the vertical) of acceleration time histories were generated for each earthquake simulation.

Step 2: Determine Response of Structures and Subsystems to Seismic Excitation

The computer program SMACS (Seismic Methodology Analysis Chain with Statistics) calculates soil-structure interaction (SSI) and response of the plant's major structures and subsystems to seismic excitation. Seismic excitation is given by ensembles of acceleration time histories in three orthogonal directions, obtained as we described above for Step 1. SSI and detailed structure response are determined simultaneously using the substructure approach to SSI. The response of subsystems is calculated by multi-support time history analysis procedures. Uncertainty is treated explicitly in each of these links of the seismic methodology chain by analyzing an ensemble of free-field acceleration time histories and by varying a discrete number of input parameters of the soil, structures, and subsystems. SMACS performs repeated deterministic analyses, each analysis simulating an earthquake occurrence. By performing many such analyses and by varying the values of the input parameters, we take account of the uncertainty inherent in any deterministic analysis.

Step 3: Determine Fragility Functions

Different subsystems, structures, parts of structures, and components have different susceptibilites to failure as a result of an earthquake. These different susceptibilites must be determined. We specify susceptibility by a fragility function, which is a cumulative probability of failure as a function

of loading. We developed fragility functions for structures and large components at Zion and for 37 categories of small components.

Step 4: Identify Accident Scenarios

All failures are not equally serious. In some accidents, safety systems will be effective, either permitting the continued operation of the plant or bringing about a safe shutdown. In other accidents, safety systems could be ineffective, and in an extreme case radioactive release would occur.

In this step of the risk analysis process, we identify the possible accident scenarios during an earthquake-induced shutdown. For the Zion plant we identified 315 accident scenarios stemming from 7 classes of initiating events. The accident scenarios varied from minor to severe. We used fault trees to determine the success or failure of each of the safety systems whose success or failure made up the accident sequence.

Once a probability is associated with each event in an accident scenario, the probability of each scenario can be calculated. This process is described in Step 5.

Step 5: Calculate Probability of Failure and Frequency of Radioactive Release.

Step 5 combines the results of Steps 1-4 to express plant risk as the frequency of 1) failure of structures and components, 2) failure of a group of structures and components, and 3) radioactive release.

(a) Calculate Cut Set Probabilities. Each accident sequence consists of the union of sets of events (successes or failures of components) which must occur together to have system failure. (In systems analysis terminology, these sets are called min cut sets). The Zion accident sequences each contained up to 5000 of these component failure groups and each component failure group (min cut set) was allowed to have up to ten basic events (component failures).

The computer code SEISIM was written expressly to calculate the probability of such component failure groups including all common-cause failures. Given the individual component responses and fragilities (in terms of the means and variances of their distributions) and given the computed correlations between the responses (obtained from the time history response calculations at each earthquake level), SEISIM constructs a multi-variate lognormal distribution for each component failure group, and then uses n-dimensional numerical integration to compute the probability of occurrence of the component failure group.

(b) Calculate Frequency of Radioactive Release Once the component failure group probabilities have been computed, the probability of each accident sequence can be found from the expression for the union of disjoint cut sets, which is an upper bound to the accident sequence probability. Then each accident sequence probability is multiplied by the probability of the earthquake's occurrence, the probability of the initiating event, and the probability of failure of the containment, to obtain the frequency of radioactive release. Several different containment failure modes of different severity were identified, ranging from rupture of the containment shell down to leakage of the containment isolation valves. Different containment failure

modes are assigned to different accident sequences according to our understanding of the physical processes involved. One accident sequence can result in one or more containment failure modes.

Finally, accident sequence probabilities are assigned to different release categories to reflect their severity with respect to radioactive release to the surrounding population. These release categories relate to the type and energy content of the radioactive fission product release, as well as the mode and timing of the release. They range from rupture of the top of the containment with a rapid, high energetic release (due to a fuel/water explosion or due to steam overpressure) down to slow melt-through of the containment concrete foundation, which is expected to have the least effect on the surrounding population. The containment failure modes and the release categories are those derived and used in the Reactor Safety Study.

Results of Zion Risk Analysis and Uncertainty Intervals

This section presents the results of the base case calculations made for the seismic risk analysis of the Zion nuclear power plant. The calculations of the median core melt frequency and the uncertainty intervals are also described.

The base case is our best estimate of the configuration of the Zion plant and its emergency procedures. A number of important assumptions have been made as described below.

1. It is assumed that "feed-and-bleed" emergency core cooling can be performed after an earthquake. In this procedure, which is employed if the auxiliary feedwater system has failed, the operator makes use of the emergency safety pumps to pump cooling water to the core. The resulting steam is bled-off through the pressurizer relief valves.

2. The identified structural failure modes are assumed to have the most serious consequences. Two structural failure modes play crucial roles.
   (i) The failure of the roof of the service water pump enclosure (at the top of the crib house) is assumed to fail all six service water pumps beneath it, leading to loss of the emergency AC power diesel generators, due to lack of cooling water.
   (ii) The failure of the wall between the turbine building and the auxiliary building is assumed to cause loss of all electrical wiring and control circuits, so both power and control to the containment building are lost.

   Both of these are assumed to fail the safety injection system (SIS), the charging system (CHG), the containment spray injection system (CSIS), and the containment spray recirculation system (CSRS).

3. Soil failure under the toe of the containment is assumed to result in sufficiently large rocking motions so as to fail the SIS, CHG, RHR, CSIS and CSRS piping between the auxiliary-fuel-turbine (AFT) building and the containment building.

4. Failure of the vertical column supports under the steam generators and reactor coolant pumps is assumed to result in a double-ended guillotine break of the primary coolant piping, equivalent to a large

LOCA. Failure of supports in two different loops is assumed to result in a reactor vessel rupture initiating event.

These assumptions all play crucial roles in the base case results.

Frequency of Core Melt. We used a Monte Carlo procedure to determine the probability function relating the probability and frequency of core melt release per year. We made repeated calculations of the core melt frequencies for the base case, while varying the median values of all input variables by sampling from distributions of input variable values. Fourteen calculations were performed, with new values for structural responses, fragility curves and hazard curves for each calculation. The median value and uncertainty intervals were inferred from these 14 calculations. We found the median frequency of core melt for the plant to be 1×10^{-5} per year. This value reflects inherent randomness in all the input variables and the hazard curve, as well as modeling uncertainties attributable to lack of exact knowledge of mean values of input variables. The 10-90% uncertainty band on the core melt frequency was found to be about 3 orders of magnitude. The core melt frequency is due primarily to the failure of certain structural elements that result in common-cause failures of the safety systems.

Results for the Base Case with Random Uncertainty Only. To illustrate the important accident scenarios, the point estimates for the base case are presented in Table 1. To obtain the values in Table 1, all input variables were assigned best-estimate values for their medians and standard deviations. A median hazard curve was used. Thus, this base case calculation gives the

Table 1. Summary of point estimates of release frequency and dose for the base case (with feed-and-bleed and structural failures).

Release category	Release frequency/yr	man-rem/yr
1	2.9E-8	0.2
2	1.4E-6	6.5
3	5.4E-7	2.9
4	0	0
5	8.3E-10	0
6	1.7E-7	0
7	1.5E-6	0
Total	3.6E-6[a]	9.6

[a] This is equivalent to frequency/yr of core melt.

risk at Zion based on best-estimate values of the input parameters. The table presents the frequencies per year of occurrence of the seven release categories and the radiation dose associated with each release category. Release categories 2 (containment failure due to overpressure) and 7 (melt-through of basemat) have the highest frequencies of occurrence, 1.4E-6 and 1.5E-6 per year, respectively. The man-rem/year released comes from release categories 2 and 3 (containment failure due to overpressure). (The conversion of release category frequencies to man-rem/year released is based on averaged values for a presssurized-water reactor taken from NUREG/CR-2800 and are not specific to Zion.) The total frequency of core melt is seen to be 3.6E-6 per year and the total release is 9.6 man-rem/year. These release category frequencies were found to be due primarily to the failures of certain local structural elements and inter-building piping, which resulted in common-cause failures of the safety systems.

In terms of both core melt frequency and dose, it was found that earthquake levels 2, 3, and 4 were dominant and the frequencies and dose were significantly smaller at earthquake levels 1 and 6. This indicates that we captured the bulk of the risk in the middle earthquake levels (2-4 SSE), and that we considered an adequate range of earthquakes.

We found that the initiating events are dominated, at the three lower earthquake levels, by the transients T1 and T2. At earthquake level 4, it is primarily the small and small-small LOCAs that are important. At earthquake level 5 the initiating event probabilities are fairly evenly spread over the initiating events and the LLOCA and RVR initiating events have become significant. Finally, at level 6 the dominant initiating events are the RVR and LLOCA events. Thus, we see that the contribution of the more severe initiating events increases as we increase the level of earthquake excitation.

The seismically-induced failure causing the two transient initiating events is primarily the loss of offsite power by failure of the ceramic insulators at the point where offsite power is brought into the switch yard. The component failures which cause the LLOCA and the RVR initiating events are the failure of the primary coolant piping due to the failure of the supports of the steam generators and reactor coolant pumps. Without these two failures the initiating events for the RVR and the LLOCA would be significantly smaller. Thus, we found that it is not failure of the piping which results in a RVR or LLOCA but rather the possibility of failure of the supports of the major components.

At the lower three earthquake levels, both the release category frequencies and the dose are dominated by failure of the auxiliary feedwater system caused by structural failures. The uplift of the containment basement causes failure of the AFWS pipes, and is also assumed to fail the containment sprays. Since the containment sprays fail, the release occurs in release category 2 (80%) and release category 7 (19%). A second contributor is failure of the crib house service-water pump enclosure room roof slab. This is assumed to fail the six service water pumps, which in turn fails the diesel generators due to lack of cooling water. This, in conjunction with loss of off-site power, results in loss of all AC power, and hence loss of both the AFWS and the containment sprays.

For earthquake levels 4, 5 and 6, significant contributions are found from release category 3 as well as 2 and 7. For the upper three earthquake levels,

the containment sprays are assumed to have failed due to ground shaking alone. (For levels 1, 2 and 3, the containment sprays were assumed to have failed only in those accident sequences caused by the structural failures.) Release category 3 is due almost entirely to small LOCA sequences, which are caused by the failure of pairs of pipes between the containment and AFT buildings. These pairs of pipes fail due to differential motion between the buildings. Failure of any one of these pipe pair combinations causes failure of both emergency core injection and the RHR systems. The release in category 7 at the upper earthquake levels is due to two small LOCA accident sequences which are both the result of loss of emergency core cooling due to uplift and service water pump room roof failures.

In summary, out of the total 9.6 man-rem/year, approximately 6.1 man-rem/year is due to accident sequences caused directly by the uplift and crib house pump room roof failures, and 2.7 man-rem/year is due to failures of pairs of pipes between the containment and AFT buildings. At the three lower earthquake levels, transient accident sequences predominate, while at the upper three earthquake levels the smaller LOCAs predominate. Thus it is seen that, for the base case computations of the seismic risk at Zion, the structural failures and the assumptions as to their consequences play a dominant role.

Sensitivity of Risk Results to Basic Assumptions

To test the fundamental assumptions on which the base case results were predicated, three additional risk assessments of Zion were performed, with the results shown in Table 2. In Case 1, the effects of the structural failures (the service water pump enclosure room roof, auxiliary building shear wall, and soil failure and basemat uplift) were removed, but the "feed-and-bleed" capability was retained. In this case, both the frequency of core melt and radioactive dose decreased by 50% relative to the base case.

In Case 2, both the effects of structural failures and the "feed-and-bleed" cooling capability were removed. For this case, the core melt frequency increased by a factor of 2-1/2 over the base case. This increase in frequency results because with no "feed-and-bleed" cooling capability, the auxiliary feedwater system (AFWS) has no back-up, and thus electrical component failures in the AFWS became significant. However, the dose is only 60% of the base case, because the additional accident scenarios caused by failures of the AFWS result in basemat melt-through (which is relatively benign) rather than over-pressure failure of the containment.

In Case 3, the effects of the structural failures are included, but no "feed-and-bleed" capability is assumed. This results in the highest (point estimate) values of both core melt frequency and radioactive release. The core melt frequency is 3 times higher than in the base case, and the radioactive release is 13% higher than for the base case.

In summary, it can be seen that, depending upon the assumptions made as to the consequences of the localized structural failures and the credibility of performing "feed-and-bleed" cooling, the core melt frequency can vary by an order of magnitude, and the release can vary by 250%.

A number of other cases were analyzed to demonstrate the importance of various aspects of modeling the Zion plant. These cases showed the local

Table 2. Comparison of cases designed to test the effects of fundamental assumptions.

	Release category	Frequency per yr	man-rem/yr
Base case (with feed-and-bleed, with structural failures)			
	1	2.9E-8	0.2
	2	1.4E-6	6.5
	3	5.4E-7	2.9
	4	0	0
	5	8.3E-10	0
	6	1.7E-7	0
	7	1.5E-6	0
	Total	3.6E-6	9.6
Case 1 (with feed-and bleed, without structural failures)			
	1	1.9E-8	0.1
	2	1.9E-7	0.9
	3	6.1E-7	3.3
	4	0	0
	5	8.8E-10	0
	6	1.2E-7	0
	7	5.3E-7	0
	Total	1.5E-6	4.3
Case 2 (without feed-and-bleed, without structural failures)			
	1	2.4E-8	0.1
	2	5.7E-7	2.7
	3	6.6E-7	3.6
	4	0	0
	5	0	0
	6	2.8E-7	0
	7	7.6E-6	0.2
	Total	9.1E-6	6.6
Case 3 (without feed-and-bleed, with structural failures)			
	1	3.3E-8	0.2
	2	1.5E-6	7.2
	3	6.0E-7	3.2
	4	0	0
	5	0	0
	6	2.9E-7	0
	7	8.6E-6	0.2
	Total	1.1E-5	10.8

amplification of the free-field motion was quite important. The effect of structure-to-structure interaction on core melt frequency was not important. The assumption of rigid foundations was appropriate. Finally, several cases were analyzed that showed the effects of correlation between responses in the plant due to the common ground shaking, and correlation between fragilities.

PART I: METHODOLOGY

CHAPTER 1: INTRODUCTION

The Seismic Safety Margins Research Program (SSMRP) is a U.S. Nuclear Regulatory Commission-funded, multiyear program conducted by Lawrence Livermore National Laboratory (LLNL). Its objective was to develop a complete, fully coupled analysis procedure (including methods and computer codes) for estimating the risk of earthquake-induced radioactive release from a commercial nuclear power plant, and to determine major contributors to the frequency of radioactive release. The analysis procedure is based upon a state-of-the-art seismic and systems analysis process and explicitly includes the uncertainties inherent in such a process. The results will be used to improve seismic licensing requirements for nuclear power plants.

The SSMRP was begun in 1978 when it became evident that an accurate seismic risk analysis must simultaneously consider all the interrelated factors that affect the final probability of radioactive release. In the traditional design procedure, by contrast, each factor is usually analyzed separately. These closely coupled factors are:

- The likelihood and magnitude of an earthquake.
- The transfer of earthquake energy from a fault source to a power plant site, a phenomenon that varies greatly with the magnitude of an earthquake.
- Interaction of the soil and structures at nuclear power plant site, a phenomenon that depends on the soil properties at the site, the dynamic characteristics of the structure, and the location of the fault source relative to the site.
- Dynamic responses of a power plant's buildings and the massive reactor vessels, piping systems, and emergency safety systems within.
- Numerous accident scenarios, which vary according to the types of failures assumed and the success or failure of the engineered safety features intended to mitigate the consequences of an accident.
- Different modes of containment failure resulting in differing types of radioactive release.

The goals of the SSMRP were to be achieved in two phases. In Phase I, the overall seismic risk assessment methodology was developed and assembled. The methodology is embodied in three computer codes: HAZARD, SMACS and SEISIM. In addition, extensive data bases on earthquake occurrence models and failure data for nuclear power components were assembled. A pressurized water reactor was selected for demonstration calculations, and fault trees were developed for its essential safety and auxiliary systems. The plant chosen was the Zion nuclear power plant, located on Lake Michigan just east of the town of Zion, Illinois, and about 40 miles north of Chicago. This plant was chosen on the basis of being reasonably typical (in terms of power, systems design and site conditions) of pressurized water reactors in the 1960's era. The limited demonstration calculations (and Phase I) were completed in February, 1981. A 10-volume final report (Ref. 1) on Phase I was issued during 1981-1982.

The goals of Phase II of the SSMRP were to complete the seismic risk methodology development and perform a complete seismic risk assessment of the Zion plant. This risk assessment was not only to compute the frequency of core melt and radioactive release, but also to include an uncertainty analysis on the entire risk assessment process so that uncertainty intervals on the core melt frequencies could be determined. This report presents the final SSMRP seismic risk assessment for the Zion nuclear power plant.

Part I of this report describes the methodology and input for the SSMRP seismic risk assessment. An overview of the entire risk assessment process is presented in Chapter 2, along with a brief discussion of the uncertainty analysis we employed. Chapter 3 describes the seismic input requirements, the development of earthquake occurrence models and ground motion models, and the family of hazard curves developed for the Zion site. A discussion of the significant effects of local site conditions on the hazard curve at Zion is presented.

The calculation of seismic responses of buildings, piping, and components is presented in Chapter 4. These calculations are performed with the SMACS code, which generates distributions of all plant responses, given uncertainty distributions on the input parameters. The basis of variation of these input parameters is discussed.

The statistically based failure relations (fragilities) for the structures and components are given in Chapter 5. Separation of the uncertainty of the fragilities into random and modeling components is discussed, and tables listing all fragilties used in the final analysis are presented.

Finally, Chapter 6 describes the systems analysis methodology by which the risk assessment is performed. Discussions of the initiating events, event trees, accident sequences and fault trees of the safety and auxiliary systems are presented. In addition, the two-loop modified Monte Carlo scheme for computing uncertainty intervals on the final results is presented.

Part II of the report presents all the numerical results, both for the base case risk analysis, and for the 12 additional risk assessments performed to evaluate the sensitivity of the final results to the operational and modeling assumptions made in defining the base case.

In each case, the frequency per year of core melt and radioactive release in each of the seven WASH-1400 radioactive release categories is presented, along with tables listing the dominant accident sequences at each earthquake level. The frequencies of release and core melt are specific to Zion.

In addition, the public exposure at the plant boundary, expressed in terms of man-rem/yr, is given for each release category. These values are computed by multiplying the release category frequencies/year by conversion factors taken from NUREG/CR-2800. The conversion factors are <u>not</u> specific to the Zion site, but are, instead, in some sense generic, being based on average population densities and average meteorological conditions. Thus it is very important to note that the man-rem/year values given in this report are not intended to apply to Zion. They are presented to assist in interpretation of the final

results, for in many cases the conclusions which can be drawn when discussing core melt frequencies are not the same conclusions which apply to man-rem/year exposure.

Chapter 7 presents the evaluation of the base case, which is our best estimate of the risk at Zion. This chapter includes the uncertainty intervals calculations. The final values of core melt and release in the Zion base case are predicated on a number of consequence and modeling assumptions. For example, in the base case, certain identified local structural failures were assumed to have the most severe consequences in causing failure of the safety systems. In Chapter 8, we examine the risk when less conservative assumptions are made. In addition, the base case included "feed-and-bleed" cooling as a viable core-cooling option. In Chapter 8, we present the risk at Zion under the assumption that the "feed-and-bleed" option is not possible following an earthquake.

The sensitivity of the risk at Zion due to the effects of earthquake-induced correlated failures is discussed in Chapter 9. Two cases were analyzed, which assess the effects of correlated responses and correlated fragilities separately.

In computing the seismic responses for the base case, amplification of the free-field ground motion due to the shallow soil layer at the Zion site was explicitly modeled. In addition, structure-to-structure interaction effects were incorporated in the soil-structure interaction calculations. These effects are not routinely included in plant design calculations, so Chapter 10 presents the results of risk analyses for Zion which do not include these effects.

Finally, Chapter 11 summarizes our Zion risk analyses, and makes recommendations for future work to extend and verify some of the crucial assumptions on which the SSMRP Zion risk assessment was based.

CHAPTER 2: OVERVIEW

2.1 Scope of the SSMRP

A nuclear power plant is designed to ensure the survival of safety-related systems,buildings and equipment in a worst-case ("safe shutdown") earthquake. The assumptions underlying this design process are deterministic. In practice, however, these assumptions are subject to uncertainty. It is not possible, for example, to accurately predict the "worst" earthquake that will occur at a given site. Soil properties and dynamic characteristics of structures and subsystems are subject to uncertainty in their definition. To model and analyze the coupled phenomena that contribute to the total risk of radioactive release it is therefore necessary to consider all significant sources of uncertainty. Total risk is then obtained by considering the entire spectrum of possible earthquakes and integrating their calculated consequences.

There are five steps for calculating the seismic risk at a nuclear power plant (Fig. 2.1).

- Characterize the seismic hazard
- Determine response of structures and subsystems to seismic excitation.
- Determine fragility functions.
- Identify accident scenarios.
- Calculate probability of failure and frequency of radioactive release.

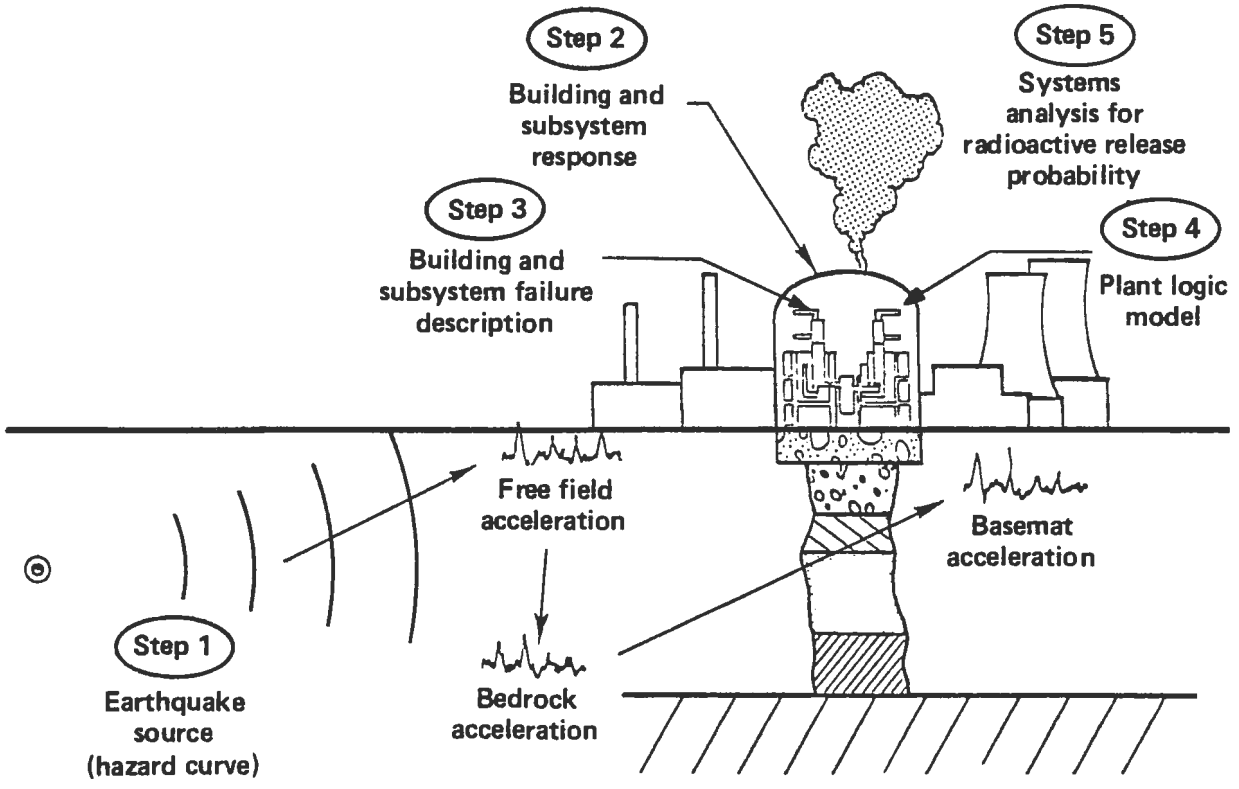

Fig. 2.1. A seismic risk analysis methodology.

A brief discussion of each of these steps is given below.

Step 1: Characterize the Seismic Hazard

The earthquake hazard at a given power plant site is characterized by a Hazard Function giving the annual probability of exceedence of a ground motion parameter (i.e., peak acceleration, peak velocity, uniform hazard response spectrum). Figure 2.2 shows an example of hazard curves for the Zion nuclear power plant used in the present study. For a given site, this curve is derived from a combination of recorded earthquake data, estimated earthquake magnitudes of known events for which no data are available, review of local geological investigations, and use of expert opinion based on a survey of seismologists and geologists familiar with the region in question. Chapter 3 describes in detail the process we used to generate the seismic hazard curves.

In addition to the seismic hazard curve, descriptions of the corresponding frequency charcteristics of the motion are required. Response spectra and/or acceleration time histories usually serve this purpose. For the SSMRP, response spectra were generated in conjunction with the seismic hazard curve using the computer program HAZARD. Artificial acceleration time histories were generated to match these response spectra and for use in Step 2, computing the seismic response of structures and subsystems. Three orthogonal components (two horizontal and one vertical) of acceleration time histories were generated for each earthquake simulation. Chapter 3 also describes this aspect of the seismic hazard in detail.

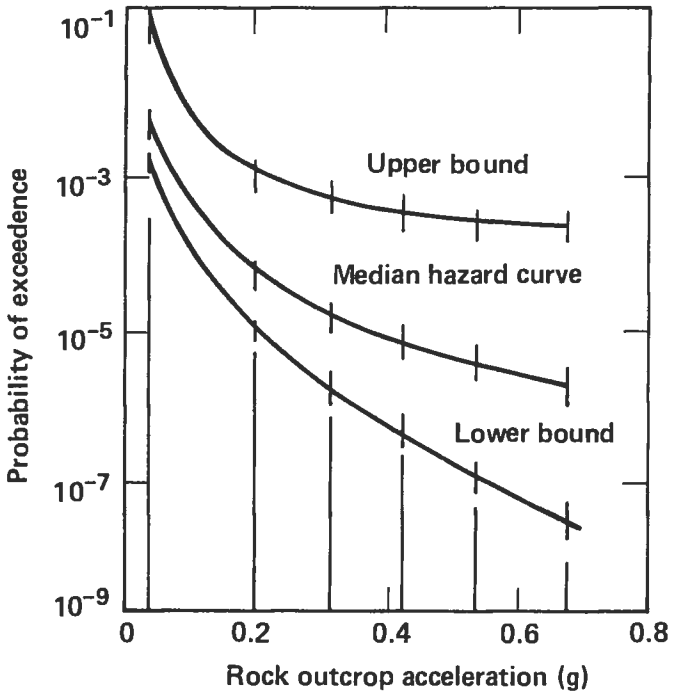

Fig. 2.2. Example of hazard curve for Zion nuclear power plant.

Step 2: Determine Response of Structures and Subsystems to Seismic Excitation

For each level of earthquake described by the seismic hazard curve (Step 1), three aspects of seismic response are necessary to perform the seismic risk analysis: Median response, variability of response, and correlation of responses. Seismic responses are required for all structures and components contained in the plant logic models (fault trees and event trees)(Step 4). The three aspects of seismic response are discussed briefly here.

- Median response--the median level seismic response given an earthquake occurrence is required. In general, the median response differs from the design values because, in the latter case, design analysis procedures, parameter selection, and qualification procedures are conservatively biased. An additional consideration due to analyzing for the range of earthquakes is the change in properties of the soil/structure/piping systems which occurs as excitation levels increase. For example, higher excitations lead to lower soil shear moduli, lower structure frequencies, and higher soil and structure damping characteristics. Such changes need to be taken into account when determining best-estimate response.

- Variability of response--variability in seismic response resulting from variations in the earthquake excitation, the physical properties of the soil/structure/piping system, and our ability to model them must be acknowledged and included in the seismic risk analysis to permit calculation of probability of component failure and uncertainty intervals on the core melt frequency.

- Correlation of responses (the tendency for pairs of responses to have simultaneously high or low values) results from two sources, the level of the earthquake and the dynamic characteristics of the system. The level of the earthquake affects correlation since a large earthquake (large peak acceleration) may cause all responses to be large, whereas a small earthquake produces the opposite effect. The second source of correlation is due to system response itself. For example, floors within a structure may all experience high values of response simultaneously due to the dynamic characteristics of the structure itself. Hence, equipment supported on these floors may simultaneously have high response. The importance of response correlation on frequencies of system failure, core melt, and radioactive release depends on correlations between fragilities and the functional characteristics of the systems themselves.

For the SSMRP, these three aspects of seismic response were determined calculationally using the computer program SMACS (Seismic Methodology Analysis Chain with Statistics).

SMACS links seismic input with the calculation of soil-structure interaction (SSI), major structure response, and subsystem response. Seismic input is defined by ensembles of acceleration time histories in three orthogonal directions. SSI and detailed structure response are determined simultaneously using the substructure approach to SSI. The response of subsystems is

calculated by multi-support time history analysis procedures. Uncertainty is treated explicitly in each of these links of the seismic methodology chain by analyzing for an ensemble of free-field acceleration time histories and by varying a discrete number of input parameters in the soil, structure, and subsystem. SMACS performs repeated deterministic analyses, each analysis simulating an earthquake occurrence. By performing many such analyses and by varying the values of the input parameters, we account for the uncertainty inherent in any deterministic analysis. Parameter values for each simulation were sampled from assumed probability distributions according to a Latin-hypercube sampling procedure. Chapter 4 describes the SMACS methodology and results of the response calculations.

Step 3: Determine Fragility Functions

The failure of structures or structural elements may occur in one of several possible modes. If the structure provides a pressure boundary, then a failure mode is loss of pressure boundary integrity. Structures whose main purpose is to support subsystems and components fail when they no longer provide adequate support. Secondary failures of subsystems and components occur when structural elements collapse causing their failure. An example of secondary failure is collapse of the pump enclosure roof on the service-water pumps. Component failure is defined as either loss of pressure boundary integrity or loss of operability. In all cases, failure (fragility) is characterized by a cumulative distribution function which describes the probability that failure has occurred given a value of loading. In the context of the SSMRP, the loading may be described by local spectral acceleration, local peak acceleration, or an internal force resultant such as moment, depending on the component and failure mode under consideration. Contrary to other studies, fragility is related to the appropriate local response, rather than being related directly to the free-field peak acceleration.

Development of the necessary fragility functions is reported in Chapter 5. Fragilities for structures and large components (such as steam generators, etc.) were developed uniquely for the Zion nuclear power plant configuration. Fragility functions for other components were treated generically. As a first step, all components identified in the fault tree analyses were grouped into 37 generic categories. Fragility functions for each generic category were developed from design analysis reports, experimental data, and an extensive expert opinion survey. Statistical methods were used to combine data from the several sources. Chapter 5 discusses development of the fragility functions in detail.

Step 4: Identify Accident Scenarios

In the event of an earthquake or other abnormal condition in a power plant, the plant safety systems act to bring the plant to a safe shutdown condition. Should the earthquake damage essential components in the safety systems, it is possible that the effectiveness of the safety systems would be diminished. In an extreme case, it is possible that damage to the fuel rods or core melt could result. In this step of the risk analysis process, we identify the possible paths that a reactor system could follow during a shutdown caused by an earthquake-related event. These paths usually involve an accident and a

subsequent failure of one or more plant systems and are referred to as accident sequences. For the SSMRP analysis of the Zion power plant, 315 accident sequences were identified.

All the identified accident sequences result from one or more seismically induced initiating events (events requiring immediate shutdown of the plant). In the SSMRP analysis of the Zion plant, we identified seven classes of initiating events. Four LOCAs of different severity were considered, and two types of transients. In addition, an initiating event "Reactor Vessel Rupture" was identified which is a LOCA for which the emergency core cooling system (ECCS) cannot effectively flood the core. For this event it is assumed that multiple coolant loop failures occur. Thus, in this case, the only mitigating safety systems are those in the containment (CSIS and CFCS). These seven initiating events are shown in Table 2.1

For each of these seven initiating events, an event tree is constructed. Each branch of an event tree is an accident sequence. We use fault trees to determine the success or failure of each of the safety systems whose success or failure make up the accident sequences.

In determining failure modes for the plant safety systems, we use the fault tree methodology developed in the aerospace industry to identify all the groups of system components whose simultaneous failure would result in failure of the system.

Construction of a fault tree begins by identifying the immediate causes of system failure. Then each of these causes is examined for more fundamental causes, until one has constructed a downward branching tree, at the bottom of which are failures not further reducible, i.e., failures of mechanical or electrical components due to all causes, such as structural failure, human error, etc. These lowest-order failures on the fault tree are called basic events.

Fault trees are required for every system identified on the event trees. For the Zion plant, seven systems were modeled. The emergency core-cooling system was modeled with fault trees for the Safety Injection System (SIS), the Charging System (CHG), the Residual Heat Removal System (RHR), and the

Table 2.1. SSMRP initiating events.

Event	Charactersitics
Vessel Rupture	ECCS ineffective
Large LOCA	ID > 6 in. diameter
Medium LOCA	3 < ID $\leq$ 6 in. diameter
Small LOCA	1.5 < ID $\leq$ 3 in. diameter
Small-Small LOCA	0.5 < ID $\leq$ 1.5 in. diameter
Transient T1	PCS initially available
Transient T2	PCS inoperative initially

Accumulator System (ACC). The emergency core-cooling function is provided by different combinations of these systems in the injection and recirculation phases of a LOCA, and also depends on break size. The auxiliary feedwater system (AFWS) is of primary importance in a risk analysis, and a complete fault tree was developed for this system. All the above systems (except the accumulators) require both electric power and service water, so detailed fault trees were developed for both these systems.

The size of the resulting fault trees varied considerably, as shown below:

System	Number of basic events	Number of logic gates
ACC	54	17
SIS	242	117
RHR	309	130
CHG	378	172
AFWS	1288	786

The basic events which resulted after all fault trees were constructed fell into three categories:

Human and maintenance errors	583
Other random failures	20
Seismically-induced failures	1905

In all, 2508 basic events were considered.

Step 5: Calculate Probability of Failure and Frequency of Radioactive Release

Step 5 combines the results of steps 1-4. With respect to the seismic hazard at the site in question, Step 5 calculates:

- Structure and component failure probability.
- Probability of failure of a group of structures and components.
- Frequency of radioactive release.

Each of these elements is discussed briefly here. The computer program SEISIM was written to perform these probabilistic calculations, including treatment of the common-cause nature of earthquakes, as discussed below. Our discussion here emphasizes the calculational process to obtain a point estimate of the quantities of interest. Section 2.2 discusses our methodology to obtain uncertainty intervals. One additional point is that the seismic response (Step 2) and systems analyses were performed for discretizations of the seismic hazard curve (Chap. 3). The final step in the process is convolution of these conditional results with the seismic hazard curve.

Structure and Component Failure Probabilities

To calculate the probability of failure of structures and components requires input from Steps 1-3. For each discretization of the seismic hazard, the results of our SMACS analysis define the response of the structures and subsystems of interest. Correlation coefficients are calculated and used in succeeding stages of Step 5. The fragility functions of Step 3 are convolved with the response functions to yield the conditional probability of failure (conditional on the earthquake occurrence). A final stage in the process is integration over the seismic hazard curve.

Frequency of Core Melt and Radioactive Release

Accident sequence probabilities must be calculated to determine radioactive release frequencies. As discussed in Step 4 above, each accident sequence consists of groups of events which must occur together. The failure of each safety system can be represented in terms of cut sets, which are groups of component failures which will cause the system to fail. These cut sets and the accident sequences are combined so that every accident sequence can be expressed in a Boolean expression of the form

$$ACC = C_1\ C_2\ C_3 \text{ or } C_4\ C_5 \text{ or } \ldots \text{ or } C_i\ C_j\ C_k \quad ,$$

in which the C_i are basic events (i.e., failures of individual components) identified on the safety system fault trees. If at least one of the component failure groups $C_i\ C_j\ C_k$ occurs, then the accident sequence occurs. As previously mentioned, in the SSMRP a total of 315 accident sequences were considered. These accident sequences contained up to 5000 component failure groups (in systems analysis terminology, called min cut sets). Each of these component failure groups was allowed to have up to ten basic event failures.

- Probability of failure of a group of structures and components. To calculate the probability of an accident sequence (that is, to evaluate the probability of simultaneous, or joint, component failures in a group $C_i \ldots C_k$), it is necessary to evaluate the probability of the component-failure groups, $\text{Prob}(C_i\ C_j \ldots C_k)$. If these events were independent of one another (so that the failure of one component had no correlation with the failure of any other component), then a well-known law in probability theory states that the probability of several independent events is equal to the product of their individual failure probabilities. That is,

  $$\text{Prob}(C_1\ C_2 \ldots C_n) = \text{Prob}(C_1)\text{Prob}(C_2) \ldots \text{Prob}(C_n) \quad .$$

  However, when failure is caused by ground shaking due to an earthquake, all parts of the plant are shaken together. Therefore, the accelerations or loads which the various buildings and components experience are highly correlated. This correlation increases the probability of occurrence of the component failure group. In fact, two components sitting side by side would experience essentially the same floor accelerations, and thus their responses would be said to be "perfectly correlated." Hence, if either component failed, it would be more likely that the other component would also fail. The computer code SEISIM was written

expressly to calculate such dependent failures. Given the individual component responses and fragilities (in terms of the means and variances of their distributions) and given the computed correlations between the responses (obtained from the SMACS analyses), SEISIM constructs a multivariate normal distribution for each component-failure group, and then uses n-dimensional numerical integration to compute the probability of the component-failure group occurring.

- Frequency of Radioactive Release
  Once the component failure group probabilities have been computed, the probability of each accident sequence can be found. To obtain the frequency of radioactive release, the accident sequence probability (which is a measure of the frequency of core melt) is then multiplied by the probability of the earthquake's occurrence and the probability of failure of the containment. Several different containment failure modes of different severity were identified, ranging from rupture of the containment shell to leakage of the containment isolation valves. Different containment-failure modes are assigned to different accident sequences, depending on our understanding of the physical processes involved. One accident sequence can result in one or more containment failure modes. Finally, radioactive releases are sorted into seven different release categories to reflect their severity with respect to the surrounding population. These release categories relate to the type and energy content of the radioactive fission product release, as well as to the mode and timing of the release. They range from rupture of the top of the containment with a rapid, energetic release (due to a fuel/water explosion or steam overpressure) to slow melt-through of the containment concrete foundation, which is expected to have the least effect on the surrounding population. The containment failure modes and the release categories are those derived for and used in the Reactor Safety Study. Each of the seven release categories can be assigned a corresponding dose to the public for a PWR at an average site. Table 2.2 lists the doses versus release category. The total public dose in terms of man-rem per year for each release category is obtained by multiplying the frequency of the release category by the corresponding dose. The frequency of core melt is the sum of release frequencies from all seven categories.

2.2 Uncertainty Analysis

In seismic risk analysis, it is important to recognize two types of uncertainty--random uncertainty and modeling uncertainty. Random uncertainty is the inherent randomness associated with the events of interest. It is fundamental to the phenomenon being represented and it is also irreducible given present state-of-the-art understanding and modeling of the phenomenon. Modeling uncertainty reflects incomplete knowledge of the models and calculational techniques used to estimate risk. Modeling uncertainty, in many cases, can be reduced within present limits of the state of the art by improved analytical models, experiments, etc. Both types of uncertainty exist in all of the elements that comprise the five steps in the SSMRP methodology described earlier. The separation of random and modeling uncertainty and the

Table 2.2 Estimated public dose in WASH-1400 release categories from NUREG/CR-2800.

Release category	Dose (man-rem)
PWR 1	5,400,000
PWR 2	4,800,000
PWR 3	5,400,000
PWR 4	2,700,000
PWR 5	1,000,000
PWR 6	150,000
PWR 7	23,000

methodology used to propagate the modeling uncertainty through the probabilistic calculations is denoted "uncertainty analysis."

One goal of the SSMRP uncertainty analysis was to describe the variation in the estimator of the frequency of radioactive release due to the uncertainties associated with the risk analysis techniques. Perhaps the optimal method for assessing the effect of analysis uncertainties on the estimator of risk would be to analytically propagate the uncertainties through the analysis. Because of the complexity of our analysis, this was not possible. Alternatively, a Monte-Carlo simulation procedure was selected to assess the variation in the output probabilities due to modeling uncertainties.

The procedure to propagate random and modeling uncertainties was a two-loop process; the outer loop treats modeling uncertainty and the inner loop treats random uncertainty. The parameters varied on the outer loop are the seismic hazard curve, the medians of structure and soil parameters in the calculations of the seismic responses (which result from the SMACS analyses), the medians of the fragilities, and the probability of failure of unmodeled systems. Usually, a simulation analysis such as the outer loop involves a large number of iterations of the basic risk analysis. However, the number of iterations can be reduced by appropriately choosing the sets of inputs to be used for each iteration. The basis of one such method is to choose the values for each input so that the entire range of values for the input is represented in the sample of inputs used. The designs of our outer and inner loops are based on using such a sampling method, called a Latin hypercube design. Using this modified Monte Carlo approach, 14 evaluations of the seismic risk at Zion were performed to span the range of modeling uncertainties in the calculational procedure. From these 14 analyses, median values of release frequencies and uncertainty intervals on the median values could be inferred. Details of the two-loop process are presented in Chapter 6.

CHAPTER 3: SEISMIC INPUT

3.1 Seismic Input Requirements

As outlined in Chapter 2, the calculation of median values and uncertainty intervals for the radioactive release frequencies at Zion required 14 complete seismic risk analyses. For each of these analyses, a separate hazard curve and separate set of time histories were required. These 14 sets of seismic hazard inputs were constructed to systematically incorporate both the random and modeling uncertainties which are inherent in the determination of the seismic hazard at Zion.

In this chapter we discuss the methodology used to develop the seismic hazard input, the systematic incorporation of uncertainties, and the 14 sets of seismic inputs used in the Zion risk analysis. For the base case (random uncertainty only) a single, nominally average hazard curve was used, and the rationale for selection of this curve is discussed. In addition, in order to assess the effects of the local site conditions under the Zion plant, a seismic hazard was developed which neglected these local site conditions, so that comparisons with the base case (which included local site conditions) could be made. Note that modeling local site conditions is a major source of modeling uncertainty.

3.2 Approach Used to Develop the Seismic Input

3.2.1 Methodology

Figure 3-1 illustrates our seismic hazard modeling approach, which is comprised of three main elements: an overall earthquake occurrence model, a ground motion model, and a hazard evaluation methodology which yields the hazard curve and associated time histories.

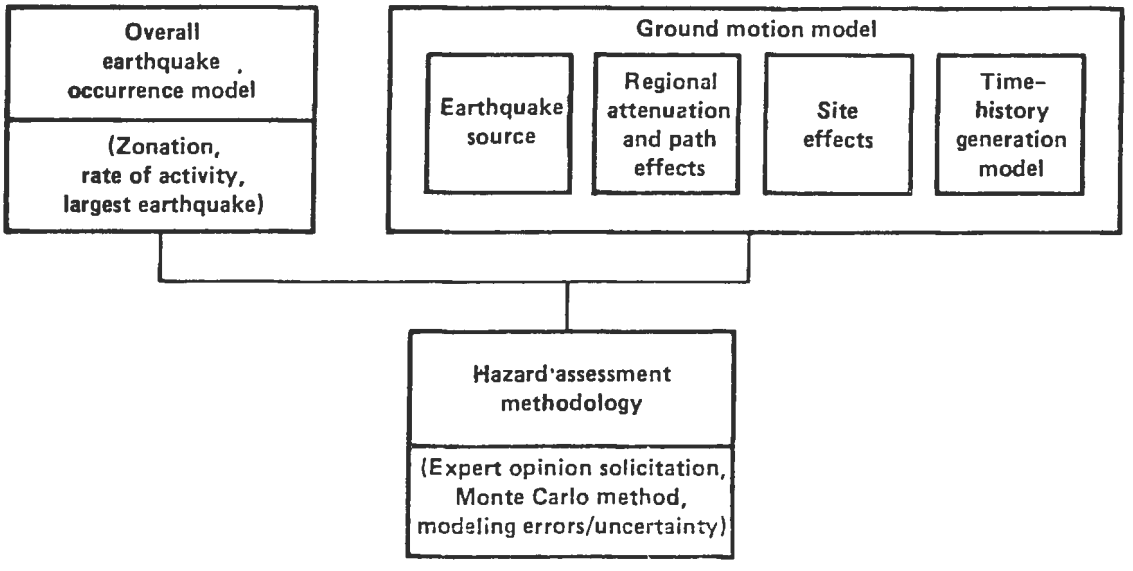

Fig. 3.1. Overall hazard model.

The overall earthquake occurrence model includes two important general features:

- An identification of earthquake source regions. These regions define areas of uniform seismicity in which earthquakes have occurred (or are expected to occur) in relation to the Zion site. Because of low seismicity and lack of geological evidence, it is difficult to correlate earthquakes with faults in the Eastern United States (EUS), and hence we assume that earthquakes occur randomly over large regions. Considerable judgment is required to define these regions of uniform seismicity.

- The use of earthquake occurrence models for each source region. These models define the distribution of earthquakes in terms of time and size (magnitude or intensity) for each source region, including estimation of the largest earthquake that is hypothesized to occur. Because of the brevity of the historical seismic record, considerable judgment is needed to estimate the largest earthquake that might occur.

The ground motion model, discussed in Sec. 3.2.2, is comprised of four elements:

- The diversity of potential acceleration levels and energy content of ground motion generated by earthquakes of a given magnitude.

- The attenuation of ground motion between the earthquake source and the site.

- The effect of the site's local geology on the ground motion.

- The spatial variation of the ground motion, both across the site and its variation with depth.

Our hazard evaluation methodology differs in two areas from the typical approach. First, other approaches typically express the exposure at a site in terms of peak ground-motion parameters or uniform hazard spectra (UHS), or both. UHS are spectra for which each ordinate has the same probability of being exceeded in a fixed period of time. All events capable of affecting a site are then considered by assessing the probability of exceedence. However, no real earthquake has a spectrum corresponding to the UHS, because different earthquakes contribute to different frequency bands of the spectrum. The use of UHS introduces conservatism, particularly when used in the generation of artificial time histories, because their frequency content is much broader than is typically found for a real earthquake. In the SSMRP, we attempt to circumvent this problem by expressing the seismic hazard in terms of event-specific response spectra corresponding to the particular types of earthquakes to which the site in question is expected to be subjected. This approach is discussed in Ref. 3.

Secondly, in addition to the event-specific approach, use of expert opinion is one of the key elements of our hazard evaluation methodology. Many elements of our hazard model are based on expert opinion, supplemented by the limited data base and, in some cases, by theoretical models. This is also discussed

in detail in Ref. 1. Direct input of expert opinion into the assessment of the seismic hazard was obtained from two panels of experts:

- Eastern United States Seismicity Panel. This panel provided the information used to develop the overall earthquake occurrence model.
- Ground Motion Panel. This panel provided us with sets of alternative ground motion models.

One important element of our approach was to keep the overall earthquake occurrence models provided by each of our members of the EUS Seismicity Panel separate from the input of the others.

The seismic hazard curve (in this study) is defined to be the function $P(A > a)$ which gives the annual probability that the PGA exceeds a at the site. We compute $P(A > a)$ by first evaluating $P_S(A > a)$ for source zone S, for each expert, given that an earthquake has occurred in source zone S, using

$$P_S(A > a) = \int_m \int_r P(A > a \mid m,r)\, f_{S_M}(m)\, f_{S_R}(r)\, dm\, dr \quad , \tag{3-1}$$

where $P(A > a \mid m,r)$ is the probability that the acceleration A at the site is greater than a, given that an earthquake of magnitude m has occurred at a distance r from the site in zone S. $P(A > a \mid m,r)$ is obtained from the ground motion model. $f_{S_M}(m)$ is the probability density function giving the distribution of the magnitudes (or epicentral intensities) of earthquakes in source zone S. This distribution is derived using input provided by panel members. There is a separate distribution for each zone for each expert. $f_{S_R}(r)$ is the probability density function for the distribution of distances from the site in source zone S and is a function only of the source zone's shape and distance from the site. This distribution is derived from the geometry of the source zones provided by each expert. The integral is evaluated over the range $M_O \leq m \leq M_{SU}$ and the entire range of distances (r) from the site to the source S. M_O was taken to be 4.0 if a given expert was expressing his occurrence model in magnitude or 4.5 if the model was expressed in epicentral intensity. The experts provided estimates of the upper magnitude cutoff M_{SU} for the distribution of the magnitude for each source zone S as well as its uncertainty. All experts derived $f_{S_M}(m)$, the distribution on earthquake magnitude (intensity), from the well-known frequency relationship proposed by Richter:

$$\log N_c = a - bM \quad , \tag{3-2}$$

where M = magnitude or epicentral intensity

N_c = cumulative number of earthquakes greater than M

a,b = parameters of the model estimated from historical data and other insights.

Evaluation of Eq. (3-1) for each source zone gives the total probability that a PGA of amplitude a will be exceeded, given an earthquake in source zone S. We assume that earthquake occurence within a zone is a Poisson process. Thus to compute the expected number of exceedences, the probability for each source zone is multiplied by the mean activity rate for each source zone. The total expected number of exceedences is calculated as the sum of expected numbers of exceedences from each source zone. Under the Poisson assumption

$$P(A > a) = 1 - \exp[-(\text{total number of exceedences of amplitude a})] \quad . \qquad (3\text{-}3)$$

Note that this brief discussion provides only a simplistic description of the process used (particularly when uncertainty in the parameters a, b, and M_{SU} are included). For a detailed discussion of our hazard evaluation program see Ref. 3.

This approach can be used to generate both the hazard curve and UHS. The event-specific seismic hazard procedure that we developed to generate time histories shares the same basic steps and models as the probabilistic hazard analysis used to generate the hazard curve. The same overall earthquake occurrence and ground motion models are used. The major variation introduced by the event-specific approach occurs in the evaluation of the hazard at the site. In standard analyses the hazard is quantified through the probability distribution of ground motion parameters at the site during a given interval of time, due to the occurrence of all possible events. In the event-specific analysis, a pseudo-random simulation allows the hazard to be defined in terms of response spectra that are functions of event-specific parameters, namely magnitude and distance.

Figure 3-2 illustrates the approach. The geometry is discretized in rings (R_i) centered at the site, and the magnitudes in intervals centered at magnitude M_j. This representation allows the use of a discrete magnitude distribution model and is advantageous in the formulation of the simulation procedure.

For a given magnitude M_j and distance R_i, we have developed from the attenuation relationships a normal distribution for the logarithm of each spectral ordinate. The spectrum cannot be generated by randomly simulating each frequency independently, because this would ignore the high level of correlation between close frequencies and would generate unrealistically large spectral variations. The procedure used instead was to assume that the spectrum generation could be modeled by a Markovian process of order 1, generating each spectral amplitude conditionally on the realization of the previous one. (See Ref. 3, for details.)

The methodology described above generates the maximum horizontal component. To determine the response spectrum in the second horizontal direction, the distribution of the ratio of the smallest horizontal PGA component to the largest horizontal PGA component is determined from the data base. For each simulation, a ratio is randomly selected from this distribution, and the PGA in the second horizontal direction is determined. The shape of the response spectrum is assumed to be the same as the one in the first horizontal direction.

The response spectrum in the vertical direction is simulated independently using the vertical ground motion model. In order to introduce the correlation between horizontal and vertical PGA components, the distribution of the ratio

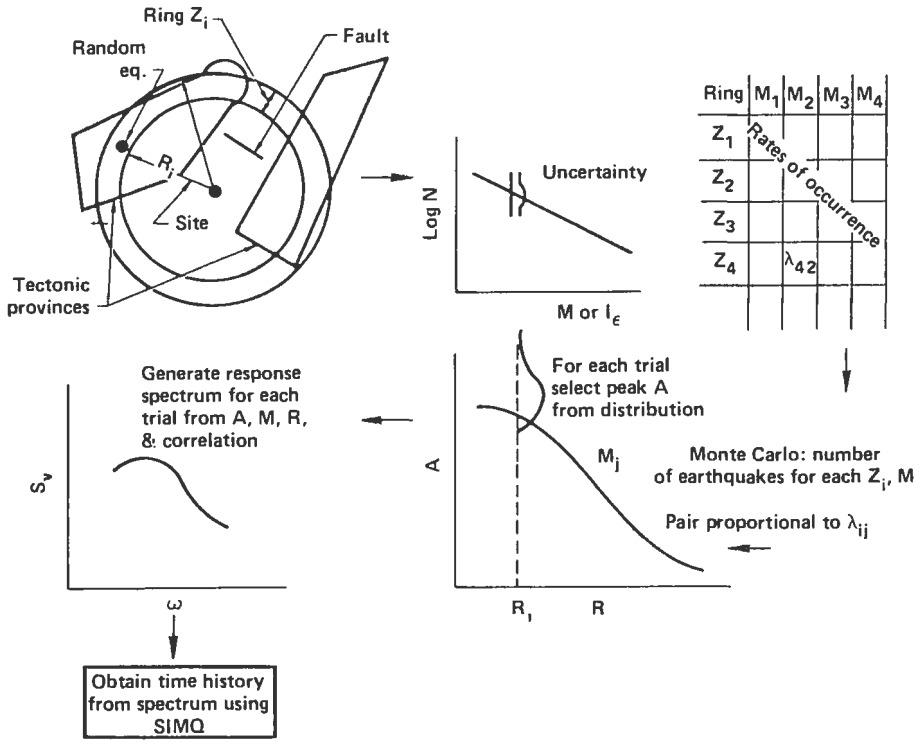

Figure 3.2. Steps in the event-specific approach. A simulation allows the hazard to be defined by response spectra that are functions of event-specific parameters, namely magnitude and distance. Both distance and magnitude are discretized: the geometry in rings (Z_i) centered at distance (R_i) from the site and the magnitudes in intervals centered at magnitude M_j. The mean rates, $\gamma_{R,\,M}$, are arranged, irrespective of source, in a matrix that completely describes the seismicity of the region under consideration. The next step consists of determining the effect at the site of the events of magnitudes M_j at distances R_i. In order to describe the hazard at the site on an event-speific basis, each M_j-R_i event is attenuated to the site separately, using simulation techniques. For the Monte Carlo simulation, a number of horizontal spectral shape intervals and PGA intervals were preselected as target spectra. A number of earthquakes (proportional to their mean rate of occurrence) were simulated from each M and R interval. All horizontal realizations at the site were then sorted in the appropriate box, keeping track of their mean rate of occurrence. The goal was to obtain a fixed number of realizations (30) in each box to take into account the randomness of events having similar characteristics. We then generated the remaining information for each selected horizontal spectrum: the second horizontal PGA, the vertical PGA, the shape, and the duration. The final product of the analysis was the description of the hazard at the site in terms of different types of events, each expressed in terms of 30 realizations and their mean rate of occurrence.

of the vertical PGA to the largest horizontal PGA component is obtained from the data base. The ratio for the present realization is randomly selected from this distribution and the PGA in the vertical direction is determined. The last piece of information necessary to generate artificial time histories is the duration of the strong ground motion shaking. This is obtained using the duration relationship developed by Trifunac and Brady (Ref. 4) and

randomly selecting a realization. Hence three parameters describe the simulation of one seismic event at the site:

- PGA in both horizontal directions and spectral shape (the same spectral shape is used for both horizontal directions).
- PGA and spectral shape in the vertical direction.
- Duration.

Earthquakes (in numbers proportional to their mean rate of occurrence) were simulated from each M and R interval. All horizontal realizations at the site were then sorted in the appropriate interval of PGA (denoted as box). The goal was to obtain a fixed number of realizations in each box to ensure that we had the correct distribution of distances and magnitudes for the future earthquakes occurring around the Zion site and to take into account the randomness of events having similar characteristics. Large numbers of simulations were necessary to simulate very rare events (large PGAs). Recall that for the SSMRP computational procedure, the seismic response and systems analyses were performed for discretizations of the seismic hazard curve and the final step in the process is convolution of these conditional results with the seismic hazard curve. In all of our analyses, the seismic hazard curve was discretized into six intervals of peak acceleration. For random-only and total uncertainty cases, 30 earthquake simulations were performed and 30 sets of acceleration time histories were generated. For our confidence interval calculations, 20 earthquake simulations were performed and a subset of 20 earthquakes were selected from the 30. Most intervals ended up with a large number of events; 30 of them were randomly selected from the sample. For each selected horizontal spectrum, the remaining information (the second horizontal PGA, the vertical PGA, the shape and the duration) was then generated.

Time histories for input into SMACS were generated using the computer program SIMQ (Ref. 5). Durations larger than 18 seconds were truncated to 18 seconds. Because of this truncation, no attempt was made to model the different wave trains. See Ref. 3 for typical results.

The target spectra used to generate the time histories were all developed using the overall earthquake occurrence model of a single expert (Expert 9). This particular model was used because the hazard curve obtained using this overall earthquake occurrence model was effectively (within a few percent) the median hazard curve for all the ground motion models used in this analysis. The Gupta-Nuttli ground motion model, discussed in Section 3.2.3, was used. The "rock" site model was used to generate the target spectra/time histories used to input into the SMACS computer program, which then corrected the frequency content and spectral level of the time histories for the influence of the soil column at the Zion site in the manner described in Sec. 3.2.4.

3.2.2 Overall Earthquake Occurrence Model

The overall earthquake occurrence model includes zonation, rate of occurrence of earthquakes of different magnitudes, and largest earthquakes that can occur in each zone. To obtain the potential range of zonation, rates of occurrence, largest earthquake for each zone, etc., we formed a panel of 10 experts knowledgeable in the history of seismicity in the Eastern United States (EUS). In a questionnaire, the experts were asked to integrate their knowledge about the geology and seismicity of the EUS.

This questionnaire had five sections, asking for input in the following areas:

- Source zone configuration.
- Maximum earthquakes.
- Earthquake occurrences.
- Attenuation.
- Self-ranking.

Questions in the first section were directed to the specification of regions that appear unique in their potential to generate earthquakes and within which the experts felt future earthquake activity would be homogeneous. In the second section, questions focused on determining the size of the largest event that, in the experts' opinion, could be expected to occur in each of the source zones for a given time interval in the future.

The experts were also asked to consider the largest event that they expected to occur within the current tectonic framework in each source zone, irrespective of the time period. We emphasized that they should base their answers not only on recorded data but also on their beliefs on two issues:

- Whether past history can be used for future predictions.
- Whether additional information can be drawn from such sources as tectonics, theoretical studies, and similarity with other regions in the world.

The third section of the questionnaire sought information about the magnitude-frequency relationship for each source zone. Experts were asked to base their answers on historical data and on their own judgment as to the validity, quality, and completeness of the data.

The fourth section of the questionnaire focused on gathering information to review existing attenuation relationships and to develop a new attenuation relationship applicable to the EUS. The experts were questioned on their knowledge of attenuation in the EUS.

In the fifth section of the questionnaire, the experts were asked to rate (on a scale of 1 to 10) the confidence they had in their own responses to the questions in the other four sections. Using this input and weighted-averaging procedures, we obtained a synthesis of opinion. The approach used to generate the subjective input, to assure reliability by feedback loops and cross-checking, and to account for biases and modes of judgment, is presented in detail in Ref. 3.

Using the information provided by the experts, seismic hazard evaluations at the site were performed. Rather than looking for a consensus at the input stage, we processed the input from each expert individually, using his complete set of responses, except for the ground motion attenuation information. The uncertainty provided by the experts about the various

parameters was also included. This procedure has the advantage of providing hazard curves for each expert and of establishing sensitivity for each set of assumptions. This method of independent analysis for each expert accounts for modeling rather than random biases in expert opinion. It should be noted that only 8 out of 10 experts in our panel provided sufficient information for us to be able to develop hazard curves.

The hazard results thus obtained using each expert's input were combined into a single synthesis using a complex weighting method. This method of obtaining a synthesis at the output stage rather than at the input stage is felt to be most appropriate since the model is nonlinear in the input parameters.

It was assumed that the different models provided by our panel of experts covered all the potential range of zonations and earthquake occurrences, including the largest earthquake for each zone. The uncertainty each expert expressed about the parameters of his earthquake occurrence models was treated as random error and included in the analysis. This is not strictly correct but sensitivity studies show that differences in the best estimate curve for each expert resulting from treating such variables as upper magnitude cutoff in this fashion and in a more correct manner are much smaller than the differences between experts and the large effects introduced by site differences and ground motion models.

There is some question as to how well our approach actually bounds the uncertainty introduced by the overall earthquake occurrence model. This is, to a large extent, a matter of subjective judgment. However, as discussed in Refs. 1 and 4, there were large variations for each of the elements of the models between the various panel members. In our view, the results reasonably span the possible alternatives and adequately bound the uncertainty.

3.2.3 Regional Ground Motion Models

The ground motion model enters the hazard analysis in a very direct way. The estimates of the probability of exceedence are strongly correlated with changes in the ground motion model. Thus the uncertainty in our estimates of ground motion plays a very significant role, directly affecting the hazard at a site. As illustrated in Fig. 3-1, the ground motion at a site can be schematically envisioned as arising from three elements. The first is the earthquake rupture process and energy release, which can be described by such source parameters as magnitude, seismic moment, dynamic stress drop, type of faulting mechanism, etc. The second is the seismic energy radiated from the source region, with a definite radiation pattern effect and both geometrical and regional inelastic attenuation (travel path effects). The third is local site effects. The ground motion model is constructed by combining all of these elements into a relationship among the specification of the earthquake's seismic energy, the distance from the site of interest, and the ground motion observed at the site.

There is considerable evidence to suggest that there is a significant systematic variation in each of these elements between the western United States (WUS) and the eastern United States (EUS). For example:

- It is generally agreed that the attenuation of seismic energy in the EUS is much different from that in the WUS.

- Recent work by Nuttli suggests that the source parameters of EUS earthquakes are significantly different from WUS earthquakes.

- There are many sites in the EUS where the site conditions are significantly different from WUS sites. These EUS sites are stiff shallow soils overlying very competent bedrock, i.e., rock with shear wave velocities of greater than 1.5 km/sec. We would expect considerable amplification of the gound motion at these sites.

There are few data on strong ground motion from EUS earthquakes which can be used to verify/resolve these differences or be used to develop EUS ground motion models directly from the data by regression analysis. Thus, it is necessary to convert WUS ground motion models into ground motion models for the EUS by accounting for the systematic differences between the two regions.

In this section, we deal with the regional ground motion model, and in Section 3.2.4 we examine the influence of the local soil column at Zion on our estimate of the seismic hazard.

We formed a panel of experts in ground motion modeling to assist us in the selection and development of appropriate ground motion models for use in our analysis. While no general agreement could be reached, four approaches were identified as "best." Given the paucity of strong ground motion data and only moderate availability of intensity data for the EUS, there are few options. Three of the approaches identified by the panel use intensity as an intermediate variable to relate ground motion in the WUS to that in the EUS. The approaches are:

- Distance-weighted:

  $I_S = f(I_O, R)$ EUS data (3-4a)

  $\text{Log GM} = G(I_S, R)$ and in some cases $G(I_S, M_L, R)$ WUS data (3-4b)

- Magnitude-weighted:

  $I_S = f(I_O, R)$ EUS data (3-5a)

  $\text{Log GM} = G(I_S, M_L)$ WUS data (3-5b)

  $m_b = M(M_L)$ WUS data (3-5c)

  $I_O = 2m_b - 3.5$ EUS data (3-5d)

- No weighting:

  $I_S = f(I_O, R)$ EUS data (3-6a)

  $\text{Log GM} = G(I_S)$ WUS data (3-6b)

where

I_s = Site intensity
I_o = Epicentral intensity
R = Epicentral distance
M_L = Local magnitude (WUS)
m_b = Body wave magnitude based on 1-second waves including Nuttli's m_{blg} scale.

In the fourth approach, various theoretical/empirical assumptions are used to construct ground motion models for the EUS. An example is the Nuttli model (Ref. 5), which combines theoretical modeling with measured regional Q values, assumes that the near-source ground motion in the EUS is the same as in the WUS, and scales only by magnitude. The implications of these various weighting schemes are discussed in Refs. 3 and 8.

For each of the above approaches a number of distinct ground motion models can be developed, depending upon the particular intensity attenuation relation used, the particular data set used, and on how the regressions are performed to get the relation between site intensity and ground motion.

Because only a limited number of hazard curves were developed which had to span the uncertainties both in ground motion modeling and in the overall earthquake occurrence model, we felt it was necessary for us to select only those that are most probable. To do this, we performed a large number of sensitivity tests to ensure that omitting certain ground motion models would not significantly bias our results, i.e., that the less probable models did not give results signficantly different from those of the models considered. Many of these studies are reported in Refs. 3 and 6. We selected what we considered to be the most probable models, basing our selection on discussions with the EUS Ground Motion Modeling Panel, on sensitivity studies, and on our subjective judgment. The rationale for our choices is discussed below.

In selecting the most probable EUS ground motion models, it must be kept in mind that, because there are so few EUS strong ground motion data, one cannot directly develop EUS ground motion models and one must rely primarily on WUS data and correct for the major differences between EUS and WUS tectonic conditions. The major factors (sources of uncertainty) that must be accounted for in converting a WUS ground motion model to an EUS ground motion model are:

(1) Regional attenuation of strong ground motion.

(2) Scaling of the ground motion as a function of earthquake magnitude.

(3) The variability in the ground motion between earthquakes of the same magnitude introduced by source, travel path, and local site effects.

The selection of the most probable models was based on our judgment of how well they accounted for the above items. For example, all of the four general approaches outlined above introduce corrections for regional attenuation. The three approaches which use intensity data make the assumption that strong ground motion in the EUS attenuates at the same rate as intensity attenuates.

This assumption is reasonably valid in the WUS. The theoretical/empirical approaches introduce a correction based on regional measurements of the attenuation of low-energy seismic waves.

For the intensity-based approaches, regional scaling of the ground motion with increasingly large earthquakes is accounted for primarily by the way intensity scales with increasing epicentral intensity, and by the regional relation between epicentral intensity and magnitude. The so-called magnitude weighting approach introduces a secondary correction for magnitude scaling; however, as discussed by Bernreuter (Ref. 6), this additional weighting is not introduced to account for regional differences in scaling of ground motion with magnitude but to help account for regional differences in attenuation and the fact that the same intensity occurs at much greater distances for large earthquakes as compared to smaller earthquakes. Some theoretical/empirical approaches introduce a regional correction for scaling of the ground motion with magnitude and others do not. We will provide several examples later in this section.

Although they have their conceptual difficulties (see Ref. 3), the class of models that we labeled theoretical/empirical leads, in our opinion, to more probable EUS ground motion models. There are several reasons for this. First, one major problem with intensity-based models is that use of intensity as an intermediate variable leads to models which generally underestimate the ground motion at smaller epicentral distance and overestimate the ground motion at large epicentral distances. Also, there are difficulties correlating ground motion with the parameters noted on the intensity scale.

Secondly, it is possible to account for regional differences in the way the ground motion scales from earthquakes of different magnitudes. As noted above, the correct scaling relation should be embedded in the relation $I_S = f(I_O, R)$. However, in actual practice the attenuation of the intensity relation is generally developed from only a few earthquakes, and thus it is difficult to get a good estimate of the scaling parameter.

Of three general intensity-based approaches, we selected the magnitude-weighted approach as best. In our judgment, the unweighted approach introduced significant bias in converting from WUS to EUS models. For data obtained in the same region, distance weighting appears to be the best approach. However, if the data is from two different regions, as is our case, where the attenuation of intensity is from the EUS and the relation between ground motion level and site intensity is from the WUS, then there are a number of conceptual problems with the distance-weighted approach (Refs. 6, 8).

Of all the possible magnitude-weighted models, we selected the one that we called the Gupta-Nuttli model in the Phase I report (Ref. 3). The details are provide in Refs. 3 and 6. Briefly, the equations are based on the attenuation-of-intensity relationship developed by Gupta and Nuttli for the Central United States (CUS). Their model is based on the smoothed isoseismals from a number of earthquakes. To account for the fact that we want to use the median distance at which a given intensity level is representative rather than isoseismal distance, we reduced the intensity by 1/2 an intensity unit. The model was completed by combining the relation between site intensity, magnitude, and ground motion we developed in Phase I with the modified Gupta-Nuttli attenuation relation to obtain the relation

$$\ln a = 0.74 + 1.12\, m_b - 0.0007\, R - 0.73 \ln R \quad . \tag{3-7}$$

A number of models fit in the general approach that we have labeled theoretical/empirical. We considered three of them. The first model, developed by Nuttli (Refs. 7 and 9) is specified by

$$a = A_o(m_b)\, R^{-5/6} \exp(-\gamma R) \quad .$$

The term $R^{-5/6}$ gives the geometric attenuation which is assumed to be the same in both EUS and WUS, and the term $\exp(-\gamma R)$ gives the regional anelastic attenuation, obtainable from regional data. To determine the scaling with magnitude, Nuttli assumed that within 20-30 km of the epicenter the ground motion from EUS earthquakes would be similar to WUS earthquakes. Thus one could determine the scaling with magnitude. Rather than directly appeal to data to obtain $A_o(m_b)$, Nuttli used a combination of theoretical assumptions and comparisons to data to obtain his scaling term. A good fit to the curves provided by Nuttli is given by

$$\ln a = A_o + 1.15\, m_b - 0.833 \ln R - \gamma R \quad , \tag{3-8}$$

where

$$\gamma \sim 0.042 \exp(-0.45\, m_b)$$
$$A_o \sim 1.48.$$

The value for A_o depends upon the analysis being performed. Generally when ground motion models are developed, regression analysis is performed using both horizontal components. Campbell (Ref. 10) examined this question and determined that the difference between regression using both components and regression using only the largest of the two horizontal components is about 12%. However, in our case we want to estimate the peak acceleration, because in the event-specific approach we randomly select the value of the other horizontal component from the distribution between the peak and the other horizontal component using available strong ground motion data. To assure that the peak does not always occur along the same structural coordinate axis, we alternated the axis of the peak.

Bernreuter et al. (Ref. 3) pointed out that the coefficient of the m_b term in Eq. (3-8), which determines how the acceleration scales with magnitude, was larger than typically found from regression analysis of WUS data, where values of range of 0.6 to 0.9 are typical. To examine this question we repeated the regression analysis on the data set used by Joyner and Boore (Ref. 11), using an approach similar to theirs. In our analysis, the coefficient of the term for geometrical attenuation was taken to be the (-5/6) power (in agreement with Nuttli's model) rather than the (-1) power assumed by Joyner and Boore. The purpose of this change was to put the model in the same form as assumed by Nuttli when he determined the regional absorption coefficient for both the EUS and WUS. In addition, the corrected value of m_b (or an estimate of the corrected value of m_b) was used for the measure of the size of the earthquakes. We determined the best fit relation

$$\ln a_w = 3.99 + 0.59\, m_b - 5/6 \ln R - 0.007\, R \,, \qquad (3\text{-}9)$$

where

$$R^2 = d^2 + h^2$$
$$h = 5.3 \,.$$

Nuttli (Ref. 7) obtained a similar estimate for γ in the WUS. For the central United States (CUS)* where Zion is located, Nuttli (Ref. 12) estimates a value of $\gamma = 0.003$. If indeed the ground motion from CUS earthquakes scales the same with magnitude as WUS earthquakes, we can convert Eq. (3-9) into a CUS ground motion model simply by replacing the value of γ with the appropriate value for the CUS. This gives

$$\ln a = 3.99 + 0.59\, m_b - 5/6 \ln R - 0.003\, R \qquad (3\text{-}10)$$

where

$$R^2 = d^2 + h^2$$
$$h = 5.3 \,.$$

In his most recent work Nuttli (Refs. 12-14) has studied the regional magnitude scaling of the source spectrum. Nuttli found that the earthquake source spectra for earthquakes larger than about magnitude 4-4.5 scale differently in the intraplate regions (such as the CUS) than in the interplate regions where the bulk of the WUS data is obtained. Nuttli's research indicates that for intraplate EUS earthquakes

$$\ln a \sim 1.15\, m_b \,,$$

whereas for interplate earthquakes (WUS) the scaling is more complex. Nuttli's model (Refs. 13 and 14) suggests that Eq. (3-10) should be written as

$$\ln a = A_o + 1.15\, m_b - 5/6 \ln R - 0.003\, R \,,$$

where the value of A_o is obtained by evaluating Eq. (3-10) in the reasonable nearfield (we used $d = 10$ km) at $m_b = 4.5$. We obtain

$$\ln a = 1.412 + 1.15\, m_b - 5/6 \ln R - 0.003\, R \,. \qquad (3\text{-}11)$$

It is interesting to note that there is very little difference between Eqs. (3-11) and (3-8), although they were derived from different hypotheses.

Up to this point we have only examined corrections for converting WUS ground motion models into CUS ground motion models by introducing corrections for differences in regional attenuation and magnitude scaling. We noted earlier that we also needed to correct for possible regional differences in the variability in ground motion between earthquakes of the same magnitude. This random variability is due to differences in the rupture process, complexity of

* The EUS comprises all the region east of the Rocky Mountains. The CUS is a sub-element of the EUS and includes the area around the Zion site.

the travel path, and local site geology. For example, there is some evidence that earthquakes of the same magnitude are more similar in mid-plate areas such as the CUS than along the plate margins. Thus we would expect to see less random variability in the ground motion, since the travel path is certainly less complex in the CUS than along plate margins. For this study the uncertainty in the estimate of the ground motion for a given magnitude and distance is assumed to be lognormally distributed. The uncertainty is measured by the standard deviation of the natural logarithm of the peak acceleration, $\sigma_{\ln a}$. Although we might expect $\sigma_{\ln a}$ for the CUS ground motion model to be smaller than for the WUS, data are not sufficient to evaluate such a hypothesis.

For our analysis there is a further complication because, as will be outlined in the next section, corrections will be introduced to account for the specific soil column at the Zion site and for the uncertainty associated with its configuration and properties. The value of $\sigma_{\ln a}$ is a measure of the total uncertainty, including the uncertainty attributable to the basing of the ground motion model on data obtained from different sites with very different site geological columns. There have been only a few studies which attempt to sort out the relative contribution to the variability in the ground motion from these factors (Refs. 15, 16). From a review of the available data we estimated that the appropriate value for the standard deviation of the logarithm of the peak ground acceleration to use in our hazard analysis (before specific correction for the local geologic column) is

$$\sigma_{\ln a} = 0.45 \ .$$

Most of the hazard curves were developed using this value for $\sigma_{\ln a}$ using either Eq. (3-7) for experts whose earthquake occurrence models are expressed in intensity, or Eq. (3-8) if the earthquake occurrence model is expressed in magnitude. Sensitivity studies showed that choice of Eq. (3-8) or Eq. (3-11) made little difference in the computed hazard curve.

To bound the uncertainty in our estimates of the seismic hazard due to our uncertainty in the ground motion models required the selection of an upper-bound and lower-bound model. The upper-bound model (the one that led to the largest estimate of the probability of exceedence for acceleration levels larger than the 0.1 g for the set of earthquake occurrence models provided by the members of EUS Seismicity Panel) was obtained using Eq. (3-7) both in its magnitude and epicentral intensity form with $\sigma_{\ln a} = 1$. This value of $\sigma_{\ln a}$ represents the upper limit of the uncertainty in ground motion estimates. It is obtained by combining the uncertainty of the attenuation of intensity relation Eq. (3-5a) with the other uncertainties associated with Eq. (3-5). See Bernreuter (Ref. 6) and Cornell et al. (Ref. 17) for added discussion. The lower bound model is given by Eq. (3-10). We also used Eq. (3-11) with $\sigma_{\ln a} = 0.2$ as the lower-bound model.

3.2.3 Correction for Local Site Factors

In the Phase I report we noted that one of the major modeling uncertainties was the manner in which the influence of the local soil column on the free-field ground motion was included in the analysis. In Phase I, local site effects were accounted for by use of a simple soil classification procedure,

such as that introduced by Trifunac and Brady (Ref. 18). However, as noted in the Phase I report, the ground motion models so developed are valid only at what could be loosely termed "average" soil sites. Such an approach can introduce two significant modeling errors in the analysis:

- Since ground motion estimates for a site are based on correlations developed from data obtained at a number of loosely correlated sites, there is little correlation among spectral peaks from site to site. Thus, the spectral peaks at one site are often averaged with spectral valleys for other sites. However, a given site may consistently amplify the incoming seismic energy at certain frequency intervals. The net result is that the projected ground motion estimates may be biased on the low side for such a site.

- The statistic (typically the standard deviation) that measures the dispersion or spread of the data about the mean may be smaller at a single fixed site than that obtained for data recorded at a number of different, loosely correlated sites.

Our concern about the first possible error was heightened for the Zion site, since the geological column there is significantly different from those at sites making up the strong-motion data set. Notably, the Zion site is underlain by rock with a higher shear-wave velocity than typical WUS sites. The Zion site also has a relatively shallow soil cover (about 110 ft) consisting of sand and stiff, highly overconsolidated glacial tills that are significantly different from soil conditions at sites in the strong-motion data set.

There is no general agreement on how best to address these two potential problems. To help assess how to model the Zion site, we performed a numerical modeling study (Ref. 19) in Phase I to determine if it was possible to model the incoming seismic waves as a one-dimensional problem. The results of this study indicated that the angle of incidence of all wave types was almost vertical. The study also showed that such was not the case for typical WUS sites. These results indicated that the use of a one-dimensional vertical wave propagation computer program such as SHAKE would be acceptable in assessing the influence of the local soil column at Zion.

The potential nonlinear behavior of the soil column at the Zion site was examined by Johnson et al. (Ref. 20). It was found that for the Zion site, use of the equivalent linear analysis incorporated in the SHAKE computer program reasonably modeled the response of the soil column when compared to a nonlinear analysis. Appendix A provides comparisons that were made between the computed response at the Zion site and that recorded at several other sites. These comparisons show that there is reasonable agreement between the computed amplification factors for the Zion site and the amplification factors recorded at several other sites.

Based on the above, the effect of the soil column at Zion was modeled in the following manner. Acceleration time histories were developed for a hypothetical rock outcrop at the Zion site, using the event-specific methodology outlined in Sec. 3.2.1. The target spectra were corrected for the difference between rock and soil sites; correction factors are given in

Bernreuter (Ref. 6). The time histories were developed using SIMQ. Each earthquake contained three components (two horizontal and a vertical component). They span the expected range of ground motion at the Zion site. That is, they have the proper distribution of earthquake magnitudes, distances, durations, and peak accelerations. For example, the PGA varies from 0.06 g to 0.7 g at the rock outcrop. These rock outcrop time histories were input into the SMACS computer program, and corrected for the Zion soil column in SMACS as described below.

The seismic input phase of SMACS is described by free-field acceleration time histories on the surface of the soils; spatial variation of the motion is taken into account in the development of the scattering matrices (Sec. 4). Transfer functions which relate rock outcrop acceleration time histories to the surface accelerations were generated based on vertically propagating shear and dilatational waves and equivalent linear viscoelastic soil properties. The resultant motion is the same as would be computed using, for example, the SHAKE computer program, provided no iterations were applied. The soil properties were corrected to the first order for the average strain level based on the peak acceleration of the event (Sec. 4).

The effect of the soil column is significant on the computed free-field time histories. Shown in Fig. 3-3 is a comparison of the average spectra at the rock outcrop and at the top of the Zion soil column. It can be seen from this comparison that there is a significant difference between the two sets of spectra, with significant amplification due to the local site column.

3.2.5 Limitations

The uncertainty in our estimate of the seismic hazard at the Zion site arises from our uncertainty in the overall earthquake occurrence model, the ground motion model including local site effects, and the assumptions required to compute the hazard. In the preceding sections we have outlined what we included in our uncertainty analysis. Here we enumerate the main elements not included.

We did not include alternative hazard analysis approaches, e.g., the "historical analysis" discussed in Bernreuter et al. (Ref. 3). Neither did we include alternatives to the Poisson assumption for the occurrence of earthquakes in time. We did ask our panel of experts to suggest alternative models. The panel generally agreed that although the earthquake occurrence model could be considerably improved, there was not at present sufficient data/judgment to come up with superior alternative models.

We note that we did not attempt to completely bound the uncertainty introduced by local site effects. All of the SMACS calculations were made including the modeling correction for local site effects. No other approaches to correct for local site effects were used to introduce our uncertainty about the correction approach used. To assess the effects of local site conditions on seismic risk, analyses including explicit modeling of the phenomenon and excluding it were performed and comparisons made.

While the impact of local site conditions on the time histories was accounted for, we included no other sources of uncertainty in our modeling of time histories, other than the approach used in Phase I. The same sets of time

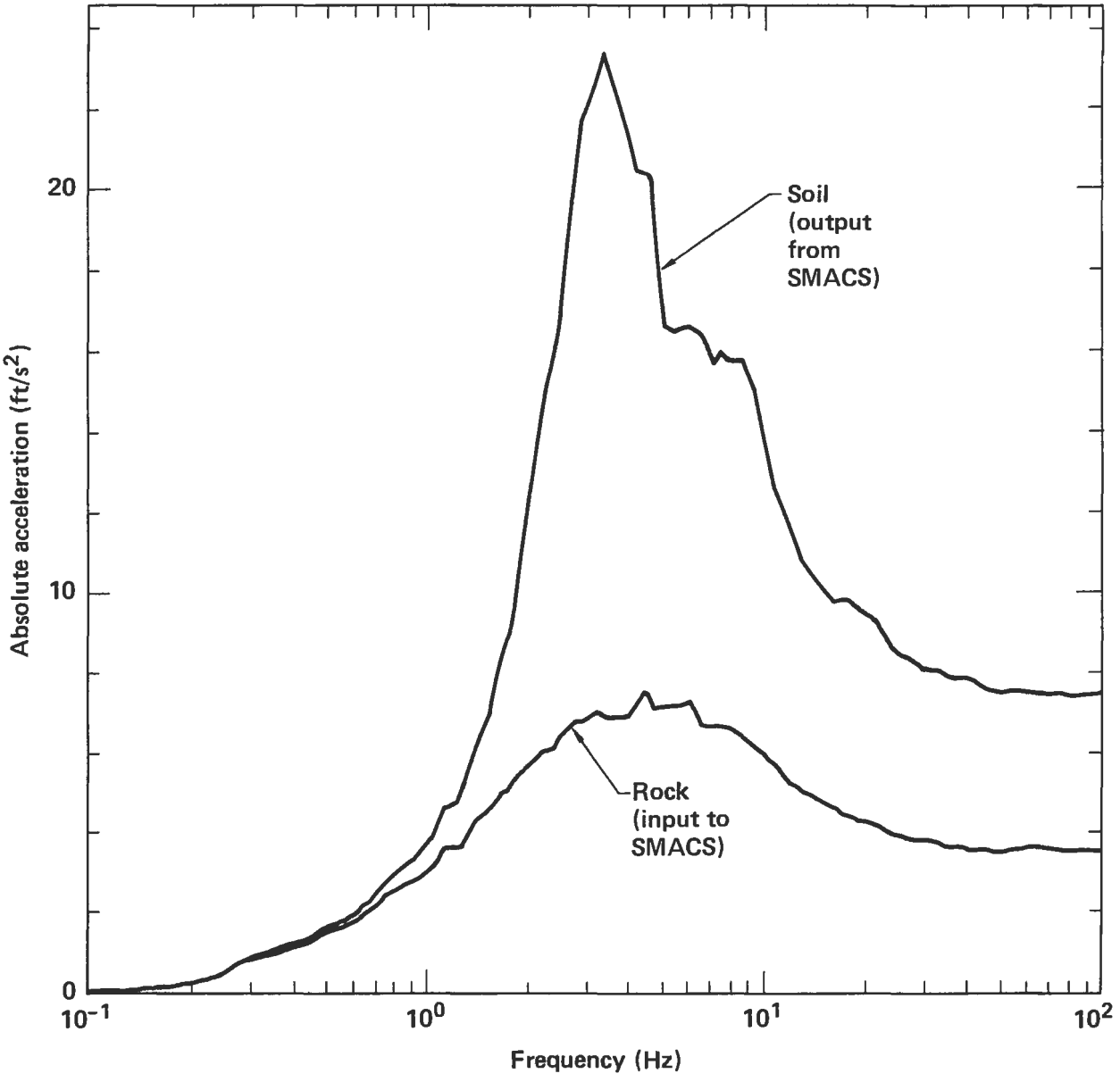

Fig. 3.3. Comparison of the average spectra at the rock outcrop and at the top of the Zion soil column.

histories were used for all hazard curves. To be more correct, we could have developed a set of time histories for each expert/ground motion model. Methods other than SIMQ (Ref. 5) could have been used to develop the time histories from the target spectra. Clearly, this would have led to an insurmountable computation problem. It was our judgment that, because the SMACS analysis is essentially linear, the impact of other sources of uncertainty on the time histories would be small compared to local site effects. This area is currently under investigation as part of the SSMRP verification program.

A number of ground motion models were used to attempt to bound the systematic error attributable to ground motion modeling. How well the ground motion models used in this analysis bound the uncertainty in the estimation of the ground motion from earthquakes around the Zion site is, of course, a matter of judgment. They were chosen to account for various hypotheses about ground motion from EUS earthquakes relative to PGA, but some hypotheses about the shape of the spectra from EUS earthquakes were not investigated.

3.3 Hazard Curves

3.3.1 Hazard Curves for Uncertainty Intervals

In this section we discuss our rationale in developing the 14 hazard curves which span the total uncertainty in the estimates of the ground motion at the Zion site. As discussed above, one of the key features of our approach is to keep each expert's model separate and distinct. We developed the 14 hazard curves, as far as possible, in keeping with this approach. Because of the limited number of runs being performed, we felt that it would be preferable if each of the 14 hazard curves had approximately the same weight. We did not formally compute weights assigned to each hazard curve by assigning weights to each of the hypotheses that were used to develop it. It is possible, in our opinion, to judge that some hypotheses are better than others. However, the assignment of actual numerical values is arbitrary and the final computed weight assigned to any one curve would imply a far greater precision than we feel is possible or justified. Figure 3-4 shows the 14 curves developed. It should be noted that the curves shown on Fig. 3-4 are for peak ground acceleration at the rock outcrop.

To span the uncertainty in zonation and earthquake occurrence models, each expert's model was used with the appropriate ground motion model. For the experts who expressed their overall earthquake occurrence model in magnitude, we used Eq. (3-8). It should be recalled that sensitivity studies showed very little difference between Eqs. (3-8) and (3-11). For the experts who expressed their earthquake occurrence model in intensity, we used Eq. (3-7). To span the uncertainty introduced by the ground motion models, we introduced different ground motion models. It is our judgment that a lower-limit ground motion model is more likely to be correct than an upper-limit ground motion model. To capture this, three curves were developed using lower-limit ground motion models, as compared with only one curve for the upper limit. As noted in the Ground Motion Model section, the curves used for upper limit and lower limit do not represent extreme bounds. The upper-limit hazard curve is constructed from the median of the three highest hazard curves (Experts 5, 7, 10) using the upper-limit ground motion. The lower-limit curve was constructed using the lowest estimate (Expert 8) zonation and earthquake occurrence model and the lower-limit ground motion model. The upper- and lower-limit curves were done differently to reduce the conservatism introduced in the different expert's earthquake occurrence models. The other two lower models were constructed using the median curve obtained using the lower-limit ground motion model and the median curve from Eq. (3-11) and $\sigma_{\ln a} = 0.2$.

Finally, to balance the relatively more numerous lower-limit models, two additional hazard curves were developed. One curve is the curve shown in Fig. 3-5 (median obtained using the Gupta-Nuttli model), and the other curve is the median using our improved EUS ground motion model, Eq. (3-11).

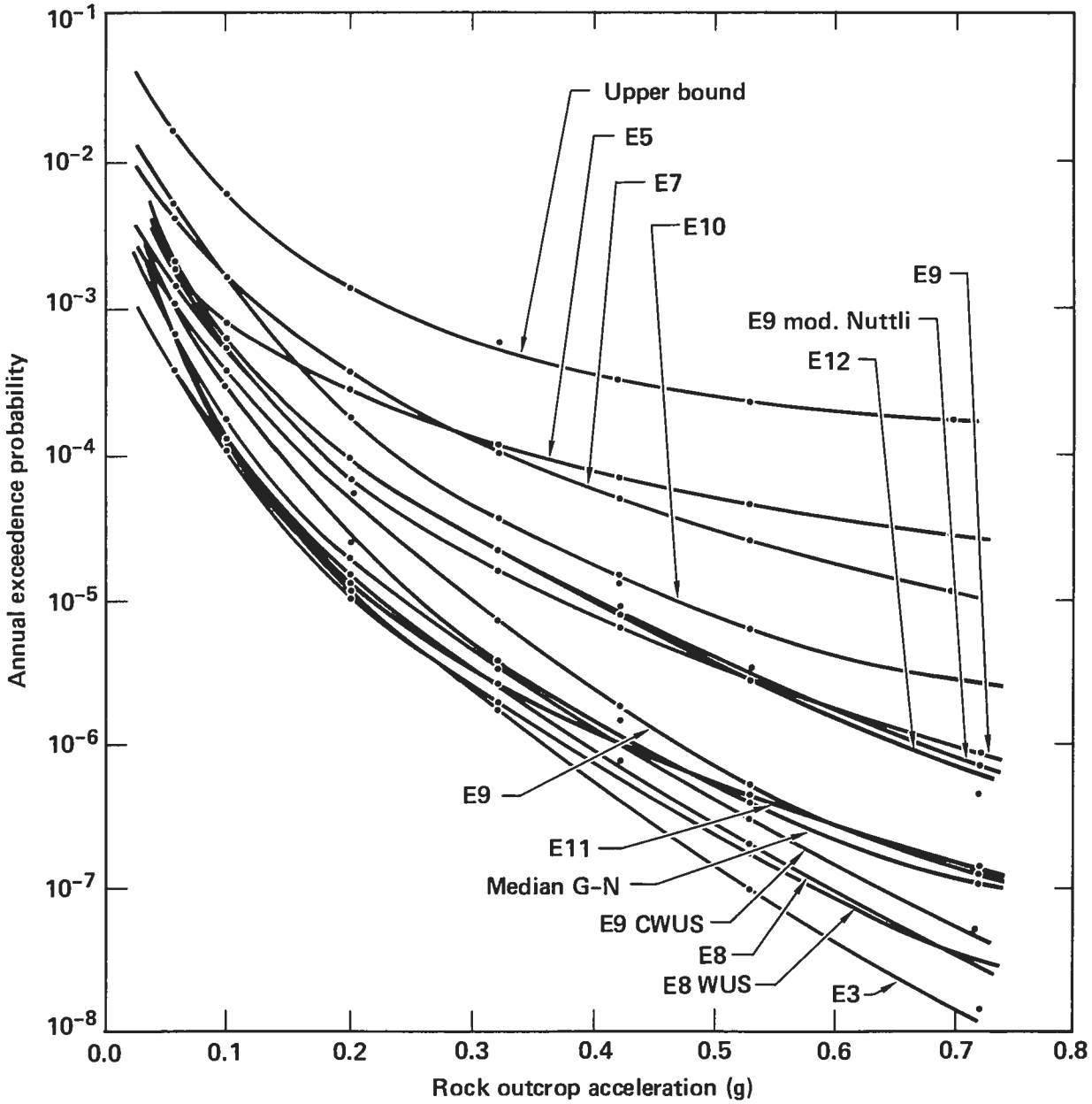

Fig. 3.4. Fourteen approximately equally weighted hazard curves for computation of the uncertainty in the final risk numbers.

3.3.2 Hazard Curve for Random-Uncertainty-Only Case

As discussed in Chapter 7, the base-case point estimates of core melt and release were computed considering random uncertainty only. Unlike other inputs, e.g., fragility curves, soil properties, etc., for which uncertainty is modeled by continuous distributions with contributions from both random and systematic uncertainties, many of the input parameters for the seismic hazard analysis are discrete. Thus, it is necessary to introduce some assumptions and approximations in order to develop a hazard curve reflecting random uncertainty only. In particular we assumed that:

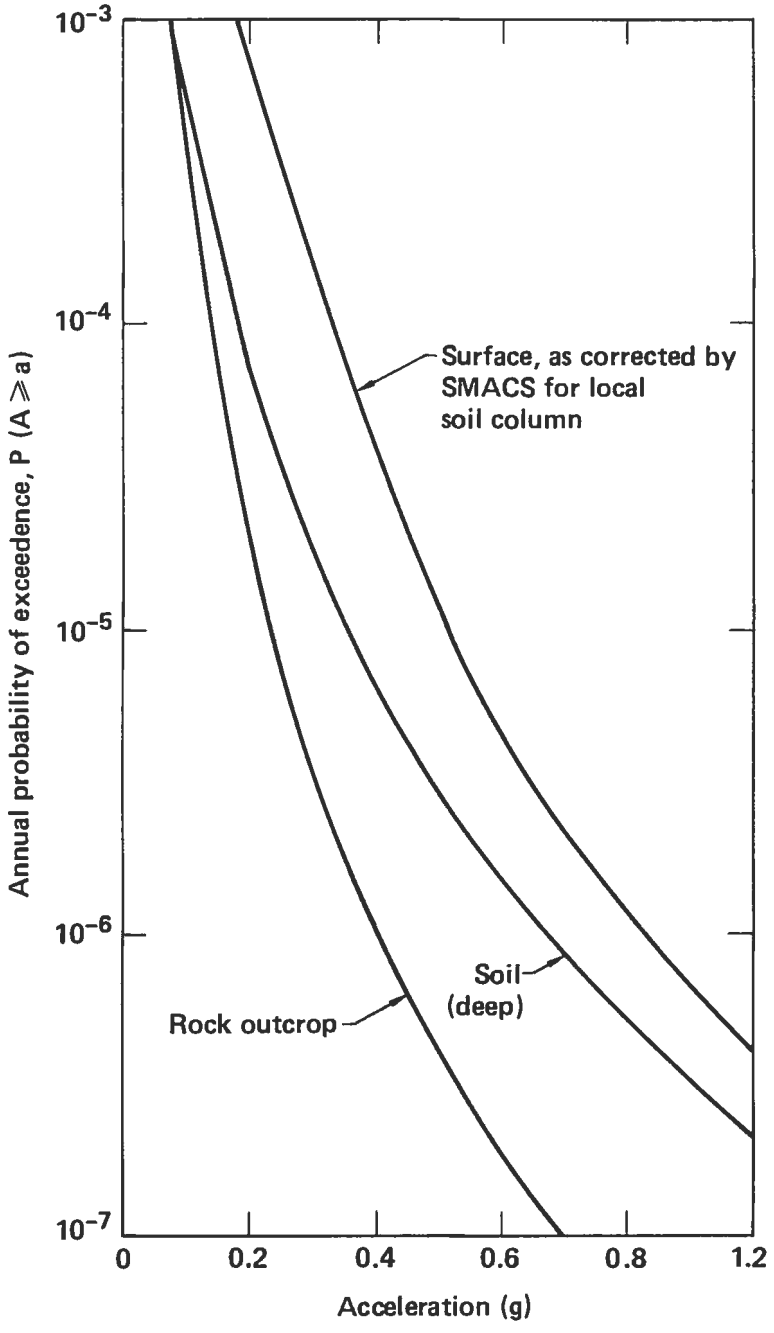

Fig. 3.5. Zion hazard curves compared. Hazard curves with and without effects of local soil column. For reference, the "rock outcrop" hazard curve is also shown.

1. Zonation was primarily a systematic uncertainty. We chose Expert 9's model as the base zonation for the random-only hazard curve.

2. The random uncertainty in the parameters of the earthquake occurrence model for each zone was taken as the uncertainty expressed by Expert 9 for each of these parameters. The systematic uncertainty was assumed to be modeled by the parameters for the earthquake occurrence model provided by each expert for his model. There is, of course, some inconsistency here, since the parameters provided by other experts are generally for a different set of zones.

3. The uncertainty of the regional ground motion model naturally separates into random and modeling parts. As noted, the regional ground motion model is assumed lognormal and the random is measured by $\sigma_{\ln a}$. The modeling uncertainty is modeled by using different ground motion models. For the random-only case we used Eq. (3-7), which is the same ground motion model that we used in Phase I, except here we used $\sigma_{\ln a} = 0.45$.

4. Local site corrections were included with only random uncertainty included for the soil properties.

The resultant hazard curve for the rock outcrop is shown in Fig. 3-5. Also shown in Fig. 3-5 is the approximate hazard curve on the soil surface.

3.3.3 Hazard Curve Neglecting Site Effects

In order to demonstrate the importance of including an explicit correction for local site effects (as compared to treating all soil sites alike, as is typically done in other hazard analyses), it is necessary to compare a compatible case with explicit correction to one without correction. The hazard curve without explicit correction for local site effects was developed using the ground motion model given by Eq. (3-7), using case $\sigma_{\ln a} = 0.6$ and Expert 9's overall earthquake occurrence model shown in Fig. 3-5 as soil (deep). Time histories were developed for this hazard curve using the soil site spectral ground motion model given in the Phase I report and the event-specific approach discussed above in Sec. 3.2.1. These time histories were used directly to compute structural response and represent the "without local site effects" case. As discussed in Chapter 10, the results from the analyses using the "without local site effects" curve were compared to the results obtained using the hazard curve discussed in Sec. 3.3.2.

3.3.4 Discretization of the Hazard Curve

The computational procedure, i.e., the seismic response and systems analysis steps, was performed for discretizations of the seismic hazard curve, and the final step in the process was convolution of these conditional results with the seismic hazard curve. In all of our analyses, the seismic hazard curve was discretized, for calculational purposes, into six intervals of peak horizontal acceleration on the rock outcrop: 0.06-0.10, 0.10-0.20, 0.20-0.32, 0.32-0.42, 0.42-0.53, and 0.53-0.69 g Discretization permits excitation-sensitive parameters to be incorporated into the calculations, and serves as

an approximate numerical integration in computing the seismic risk over the entire range of hypothesized earthquake levels. These six intervals were chosen so that each interval (set of time histories) had the same probability as for the Phase I analysis. This discretization is somewhat arbitrary, but was judged to be reasonable and adequate.

CHAPTER 4: STRUCTURE AND PIPING RESPONSE

Chapter 2 described the basic steps of a seismic risk analysis. In the seismic response step, responses of structures and components for all basic events in the fault trees and for the calculation of initiating event probabilities are required. These responses must be compatible with the fragility descriptions (Chapter 5), and must be estimated for the range of possible earthquakes at the site, i.e., for the range of earthquakes represented by the seismic hazard curve (Chapter 3). Three aspects of seismic response are necessary for seismic risk analysis:

- Median response--the median level seismic response given an earthquake occurrence is required. In general, the median response differs from the design values because design analysis procedures, parameter selection, and qualification procedures, in the latter case, are conservatively biased. The change in properties of the soil/structure/piping systems which occurs as excitation levels increase is an additional consideration in the analysis of the range of earthquakes. For example, higher excitations lead to lower soil shear moduli, lower structure frequencies, and higher soil and structure damping characteristics. Such changes need to be taken into account when determining median response.

- Variability of response--variability in seismic response resulting from variations in the earthquake excitation, and the physical properties of the soil/structure/piping system, and our ability to model it must be included in the seismic risk analysis.

- Correlation of responses--correlation of responses (the tendency for pairs of responses to have simultaneously high or low values) results from two sources--the level of the earthquake and the dynamic characteristics of the system. The level of the earthquake affects correlation, since a large earthquake (large peak acceleration) may cause all responses to be large, whereas a small earthquake produces the opposite effect. The second source of correlation is the system response itself. For example, floors within a structure may all experience high values of response simultaneously due to the dynamic characteristics of the structure itself. Hence, equipment supported on these floors may simultaneously have high response. The importance of response correlation on frequencies of system failure, core melt, and radioactive release depends on correlations between fragilities and the functional characteristics of the systems themselves.

For the SSMRP seismic risk analysis of the Zion nuclear power plant, these three aspects of seismic response were calculated by the computer program SMACS (Seismic Methodology Analysis Chain with Statistics). The following sections describe the SMACS methodology, the Zion nuclear power plant (soil/structures/piping models), parameters of the SMACS analyses, and results in the form of seismic responses.

4.1 SMACS Methodology

The computer program SMACS links the seismic input, soil-structure interaction (SSI), major structure response, and subsystem response calculations.

A detailed description of the methodology is contained in Ref. 1 and summarized here. The seismic input is defined by ensembles of acceleration time histories in three orthogonal directions (two horizontal and one vertical) in the free-field. Soil-structure interaction and detailed structure response are determined simultaneously, using the substructure approach (Refs. 21 and 22). This approach, as implemented in the CLASSI family of computer programs (Ref. 23), was used extensively. It permits very detailed models of the structure to be considered in the final step of the substructure approach (analysis of the coupled soil-structure system). Section 4.2 describes models of the Zion site (soil configuration and material properties) and structures used in the analysis. Detailed structure response in the form of time histories and peak values of accelerations, displacements, and forces is computed. Structure response serves two main purposes in the analysis.

First, a measure of response (peak value) is compared with a fragility description of the structure to assess its ability to perform its design function during or after the earthquake. For buildings, this function includes providing support for systems contained within. Second, because structures act as transmitters of vibratory motion to the support systems of emergency and power-generation equipment, structure response becomes an input to the calculation of subsystem response. SMACS likewise calculates time-history response of subsystems. Piping systems are analyzed assuming independent piping-support motions obtained from the detailed structure response. The pseudostatic mode method was used. Section 4.2 describes the models of the Zion nuclear power plant piping systems which were analyzed.

Dynamic responses determined by SMACS constitute one of the essential ingredients of the seismic risk analysis. Compatibility between these responses and the fragility descriptions of structures, components, and systems must be maintained. Locations within structures and piping systems at which responses were calculated were therefore selected according to the requirements of the fault trees and the fragility descriptions. Similarly, response quantities were selected to correspond to quantities on which the fragilities were based. The fragilities of structures and floor-mounted equipment are expressed in terms of structural accelerations; the fragilities of valves mounted on piping systems are tied to their local accelerations; and the fragilities of the pipes themselves are characterized by peak resultant moments over the duration of the earthquake.

The SMACS methodology, the models of the Zion soil, structures, and piping systems, and parameter values for the analysis were selected to produce median responses and provide a measure of variability and correlation of responses. The modus operandi of SMACS is to perform repeated deterministic analyses, each simulating an earthquake occurrence. By performing many such analyses and by varying the values of the input parameters, the uncertainty inherent in any deterministic analysis is taken into account. Variability in the seismic input is included by sampling to obtain a different set of earthquake time histories for each simulation. Variability in the soil-structure-subsystem behavior is introduced by varying a number of parameters: in the SSI analysis, the mechanism for introducing uncertainty was to vary the shear modulus and material damping in the soil; in the calculation of major structure and subsystem responses, frequencies and modal damping properties

were varied. This variability was introduced by sampling values of these input parameters from assumed probability distributions for each simulation. Values for these SSI, structure, and subsystem parameters were selected according to a Latin hypercube sampling method, which efficiently spanned the parameter spaces. The remainder of Sec. 4 describes the distributions of the parameters and the sampling schemes used.

Section 3 described the seismic hazard curves and their discretization for the response calculations and the systems analysis. In terms of SMACS analyses, 30 deterministic analyses were performed for each of the 6 ranges of peak ground accelerations on the rock outcrop (0.06-0.10 g, 0.10-0.20 g, 0.20-0.32 g, 0.32-0.42 g, 0.42-0.53 g, 0.53-0.69 g) for our base cases (Chapter 7). Analyses leading to estimates of uncertainty intervals used 20 earthquake simulations (Chapter 7). Note, as discussed in Chapter 3, that these accelerations are relative to the rock outcrop. The following discussion assumes 30 earthquake simulations but is equally applicable to 20 simulations. Therefore, in our Latin hypercube sampling method, 30 sets of time histories were generated for each acceleration range. (Each set included two horizontal and one vertical time history.) Within each range, the peak acceleration of the 30 earthquakes varied according to the relative probability of their occurrence. The distribution of each variable input parameter was then divided into 30 equal-probability intervals. Next, a value was randomly selected from each interval, and the 30 values for each variable were rearranged randomly. The 30 sets of time histories and the permuted values of the variable parameters were then grouped to give 30 combinations of input values for the dynamic analyses. Therefore, in a series of 30 analyses, which results in a distribution of responses for the acceleration range of interest, each time history set was used once, and a parameter value was selected once from each of the 30 intervals in each of the parameter distributions. Each set of 30 input parameter combinations is called a Latin hypercube sample. More will be said concerning parameter variations in subsequent sections.

Variability of responses and their correlation are a result of the SMACS analyses. Responses for each of the 30 earthquake simulations were saved, and variability in response was represented by parameters of a lognormal distribution fitted to the calculated responses. Similarly, correlation between responses was estimated by calculating correlation coefficients.

4.2 Modeling the Zion Nuclear Power Plant

4.2.1 Zion Nuclear Power Plant

The Zion nuclear power plant, north of Chicago, Illinois, is the subject of our analysis. Figure 4.1 shows a layout of the Zion facility. It is founded on a site characterized by about 110 feet of soil overlying a bedrock of Niagara Dolomite. The top layer of soil, about 35 ft thick, consists of granular lake deposits of dense, fine-to-medium sands, together with variable amounts of coarse sand and gravel. The second layer, 30 ft thick, is a cohesive, firm-to-hard glacial till. The remaining 45-ft layer of soil is a cohesionless glacial deposit of dense sands and gravel. This soil configuration was discretized for the SMACS computations as three soil layers underlain by a half space. The soil layers were distinguished by the choice of values for shear modulus and material damping, which will be discussed in Section 4.2.2.

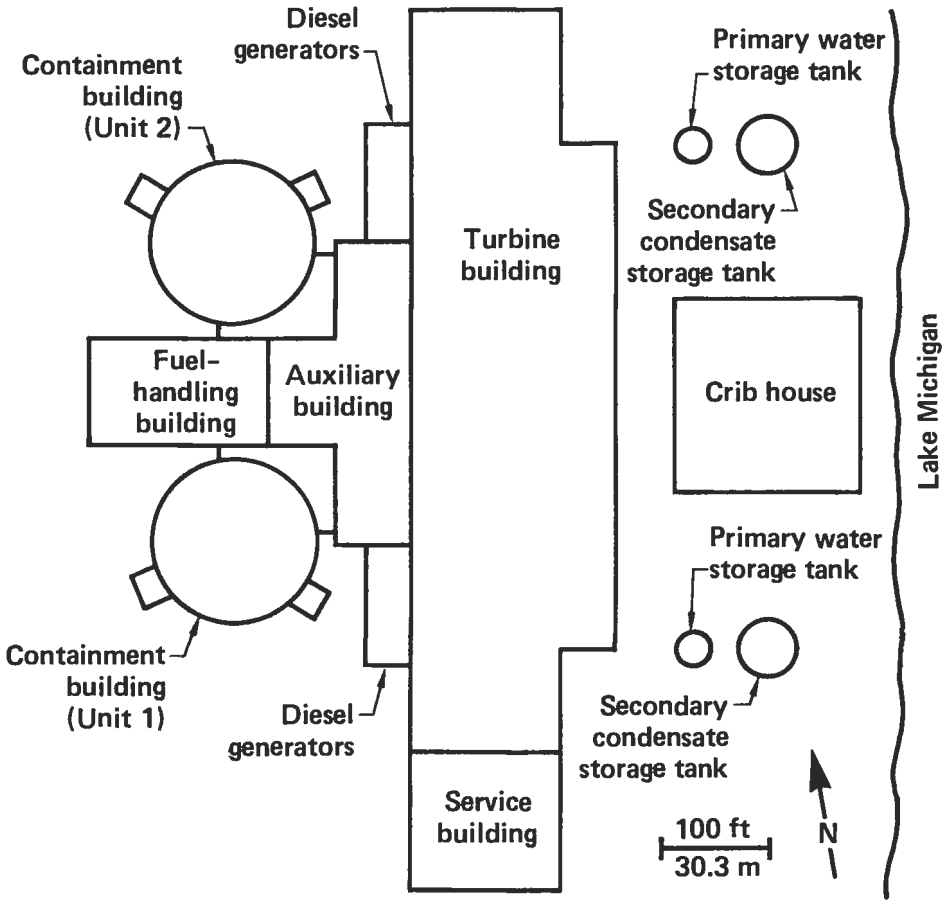

Fig. 4.1. Site plan of the Zion nuclear power plant.

Zion Unit 1 was the subject of our analysis. The Unit 1 containment building at the Zion plant comprises two essentially independent structures--a containment shell and a concrete internal structure. As shown in Fig. 4.2, the common foundation for these two structures is embedded in the second soil layer. In the SSI phase of the SMACS computations, the foundation was assumed flat bottomed and rigid; the deeply embedded sump was not modeled, though the effects of its mass were included. The cylindrical, prestressed concrete containment shell was modeled with a series of beam elements. Masses and rotary inertias were lumped at nodal points. Rotary inertias affecting bending and torsional response of the shell were included. The internal structure, including a simplified model of the nuclear steam supply system, was modeled with three-dimensional beam and plate finite elements. Masses were again lumped at selected nodes. These two structures, together with several of the nodes at which responses were calculated, are shown in Fig. 4.2.

The second structure studied at the Zion site, the AFT complex, consists of the T-shaped auxiliary building, the fuel-handling building, the turbine buildings, and the two diesel generator buildings. These structures are founded on a common base slab of varying elevation. Common floor slabs in the superstructure provide additional structural connections. We developed a finite-element model of the AFT complex, employing thin plate and shell elements to represent the concrete shear walls, and beam and truss elements to

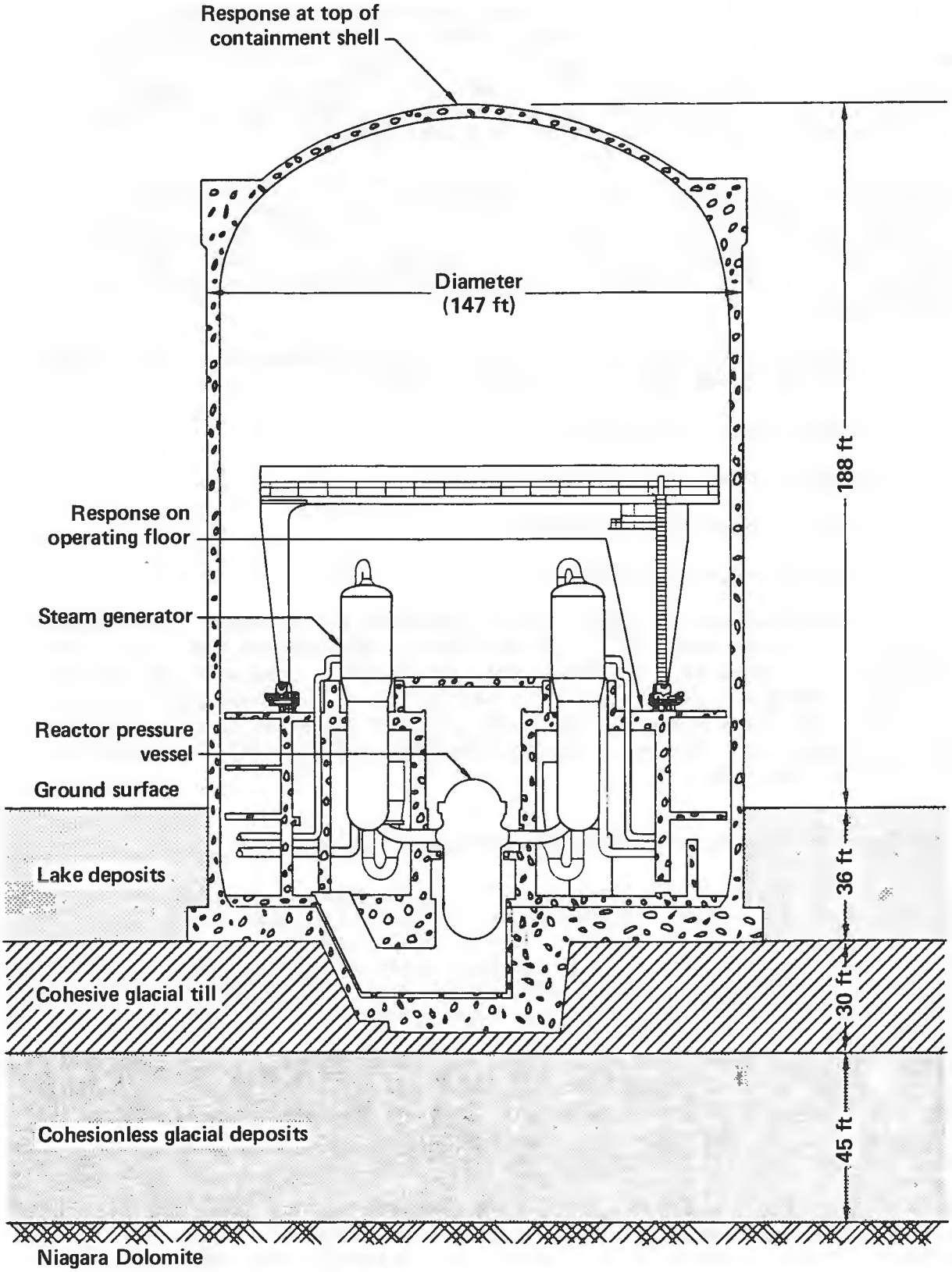

Fig. 4.2. Simplified elevation view of the containment shell and internal structure at Zion.

model the braced frames. Because of the symmetry of the structure, only half of the AFT complex was modeled. Masses were lumped at selected nodes, but the locations of the nodes were chosen so as to minimize the effects of this simplification on the responses in the auxiliary building and to suppress "local modes" in the turbine building. Figure 4.3 shows the AFT complex, including several points at which we computed responses.

The Zion Unit 1 systems of potential importance to risk, which were identified in conjunction with the systems analysis, include the auxiliary feedwater system, the safety injection system, the component-cooling water system, the containment spray system, the reactor coolant system, and the main steam and main feedwater system. Five systems were identified for detailed piping analysis:

1. Auxiliary Feedwater (AFW) System, including appropriate portions of the main steam and main feedwater lines.

2. Service-Water (SW) System.

3. Residual Heat Removal (RHR) System.

4. Safety Injection (SI) System.

5. Reactor Coolant (RC) System.

A total of 20 mathematical models were constructed and analyzed in the SMACS analysis; 13 were included in the SSMRP Phase I calculations and 7 were new models added in Phase II. The seven additional models consisted of portions of the main steam and auxiliary main steam lines. The AFW system was found to be the most important system in the SSMRP Phase I analysis; hence, a complete model was generated. The seven new mathematical piping models are shown in Figs. 4.4 through 4.10.

4.2.2 SSI, Structure, and Subsystem Models and Parameter Values

SMACS uses the substructure approach to solve for SSI and detailed structure response. The substructure approach divides the SSI problem into a series of simpler problems (typically three), solves each independently, and superposes the results. The three steps are: determination of the foundation input motion; determination of the foundation impedances; and analysis of the coupled soil-structure system. The first two steps are performed outside SMACS and serve as input data. The procedure is described in detail in Ref. 1. Of importance to the present discussion are the input quantities to SMACS: the frequency-dependent scattering matrices which, when multiplied by the Fourier transform of the free-field ground motion, yield foundation input motion; the impedance matrices which are also frequency-dependent; and the structures models, represented by their fixed-base eigensystem.

The scattering and impedance matrices are dependent on the characteristics of the soil deposit (configuration and material behavior) and the geometry and stiffness of the structure's foundation. The material model selected to represent the stress-strain behavior of the soil is based on linear visco-elastic theory. The parameters defining the model produce constant hysteretic-type damping and consist of two elastic constants (typically, shear modulus

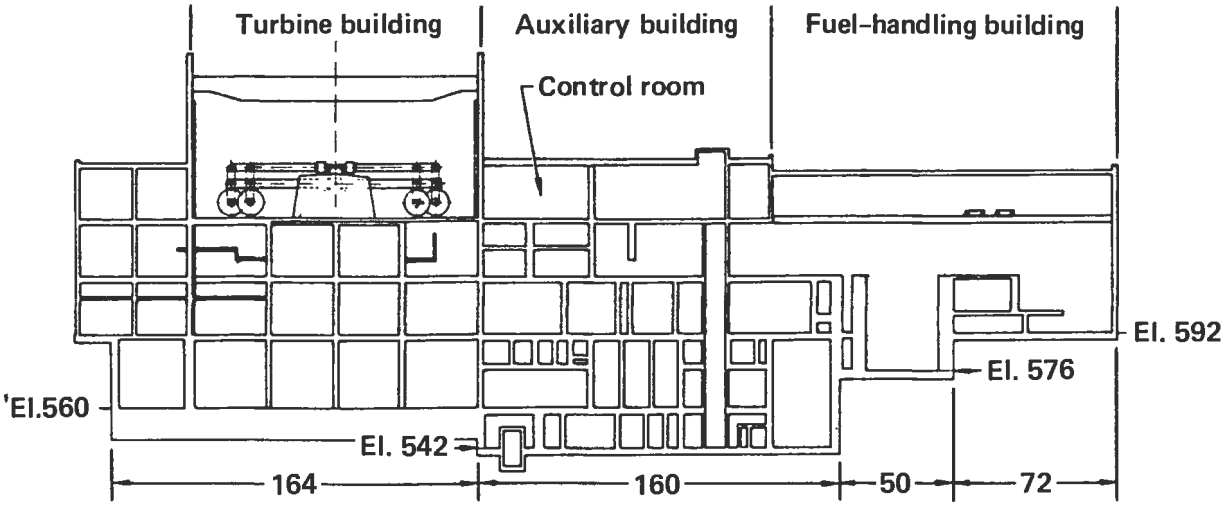

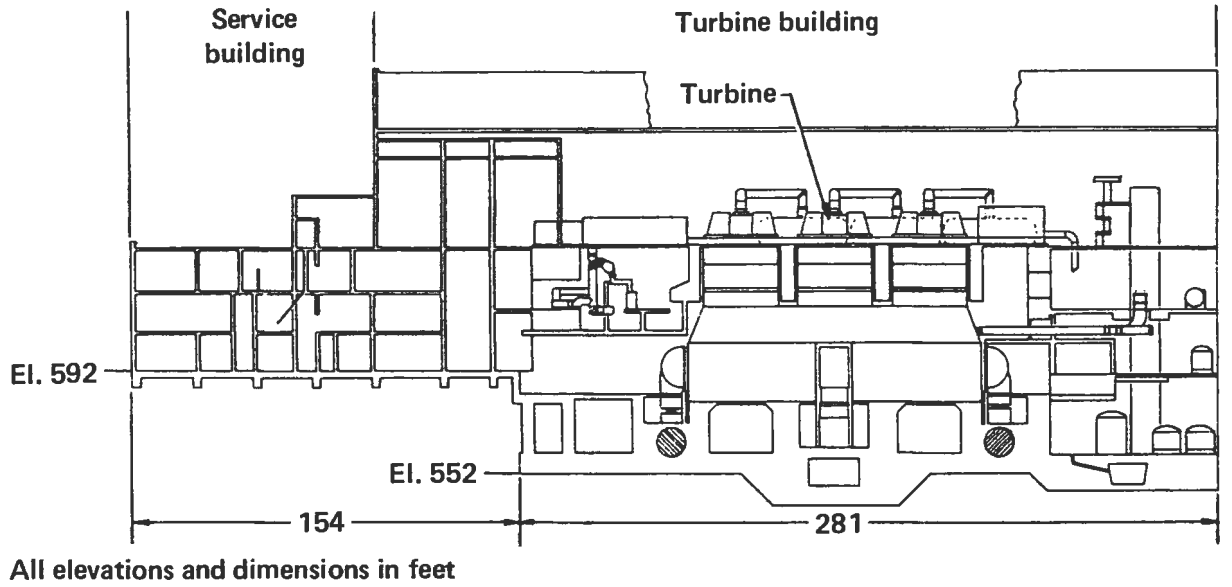

Fig. 4.3. Simplified elevation views of the AFT complex.

and Poisson's ratio) and a damping factor. The nonlinear behavior of soil was taken into account by equivalent linear techniques. Only the "primary nonlinearity," i.e., the nonlinear behavior induced in the free-field by the earthquake itself, is treated. The procedure used to generate equivalent linear soil properties is described in detail in Ref. 1, Vol. 4. The soil property study (Ref. 1) discretized the Zion site into 18 layers and an underlying half space. Preliminary calculations indicated that a discretization of three distinct layers and an underlying half space was adequate for the determination of the scattering matrices and impedances for SSI.

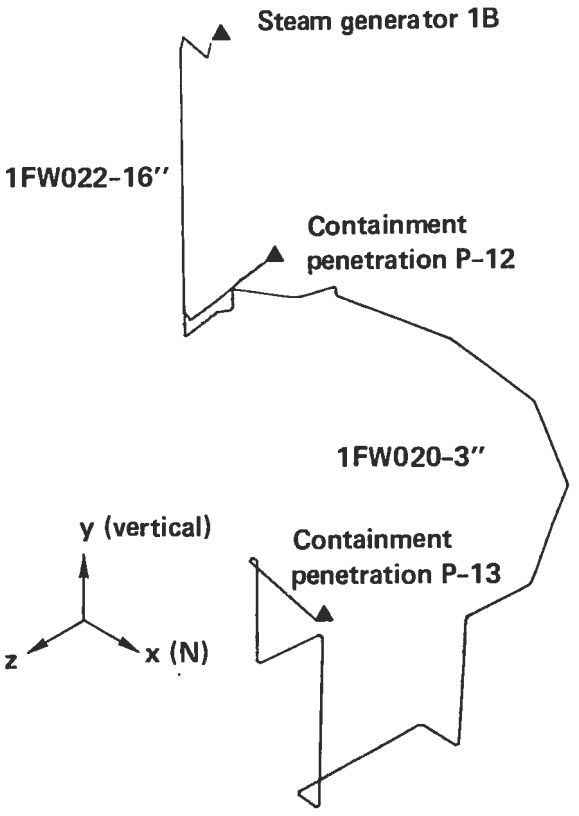

Fig. 4.4. Mathematical model of the auxiliary feedwater piping configuration--steam generator 1B to containment penetrations.

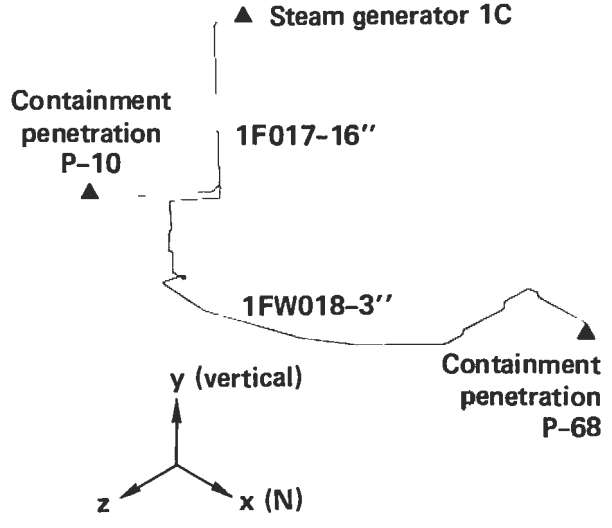

Fig. 4.5. Mathematical model of the auxiliary feedwater piping configuration--steam generator 1C to containment penetrations.

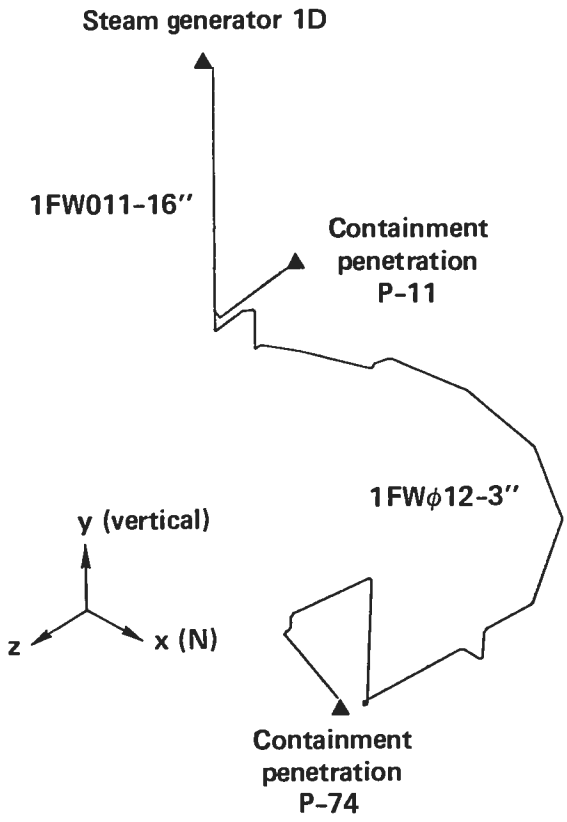

Fig. 4.6. Mathematical model of the auxiliary feedwater piping configuration--steam generator 1D to containment penetrations.

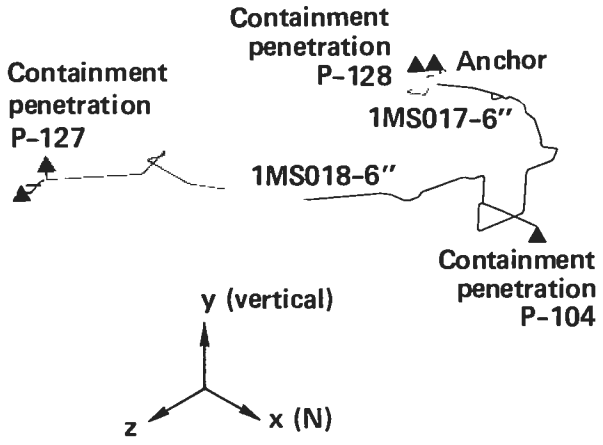

Fig. 4.7. Mathematical model of the auxiliary main steam piping configuration--inside containment.

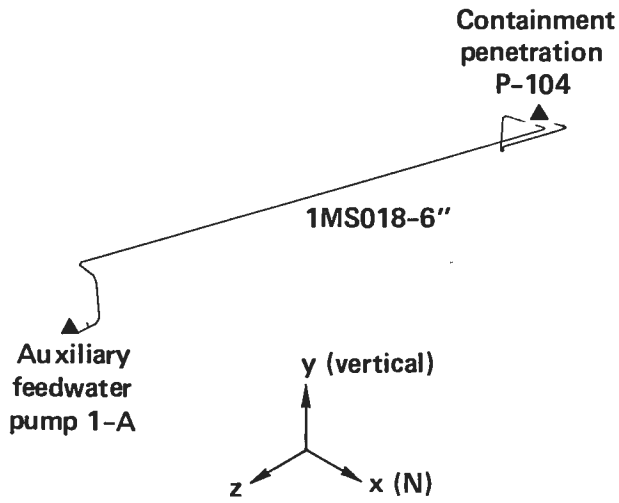

Fig. 4.8. Mathematical model of the auxiliary main steam piping configuration--outside containment.

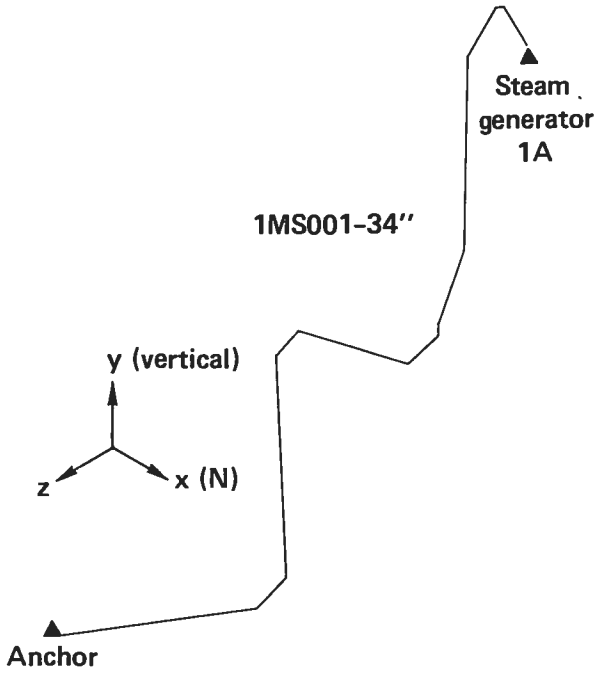

Fig. 4.9. Mathematical model of the main steam piping configuration--inside containment.

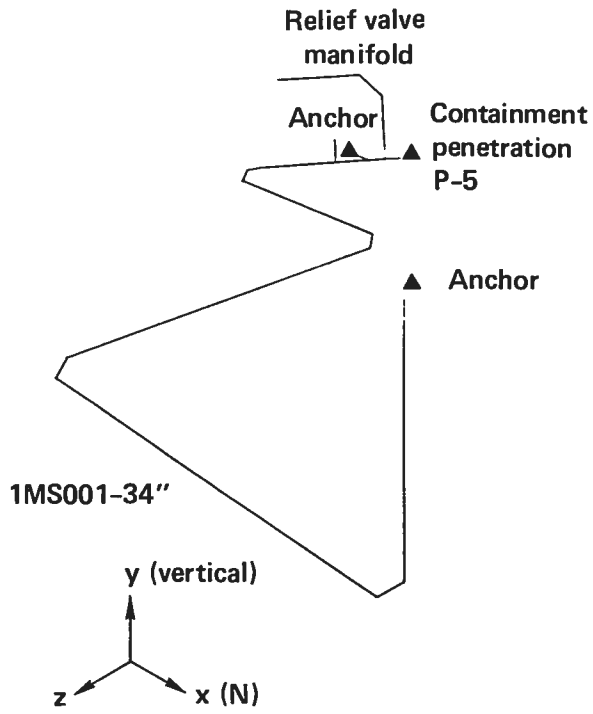

Fig. 4.10. Mathematical model of the main steam piping configuration--outside containment.

Two aspects of soil properties are important to our analysis: nominal equivalent linear values for each of the six acceleration ranges and variability in soil properties. Variability will be discussed later. Nominal soil properties for the six acceleration ranges will be discussed next.

We calculated impedances and scattering matrices for one set of material properties. These properties are shown in Table 4.1 (Ref. 41). Variations in soil properties from newly defined nominal values for each acceleration range and for specified variations within each range were achieved by the approximate scheme used in SMACS and described in detail in Ref. 1. The soil profile for these modifications is dictated by the values of shear modulus and material damping in layer 3. Table 4.2 itemizes values of these two constants for each of the six acceleration ranges.

Modeling the foundations of the containment building and the AFT complex is necessary to calculate the impedances and scattering matrices. Modeling the containment building foundation was straightforward--it was modeled by a circular cylindrical foundation, 157 ft in diameter, embedded 36 ft. Modeling the complicated geometry and embedment of the AFT complex was more difficult. Alternative models were investigated and reported in Ref. 1.

Table 4.1. Zion soil characteristics for calculated impedances and scattering matrices.

	Layer number			
	1	2	3	4
Thickness (ft)	6	30	75	∞
Density (lb/ft^3)	116	131	142	160
Poisson's ratio	0.39	0.39	0.46	0.27
Shear modulus (10^6 lb/ft^2)	1.46	3.46	8.57	423
Damping ratio	0.018	0.026	0.025	0.01

Table 4.2. Reference shear modulus and damping ratios for the six acceleration ranges. Layer 3 is the reference layer (see Table 4.1).

Range	Range of peak accelerations-rock outcrop (g) [median surface acceleration]	Shear modulus (10^6 lb/ft^2)	Shear-wave velocity (ft/s)	Damping ratio
1	0.06-0.10 [0.163]	8.70	1405	0.043
2	0.10-0.20 [0.258]	8.35	1376	0.049
3	0.20-0.32 [0.512]	7.54	1308	0.062
4	0.32-0.42 [0.722]	6.85	1246	0.072
5	0.42-0.53 [0.943]	6.51	1215	0.076
6	0.53-0.69 [1.135]	5.83	1149	0.084

Impedances for the AFT complex were generated for a flat surface foundation identical in shape to the AFT complex, resting on a soil layer of depth equal to the average soil depth under the real foundation. This representation maintains the general characteristics of the foundation's dynamic behavior--differing horizontal translation and rocking impedances in each direction and appropriate coupling terms. To account for embedment, we considered an equivalent cylindrical shape with dimensions obtained by matching the total volume and the area of the deepest portions of the foundation. Scattering matrices were generated for this equivalent cylinder and were used in our analysis. Several two-dimensional analyses were performed to gain insight into the effect of irregular foundation geometry on the scattering matrices. These studies aided the selection of equivalent dimensions. To correct the impedances for embedment, a correction term was obtained by comparing impedances for the equivalent cylinder with those for an assumed circular disk resting on the same soil layer as the AFT foundation. This comparison yielded minimal differences for most components; however, embedment had a significant effect on horizontal translations, due largely to radiation damping effects (Ref. 1).

The major differences between SSMRP Phase I and Phase II models was the inclusion of structure-to-structure interaction in Phase II models. In this case, three foundations were considered--two containment building foundations and the AFT complex. In modeling foundation-to-foundation interaction, the scattering matrices were assumed to be unaltered by the phenomenon. The impedances, however, were modified to include the effects of foundation-to-foundation interaction. In the present case, the impedance matrix was an 18 x 18 matrix (for each frequency), with 6 x 6 off-diagonal blocks representing the coupling terms between foundations. Calculation of the coupled impedances is described in detail in Ref. 1.

As discussed in Sec. 4.2.1, the Zion containment building and AFT complex were the subject structures of our analysis. Zion Units 1 and 2 containment buildings were represented by identical models. Structure models were based on actual material property data rather than design values. Typically, the actual median concrete strength is greater than the design strength, because a contractor creates a mix that has an average strength above the design strength to ensure that the design specification is met. Moreover, concrete becomes stronger with age. Both of these facts were taken into account in the estimates of material properties used in the structure models. The substructure approach uses the fixed-base modes to represent the dynamic characteristics of the structures. The eigensystems obtained from our structure models were assumed to represent the nominal frequency characteristics of the structures for the entire range of earthquakes considered.

Modal damping of the structures was selected to correspond to stress levels developed in the structures (Ref. 24). For excitation levels that produce stresses below approximately half the yield stress of both reinforced and prestressed concrete, a nominal value of structure damping of 3% of critical is expected. Somewhat less damping is expected for very low stress levels. For excitations producing stresses approximately equal to yield and above, damping equal to 10% of critical is expected for reinforced concrete. Depending on the amount of prestressing remaining at yield, damping equal to

7% to 10% of critical is expected for the prestressed concrete containment shell. Preliminary stress analyses of the Zion structures provided guidance as to the median stress levels expected in the SMACS calculations. The damping values of Table 4.3 were used as nominal values in the analysis.

Twenty piping system models were analyzed in detail with SMACS. Mathematical models were developed using state-of-the-art techniques, with the following assumptions:

- Piping systems were assumed to be linear elastic.
- Piping supports, rigid hangers, and snubbers were assumed to be rigid.
- Constant and variable spring hangers were not included, because their stiffness was small compared to the stiffness of other restraints.
- Pipe whip restraints were not included in the model because gaps between the restraints and the pipe were assumed to be large enough to accommodate the seismic movement.
- The effect of internal pressure on bend flexibility was included in the stiffness formulation of the elbow/pipe bend model.

The piping system models were developed for best-estimate assumptions and the resulting eigensystem was assumed to be the nominal case. Multi-support time history analysis as described in Ref. 1 was performed to calculate piping response. Two parameters were varied to incorporate uncertainty in piping systems--frequency and modal damping. The nominal value of modal damping for piping systems was selected to correspond to stress levels in the pipes. Table 4.3 lists nominal damping values for the piping system. Table 4.4 lists the piping models analyzed and some pertinent characteristics.

Table 4.3. Nominal modal damping ratios for SMACS calculations.

Range	Containment shell	Internal structure	AFT complex	Piping systems
1	0.020	0.020	0.020	0.020
2	0.030	0.022	0.036	0.024
3	0.040	0.024	0.052	0.028
4	0.050	0.026	0.068	0.032
5	0.060	0.028	0.084	0.036
6	0.070	0.030	0.100	0.040

Table 4.4. Piping system model characteristics.

	Fundamental frequency (Hz)	No. of modes considered	No. of support motions	No. of components calculated
Phase I:				
AFW SG-1A to containment penetrations P-9, P-69	2.9	36	45	24
AFW containment penetrations P-13, P-68, P-69, P-74 to AFW pumps (outside containment)	3.2	93	47	141
SW pumps discharge to SW strainers 1, 2	12.9	20	3	34
SW strainers 1 and 2 to Auxiliary Building	16.0	7	3	36
SW from SW013-48" to AFW pumps, heat exchangers and containment ventilation coolers	2.0	57	44	145
RHR pumps 1A and 1B suction to containment penetration P-124	4.3	32	33	58
RHR pumps 1A and 1B discharge to residual heat exchangers 1A and 1B	9.8	10	10	43
RHR and SI-1 refueling water storage to containment penetration P-22	3.9	18	21	24
RHR and SI-2 residual heat exchangers 1A and 1B to containment penetrations P-108, P-170	2.7	115	49	190
Charging pumps discharge to boron injection tank #1	3.2	87	35	125
Boron injection tank #1 to containment penetration P-4	9.1	8	19	17
RCL and branch lines	1.4	130	127	135
Pressurizer to pressurizer relief tank	3.5	34	28	33
TOTAL				1005

Table 4.4. (continued)

	Fundamental frequency (Hz)	No. of modes considered	No. of support motions	No. of components calculated
Phase II:				
MS SG-1A to containment penetration P-5	9.7	9	21	8
MS containment penetration P-5 to safety valve manifold, auxiliary main steam line	5.0	12	24	14
MS lines of steam generators 1A and 1D to containment penetration P-104	2.9	50	58	56
MS containment penetration P-104 to AFW pump 1A	5.4	23	32	14
AFW SG-1B to containment penetrations P-12, P-13	3.5	50	57	28
AFW SG-1C to containment penetrations P-10, P-68	2.2	35	51	29
AFW SG-1D to containment penetrations P-11, P-74	2.1	46	51	28
TOTAL				177

4.3 Variation of Input Parameters

As described in previous sections, SMACS performs repeated deterministic analyses, each analysis simulating an earthquake occurrence. By performing many such analyses and by varying the input parameters, we take account of the uncertainty inherent in any deterministic analysis. A limited number of input parameters is used to represent uncertainty in each element of the seismic methodology chain--ensemble of free-field acceleration time histories for seismic input, soil shear modulus and material damping for SSI, frequencies and modal damping for structure and subsystems. Parameter values for each simulation were sampled from assumed probability distributions according to a Latin hypercube sampling procedure.

Section 2 introduced the concept of random and modeling uncertainty. Random uncertainty is fundamental to the phenomenon being represented and is irreducible given present state-of-the-art understanding and modeling of the phenomenon. Modeling uncertainty can be reduced within present limits of the

state of the art by improved analytical models, tests, etc. To perform the required analyses, variations in our input parameters were separated into random and modeling components. The combination of the two is denoted total uncertainty.

Table 4.5 tabulates the separation of total uncertainty into random and modeling components for the input parameters to SMACS. The values representing total uncertainty are identical to those of SSMRP Phase I. Lognormal distributions were assumed for the input parameters. Coefficients of variation are shown in Table 4.5. The variations in Table 4.5 apply to each of the six acceleration ranges of the discretized seismic hazard curve. The nominal values of the input parameters were varied according to excitation level (Sec. 4.2). The separation of random and modeling uncertainty was accomplished by examining in detail uncertainty attributed to random sources. A two-fold approach was taken:

- Examine recorded data of the input parameters themselves (soil shear modulus and damping, structure and subsystem frequency and damping) and assign COVs accounting for the range of excitations and the phenomenon represented by the parameter. An example is soil shear modulus. Reference 25 recommends a range of COV values of 0.5-1.0 for soil "stress-strain behavior." Reference 26 contains a series of data recorded for a variety of sites and soil conditions with COVs in the range of 0.5 and above. The former estimate undoubtedly contains random and modeling uncertainty, whereas modeling uncertainty in the latter estimate should be less. A COV of 0.4 for soil shear modulus was used in the analysis to represent random uncertainty. Similar estimates were made for the remaining input parameters.

- Perform preliminary response calculations for the selected variations and compare the calculated response distributions with recorded data. One of the only sources of recorded response data for multiple earthquakes on a structure and on equipment and piping supported on the structure is a report by Shibata (Ref. 27) for the Chiba Field Station. Table 4.6 tabulates results taken from Ref. 27. Note that these data are normalized--horizontal response is normalized by peak ground acceleration in the horizontal direction and vertical response is normalized by peak ground acceleration in the vertical direction. The range of COVs for response is approximately 0.3 to 0.7. These values can be interpreted as due to random sources of uncertainty in the seismic input, SSI, structure, and subsystem characteristics. Section 4.4 displays results from our SMACS analyses, which show comparable variability for the random-only case.

4.4 Numerical Results

4.4.1 Typical responses

The results of the SMACS calculations and selected post-processors of the data are displayed here in a form consistent with systems analysis requirements, i.e., scalar quantities such as in-structure accelerations (peak and spectral) and subsystem accelerations and moments, as required by fragility characterizations. The results presented here are for 30 earthquake

Table 4.5. Uncertainty in the normalized input parameters. Values of the coefficients of variation (COV) are given.

Parameter	Total uncertainty COV	Random uncertainty COV	Modeling uncertainty COV
Soil shear modulus	0.7	0.4	0.57
Soil damping	1.0	0.5	0.866
Structure frequency	0.5	0.25	0.43
Structure damping	0.7	0.35	0.606
Subsystem frequency	0.5	0.25	0.43
Subsystem damping	0.7	0.35	0.606

Table 4.6. Summary of Shibata's data (Ref. 27) on coefficient of variation of normalized response structure/piping/equipment at the Chiba Field Station due to natural earthquakes. North-south data were normalized by peak acceleration in north-south direction. Vertical data were normalized by vertical peak ground acceleration.

Location	Number of earthquakes	Coefficent of variation
North-south:		
Hung tank[a]	77	0.492 (0.262)[b]
Piping[a]	57	0.345
Saddle tank[a]	58	0.538
Self-standing tank[a]	58	0.248
Frame structure[c]	21	0.30
Horizontal tank[c]	21	0.33
Vertical:		
Foundation[d]	12	0.136
Hung tank[d]	16	0.39
Piping[d]	17	0.35
Horizontal tank[d]	9	0.70
Frame structure[e]	15	0.45

[a] From Table 3(a) of Ref. 27.
[b] Abnormal data omitted.
[c] Estimated from Fig. 6 of Ref. 27.
[d] From Table 3(b) of Ref. 27.
[e] Estimated from Fig. 7 of Ref. 27.

simulations and the majority are for random uncertainty only. Selected comparisons of responses calculated with only random uncertainty vs responses calculated with total uncertainty (random plus modeling) are presented.

The dynamic responses calculated by SMACS constitute one of the inputs to the systems analysis program SEISIM (Sec. 6). The other inputs are the seismic hazard curve (Sec. 3), the event and fault trees (Sec. 6), and the fragility descriptions of the structures and subsystems (Sec. 5). The response quantities (accelerations or moments) and the locations at which responses were computed were selected according to the requirements of the fragility descriptions and the fault trees. The fragilities of the structures and floor-mounted equipment were expressed in terms of free-field or structural accelerations. The fragilities of valves mounted on piping systems were tied to subsystem accelerations. The fragilities of the pipes themselves were characterized by peak resultant moments over the duration of the earthquake. The dynamic responses calculated by SMACS explicitly contain the three aspects of seismic response necessary for seismic risk analysis--medians, variability, and correlation.

Selected results are presented here for acceleration range 2 (Sec. 3) with peak accelerations on the rock outcrop of 0.10-0.20 g. Figures 4.11-4.15 illustrate results typical of the SMACS calculations: Fig. 4.11 shows free-field acceleration on the rock outcrop, Fig. 4.12 shows free-field acceleration on the soil free surface, Fig. 4.13 shows foundation response, Fig. 4.14 shows structure responses, and Fig. 4.15 shows selected subsystem responses. Each plot shows 30 responses, corresponding to the 30 earthquake simulations, plotted as a cumulative distribution histogram. Each simulation assumed different values of the input parameters, selected according to the Latin hypercube sampling procedure outlined in Sec. 4.3. Hence, variability in responses is a result of variations in all elements of the seismic methodology

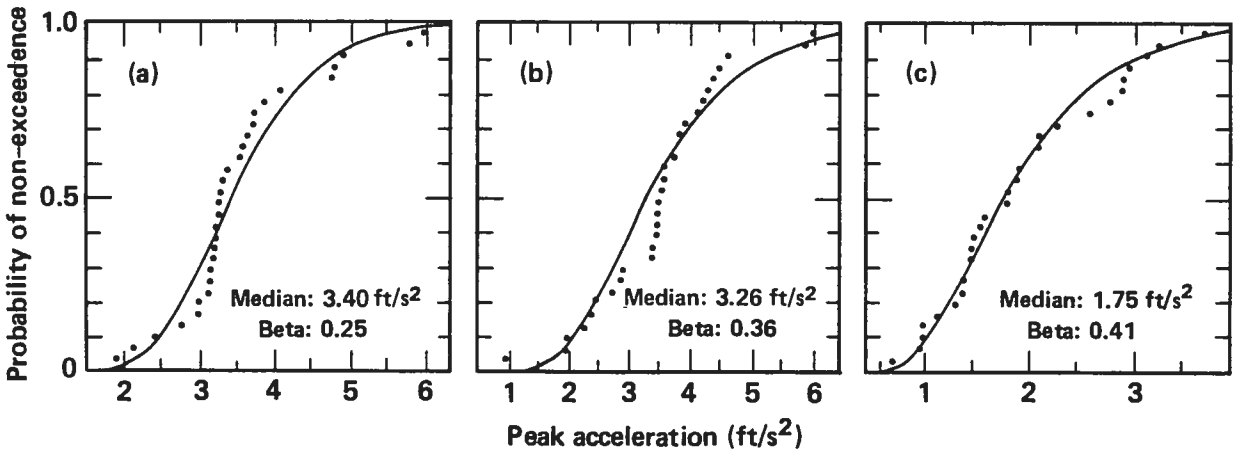

Fig. 4.11. Cumulative distributions of free-field peak accelerations on the rock outcrop. (a) X direction (west), (b) Y direction (south), (c) Z direction (vertical).

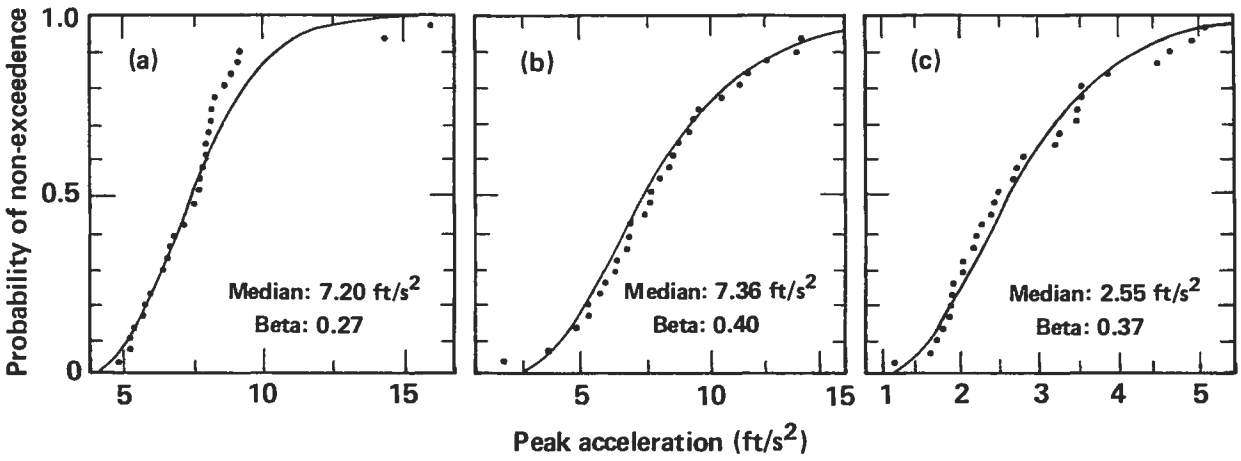

Fig. 4.12. Cumulative distributions of computed free-field peak accelerations. (a) X direction (west), (b) Y direction (south), (c) Z direction (vertical).

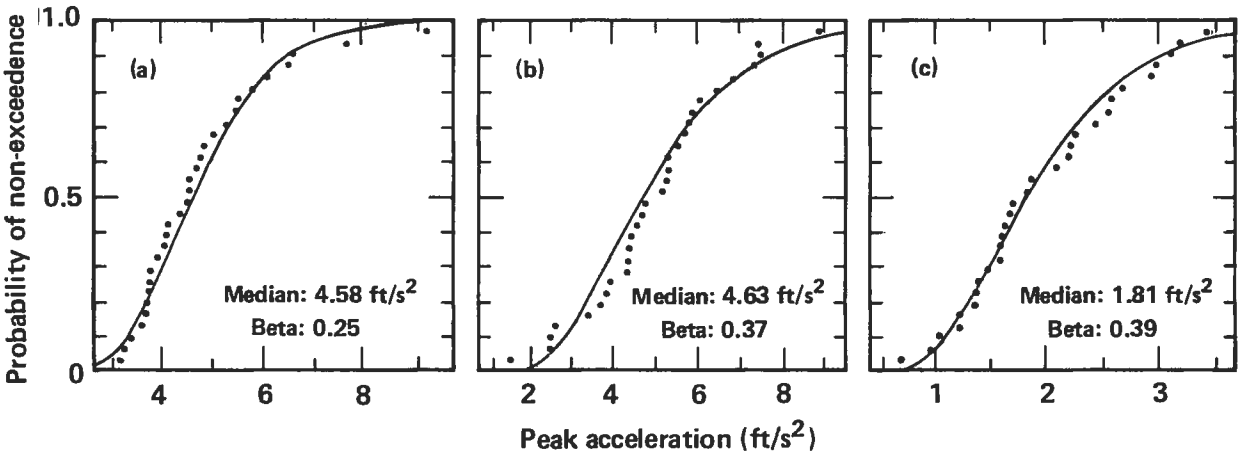

Fig. 4.13. Cumulative distributions of reactor building foundation responses. (a) X direction (west), (b) Y direction (south), (c) Z direction (vertical).

chain. The systems analysis assumes lognormal distributions; therefore, the calculated responses were fit by lognormal distributions shown in Figs. 4.11-4.15 as cumulative distribution functions (the solid lines). We denote the standard deviation of the logarithms of response (the measure of uncertainty in the result) as beta (ß). The median response and calculated ß value of the fitted lognormal distribution are shown on each of Figs. 4.11 through 4.15

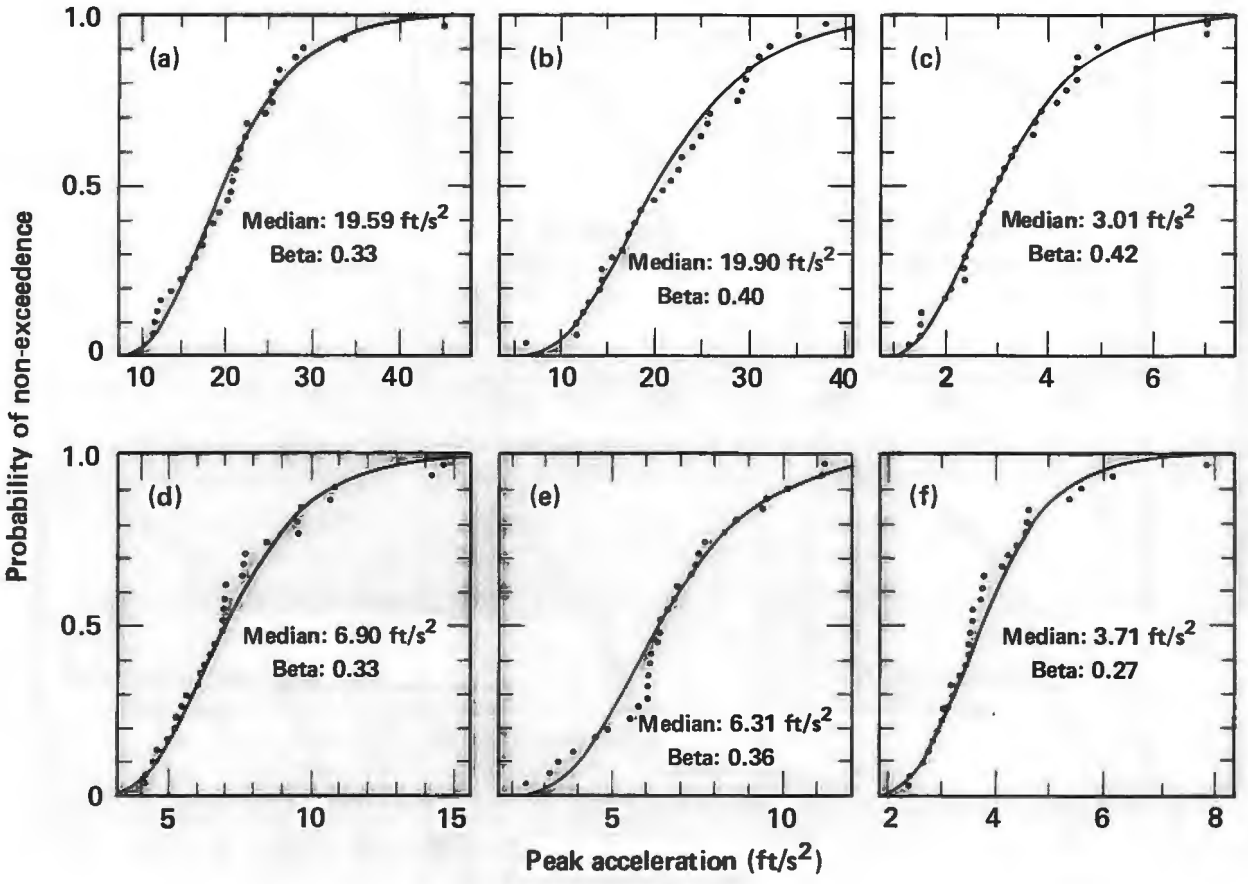

Fig. 4.14. Cumulative distribution of computed peak structural accelerations.
(a,b,c) X, Y, Z components for the top of containment shell.
(d,e,f) X, Y, Z components for the internal structure.
Note: the X direction is west, Y is south, and Z is vertical.

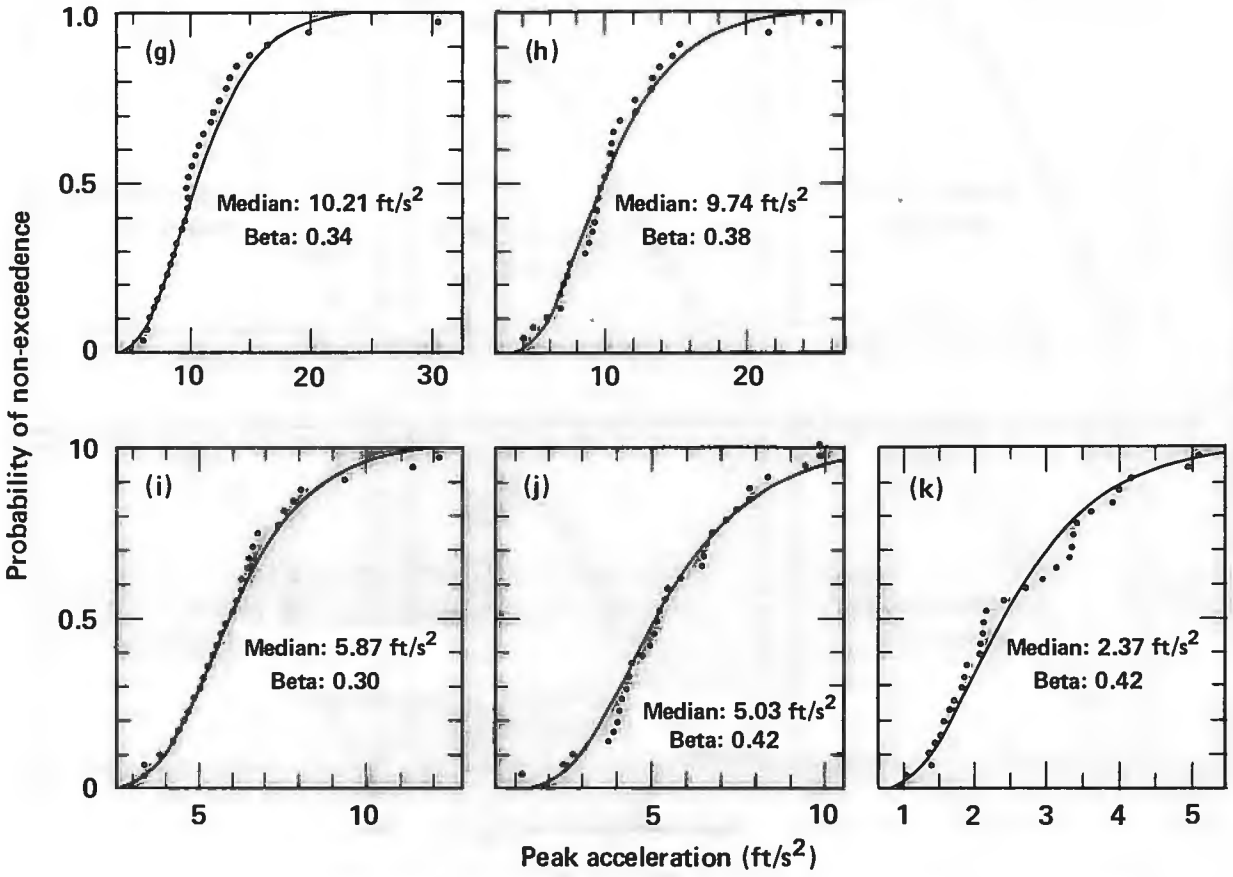

Fig. 4.14 Cumulative distribution of computed peak structural accelerations.
(g,h) X, Y components for the steam generator.
(i,j,k) X, Y, Z components for a point near the control room in the AFT complex.
Note: the X direction is west, Y is south, and Z is vertical.

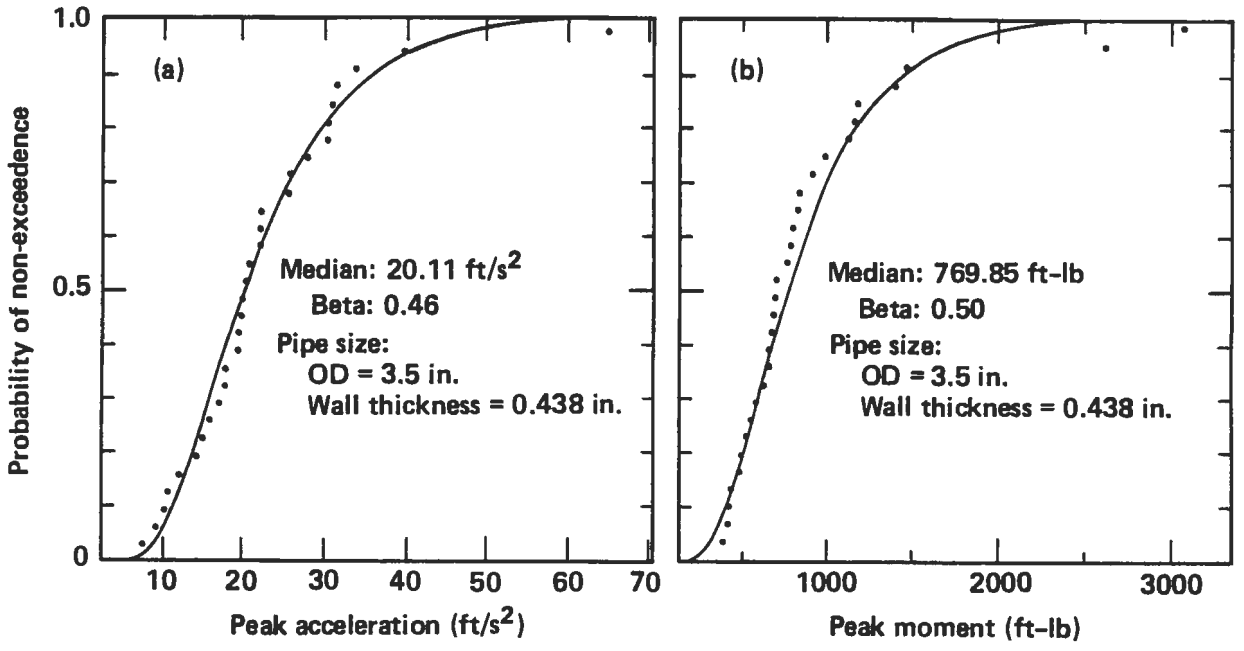

Fig. 4.15. Cumulative distribution for peak resultant responses for:
(a) auxiliary feedwater system, inside containment--check valve.
(b) auxiliary feedwater systems, inside containment--nozzle.

Figure 4.11 shows the three components of peak free-field acceleration on the rock outcrop (two horizontal and the vertical). The x and y directions are horizontal (x is west, y is south) and the z direction corresponds to the vertical. The median peak accelerations for the three directions are 0.11, 0.10, and 0.05 g (vertical). Note that the seimsic hazard curve (Chapter 3) is a function of peak horizontal acceleration, which for a specific earthquake is randomly aligned in the x or y direction. The median peak horizontal acceleration is 0.115 g, which reflects the probability distribution of earthquakes falling in the range of 0.10-0.20 g (Chapter 3). The ß values for peak acceleration are 0.25, 0.36, and 0.41 for the x, y, and z directions, respectively. As we have mentioned before, earthquakes were categorized according to peak horizontal acceleration. Hence, the peak horizontal component on the rock outcrop will fall within the specified acceleration range. A truncated distribution would be appropriate. However, systems analysis (SEISIM) requires the assumption of a lognormal distribution, which is a reasonable approximation to the appropriately truncated distribution.

Figure 4.12 shows peak free-field accelerations in three directions on the free surface of the soil resulting from wave propagation through the soil column (Chapter 3). Variability in peak acceleration is due to variability in the input motions defined on the rock outcrop and in the soil properties (shear modulus and material damping). The median peak surface accelerations are higher than the corresponding values on the rock outcrop due to amplification through the soil column (7.20 vs 3.40, 7.36 vs 3.26, and 2.55 vs 1.75). Variability in these peak values (measured by ß) increases slightly for horizontal motions (0.27 vs 0.25 and 0.40 vs 0.36) and decreases slightly

for vertical motions (0.37 vs 0.41). Hence, introduction of soil property variation did not significantly alter the variability in peak acceleration.

Response spectra and their statistics provide additional insight into the variability of free-field and in-structure response. Figure 4.16 shows the response spectra for the free-field motion. All three directions are shown. (Note, response spectra and their statistics presented herein are shown in normal distribution form for display purposes.) Figures 4.16a, b, and c show response spectra of the free-field motion on the rock outcrop for the x, y, and z directions respectively. Figures 4.16d, e, and f show the corresponding response spectra on the free surface of the soil. The first observation concerns the overall amplification of the motion from the rock outcrop to the free soil surface. Amplification factors are between 2 and 2.5 for horizontal motions in the high frequency range, and somewhat less for vertical motions. In the low frequency range (1 to 10 Hz), amplification factors are 3 to 4 on spectral acceleration for horizontal motions, and again, somewhat less for vertical motions. The effects of local site amplification are discussed in more detail in Chapter 3. A second observation pertains to variability of the response spectra. Further evaluation of the data yields coefficients of variation (COVs) of 0.25 to 0.40 for spectral accelerations over the frequency range of interest (greater than 1 Hz) in the x and y directions on the rock outcrop, and higher values in the y direction. Corresponding COVs for the vertical directions were 0.40 to 0.46. The COVs for spectral accelerations on

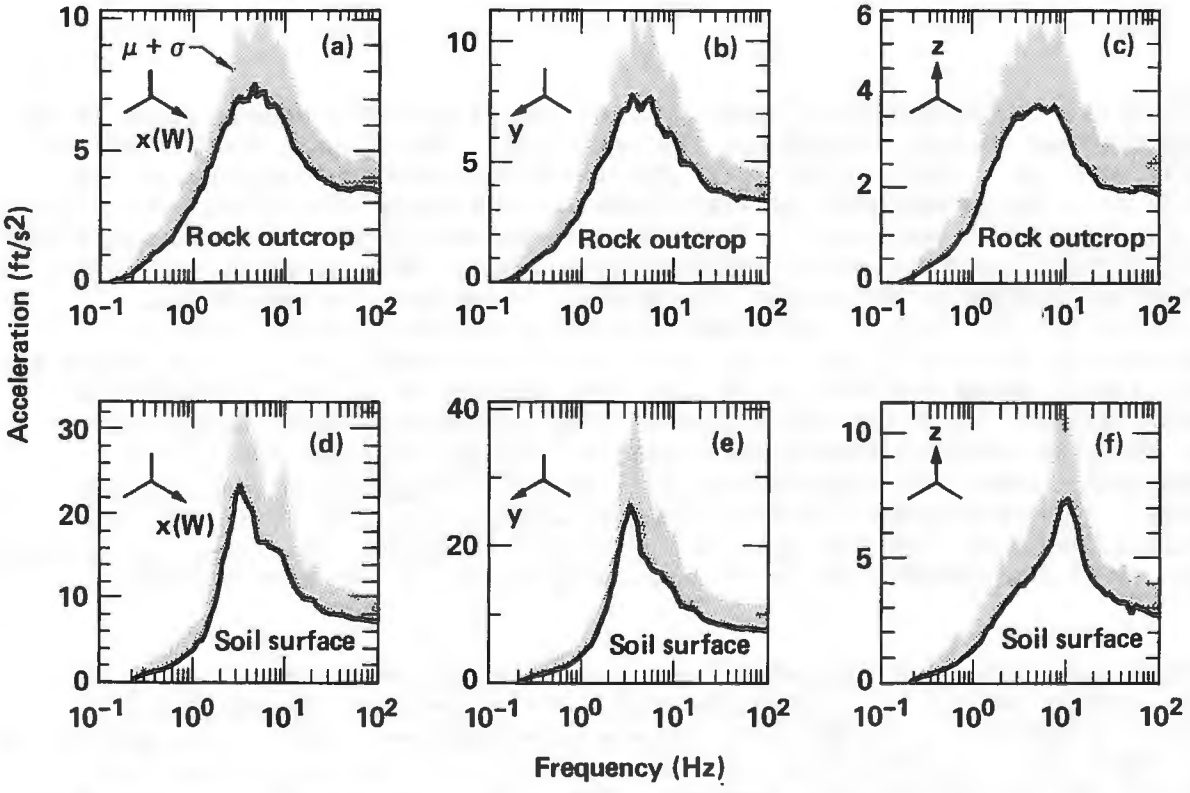

Fig. 4.16. Response spectra of the free-field motion with 5% damping: (a) X direction (west), (b) Y direction (south), (c) Z direction (vertical). The solid line is the mean of 30 spectral ratios, and the shading marks the variation in the mean (+1 standard deviation).

the free soil surface range from: 0.30 to 0.67 for the x direction; 0.35 to 0.58 for the y direction; and 0.33 to 0.60 for the z direction. The general trend is an increase in variability in the frequency range of 1 to 10 Hz for horizontal response over that on the rock outcrop. For the vertical direction, a slight increase in variability of spectral acceleration at selected frequencies in the range of 1 to 10 Hz is observed. Variability in the rock outcrop motion reflects uncertainty in the seismic input, whereas variability in the motion on the surface of the soil reflects uncertainty in the seismic input and the soil properties.

Figure 4.13 shows the peak acceleration of the reactor building foundation in the three directions. The median responses are lower than the corresponding values in the free field on the soil surface (4.58 vs 7.20, 4.63 vs 7.36, and 1.81 vs 2.55). Variability in these peak accelerations (measured by ß) is approximately the same as in the free field on the soil surface (0.25 vs 0.27, 0.37 vs 0.40, and 0.39 vs 0.37). Figure 4.17 shows response spectra on the foundation. Comparing Figs. 4.17a, b, and c with Figs. 4.16d, e, and f, respectively, shows an overall reduction in response on the foundation from the motion in the free field. Note also, however, that the general shape of the response spectra on the foundation and on the soil free surface is the same. COVs for spectral accelerations on the foundation are approximately equal to corresponding values in the free field. This is somewhat surprising, since foundation response is a function of the soil and structure characteristics. Hence, the variability in foundation response is due to variability in the parameters describing soil and structures, as well as to variability in the free-field motion.

Next, let us examine in-structure response. Figures 4.14a, b, and c show peak accelerations in three directions at the top of the containment shell, 210 ft above the basemat. The containment shell is a flexible structure with a fundamental fixed-base frequency of 4.1 Hz. The foundation response (translations and rotations) is amplified through the structure, as shown by the increase in median response (19.59 vs 4.58, 19.90 vs 4.63, and 3.01 vs

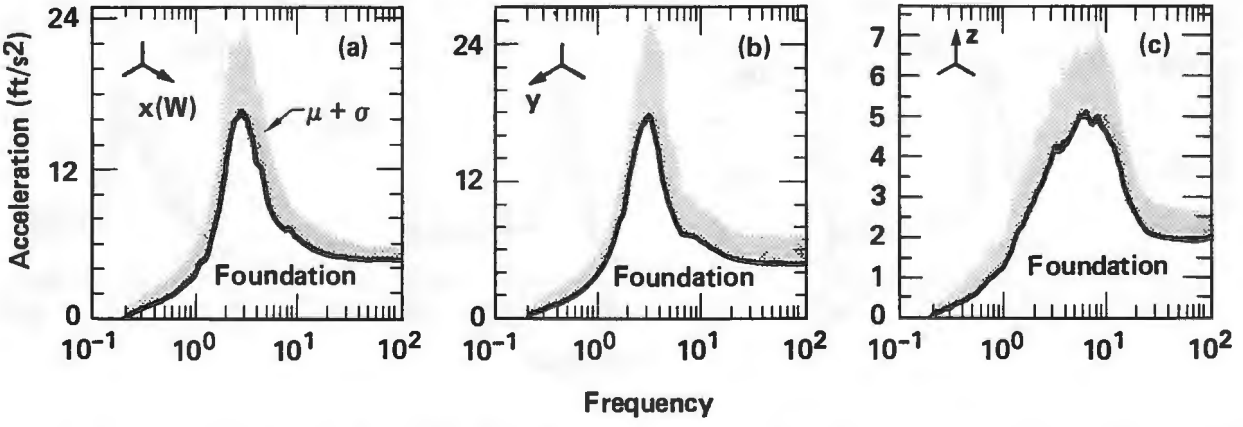

Fig. 4.17. Response spectra of reactor building foundation motion with 5% damping: (a) X direction (west), (b) Y direction (south), (c) Z direction (vertical). The solid line is the mean of 30 spectral ratios, and the shading marks the variation in the mean (+1 standard deviation).

1.81). Figure 4.18 shows response spectra at the top of the containment shell. Amplification of spectral accelerations in the 2-3 Hz frequency range for horizontal motions is apparent. This frequency range corresponds to horizontal frequencies of the coupled soil-structure system. Less amplification is seen in the vertical directions (Fig. 4.18c); the character of the motion on the foundation is propagated to the top of the containment shell. Variability in peak acceleration increases somewhat for horizontal motions (0.33 vs 0.25 and 0.42 vs 0.37) and decreases slightly for vertical motion (0.33 vs 0.39). An inspection of the response spectra and their statistics shows increases in COVs of spectral accelerations of approximately 15% from foundation to the top of the containment shell.

Results at three additional points within the Zion structures are presented here: at the top of the internal structure (Figs. 4.14d, e, and f and Figs. 4.19a, b, and c); at the steam generator support (Figs. 4.14g, and h and Figs. 4.19d and e); and at a point near the control room in the AFT complex (Figs. 4.14i, j, and k and Figs. 4.20a, b, and c). The general trend is an amplification of the input motions, as expected, and an increase in variability. COVs of peak acceleration range from 0.30 to 0.42 for horizontal motion and from 0.27 to 0.42 for vertical motion. COVs of spectral acceleration in the amplified frequency range (1-10 Hz) were irregular, with maxima higher than the COVs of peak accelerations; COVs ranged from 0.30 to 0.90 in the frequency range of 1-10 Hz. In all cases, the maximum COVs occur in narrow frequency bands. This result is obtained because extreme response values are computed in some simulations. Spectral accelerations are important because fragility descriptions of components supported near the structure response locations are based on spectral accelerations.

Finally, Fig. 4.15 shows acceleration and moment response in a typical subsystem (AFW) for the six ranges of earthquake acceleration.

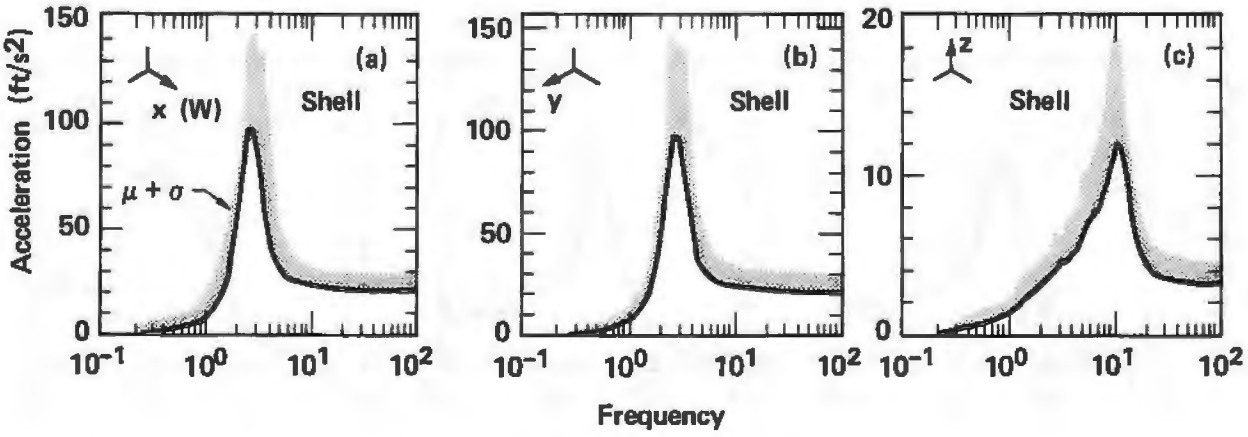

Fig. 4.18. Response spectra of the top of containment shell motion. (a) X direction (west), (b) Y direction (south), (c) Z direction (vertical). The solid line is the mean of 30 spectral ratios, and the shading marks the variation in the mean (+1 standard deviation).

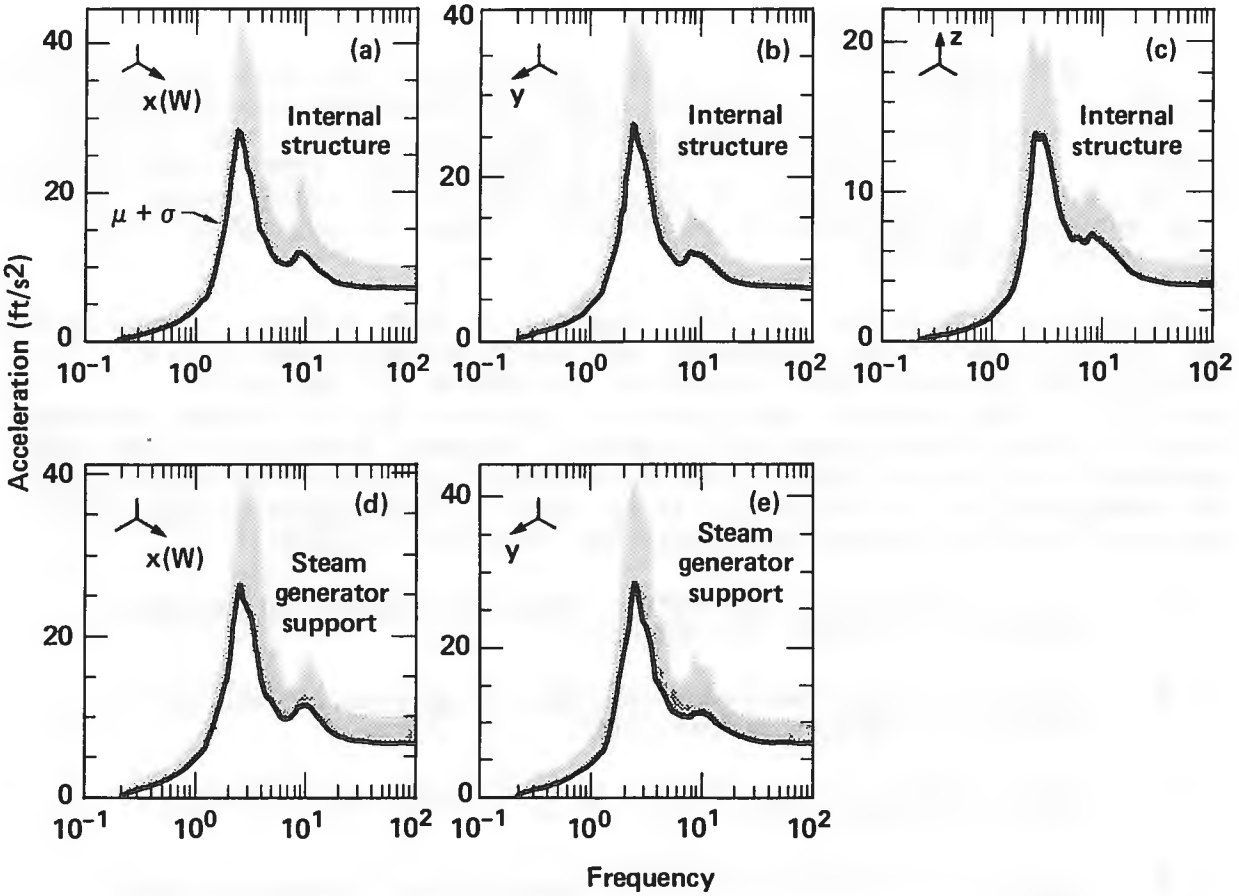

Fig. 4.19. Response spectra at the top of the internal structure [(a) X direction (west), (b) Y direction (south), (c) Z direction (vertical)] and the steam generator support [(d) X direction, (e) Y direction]. The solid line is the mean of 30 spectral ratios, and the shading marks the variation in the mean (+1 standard deviation).

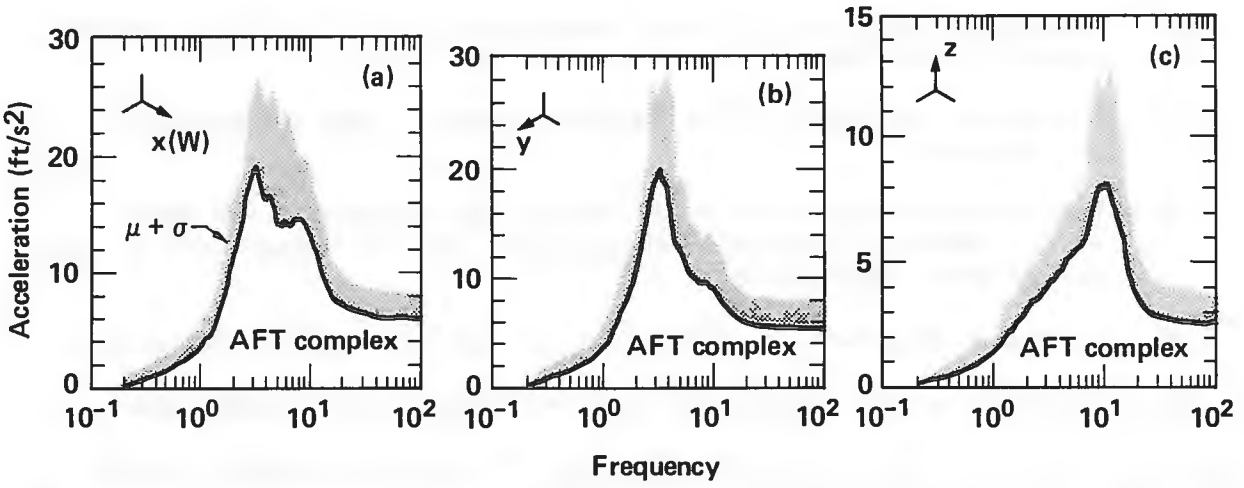

Fig. 4.20. Response spectra at a point near the control room in the AFT complex. (a) X direction (west), (b) Y direction (south), (c) Z direction (vertical). The solid line is the mean of 30 spectral ratios, and the shading marks the variation in the mean (+1 standard deviation).

4.4.2 Summary of Results

Results presented in Sec. 4.4.1 are typical of the responses calculated by SMACS. In the SSMRP Phase II analyses, 1337 such responses were calculated, 155 in the free-field and structures, 1182 in the subsystems. Further, many additional responses, not tied to fragility descriptions, were calculated for the structures as needed input to the subsystem response calculations. Where responses were used as subsystem inputs, time histories, not simply peak values, were calculated.

It is convenient to examine the 1337 responses in summary form. Figures 4.21 and 4.22 show statistical information for the free-field input and for numerous response locations--foundation, structures, and 20 piping subsystems. The horizontal axis assigns a "response number" to each computed response. These "response points" represent different locations, directional components, or spectral frequencies, as selected for use in systems analysis. The response points are identified in Appendix F. The response points were separated into five groups. The groups are, from left to right:

- Free-field surface accelerations--peak or spectral acceleration components (Response number 1-12).
- Basemat of containment building--peak or spectral acceleration components (Response number 33-44).
- Major structure nodes--peak or spectral acceleration components (Response number 65-195).
- Subsystem nodes--peak resultant accelerations (Response number 216-363).
- Subsystem elements--peak resultant moments (Response number 384-1417).

In addition, within each group, the response points are sorted into progressively finer subsets, as follows:

- Free-field acceleration: by direction--x, y, or z--and by peak or spectral acceleration.
- Foundation acceleration: by direction and by peak or spectral acceleration.
- Structure acceleration: by direction, by structure (containment shell, internal structure, AFT complex), by node number, and by peak or spectral acceleration.
- Subsystem resultant acceleration: by subsystem and by node number.
- Subsystem resultant moment: by subsystem and by element number.

Figure 4.21 shows ß values for the six ranges of peak acceleration for the base case, i.e., random variability only. Several general observations can be made:

- Response statistics vary considerably from category to category and point to point. A detailed evaluation of the data shows on the

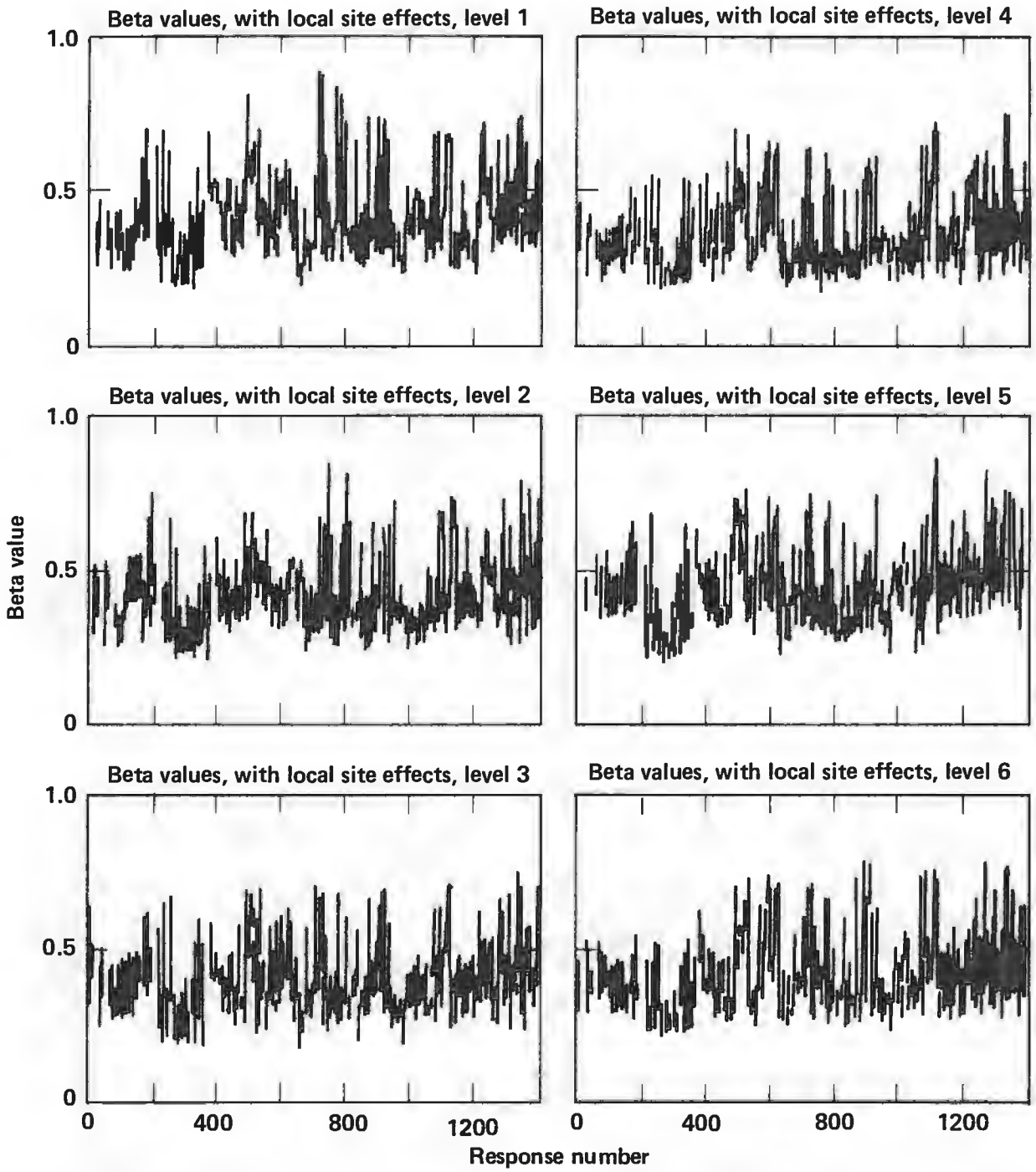

Fig. 4.21. ß values for six levels of peak acceleration--random variability only.

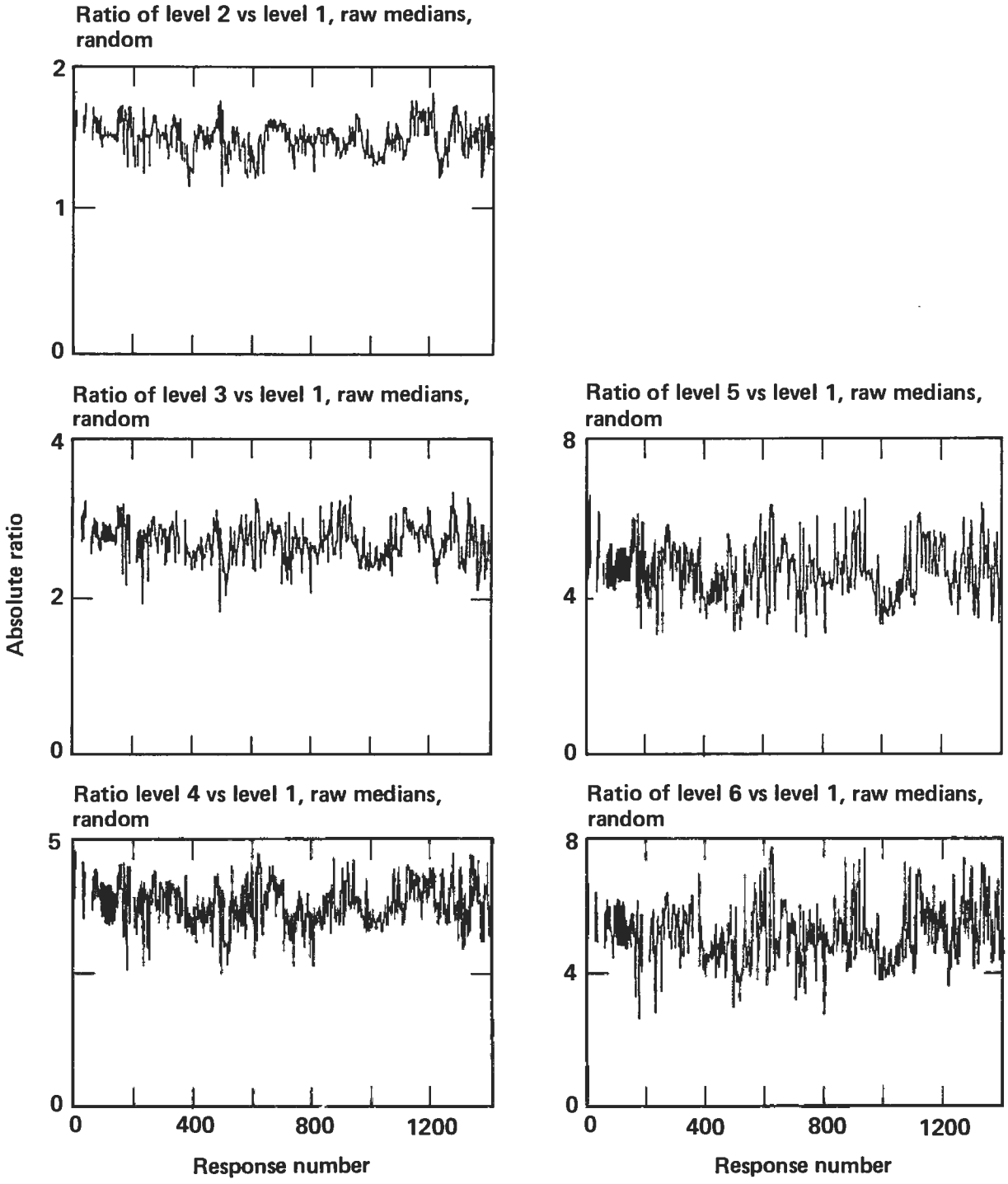

Fig. 4.22. Variations in medians of response for acceleration levels 2 to 6 relative to acceleration level 1.

average a relatively constant ß value as one moves through free-field, foundation, structure response, subsystem accelerations, and subsystems moments. Beta values, averaged over the six ranges of acceleration for the above categories are as follows:

x direction: 0.36, 0.35, 0.36, 0.31, and 0.42

y direction: 0.39, 0.36, 0.38, 0.31, and 0.42

z direction: 0.46, 0.42, 0.41, 0.31, and 0.42.

Note that the last two entries in each comparison are for a resultant over 3 directions, computed by vector sum. It is perhaps for this reason that the average ß values for subsystem accelerations (0.31) is smaller. Although these average values do not vary significantly from category to category, the scatter within a category of the ß value of the response increases significantly as one progresses from the free-field through the structure and subsystem response.

- ß values follow a consistent pattern and do not change significantly for differing excitation levels. This is due, in large measure, to the assumed variability in input parameters (soil shear modulus, damping, etc.) being identical for each acceleration range. This result is significant for simplification of the SSMRP process; an estimate of ß for one acceleration range may be used in other ranges.

Figure 4.22 shows the variations in the medians of response for acceleration ranges 2 to 6 relative to acceleration range 1. A correlation between increased excitation level and increased response is obvious, although the response variability is not linear with peak free-field acceleration.

4.4.3 Random vs Total Uncertainty

Figures 4.23 and 4.24 compare median response values and ß values for the base case (random uncertainty only) vs the case of total uncertainty, for acceleration ranges 2 and 5. The comparison of medians shows a slight decrease (10%) for all response categories, except subsystem moments, which show a slight increase (<6%). The comparison of ß values is more dramatic, as expected. Ratios of beta values averaged over the two ranges of acceleration for the categories free-field, foundation, structure response, subsystem accelerations, and subsystem moments are:

1.23--1.28--1.31--1.49--1.48 for the x-direction,

1.23--1.24--1.24--1.49--1.48 for the y-direction, and

1.04--1.09--1.09--1.49--1.48 for the z-direction.

Note that the greatest variability in beta values occurs for the subsystem accelerations and moments.

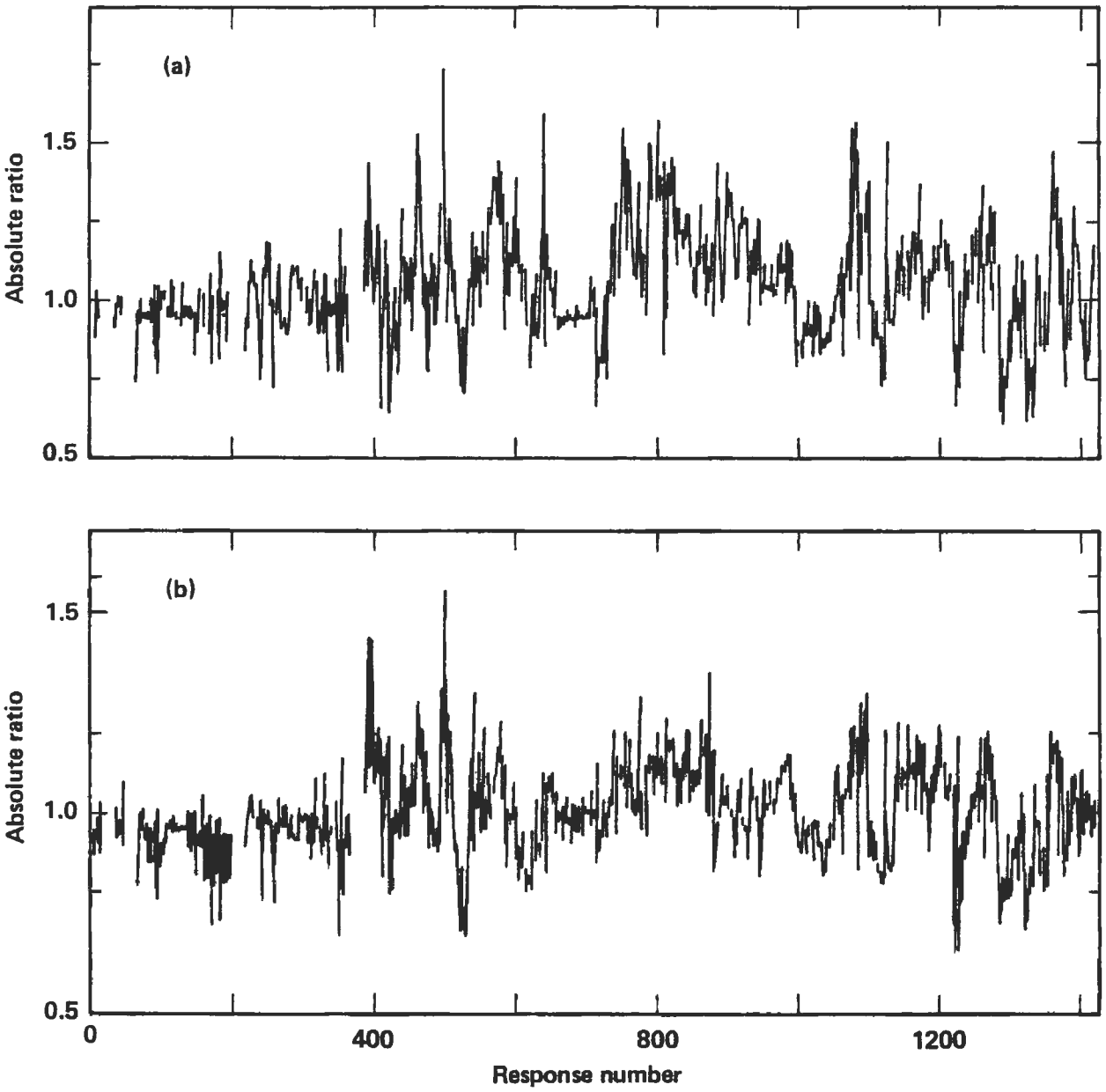

Fig. 4.23. Comparison of median response values assuming total uncertainty vs assuming random uncertainty. (a) acceleration level 2, (b) acceleration level 5.

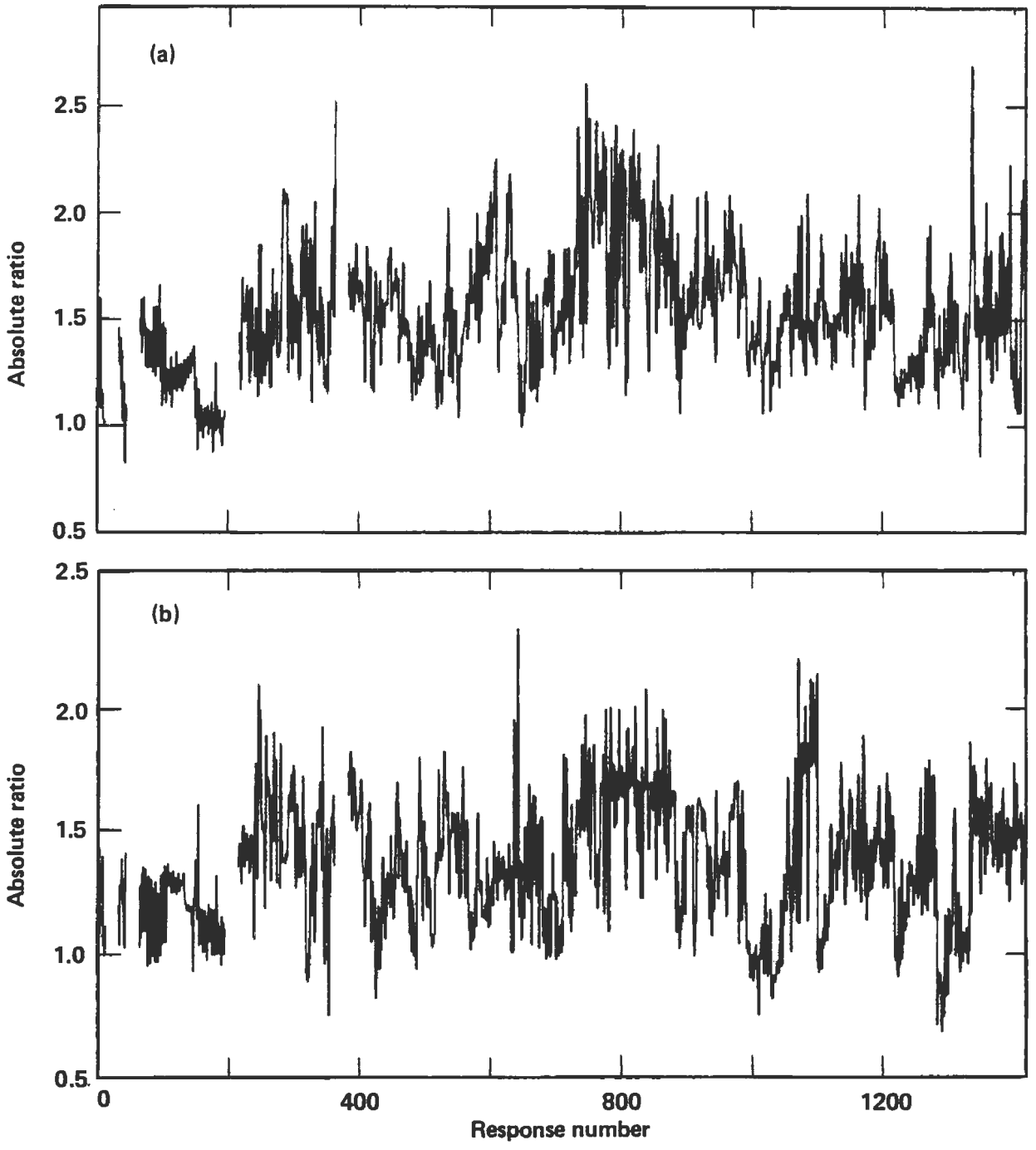

Fig. 4.24. Comparison of ß values assuming total uncertainty vs assuming random uncertainty. (a) acceleration level 2, (b) acceleration level 5.

CHAPTER 5: FRAGILITIES

5.1 Fragility Requirements for SSMRP

One of the major inputs to the program SEISIM for calculation of release category frequency is fragility descriptions of the structures and components. Fragility curves express failure probability as a function of the local parameter that is critical for the given structure or component, where failure is defined as the inability of the item to serve its intended safety-related function. Spectral acceleration is the fragility parameter for all structures and components, except for piping and valves, whose resultant moment and resultant acceleration are the parameters.

The uncertainties associated with fragilities are separated into two categories, random uncertainty and modeling uncertainty. For the demonstration calculations in Phase I these two types of uncertainty were combined in a single expression of variation. The fragilities were described by lognormal distributions with median values and coefficients of variation (β_T). For Phase II these two sources of variation were separated. The fragility descriptions consisted of the lognormal distributions with parameters median and coefficient of variation (COV) due to random uncertainty (β_R). The modeling uncertainty is introduced by treating the median as uncertain and having a lognormal distribution with a COV due to systematic or modeling uncertainty (B_U).

5.2 Methodology

Fragility relations are required for the buildings, piping, and safety-related components. Building fragilities are necessarily specific to the plant being analyzed. For the Zion Unit 1 reactor being studied in the SSMRP, fragilities for structures were developed for the reactor containment, turbine, auxiliary, fuel handling, and crib house buildings.

5.2.1 Building Fragilities

Since no actual tests to failure of typical power plant buildings exist, it is necessary to base the development of the building fragilities on a comparison of analytically calculated loads with experimentally determined wall, slab, and beam capacities. The starting point for this comparison is a dynamic structural analysis of the building under consideration, one that provides accelerations and stress resultants at various points within the structure. This analysis can be based on design calculations, which are usually based on the response spectra method, or a time history analysis. From this analysis, we relate the stress resultants in walls, slabs, and beams to the acceleration level at some convenient reference point in the building. The acceleration at failure is then computed using the relation

$$A_F = A\ F_S\ F_\mu \quad ,$$

where

A_F = acceleration at failure,
A = reference acceleration for which stress resultants are known,
F_S = factor relating the design strength capacity to the actual strength capacity,
F_μ = factor that represents the inelastic energy absorption capability of the structure.

The strength factor F_S is computed from the relation

$$F_S = \frac{\sigma_{lim} - \sigma_{dead}}{\sigma_{seismic}} ,$$

where σ_{lim} is the limit strength (the load at which structure or component ceases to function), σ_{dead} are the loads or stresses due to weight, thermal or pressure forces, and $\sigma_{seismic}$ are the loads or stresses induced by the seismic excitation. Thus, F_S increases the reference load to the actual limit load capacity, since the loads or stresses are proportional to acceleration in a linear analysis. After yield, the actual increase in stress with acceleration is highly nonlinear, so that in the plastic portion of the stress-strain relationship, the stress actually increases more slowly than the acceleration. This is taken into account by the ductility factor F_μ. The ductility factor F_μ provides the ratio between the stress calculated in a linear analysis and the stress calculated from a nonlinear analysis with a given ductility. Thus, in our analysis we estimate the ductility that the wall, slab, or beam can reach before failure, and then use the corresponding factor F_μ to increase the acceleration capacity.

The original analysis of the crib house roof was based on inherently conservative assumptions, and therefore the additional factor F_R is used to increase the load capacity according to our estimate of the degree of conservatism present. The calculation of these factors and the development of the fragilities for each of the structures mentioned above is described in Vol. 7 of Ref. 1.

The lognormal parameters of the building fragilities are presented in Table 5.1, along with those used for the demonstration calculations of Phase I. The log standard deviation used in the demonstration calculations (β_T) was simply the square root of the sum of the squares of the random uncertainty (β_R) and modeling uncertainty (β_U) components of variability.

5.2.2 Component Fragilities

The components for which fragility curves must be developed are determined by the depth of detail in the event and fault tree analyses of the reactor system under consideration. For Zion, 7 event trees and 11 fault trees have been devised to cover all the hypothesized reactor transients and potential modes of release of radioactivity. Taken together, these event and fault trees require the determination of the probability of failure (due to seismic loading) of over 2300 basic events. (A basic event could, for example, be failure of a certain valve.) Since it was clearly not feasible to generate

Table 5.1. Structural fragilities in units of gravity.

Structure	Phase I[a]		Phase II[b]			
	Median	β_T	Median	β_R	β_U	β_T
Crib house NS intake walls	2.50	0.35	2.50	0.23	0.27	0.35
Crib house EW intake walls	5.50	0.38	5.40	0.27	0.27	0.38
Crib house pump enclosure roof	0.81	0.23	0.86	0.24	0.27	0.36
Crob house NS guide walls	3.90	0.35	3.90	0.22	0.27	0.35
Aux. bldg. roof diaphragm	3.00	0.31	3.00	0.15	0.27	0.31
Aux. bldg. NS shear walls	11.00	0.23	11.00	0.12	0.20	0.23
Aux. bldg. EW shear walls	2.70	0.28	2.70	0.11	0.26	0.28
Diesel generator bldg. walls	1.10	0.19	1.10	0.07	0.18	0.19
Containment basemat	13.00	0.24	13.00	0.15	0.18	0.23
Control room masonry wall	1.70	0.33	1.70	0.23	0.24	0.33
Condensate storage tank	0.81	0.41	0.81	0.28	0.30	0.41

[a] β_T = single value representing total variability.
[b] β_R = variability due to random uncertainty.
β_U = variability due to systematic or modeling uncertainty.

fragility curves for thousands of specific components, the first step in the development of the fragility data base was to group all the components identified on the event and fault trees into a set of generic categories. For example, all motor-operated valves with piping diameters between 2 1/2 and 8 inches were placed in a single generic category, and similarly all electrical motor control centers were placed in another generic category. Then a single fragility curve was derived for each generic category. A detailed review of the components showed that a set of 37 different categories would suffice to cover all the required fragilities. These categories were selected on the basis of equipment functions, governing design criteria, method of seismic qualification, and response characteristics.

Actual experimental data on failure of components as a function of local base acceleration are scarce. The type of data most commonly available results from qualification tests in which the component is experimentally shown to function as designed for a prescribed acceleration spectrum input. While such data do provide a lower limit to the fragility level, it is difficult to extrapolate from these data to higher response levels. One notable exception to the lack of actual fragility data was the data obtained in the U.S. Army Corps of Engineers SAFEGUARD program. This 11-year program, conducted as part of a missile-site hardening effort, included tests of both mechanical and electrical components. The items tested were off-the-shelf and were typical of components used in commercial reactors in the late 1960s, and some of the results are thus directly applicable to the Zion power plant. Sixty-four test programs involving shaker table tests of approximately 300 items were conducted. Excitation consisted of sine beat pulse tests, selected to fit a prescribed acceleration spectrum. Equipment function was monitored during the test. Thus these were truly tests of fragility with respect to both functional and structural failure. Typically, components were tested to over 15 g peak

acceleration. Out of the nearly 300 reports generated in the SAFEGUARD program, 64 were found to be directly applicable to components needed in the SSMRP. In particular, these data were the only data available for electrical components, and thus all our electrical component fragilities are derived from this source.

A second source of information was the generic design analyses performed by Westinghouse and manufacturers of various components used in the Zion plant. In these analyses, the component was assumed to be excited by a base acceleration corresponding to a prescribed design spectrum. Then an analytical solution for the stresses or loads in the component was obtained. From these analytical solutions we obtained the acceleration at failure by extrapolating the stresses to our estimate of the ultimate stress capacity, using the same procedure mentioned above for structural fragilities.

The final source of information on fragility of components was an expert opinion survey performed in the spring of 1980. In this survey, a carefully worded questionnaire was mailed to several hundred well-known specialists in the nuclear industry. These individuals were selected from NSSS vendors, architect/engineering firms, consultants to the nuclear industry, and colleges and universities. In each case, the individual was asked to respond only for those components for which he felt a high degree of expertise. For each component, the respondent was asked to provide:

a) The three lowest (weakest) failure modes.

b) The appropriate response quantity for each mode (e.g., peak acceleration, spectral acceleration at some frequency and damping or force resultant, etc.).

c) The response values at 10%, 50%, and 90% probability of failure.

d) The primary source of his information (i.e., experience, test data, etc.).

The expert opinion responses covered virtually every category of component needed for Phase I of the SSMRP, with 147 detailed responses being returned.

The development of the component fragilities from these sources of data is too extensive to include here, but may be found detailed in Vol. 7 of Ref. 1.

The method of accounting for the variety of fragility possibilities for different combinations of piping elements that might occur has been based on a load scale factor. This approach related individual pipe element fragilities to a master pipe element fragility by means of a load scale factor, F_p, defined as

$$F_p = \frac{\text{Capacity Of reference pipe element}}{\text{Capacity Of pipe element under consideration}} .$$

Load scale factors were computed for several sizes and schedules of pipe elements, including straight pipe, butt welds, elbows, miter joints, and branch connections. The development of the load scale factors is discussed in detail in Ref. 28, and the results are tabulated in both Ref. 28 and Ref. 29.

For Phase I demonstration calculations, fragility descriptions consisted of the lognormal parameters of median fragility measure (m) and β_T (a single value representing total variability, from both random and modeling uncertainty). For the final calculations the random and modeling uncertainty had to be separated. For most categories of equipment, we could choose from more than one set of fragilities; different sets represented different failure modes and/or different sources of data. In some cases, our choice was obvious, but in other cases the data were combined to give one set of values for a category. The fragility values before separation of uncertainty and associated information are collected in Table 5.2. Table 5.3 relates the fragilities to the component with which they were used in SEISIM calculations.

5.2.3 Separation of Uncertainty

In order to construct uncertainty intervals for release frequencies, component fragilities with separate values of variability of randomness and modeling uncertainty (β_R and β_U) are needed. This separation had been estimated for the fragilities based either on SAFEGUARD test data and design report data from NUREG/CR-2405, hereafter called TYPE A data. However, the expert-opinion data which were used to develop fragilities were not separated, and there was insufficient information from the expert-opinion survey to make such a separation. In many cases TYPE A data and expert-opinion data were combined to yield one fragility with only the total Beta (β_T) known.

In order to provide the required separation of variability, we essentially applied the same separation as was determined for the various categories of equipment by TYPE A data, but modified the values to accommodate the additional uncertainty introduced by the expert-opinion data.

The following procedure was used for each category of components:

Given:

β_{TEO} = total variability from expert opinion or a combination of expert opinion and TYPE A data.

β_{TS} = total variability from TYPE A data.

β_{RS} = variability due to randomness only from TYPE A data.

β_{US} = variability due to modeling uncertainty from TYPE A data.

β_T, β_R, β_U } total, random, and modeling uncertainty values to be used for result.

1. If $\beta_{TS} < \beta_{TEO}$
   then assume

Table 5.2. Summary of component fragilities.

Category	Phase II fragility Median	Beta (β_T)	Load parameter	Freq. (Hz)	% of critical damping	Failure mode[a]	Key for Table 5.2[b]
Reactor core assembly	2.06	0.40	Spectral acceleration g	5-15	5	Deformation of guide tubes	A
Reactor pressure vessel	3.83	0.45	Spectral acceleration g	5	5	Fracture of RPV outlet nozzle	A
Pressurizer	2.00	0.40	Spectral acceleration g	20	5	Failure of support skirt bolting	A
Steam generator	2.45	0.44	Spectral acceleration g	5	5	Support failure	B
Reactor coolant pump	2.64	0.44	Spectral acceleration g	5	5	Support failure	R
Piping (master fragility)	2.44×10^6	0.38	Moment in.-lb	-	-	Plastic collapse	C
Large vertical vessels with formed heads	1.46	0.40	ZPA g	Rigid	-	Failure of anchor bolts	D
Large vertical tanks	2.01	0.38	ZPA g	Rigid	-	Failure of anchor bolts	A
Large horizontal vessels	3.91	0.61	Spectral acceleration g	12-20	5	Failure of anchor bolts	A
Small to medium vessels and heat exchangers	1.84	0.51	Spectral acceleration g	20	5	Failure of anchor bolts	E

Table 5.2. (continued)

Category	Phase II fragility Median	Beta (β_T)	Load parameter	Freq. (Hz)	% of critical damping	Failure mode[a]	Key for Table 5.2[b]
Large vertical centrifugal pumps with motor drive	2.21	0.39	Spectral acceleration g	5	5	Failure of support connection	F
Motor-driven pumps and compressors	3.19	0.34	Spectral acceleration g	7	5	Impeller deflection	A
Large motor-operated valves	4.83	0.65	Piping peak acceleration g	Rigid	-	Distortion of extended operator	G
Small motor-operated valves	6.50	0.55	Piping peak acceleration g	Rigid	-	Loss of control air operator	A
Large relief, manual air actuated valves	6.50	0.55	Piping peak acceleration g	Rigid	-	Loss of control air	A
Large relief, manual, and check valves	6.50	0.55	Piping peak acceleration g	Rigid	-	Internal damage	A
Miscellaneous small valves	6.50	0.55	Piping peak	Rigid	-	Internal damage	A
Horizontal motors	12.10	0.41	ZPA	Rigid	-	Binding of rotating parts	H
Generators	0.65	0.40	Spectral acceleration g	22	5	Shutdown valve trip	I
Battery racks	2.29	0.50	ZPA	Rigid	-	Failure of battens	J

Table 5-2. (continued)

Category	Phase II fragility Median	Beta (β_T)	Load parameter	Freq. (Hz)	% of critical damping	Failure mode[a]	Key for Table 5.2[b]
Switchgear	2.33	0.81	Special acceleration g	5-10	5	Spurious operation of a protective relay	K
Dry transformers	2.78	0.41	Special acceleration g	10	5	Failure of anchor bolts	L
Control panels and racks	11.50	0.88	Spectral acceleration g	5-10	5	Dislodging or malfunction of component	A
Auxiliary relay cabinets	7.63	0.82	Spectral acceleration g	5-10	5	Breaker trip	A
Local instruments	7.68	0.40	Spectral acceleration g	5-35	5	Loosening of fasteners	M
Motor-control centers	7.63	0.88	Spectral acceleration g	5-10	5	Breaker trip	A
Communications equipment	5.00	0.40	Spectral acceleration g	10-50	5	Dislodging of components	A
Light fixtures	9.20	0.20	Spectral acceleration g	20-30	2	Dislodging of components	A
Inverters	15.60	0.44	Spectral acceleration g	5-10	5	Relay trip	N
Cable trays	2.23	0.39	ZPA g	Rigid	-	Support system failure	O

Table 5-2. (continued)

Category	Phase II fragility Median	Beta (β_T)	Load parameter	Freq. (Hz)	% of critical damping	Failure mode[a]	Key for Table 5.2[b]
Circuit breakers	7.63	0.88	Spectral acceleration g	5-10	5	Breaker trip	P
Relays	4.00	0.89	Spectral acceleration g	5-10	5	Relay chatter	A
Ceramic insulators	0.20	0.35	PGA g	2-8	5	Fracture of porcelain	Q
Air-handling units	2.24	0.41	Spectral acceleration g	5	5	Rubbing of fan on housing	A A
Instrument racks	1.15	0.82	Spectral acceleration g	5-10	7	Structural failure	A
Duct work	3.97	0.54	Spectral acceleration g	5-10	7	Structural failure	A
Hydraulic snubbers, pipe supports	1.46	0.54	ZPA g	Rigid	-	Weld failure	A

[a] Only the most likely failure mode is listed, although the fragility may be based on a combination of modes.

[b] See Table 5.3.

Table 5.3. Fragilities related to components.

Key for Table 5.2	Component
A	None (i.e., not used)
B	Steam generator and steam generator tubes
C	Piping and piping components
D	Tanks in the safety injection system and chemical and volume control system
E	Coolers in the reactor containment ventilation system, service-water system, and residual heat removal system
F	Centrifugal pumps
G	Used for all valves
H	Electrical heaters in the safety injection system
I	Generator, diesel generator, and diesel generator components in the main power and service-water systems
J	Batteries in main electrical power system
K	Relays and protective switchgear
L	Dry transformers and battery chargers
M	Local instruments, including sensors, detectors, and controllers
N	Inverters in main electrical power system
O	Electrical conductors in both main power and instrumentation power systems
P	Circuit breakers, controller, starters, and switches
Q	Loss of off-site power and turbine trip
R	Reactor coolant pump

$$\beta_{RS} < \beta_{TS} < \beta_{TEO}$$

$$\beta_R = \beta_{RS}$$

$$\beta_U = \beta_{TEO}^2 - \beta_{RS}^2$$

$$\beta_T = \beta_R^2 + \beta_U^2 \quad .$$

2. If $\beta_{TS} > \beta_{TEO}$ and $\beta_{TEO} > \beta_{RS}$, then assume

$$\beta_{RS} < \beta_{TEO} < \beta_{TS}$$

$$\beta_R = \beta_{RS}$$

$$\beta_U = \beta_{US}$$

$$\beta_T = \beta_R^2 + \beta_U^2 \quad .$$

(I.e., for this case the results are the same as the TYPE A data.)

3. If $\beta_{TS} > \beta_{TEO}$ and $\beta_{TEO} < \beta_{RS}$, then assume

$$\beta_{TEO} < \beta_{RS} < \beta_{TS}$$

$$\beta_R = \beta_{TEO}$$

$$\beta_U = \beta_{US}$$

$$\beta_T = \beta_R^2 + \beta_U^2 \quad .$$

Table 5.4 shows the resulting lognormal parameters of the component fragilities as used for final calculations.

All of the fragilities used in SSMRP are developed for local responses. Table 5.5 is included here to document the relationship of the SEISIM response vectors with the physical locations throughout the areas of analysis.

5.2.4 Differences in Phase I and Phase II Median Fragilities

A few of the median values of fragilities used in Phase I demonstration calculations were revised for use in the final Zion calculations. The following were the only revisions of consequence.

Table 5.4. Final Zion component fragilities, in units of gravity (g), except for piping entries, which are in units of moment (in.-lb).

Category	Median	β_R	β_U	β_T
Reactor core assembly	2.06	0.24	0.32	0.40
Reactor pressure vessel	3.83	0.23	0.39	0.45
Pressurizer	2.00	0.21	0.34	0.40
Steam generator	2.45	0.24	0.37	0.44
Piping (master fragility)	2.44×10^6	0.18	0.33	0.38
Large vertical vessels with formed heads	1.46	0.20	0.35	0.40
Large vertical tanks with flat bottoms	2.01	0.25	0.29	0.38
Large horizontal vessels	3.91	0.30	0.53	0.61
Small medium vessels with heat exchangers	1.84	0.25	0.45	0.51
Reactor coolant pump	2.64	0.24	0.37	0.44
Large vertical centrifugal pumps	2.21	0.22	0.32	0.39
Large vertical pumps	2.21	0.22	0.32	0.39
Motor driven pumps and compressors	3.19	0.21	0.27	0.34
Large motor operated valves (>4 in.)	4.83	0.26	0.60	0.65
Large relief, manual, and check valves	8.90	0.20	0.35	0.40
Misc. small valves	12.50	0.33	0.43	.54
Horizontal motors	12.10	0.27	0.31	.41
Generators	0.65	0.25	0.31	0.40
Battery racks	2.29	0.31	0.39	0.50
Switchgear	2.33	0.47	0.66	0.81
Dry transformers	2.78	0.28	0.30	0.41
Air handling units	2.24	0.27	0.31	0.41
Instrument racks and panels	1.15	0.48	0.66	0.82
Control panels and racks	11.50	0.48	0.74	.88
Auxiliary relay cabinets	7.63	0.48	0.66	0.82
Local instruments	7.68	0.20	0.35	0.40
Motor control centers	7.63	0.48	0.74	0.88
Condensate storage tank	0.81	0.28	0.30	0.41
Local instruments	7.68	0.20	0.35	0.40
Light fixtures	9.20	0.14	0.14	0.20
Inverters	15.6	0.26	0.35	0.44
Cable trays	2.23	0.34	0.19	0.39
Ducting	3.97	0.29	0.46	0.54
Hydraulic snubbers and pipe supports	1.46	0.22	0.49	0.54
Relays	4.00	0.48	0.75	0.89
Circuit breakers	7.63	0.48	0.74	0.88
Large motor-operated valves (rupture)	14.40	0.28	0.56	0.63
Ceramic insulators	0.20	0.25	0.25	0.35

Table 5-5. Response position in SEISIM vector.

SEISIM ref. vector	Response[a]	Location in SMACS model[b]	Location
1	A	Free field	Free field
2	S_A (4)	Free field	
3	S_A (8)	Free field	
4	S_A (16)	Free field	
5	A	CLASSI Ref. Pt.	Reactor bldg.
6	S_A (4)	CLASSI Ref. Pt.	basemat
7	S_A (8)	CLASSI Ref. Pt.	containment
8	S_A (16)	CLASSI Ref. Pt.	elevation 556'
9	A	20	Reactor bldg. ring girder
10	A	936	Reactor bldg.
11	S_A (4)	936	operating floor
12	S_A (8)	936	
13	S_A (16)	936	
14	S_A (4)	1412	Reactor bldg. RC pumps
15	S_A (8)	1418	Reactor bldg. steam generator
16	S_A (16)	1462x,y 1463z	Reactor bldg. RV nozzles
17	A	13y,z 21x	Turbine/aux. bldg.
18	S_A (4)	13y,z 21x	lowest floor
19	S_A (8)	13y,z 21x	elevation 542'
20	S_A (16)	13y,z 21x	
21	A	505y,z 530x	Turbine/aux. bldg.
22	S_A (4)	505y,z 530x	basemat floor
23	S_A (8)	505y,z 530x	elevation 560'
24	S_A (16)	505y,z 530x	

Table 5.5. (Continued)

SEISIM ref. vector	Response[a]	Location in SMACS model[b]	Location
25	A	530x 544y,z	Turbine/aux. bldg.
26	S_A (4)	530x 544y,z	elevation 567'
27	S_A (8)	530x 544y,z	DG oil pumps and
28	S_A (16)	530x 544y,z	storage tanks
29	A	1511y,z 1543x	Aux. bldg. ground
30	S_A (4)	1511y,z 1543x	floor elevation
31	S_A (8)	1511y,z 1543x	592'
32	S_A (16)	1511y,z 1543x	
33	A	1530y,z 1543x	Turbine bldg.
34	S_A (4)	1530y,z 1543x	ground floor
35	S_A (8)	1530y,z 1543x	elevation 592'
36	S_A (16)	1530y,z 1543x	
37	A	1537y,z 1543x	Fuel handling
38	S_A (4)	1537y,z 1543x	bldg. floor slab
39	S_A (8)	1537y,z 1543x	elevation 592'
40	S_A (16)	1537y,z 1543x	
302[c]	A	1543x 1562y,z	Turbine/aux. bldg.
303	S_A (4)	1543x 1562y,z	elevation 591'
304	S_A (8)	1543x 1562y,z	(diesel gen.)
305	S_A (16)	1543x 1562y,z	
306	A	2012x,y,z	Turbine/aux. bldg.
307	S_S (4)	2012x,y,z	mezzanine floor
308	S_S (8)	2012x,y,z	elevation 617'
309	S_S (16)	2012x,y,z	
310	A	3005x 3006	Turbine/aux. bldg.
311	S_A (4)	3005x 3006	top floor
312	S_A (8)	3005x 3006	elevation 642'
313	S_A (16)	3005x 3006	

Note: S_A denotes spectral acceleration at given frequency and 5% damping. Numbers in parentheses are the frequency in Hz at which the spectral acceleration occurs.

[a] A denotes peak acceleration.

[b] See Section 4.2.2 of this report for description of SMACS model.

[c] Pipe and valve responses are in positions 41 through 301 and are not included in this table.

Category Description	Phase I median (g)	Phase II median (g)
• Steam generator	4.00	2.45
• Large motor-operated valves (failure mode--deformation of valve stem)	6.50	4.83
• Large motor-operated valves (failure mode--rupture)	Not used	14.40
• Battery racks	2.16	2.29
• Local instruments	10.00	7.68
• Switchgear	1.68	2.33
• Motor-control centers	7.07	7.63
• Circuit breakers	7.07	7.63

The explanations for these differences are as follows.

Steam Generators

The value used in Phase I was incorrect due to a typographical error in Table 4-2 of NUREG/CR-2405. The median capacity recorded there for the steam generator should have been 3.3 g rather than 5.2 g. The correct value was used in the development of the fragility used for final Zion calculations.

Large Motor-Operated Valves

A separation of this category to account for two separate failure modes resulted in the differences here. In Phase I, the combination of contributors to the fragility included failures due to valve rupture. These were removed to a separate category, as indicated in the table above for the final Zion calculations.

Battery Racks

The Phase I fragility for this category was obtained from expert opinion alone, whereas design data were included in the development of the fragility for final Zion calculations.

Local Instruments

In the development of the Phase I fragility for this category, the units of fragility for one set of expert opinions was interpreted incorrectly. This error was subsequently corrected, resulting in the value used for the final Zion calculations.

Switchgear, Motor-Control Center, and Circuit Breakers

Revisions in the choices of contributors used for the categories of switchgear and motor-control centers gave a more consistent basis of separation between these two categories. As a result, the median values for both of these categories were slightly altered. The data for circuit breakers and motor-control centers were so closely related that a separation was not attempted. Therefore, the values used for these categories are the same.

5.3 Unmodeled Safety Systems

The fault tree analysis described in Chapter 6 generates the system failure events identified by the event trees. Table 5.6 lists the systems that appear on the event trees and indicates those for which fault trees were generated in the SSMRP. These fault trees, except for feed-and-bleed, were described in the Phase I final report for Systems Analysis (Vol. 8 of Ref. 1). In order to assign fragilities to those systems that were not modeled, it was necessary to study previous seismic studies reports (Ref. 30) and to see how the results of those studies applied to Zion. In studying Table 5.6, we note that the auxiliary feedwater system, charging system, safety injection system, residual-heat-removal system, the accumulators, the feed-and-bleed capability, the electric power, and the service-water system were modeled for the Zion analysis. The remaining systems, which were viewed as less important, were not modeled, due to budgetary constraints. The unmodeled systems include the containment fan cooler system, the containment spray system, the chemical volume and control system, the power-conversion system, the reactor protection system, the heating and ventilation system, the component-cooling water system, and the instrumentation and control system. Some of these systems have been modeled to a lesser extent. For example, the model of the power-conversion system was based on the model of the main feedwater system. Details of the component-cooling water system were not studied, due to the high probability of failure of the roof of the crib house service-water pump enclosure, which disables the component-cooling water system. The instrumentation and control system was studied, but no fault tree was developed. This particular system is assumed to be disabled by failure of the shear wall, which causes loss of control. The systems that will be discussed in this section are the containment fan cooler system, the containment spray system, the chemical volume and control system, and the reactor protection system.

Table 5.6. Zion 1 safety and supporting systems.

Systems listed on event trees	Supporting systems
Auxiliary feedwater system[a]	Electric power[a]
Containment fan cooler system	Service water[a]
Containment spray system	Heating and ventilating system
Chemical volume and control system	Component-cooling water system
Emergency core-cooling system:[a]	Instrumentation and control system
Charging pumps	
Safety injection system	
Residual heat removal system	
Accumulators	
Power-conversion system	
Reactor protection system	
Feed-and-bleed[a]	

[a]SSMRP fault trees developed

The CSIS and CFCS(I) are designed to remove heat from the containment atmosphere to prevent overpressurization during the injection phase of a LOCA[a]. The CFCS, which consists of five fan cooler units, condenses the steam in the containment atmosphere. The heat removed from the steam is passed to the service-water system. The CSIS consists of three containment spray pumps (two motor-driven, one diesel-driven) which deliver water from the RWST to spray headers in the containment. This spray condenses the steam in the containment atmosphere. Success is defined as (1) at least two out of five containment fans passing heat to the service-water system, or (2) at least one out of three containment spray pumps delivering water to the containment atmosphere through the spray header nozzles. After studying this system, studying other facilities, and discussions with personnel involved in Diablo Canyon's seismic study, it was decided that median failure would occur between earthquake levels 3 and 4 of our analysis. It was therefore decided to use a step fragility function. That is, the CSIS and CFCS(I) were assumed not to fail for earthquake levels 1, 2, and 3 and were assumed to fail at earthquake levels 4, 5, and 6 of our analysis.

The CSRS is designed to remove heat from the containment atmosphere to prevent containment overpressure during the recirculation phase of a LOCA[a]. The CSRS consists of two RHR pumps delivering water from the containment sump to spray headers in the containment atmosphere. Success is defined as at least one out two RHR pumps delivering water from the containment sump to the containment atmosphere through spray header nozzles. The CSRS was assumed not to fail during earthquake levels 1, 2, and 3 and was assumed to fail at earthquake levels 4, 5, and 6.

The CVCS is designed to maintain water inventory in the RCS for most normal operations and transients. Excess water is drained from the RCS and eventually brought to the volume control tank. If water is needed, it is added from the volume control tank by three charging pumps. During a transient, success is defined as maintaining water inventory in the RCS above the core. The CVCS was assumed not to fail for earthquake levels 1, 2, and 3 and was assumed to fail at earthquake levels 4, 5, and 6.

The RPS is designed to shut down the nuclear reaction in the core if an abnormal condition exists. The purpose is to reduce the amount of heat and make it possible to bring the plant to a safe condition. Success is defined as bringing the reactor to a subcritical (shutdown) condition. A failure rate of 3×10^{-5} was assumed over the first six acceleration levels; this estimate was based on the Diablo Canyon analysis.

5.4 Soil Failure

When one considers the range of earthquakes for the seismic risk analysis, it is essential to include consideration of phenomena which may not be of major

[a] It is recognized that both the containment spray system and the containment fan cooler system have a functional capability to perform PARR. However, their relative efficiencies in performing this function have not been determined. It is therefore assumed for this analysis that the difference in their efficiencies is not significant enough to result in substantially different consequences. This assumption greatly simplifies the event trees.

consequence in the design process. One such consideration is soil-foundation separation or uplift. For the Zion reactor building, as for other structures having a large height-to-diameter ratio, overturning moments due to its seismic response lead to a prediction of uplift. Soil-foundation separation, per se, is not critical. The consequences of uplift on structure response are usually a reduction in member loads and introduction of additional high-frequency response. These effects are generally considered to be of second order, particularly for a seismic risk analysis, and were not explicitly included in our analysis. In addition, the potential exists for large soil pressures to occur due to a redistribution of stress. Peak toe pressures may, in fact, increase to the point of exceeding the soil bearing capacity, causing failure. A further consequence of uplift itself and potential soil failure is increased relative displacement between adjacent structures which then causes failure of interconnecting pipes. At Zion, large relative displacements would be predicted to occur between the reactor building and the AFT complex. In the SSMRP Phase II analyses, we included basemat uplift as a potential failure mode of interconnecting pipes.

To estimate the excitation levels at which uplift and soil failure occur, a series of linear analyses was performed, using SMACS, for a range of earthquakes. Ensembles of earthquakes represented the seismic input and variations in soil and structure input parameters were included. A post-processing of SMACS' results combined each horizontal response with the vertical response to determine overturning moments and peak toe pressures. In post-processing, the effects of dead weight, buoyancy, and an estimate of the portion of response distributed to the side soil were taken into account. The results were estimates of overturning moments, peak toe pressures, and vertical displacements. Such an analysis greatly overpredicts peak soil pressure. Several studies (Refs. 42, 43) have made comparisons between peak toe pressures calculated by linear and nonlinear analyses. Using these data as a basis, the linearly calculated toe pressures were adjusted for nonlinear effects. These scaled values of toe pressures were compared with the ultimate soil capacity of 45 KSF (Ref. 41). A median toe pressure of 45 KSF was estimated at a 0.70-g peak horizontal acceleration of the reactor building foundation. The consequences of soil failure, which were relative displacements of 2 in. or more, were assumed to cause rupture of piping between the reactor building and the AFT complex.

CHAPTER 6: SYSTEMS ANALYSIS AND RISK ASSESSMENT

The calculations of the frequencies of core melt and radioactive release are performed using the SEISIM computer code (Ref. 31). This code, designed and developed in the SSMRP, embodies a general probabilistic risk assessment methodology which can address complex systems whose failure modes are defined by many accident scenarios and for which failures of different components within the system can be highly dependent. The capacity to handle dependent failures having any degree of correlation is what sets SEISIM apart from any other existing quantitative risk assessment code.

6.1 The SEISIM Methodology

The calculation of radioactive release frequencies for a nuclear power plant subjected to an earthquake requires, first of all, identification of seismically-induced initiating events which require shut-down of the reactor system. Then potential accident scenarios leading to core melt and radioactive release which could occur following an initiating event are hypothesized, and characterized by event trees (Ref. 32). Failure modes for the safety and auxiliary systems are identified and expressed in terms of fault trees (Ref. 33) for each system. Quantifications of the event and fault trees yield Boolean expressions which specify the logical relationships between failures of structures, piping, and components that can lead to core melt. These logical relationships are input in the form of minimal-cut-set expressions that define the failure modes of systems in terms of their basic events. The SEISIM code was designed to compute the probabilities of the accident sequences by computing the probabilities of the minimal cut sets that define the accident sequences.

SEISIM uses the response data and fragility functions to compute the failure probabilities of structures and components, to calculate system failure probabilities, initiating event probabilities, accident sequence probabilities, and radioactive release frequencies, as shown in Fig. 6.1.

6.1.1 Cut Set Probabilities

All accident sequences evaluated in SEISIM are expressed as unions of min cut sets in the form

$$P(\text{ACC SEQ}) = P(C_1C_2C_3 \text{ or } \ldots \text{ or } C_iC_jC_kC_l \text{ or } \ldots)$$

Each cut set is allowed to have up to 10 correlated basic events, C_i.

The cut set occurs when failure of all the components in the cut set occurs, that is, when all component responses exceed their strengths. Let

$$\{R\} = \{R_1, R_2, \ldots, R_n\}$$
$$\{S\} = \{S_1, S_2, \ldots, S_n\}$$

be the vectors of responses and strengths of components in a cut set of size n. Let $\{\hat{R}\}$ and $\{\hat{S}\}$ be the vectors of the corresponding medians of response and strength, respectively. Denote by the variable

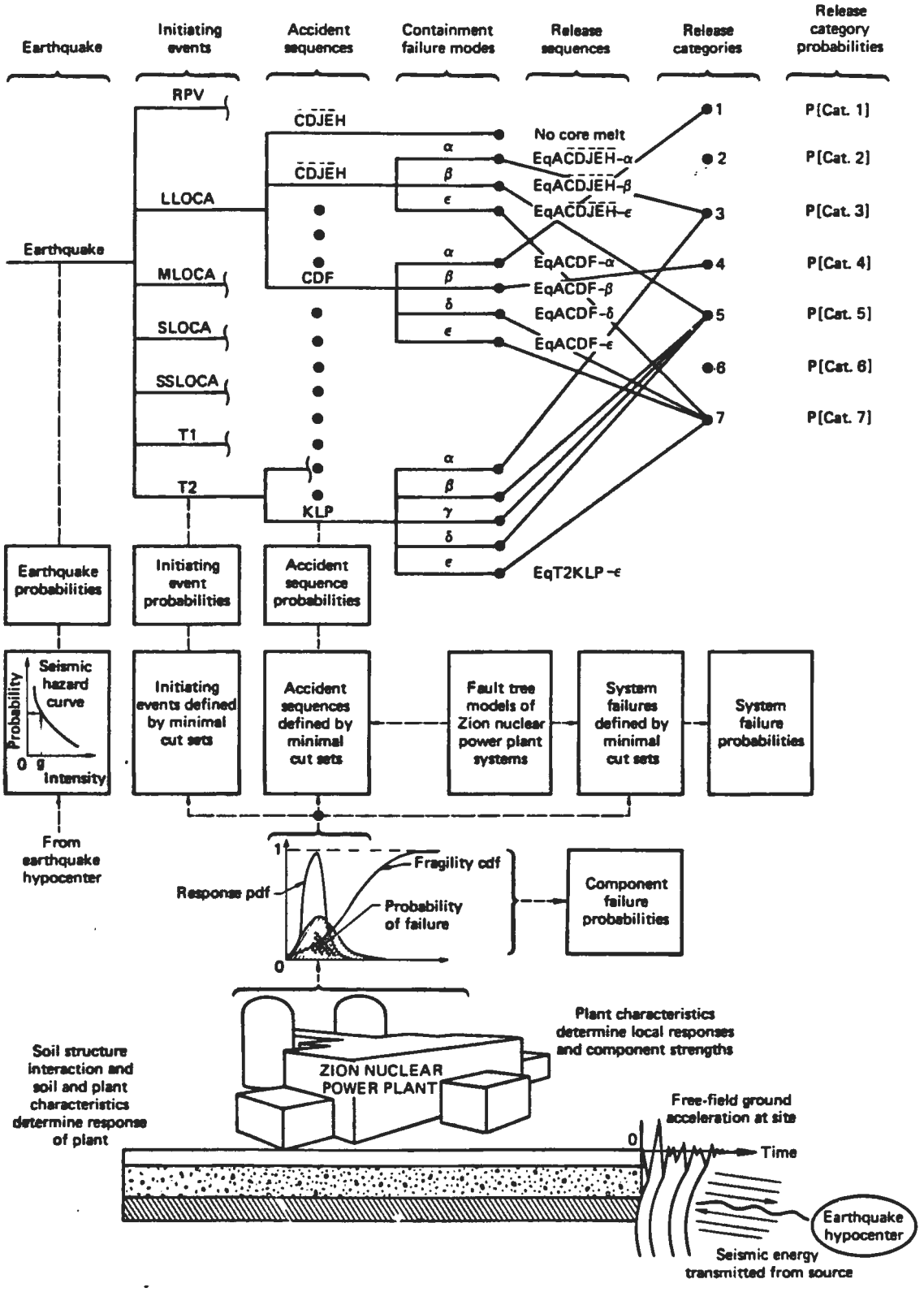

Fig. 6.1. Description of the computational procedure embodied in SEISIM.

$\{Z\}$ the difference $\{R-S\}$. Then the probability of the cut set occurring is

$$P[Z_1>0,\ Z_2>0,\ \ldots\ Z_n>0] =$$

$$\int_0^\infty \int_0^\infty \cdots \int_0^\infty \int_0^\infty f_Z(Z_1, Z_2, \ldots Z_n) dZ_1, dZ_2 \ldots dZ_n \quad ,$$

where f_Z is the joint probability density function. Since $\{Z\}$ is assumed to be multinormal, the density is given by

$$f_Z = \frac{1}{(2\pi)^{n/2} \Sigma^{1/2}} \exp\left[-\frac{1}{2}\{Z - \hat{Z}\}^T \left[\sum\right]^{-1}\{Z - \hat{Z}\}\right] \quad ,$$

in which $\{\hat{Z}\} = \{\hat{R}\} - \{\hat{S}\}$ and Σ is the covariance matrix defined by

$$[\Sigma]_{ij} = COV(R_i,R_j) + COV(S_i,S_j) - COV(R_i,S_j) - COV(R_j,S_i)$$

The covariances between responses are computed in SMACS, and the covariances between strengths are user-specified.

SEISIM computes cut set probabilities given any degree of dependence among basic event failures (Refs. 34, 35). Each cut set probability is expressed in terms of a multinormal integral whose integrand is specified by the means, standard deviations, and correlations of the responses for the cut set basic events. SEISIM processes the inputs shown in Fig. 6.2 to derive the multinormal integral parameters. The probabilities are computed in the sequence illustrated in Fig. 6.3. Correlations between local responses are accounted for as well as correlations between component strengths (fragilities). If the local responses of two components are positively correlated, the components will tend to fail or survive together, with the frequency of both failing being higher than if their responses were uncorrelated. Correlations between local responses occur because of the nature of the seismic forcing function and types of systems being analyzed.

The initiating event probabilities are also computed from Boolean equations expressed as the union of cut sets. A hierarchy of initiating events is defined and implemented in SEISIM, i.e., occurrence of a large LOCA implies non-occurrence of reactor pressure vessel rupture, etc.

The frequency of radioactive release in each WASH-1400 release category is defined as the sum of the frequencies of all the terminal event sequences that lead to a release in the specified category. (Category 1 is the most severe, and category 7 is the least severe.) Terminal event sequence frequencies are defined as the products of the probabilities of the earthquake, initiating event, accident sequence, and containment failure mode. Frequency of core melt is defined as the sum of all release category frequencies.

In addition to computing the frequencies of radioactive release, SEISIM can perform sensitivity analyses. Two types of sensitivity analyses are

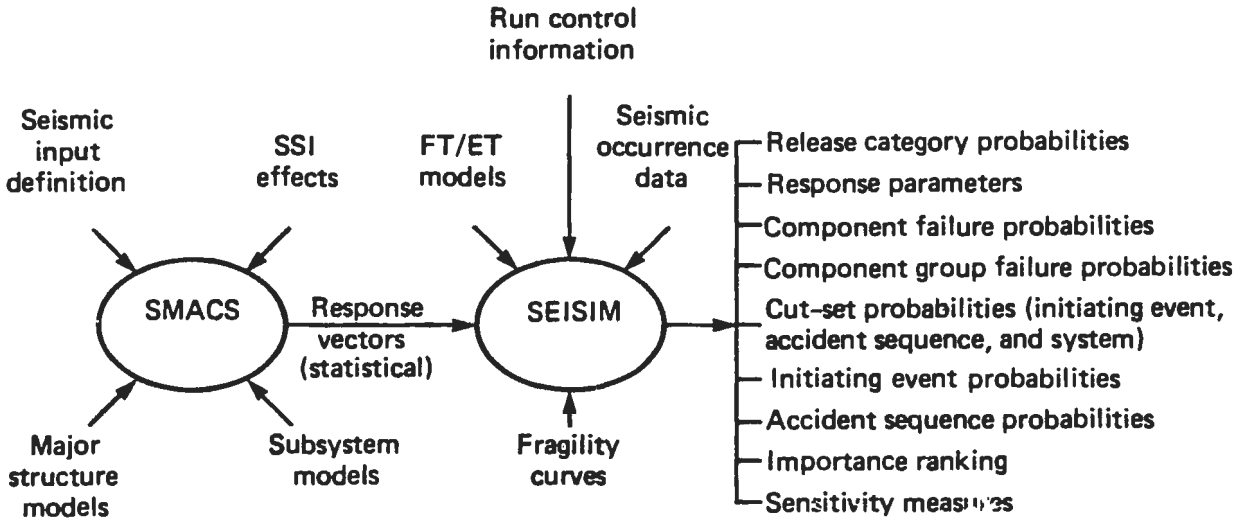

Fig. 6.2. SEISIM inputs and outputs.

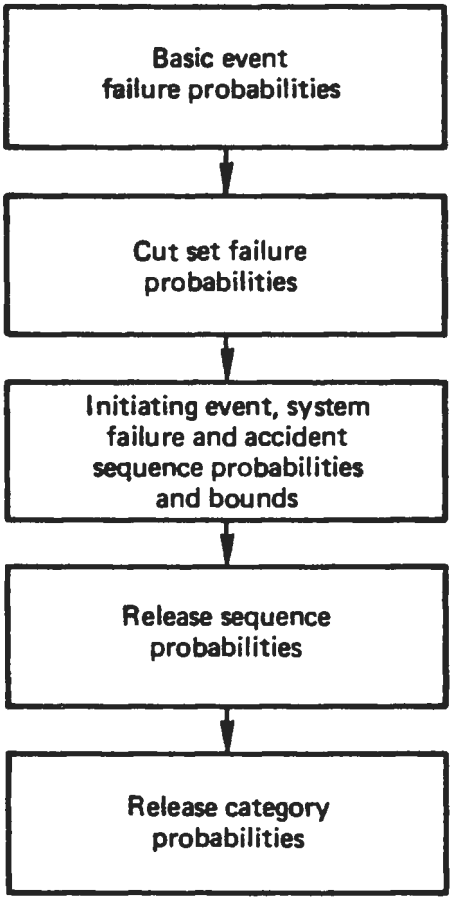

Fig. 6.3. SEISIM probability computation sequence.

incorporated into the SEISIM computational methodology. One is the sensitivity of outputs to changes in significant input parameters, expressed in terms of partial derivatives. The second type of sensitivity computation performed by SEISIM is called dominance analysis, in which the components, accident sequences, etc., that most influence the final results are identified (Ref. 36).

6.2 Description of SEISIM Input

The input required by the SEISIM code consists of the following:

- Earthquake occurrence data.
- Seismic responses for buildings, pipes, and components.
- Fragility functions for buildings, pipes, and components.
- Initiating events (defined by min cut sets).
- Accident sequences (defined by min cut sets).
- Containment event trees.

Each of these is described below.

6.2.1 Earthquake Occurrence Data

This is merely the probabilities of occurrence of earthquakes having peak ground accelerations in each of the discretized ranges of accelerations on the hazard curve, as described in Chapter 3. These probabilities for the median Zion hazard curve shown in Fig. 3-5 are given below:

Earthquake level	Rock out-crop acceleration range	Probability (per year)
1	0.06 - 0.10	5.483E-4
2	0.10 - 0.20	2.657E-4
3	0.20 - 0.32	1.322E-5
4	0.32 - 0.42	1.617E-6
5	0.42 - 0.53	4.183E-7
6	0.53 - 0.69	1.617E-7

6.2.2 Structural, Piping, and Component Seismic Responses

The input response data are the peak responses computed using the computer program SMACS. These responses are associated with specific points within the plant and include structural, piping, and component responses. For each location, SMACS generates multiple sample responses. These sample responses

are generated using the 20 time history SMACS analyses for uncertainty intervals as described in Chap. 4, for each of the 6 acceleration ranges.

SEISIM uses these responses to estimate the means, standard deviations, and covariances of the peak local responses resulting from each earthquake simulation. SEISIM assumes that the local responses are described by lognormal distributions.

6.2.3 Fragility Functions

A fragility function defines the strength or capacity of a component (or structural element). The fragility function must have the same units as its associated response. Strengths are assumed to be lognormally distributed; therefore, fragility functions can be uniquely defined by their mean strength and standard deviation. The correlations among component fragilities can be accounted for in SEISIM by a user-specified fragility correlation matrix.

6.2.4 Initiating Events

An initiating event is any event which requires shutdown of the reactor. The two general classes of initiating events are loss of coolant accidents (LOCAs) and power-coolant mismatch transients. Seven initiating events were defined for the analysis of Zion, as shown in Table 6.1. These initiating events are defined in terms of individual failure events, by unions of cut sets which represent the failure of one or more basic events. The failures of these events are the direct cause of the initiating events.

Loss of coolant by leakage occurs when there is a break in the primary coolant system boundary. The most serious primary system break is one which prevents the reflooding of the core by the emergency core-cooling system (ECCS). Such a break is called a Reactor Pressure Vessel rupture (RVR), and it is defined as a rupture large enough to negate the effectiveness of the ECCS measures to prevent core melt. Although this event is called a vessel rupture, it can also be caused by combinations of primary-system piping breaks that cannot be mitigated by the ECCS.

The second most serious break is one in the primary system where the loss of coolant can be mitigated by successful operation of the ECCS. Such breaks are called Loss of Coolant Accidents (LOCAs), and event trees have been developed for four sizes of such breaks. The four sizes were determined by evaluation of ECCS pump and accumulator combinations which would be capable of reflooding the core for the various size breaks. Breaks smaller than the smallest LOCA break for which an event tree was developed will not uncover the core, because of the slow rate of coolant loss and the operation of the normal make-up water system.

The discussion thus far has been limited to pipe and vessel failures which lead to a LOCA. However, a PWR primary system also contains a pressurizer, steam generators, primary relief valves, and primary coolant pumps. Failures in any of these components could also lead to loss of coolant. The pressurizer relief valves could rupture or fail to reclose, thus causing a loss of coolant. If such a failure occurs, the break size is equivalent to one of the LOCA sizes

Table 6.1. Definition of initiating events.

Reactor Vessel Rupture (RVR)	A vessel rupture large enough to negate the effectiveness of the ECC systems required to prevent core melt, or rupture of sufficient primary coolant piping in a pattern that negates the effectiveness of those same ECC systems.
Large LOCA (LLOCA)	A rupture of primary coolant piping equivalent to the break of a single pipe whose inside diameter is greater than 6 in., but which does not negate the effectiveness of the ECC systems required to prevent core melt.
Medium LOCA (MLOCA)	A rupture of primary coolant piping equivalent to break of a single pipe whose inside diameter is greater than 3 in. and less than or equal to 6 in.
Small LOCA (SLOCA)	A rupture of primary coolant piping equivalent to break of a single pipe whose inside diameter is greater than 1.5 in. but less than or equal to 3 in.
Small-small LOCA (SSLOCA)	A rupture of primary coolant piping equivalent to break of a single pipe whose inside diameter is greater than 0.5 in. and less than or equal to 1.5 in.
Class 2 Transient (T2)	An abnormal condition in the plant which requires that the plant be shut down and which directly affects the operability of the PCS, causing it to become inoperative, but which does not qualify as a LOCA or vessel rupture.
Class 1 Transient (T1)	Any abnormal condition in the plant which requires that the plant be shut down but which does not directly effect the operability of the PCS and does not qualify as a LOCA or vessel rupture.

for which an event tree was developed. Like reasoning applies to a pressurizer rupture accident. Similarly, an external rupture of a primary coolant-pump seal can be categorized as a LOCA.

In summary, all piping and components in the primary system have been analyzed for a leakage-type loss of coolant. The primary piping includes the main loops and all interfacing piping out to the first isolation component, such as a check valve or a normally closed valve. Adequate coverage of the potential leakage-type loss of coolant has been achieved with the event trees shown in this section.

The loss of coolant by boil-off occurs when insufficient heat is removed from the primary system. There are many ways in which this could occur. However,

no matter which failure mode causes the initial problem, the same series of events are required to mitigate the situation and prevent core melt. The first functional requirement is to shut down the reaction in the core, followed by removal of decay heat. The design used at Zion requires the relieving of excess pressure from the primary system, if decay heat is not being adequately removed, and the replacement of water lost by boil-off to maintain adequate coolant volume during the temperature and pressure changes. Ultimately, to reach a cold-shutdown mode requires additional heat removal from the primary system.

The mitigating actions described above are all considered in the transient event trees. All of these actions are concerned with prevention of core melt due to loss of coolant by boil-off. The initiating event that could be the cause of the potential boil-off can occur in either the primary or secondary coolant systems or in their supporting systems. These initiators have been defined as transient events. Events which in themselves are not transients, but which lead to transient events, still require the same mitigating systems and are therefore considered within the transient event trees.

Two transient event trees have been constructed for this study to describe two classes of transients: those which leave the power-conversion system (PCS) operable, and those which disable the PCS. Although these two classes have been treated separately, the plant response is functionally identical for both classes.

By definition, initiating events are mutually exclusive, i.e., one cannot have both a transient and a LOCA . Therefore, a hierarchy of precedence for the initiating events has been established. The hierarchial order is defined as follows: RVR, LLOCA, MLOCA, SLOCA, SSLOCA, T2, T1. For example, we use the cut sets of the RVR to compute its probability of occurrence. Then, since a large LOCA cannot occur if there is an RVR, we compute the probability of the combined event large LOCA and no RVR. And so on, we compute the probabilities of small LOCA, small-small LOCA, and Class 2 Transient. Finally, since we assume that some initiating event occurs, we compute the probability of a Class 1 Transient as one minus the sum of the probabilities of all the other initiating events.

6.2.5 Accident Sequences

Given that an initiating event has occurred, safety systems are required to operate in order to either prevent a core melt or to reduce the severity of its consequences. Event trees are used to identify the possible paths that a reactor could follow during a shutdown. These paths usually involve an accident and a subsequent failure of one or more safety systems.

The accident sequences for each event tree are input into SEISIM by specifying all the min cut sets associated with each sequence. Generation of these min cut sets is a two-step process. First, the safety and auxiliary systems whose success or failure determines the various accident sequences are analyzed for all their failure modes. Fault trees are developed for each safety or auxiliary system identified on the event trees. The fault trees for the systems are quantified by using standard Boolean reduction schemes. For the SSMRP, the computer codes SETS (Refs. 37, 38) and FTAP (Ref. 39) were used. In this section, we describe the event trees and the fault trees developed for the Zion systems.

6.2.5.1 Event Trees

An event tree is developed for each of the seven initiating events. Each of these is described below. More detail is provided in Vol. 8 of Ref. 1.

Vessel Rupture Event Tree

The vessel-rupture event tree developed for the SSMRP is shown in Fig. 6.4. It includes the functions of post-accident heat removal (PAHR) and post-accident radioactivity removal (PARR) from the containment, in both the injection and recirulation phases. In the injection phase, PAHR is accomplished by operation of (1) the CFCS(I), (2) the CSIS, or (3) a combination of the CFCS(I) and the CSIS.

In the recirculation phase, PAHR is accomplished by (1) the CFCS(R) or (2) a combination of the CSRS and the RHRS. PARR in this phase is performed by (1) the CFCS(R) or (2) the CSRS.

The event tree was constructed by considering the timing sequence of the accident as well as the functionability/operability relationships between systems. First, the heat and radioactivity removal capabilities of the CSIS and CFCS(I) during the injection phase are considered in event C. Given the success or failure of these systems in the injection mode, they are then considered during the recirulation mode. It is necessary to consider the CFCS and CSRS separately in this mode because the CFCS will fail in the recirculation mode if it failed in the injection mode, while the CSRS can succeed if the CSIS fails, because sufficient water will accumulate in the containment sump as a result of the vessel rupture to permit the RHR pumps to drive the CSRS headers and nozzles. Finally, given event F, heat removal from the containment is provided by the RHRS in those cases where the CFCS(R) does not function. Descriptions of the events and their success criteria have been described in Vol. 8 of Ref. 1.

Large LOCA Event Tree

The large LOCA event tree (LLOCA) is shown in Fig. 6.5. This event tree includes the functions of post-accident heat removal (PAHR), post-accident radioactivity removal (PARR), core reflood, and long-term heat removal. The event tree was constructed by considering the timing sequence of the accident, as well as the functionability/operability relationships between systems. Event A on the tree represents the large-LOCA accident initiator. Event C considers the heat-radioactivity-removal capabilities of the CSIS and CFCS(I) during the injection phase. Event D represents emergency core injection (ECI) or core reflood. The success criteria for this function have been previously defined. Event J is emergency core functionability (ECF). In event J, the ECI functions but, due to other factors, it is unable to reflood the core effectively. Events C, D, and J collectively make up the injection phase of the response to initiating event A.

The events which make up the recirculation phase are considered next. The first of these is event E, which represents the recirculation capability designed into the CFCS(R). Event F represents heat removal from unspecified damage or failures within the pressure vessel itself, so that ECI is provided by the RHRS for those cases where the CFCS(R) fails. Event G represents the recirculation capability of the containment spray system or CSRS. The CFCS

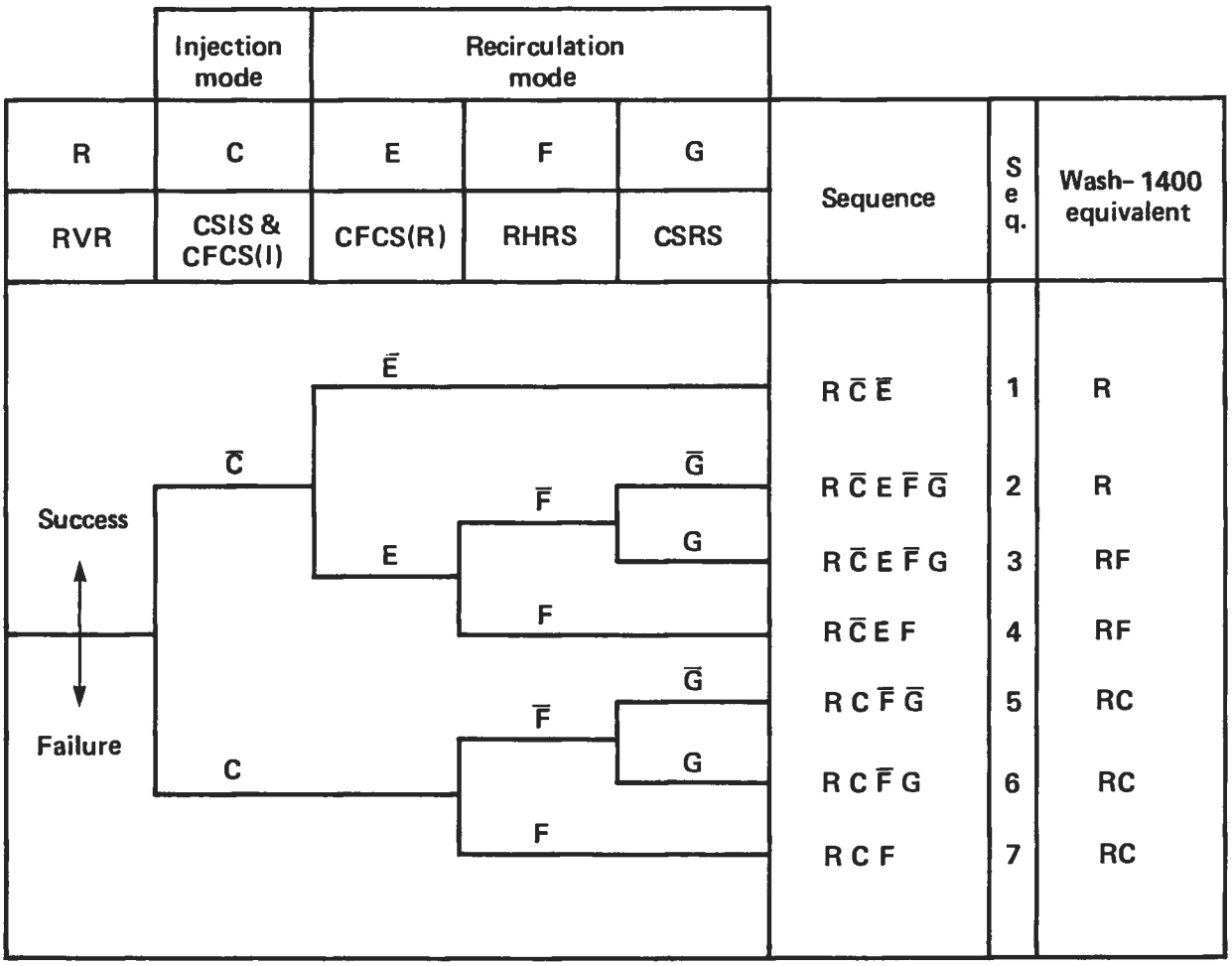

Fig. 6.4. Reactor vessel rupture event tree.

and CSRS are treated as separate events in this mode due to the assumption that the CFCS will fail in the recirculation mode if it failed in the injection mode, but the CSRS can succeed if the CSIS fails because the large LOCA will cause sufficient water to accumulate in the containment sump to permit the RHR pumps to drive the CSRS headers and nozzles. Event H represent emergency coolant recirculation (ECR). This event is concerned with the continual flow of water to the vessel in order to keep the core covered once it has been reflooded in the injection mode.

Of the 28 sequences in Fig. 6.5, the 5 marked with asterisks do not result in core melt. The fact that non-melt sequence numbers 5 and 19 are present illustrates one of the differences between the plant designs analyzed in the RSS and this study. In these sequences, failure of both CFCS(R) and CSRS (events E and G) implies that steam in containment will not be condensed--the containment will eventually rupture from overpressure. In the RSS, containment failure results in failure of the ECR function, since the PWR system design analyzed in the RSS required pressure in the containment to supply enough net positive suction head (NPSH) to operate the recirculation pumps. If the containment ruptures, sufficient NPSH to the pumps is lost, and

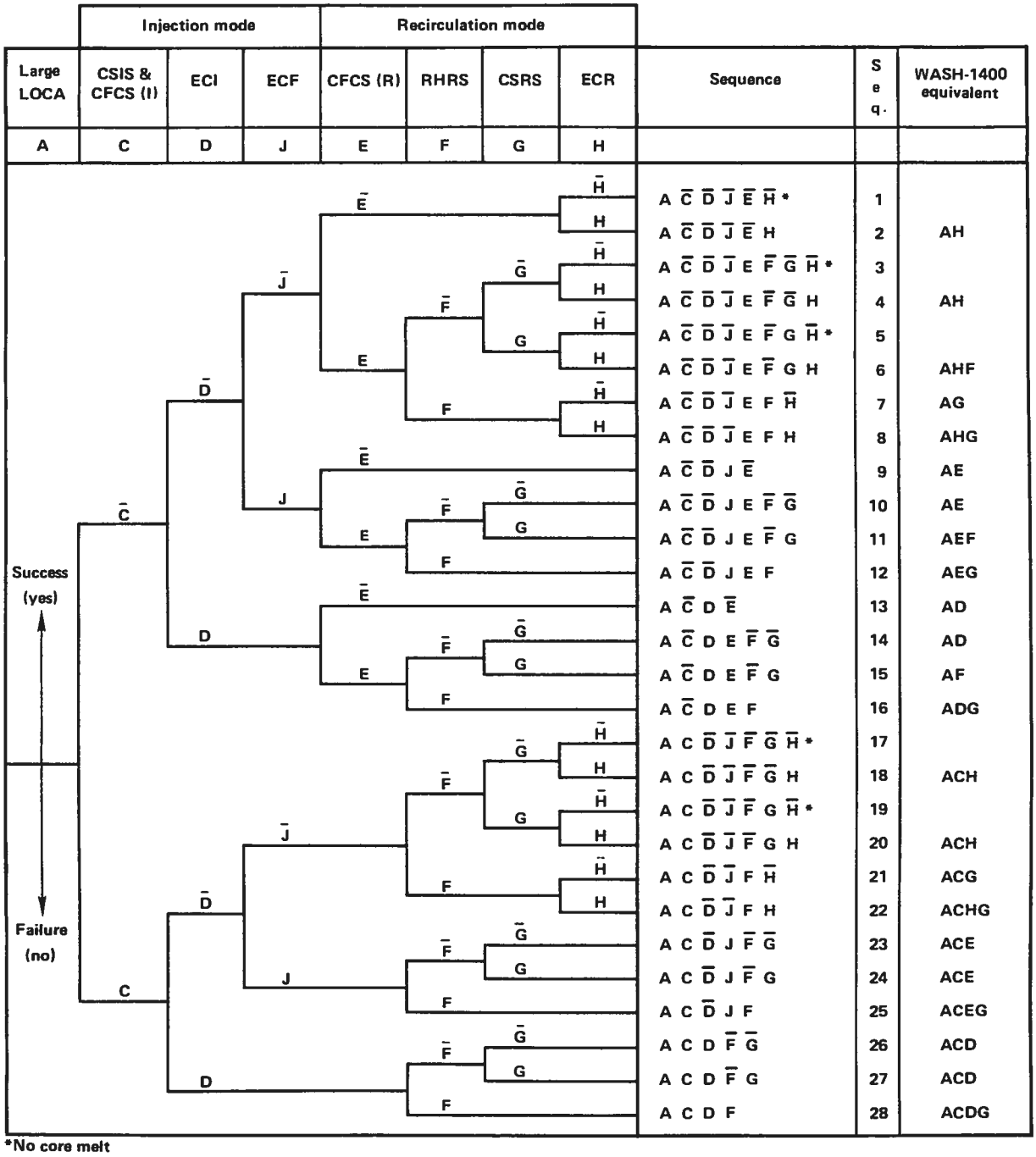

Seq.	Sequence	WASH-1400 equivalent
1	A C̄ D̄ J̄ Ē H̄ *	
2	A C̄ D̄ J̄ Ē H	AH
3	A C̄ D̄ J̄ E F̄ Ḡ H̄ *	
4	A C̄ D̄ J̄ E F̄ Ḡ H	AH
5	A C̄ D̄ J̄ E F̄ G H̄ *	
6	A C̄ D̄ J̄ E F̄ G H	AHF
7	A C̄ D̄ J̄ E F H̄	AG
8	A C̄ D̄ J̄ E F H	AHG
9	A C̄ D̄ J Ē	AE
10	A C̄ D̄ J E F̄ Ḡ	AE
11	A C̄ D̄ J E F̄ G	AEF
12	A C̄ D̄ J E F	AEG
13	A C̄ D Ē	AD
14	A C̄ D E F̄ Ḡ	AD
15	A C̄ D E F̄ G	AF
16	A C̄ D E F	ADG
17	A C D̄ J̄ F̄ Ḡ H̄ *	
18	A C D̄ J̄ F̄ Ḡ H	ACH
19	A C D̄ J̄ F̄ G H̄ *	
20	A C D̄ J̄ F̄ G H	ACH
21	A C D̄ J̄ F H̄	ACG
22	A C D̄ J̄ F H	ACHG
23	A C D̄ J F̄ Ḡ	ACE
24	A C D̄ J F̄ G	ACE
25	A C D̄ J F	ACEG
26	A C D F̄ Ḡ	ACD
27	A C D F̄ G	ACD
28	A C D F	ACDG

Fig. 6.5. Large LOCA event tree.

the pumps will activate and fail, causing loss of ECR and eventually core melt. The plant used in the present study does not require pressure in the containment to provide sufficient NPSH to the ECR pumps, so the ECR can function even if the containment fails (as it will for sequences 5 and 19). Thus, core melt can be prevented as long as both the ECR and RHRS are successful.

In three other ways this large-LOCA event tree differs from the equivalent tree in the RSS: (1) the addition of the CFCS, (2) the decision not to include electrical power, and (3) the sodium hydroxide addition (SHA) system. Loss of electrical power will be considered in the fault trees of the systems requiring electrical power. The SHA system was not included because its contribution to the post-accident radioactivity removal (PARR), as we know from WASH-1400 results, is not significant enough to merit inclusion in the event tree.

In summary, the large-LOCA event tree identifies 28 accident sequences involving the operation (and operability) of 6 safety systems: the CSIS & CFCS(I), ECI, CFCS(R), RHRS, CSRS, and ECR. Successful operation of these systems will prevent a large LOCA from resulting in a core melt accident.

Medium LOCA Event Tree

The medium-LOCA event tree developed for Zion is shown in Fig. 6.6. This event tree contains one event more than the large-LOCA tree for Zion. The addition is event K, the Reactor Protection System (RPS), which was not required in the large-LOCA tree because the very rapid blow-down and replacement of the coolant with highly borated water would bring the reactor to a subcritical point. The same effect would not occur in the medium LOCA (nor in the small or small-small LOCAs) because of the slower rate of blow-down. Thus, RPS is necessary on the medium-LOCA event tree. It is also important to note that the ECI and ECR functions (event D and H) have different success criteria for the medium LOCA than they do for the large LOCA.

There are five sequences which do not result in core melt. These sequences are nominally identical to the five non-melt sequences on the large-LOCA tree.

In summary, the medium-LOCA event tree identifies 35 accident sequences involving the operation or operability of 7 safety systems: the RPS, CSIS and CFCS(I), ECI, CFCS(R), RHR, CSRS, and ECR. Successful operation of these systems will prevent a medium LOCA from resulting in a core melt accident.

Small LOCA Event Trees

The small LOCA event tree developed for Zion is shown in Fig. 6.7. This tree is logically identical to the medium-LOCA tree because there are no significant differences in the functions required for the plant response to that break. The difference between the two break categories concerns only the success criteria for the ECI and ECR (events D and H). Since the small-LOCA and medium-LOCA event trees are logically identical, all of the descriptive text on the medium-LOCA tree applies to the small-LOCA tree. The small-LOCA event tree for Zion is a newly developed tree that was not done for the RSS.

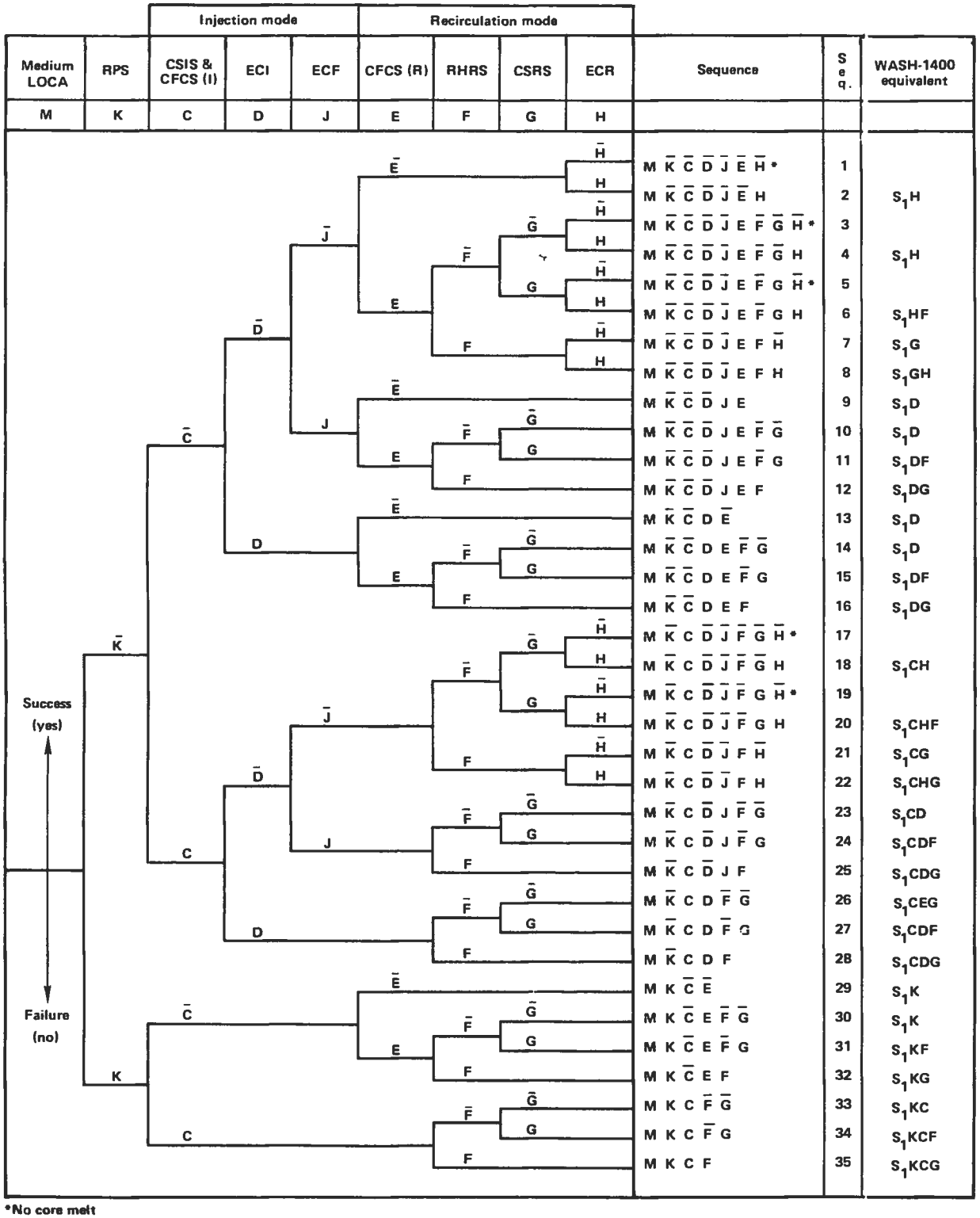

*No core melt

Fig. 6.6. Medium LOCA event tree.

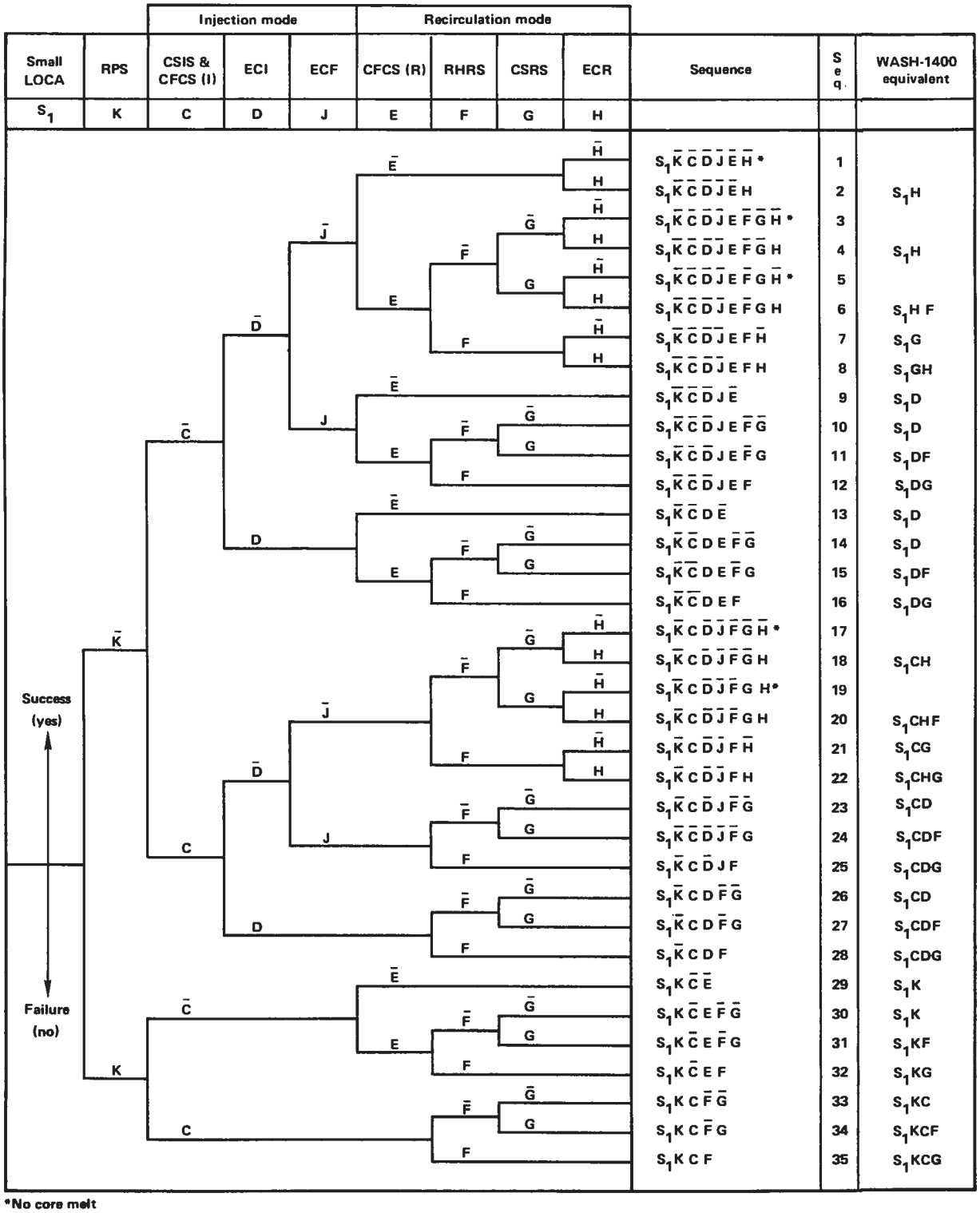

*No core melt

Fig. 6.7. Small LOCA event tree.

Small-Small LOCA Event Trees

Two small-small-LOCA event trees were developed for Zion. The first, shown in Fig. 6.8, assumes no feed-and-bleed capablity. The second tree, shown in Fig. 6.9, assumes that feed-and-bleed capability is available.

The small-small-LOCA event tree, assuming no feed-and-bleed capability, contains one more event than the small- and medium-LOCA trees for Zion. The addition is event L (the auxiliary feedwater system and secondary steam relief, AFWS and SSR), which was not required in the larger break LOCAs because the high blowdown rate would remove sufficient core heat to reduce RCS pressure. This would not occur in the small-small LOCA because of the slower blowdown. Thus, the AFWS and SSR are required to remove the excess heat. As in the previous event trees, the success criteria for ECI and ECR (events D and H) for the small-small LOCA differ from that of the other LOCA trees.

Descriptions of the events and their success criteria have been described in Vol. 8 of Ref. 1.

There are five sequences which do not result in core melt. These sequences are nominally identical to the five non-melt sequences on the other LOCA trees.

In summary, the small-small-LOCA event tree shown in Fig. 6.8 identifies 42 accident sequences involving the operation or operability of 8 safety systems: the RPS, AFWS & SSR, CSIS & CFCS(I), ECI, CFCS(R), RHRS, CSRS, and ECR.

For the small-small-LOCA event tree shown in Fig. 6.9, the feed-and-bleed procedure can be utilized for post shutdown decay heat removal. Feed-and-bleed can be utilized during small-small LOCAs and transients if the AFWS fails. To initiate feed-and-bleed, the operator must first recognize that the AFWS and secondary heat removal has failed, start a charging/safety injection pump and establish valve lineup if needed, open power-operated pressurizer relief valves and their associated block valves if required, and verify that adequate heat removal is taking place.

Transients with PCS (Tl) Event Trees

Two sets of transient event trees were developed for Zion. The first one, shown in Fig. 6.10, assumes that no feed-and-bleed is available. The second event tree, shown in Fig. 6.11, assumes that feed-and-bleed is available.

The event trees developed for transients with PCS (Tl) include all the functions required to bring the plant to a cold shutdown condition. Shutting down of the nuclear reaction is accomplished by the RPS. Removing the heat from the RCS is accomplished by either (a) the PCS or (b) the AFWS and SSR. Prevention of RCS overpressure is accomplished by S/RV-O. S/RV-R prevents the transient from becoming a LOCA. The CVCS maintains the water level in the reactor vessel, and the RHRS allows the plant to be brought to a cold shutdown.

There are six sequences on the event trees which lead to LOCAs. These are indicated on Fig. 6.10. It is important to note that even though core melt is conservatively indicated for these sequences, core melt is avoidable if the LOCA-mitigating systems are capable of functioning.

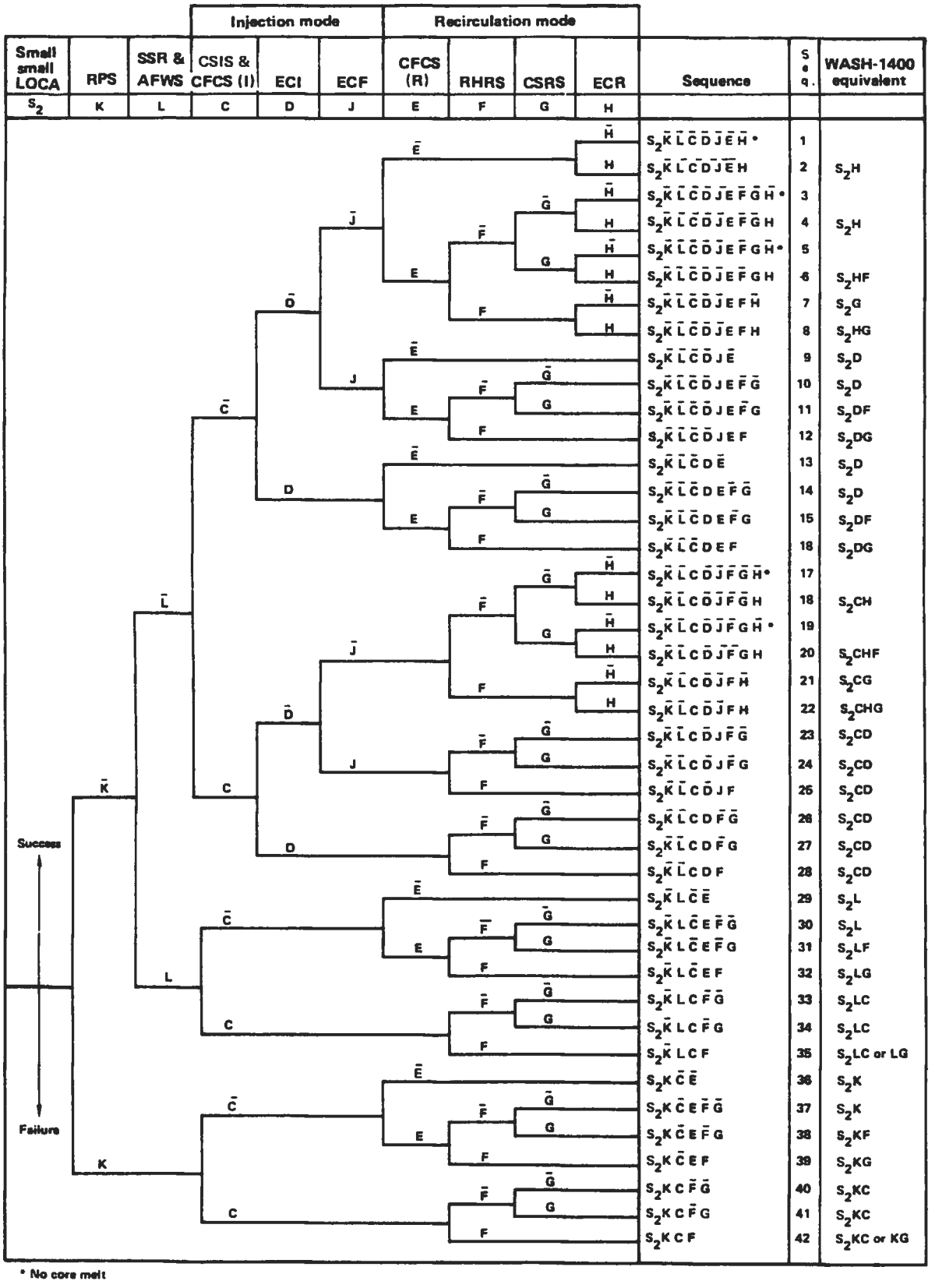

Fig. 6.8. Small-small LOCA event tree assuming no feed-and-bleed capability.

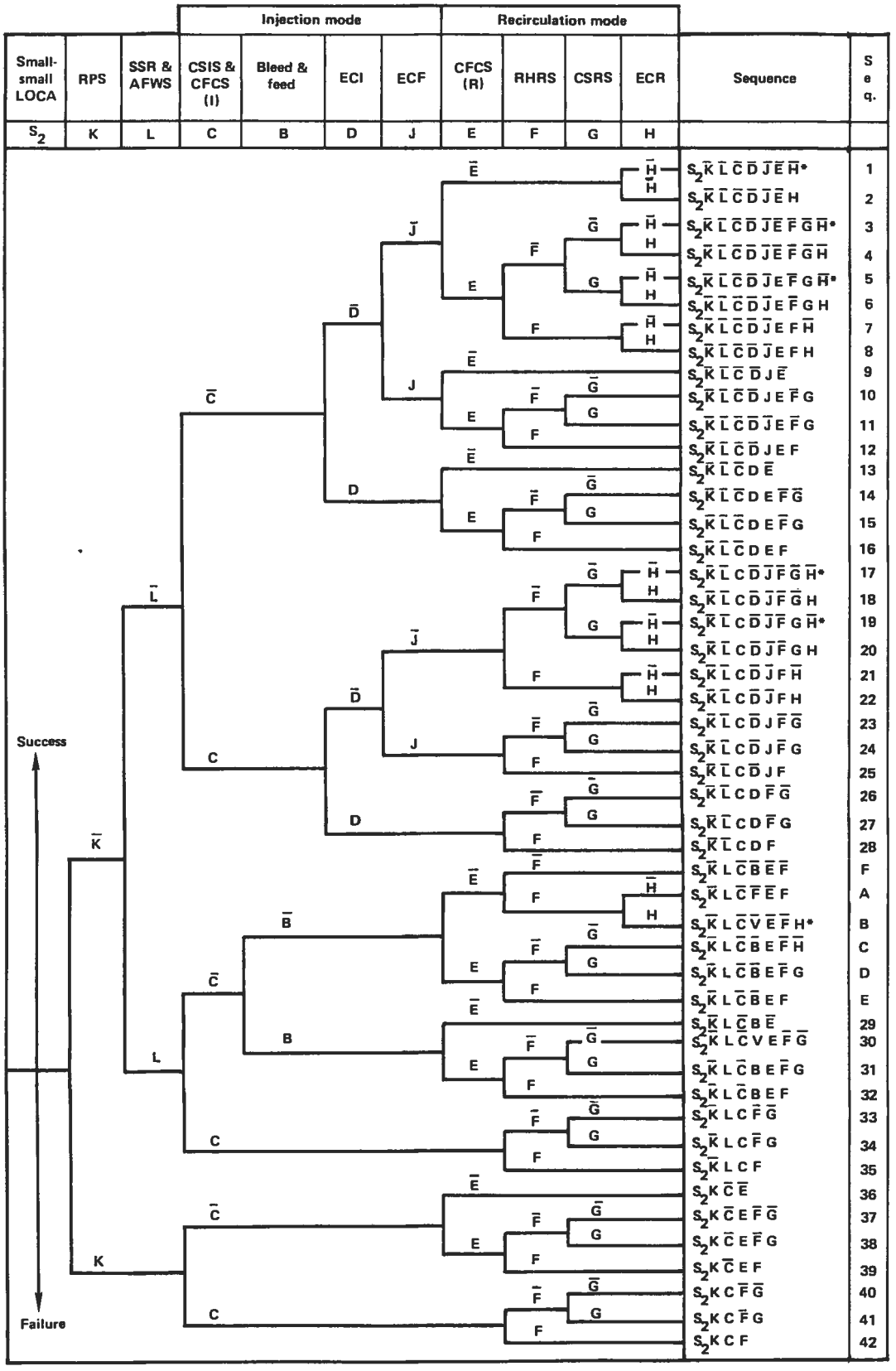

*No core melt

Fig. 6.9. Small-small LOCA event tree assuming feed-and-bleed capability.

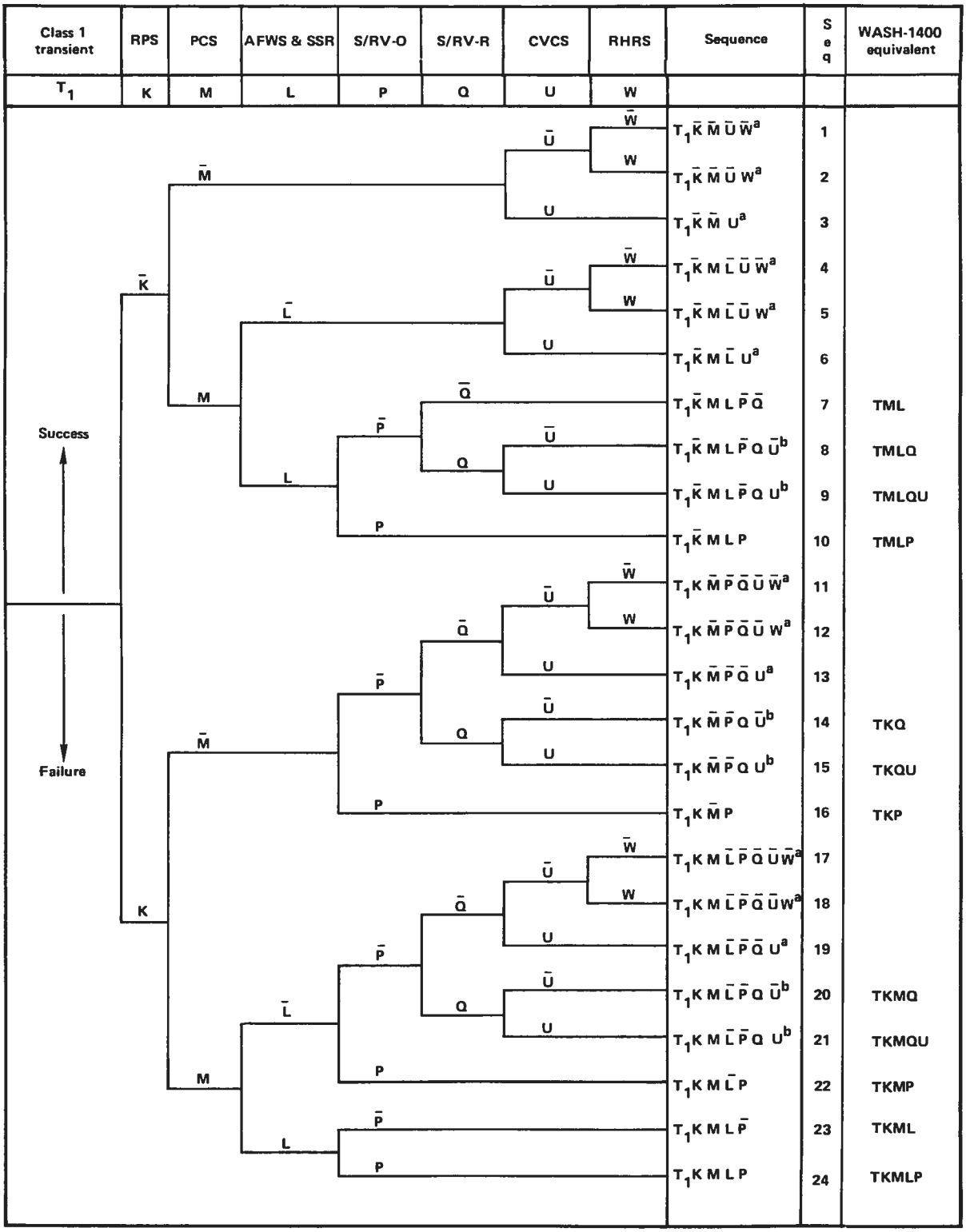

[a] No core melt

[b] These accident sequences include the events safety relief valve opens and fails to reclose which initiates a small-small LOCA. The small-small LOCA event tree is appended to the footnoted sequences.

Fig. 6.10. Class 1 transient event tree assuming no feed-and-bleed capability.

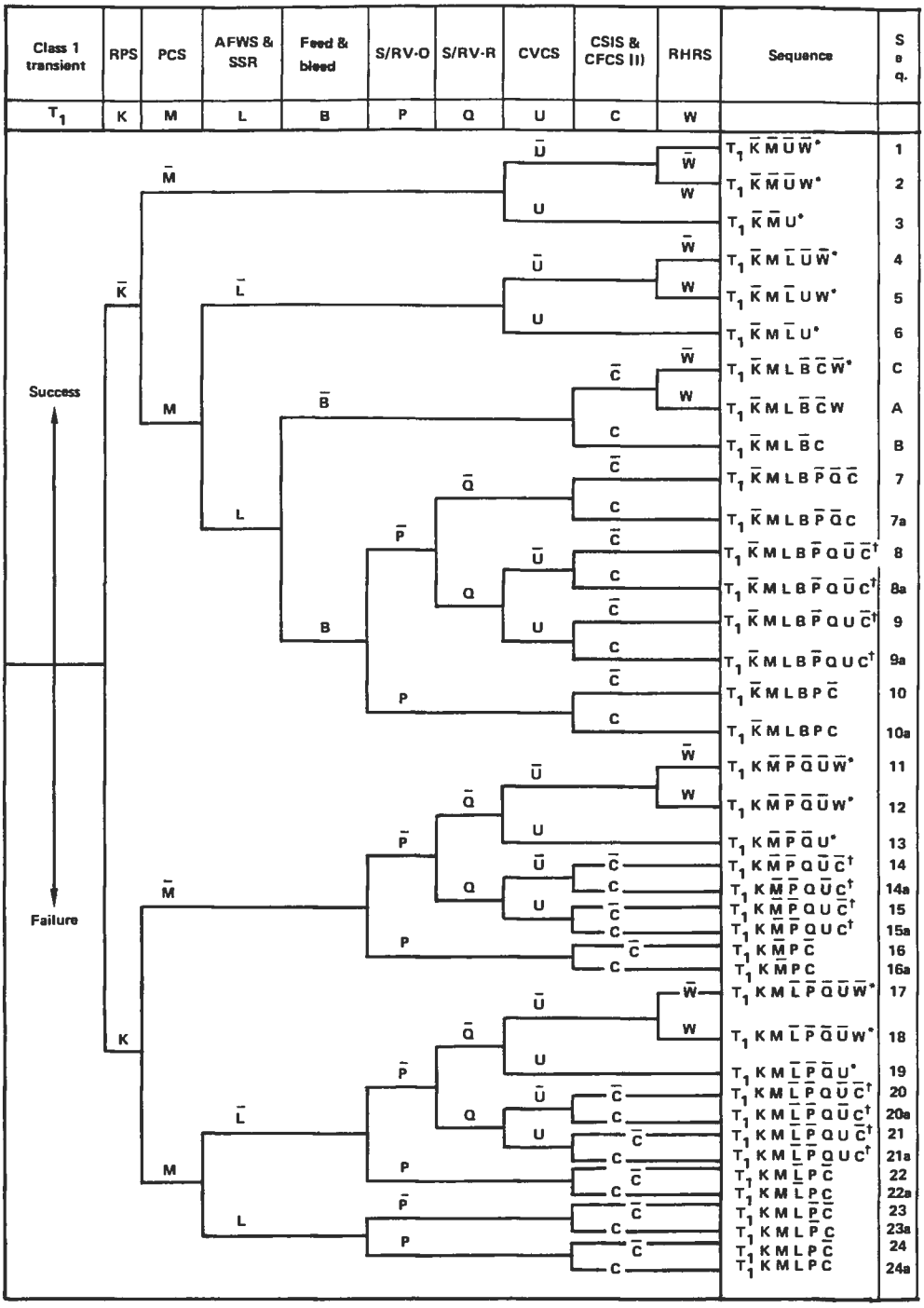

*No core melt

†These accident sequences include the following events: safety relief valve opens and fails to reclose, which initiates a LOCA. The LOCA event tree is appended to the footnoted sequences.

Fig. 6-11. Class 1 transient event tree assuming feed-and-bleed capability.

In summary, the Class 1 transient event trees identify accident sequences involving the operation (and operability) of seven mitigating systems: the RPS, PCS, AFWS & SSR, S/RV-O, S/RV-R, CVCS, and RHRS. Successful operation of these systems will prevent a Class 1 transient from resulting in core melt.

Transients without PCS (T2) Event Trees

Two T2 event trees were developed for Zion. The first one, shown in Fig. 6.12, assumes that no feed-and-bleed is available. The second event tree, shown in Fig. 6.13, assumes that feed-and-bleed is available.

The event trees developed for a Class 2 transient (T2) include the same functions as the Class 1 transient trees discussed in the previous section. The difference between the two trees is that in T2 the PCS will not be available to remove heat from the RCS, so that only the AFWS & SSR will be able to perform this function.

There are six non-melt sequences on the event trees. These sequences are indicated in Fig. 6.12. The reason for declaring these to be non-melt sequences is the same as that described in the previous section for the Class 1 transient trees. The sequences numbered 1-3 on the Class 2 transient trees correspond to the sequences numbered 4-6 on the Class 1 transient trees. The sequences numbered 8-10 on the Class 2 transient trees correspond to the sequences numbered 17-19 on the Class 1 transient trees.

There are four sequences on the event trees which lead to LOCAs. These are also indicated in Fig. 6.12. The explanation of these sequences is detailed in another earlier section and is the same as that for the similarly indicated sequences on the Class 1 transient tree.

In summary, the Class 2 transient event trees identified accident sequences involving the operation (and operability) of 6 mitigating systems: the RPS, AFWS & SSR, S/RV-O, S/RV-R, CVCS, and RHRS. Successful operation of these systems will prevent a Class 2 transient from resulting in a core melt.

6.2.5.2 Fault Trees

A fault tree is structured so that the undesired event (system failure) appears as the top event in the fault tree. The sequences of events that lead to the undesired event (high-order events) are depicted below the top event and are logically linked by branches to the undesired event by standard OR and AND gates. Those events that have a more basic cause (low-order events) are developed even further until the sequences finally lead to the primary causes for which there are failure rate data available. These primary causes appear as circles on the bottom of the fault tree and represent its limit of resolution. The fault tree technique has the advantage of locating only those system elements that contribute to the occurrence of the undesired event. Inductively finding these contributory components states (i.e., by a bottom-to-top evaluation) can be quite tedious and an almost impossible task because of the large number of component states that must be considered, particularly with complex systems. When the fault tree structure is complete, both qualitative and quantitative evaluation is possible. Of primary importance is the qualitative determination of the minimal sets of components that, when failed, will cause the system to fail. These sets are known as minimal cut sets.

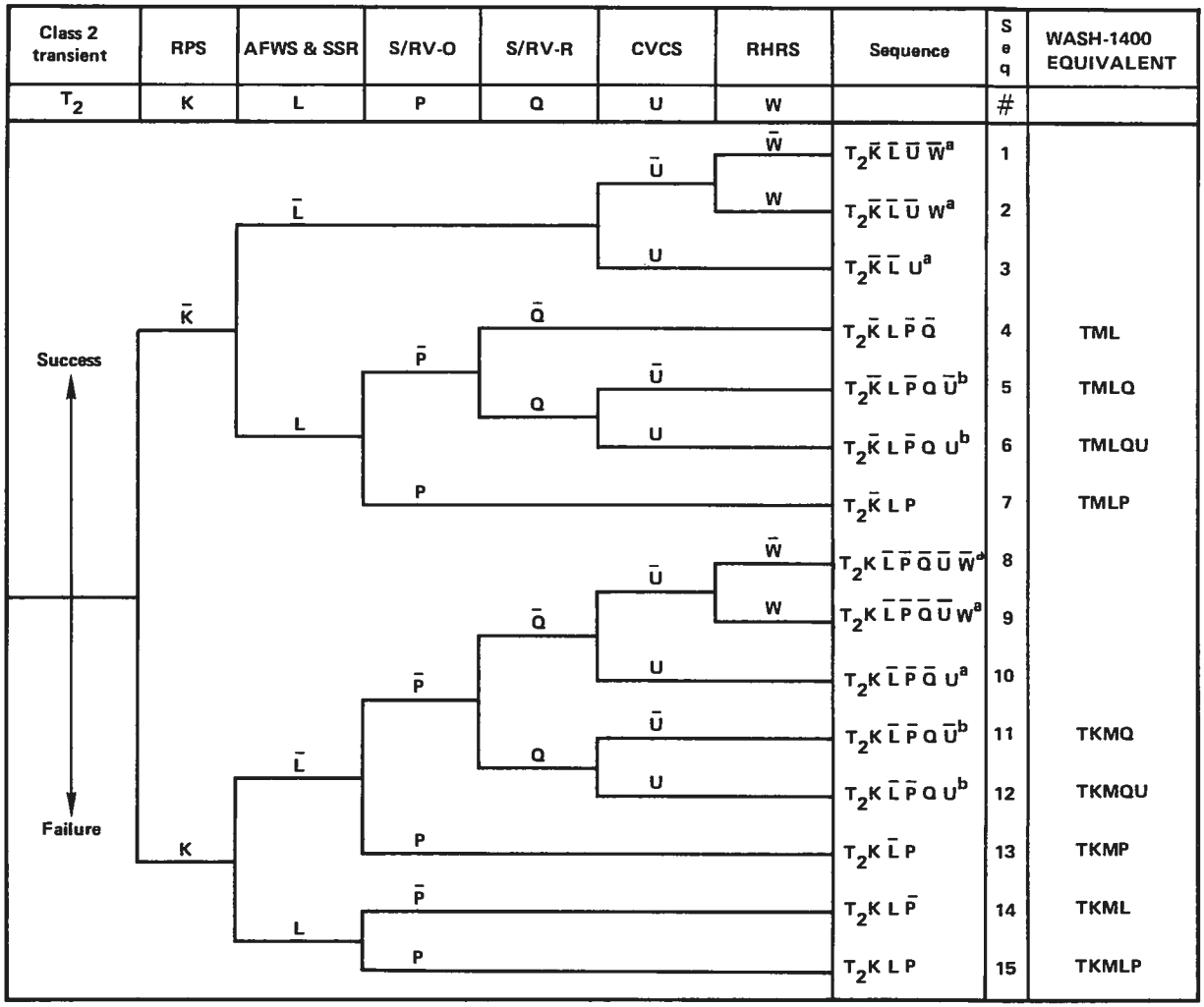

[a]No core melt

[b]These accident sequences include the events safety relief valve opens and fails to reclose which initiates a small-small LOCA. The small-small LOCA event tree is appended to the footnoted sequences.

Fig. 6.12. Class 2 transient event tree assuming no feed-and-bleed capability.

Fault trees are required for every system identified on the event trees. For the Zion plant, seven safety systems were modeled. Descriptions of these systems can be found in Appendix B. The emergency core-cooling system was modeled with fault trees for the Safety Injection System (SIS), charging system (CHG), residual-heat-removal System (RHR) and the accumulator system (ACC). The emergency core-cooling function is provided by different combinations of these systems in the injection and recirculation phases of a LOCA; the actual combination also depends on break size. The Auxiliary Feedwater System (AFWS) is of primary importance in a risk analysis, and a

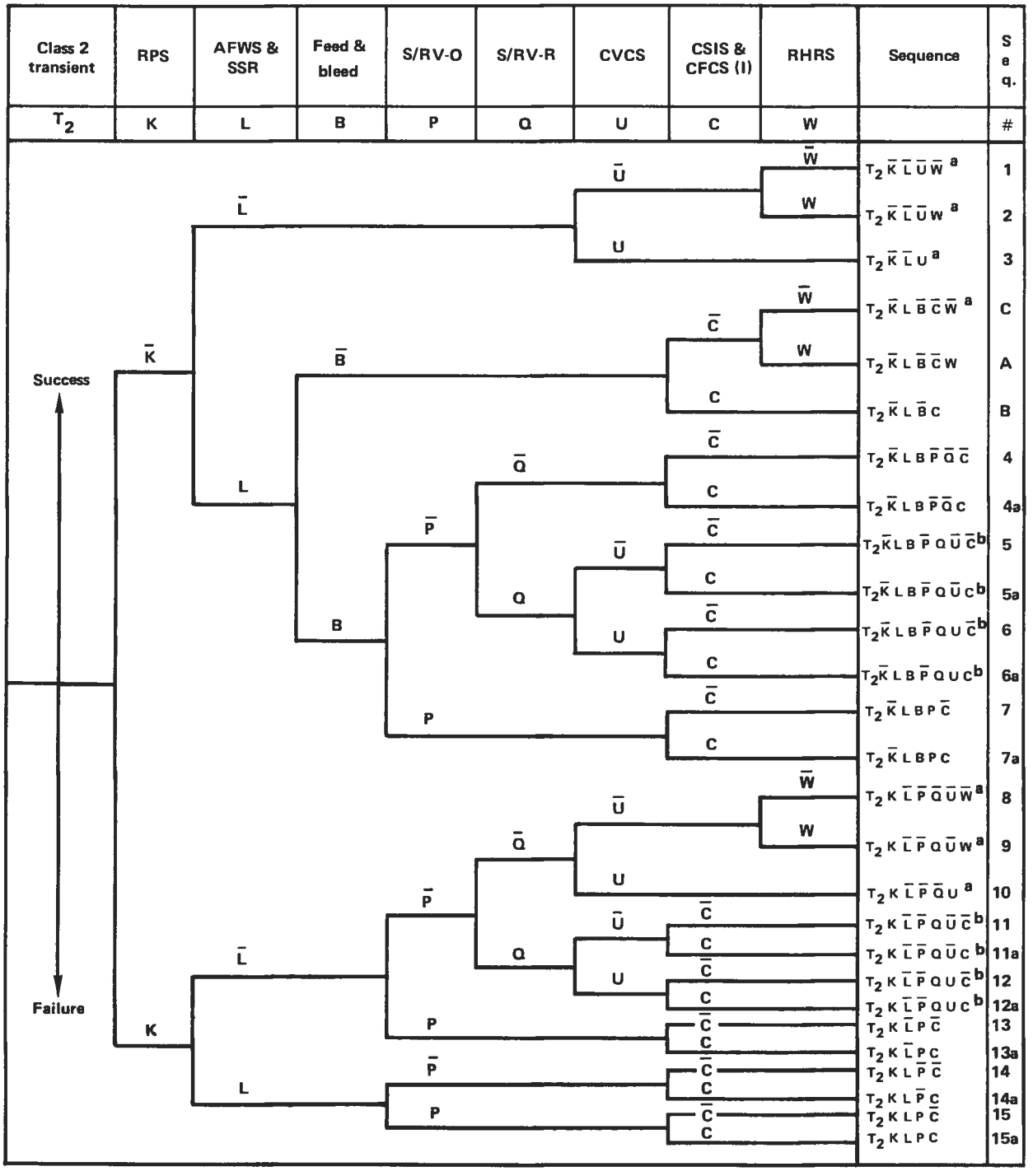

[a] No core melt

[b] These accident sequences include the following events: safety relief valve opens and fails to reclose, which initiates a LOCA. The LOCA event tree is appended to the footnoted sequences.

Fig. 6-13. Class 2 transient event tree assuming feed-and-bleed capability.

complete fault tree was developed for this system. All the above systems (except the accumulators) require both electric power and service water, so detailed fault trees were developed for both these systems. Prior to Boolean reduction and culling, the size of the resulting fault trees varied considerably, as shown below.

System	Number of basic events	Number of logic gates
ACC	54	17
SIS	242	117
RHR	309	130
CHG	378	172
AFWS	1288	786

The fault trees used in the Zion study contain two types of basic events. The first type were basic events whose failure probabilities are obtained by using response/fragility curves. These basic events are, typically, failures of hardware components. The second type are the random basic events. They consist mostly of non-hardware failures, such as human errors and other events. Their failure probabilities are randomly selected from a distribution which is defined for each event. In our study, all random basic events are treated as independent events.

A number of human error basic events were included on the fault trees. These events represent errors committed by plant personnel before, during and after the earthquake. They include operator errors, calibration errors, and maintenance errors. The human errors have been assigned failure probabilities based on available data, with corrections made to account for earthquake-induced operator stress. For simplicity, we assumed that the probability is not a function of the earthquake level.

A typical example of a human error is basic event MVD100760J, representing the leak or rupture of auxiliary feedwater isolation valve 0076 as a result of maintenance errors. This failure is not a function of earthquake level since the error preceded the earthquake.

Another example of a human error is basic event 6VG1013AOD, representing inadvertent operator closure of safety injection flow control valve 013A. Here, probability is dependent on earthquake level. Operator stress (and

thus, error probability) increases with the strength of the earthquake. However, this error may take place prior to the earthquake, divorcing it from the earthquake level. This and other complicating factors led us to assume that human error basic events were independent of earthquake magnitude.

Because of the size of system fault trees, a method was needed to reduce the resulting Boolean expressions. Probabilistic culling was selected (Ref. 40). Probabilistic culling discards cut sets that do not contribute signficantly to the probability of the top event. Cut sets do not contribute significantly if their probabilities are small. Because basic events in a cut set are dependent, it is not efficient to compute cut set probabilities in order to cull them. We can, however, compute bounds or approximations to cut set probabilities and cull them if the bounds or approximations satisfy some probability conditions.

We require that two conditions be satisfied before we discard a cut set. If the minimum of the basic event probabilities in a cut set is sufficiently small and if the product of basic event probabilties in a cut set is sufficiently small, we discard the cut set. The first criterion, culling on the minimum probability basic events, is needed because of the common-cause aspect of the problem. If all basic events are fully correlated, then the upper bound to the cut set probability is the probability of the minimum probability basic event. The second criterion, culling on the product of the basic event probabilities in a cut set, is based on the assumption that all basic events in the cut set are independent. A modified version of the FTAP computer program (Ref. 37) was used to generate the culled min cut sets.

The basic events which resulted after all fault trees were constructed fell into three categories:

Human and maintenance errors	583
Other random failures	20
Seismically-induced failures	1905

In all, 2508 basic events were considered.

6.2.6 Containment Event Trees

The containment event tree developed for the Zion PWR for use in the SSMRP analysis of earthquake-initiated events is shown in Fig. 6.14. It is similar to the event tree developed for random events in the Reactor Safety Study (RSS). This event tree identifies the same five failure modes for the PWR containment, as follows.

(1) Containment rupture due to a steam explosion in the reactor vessel.

(2) Containment rupture due to hydrogen burning, resulting in containment overpressure.

(3) Containment rupture due to overpressure from other physical processes.

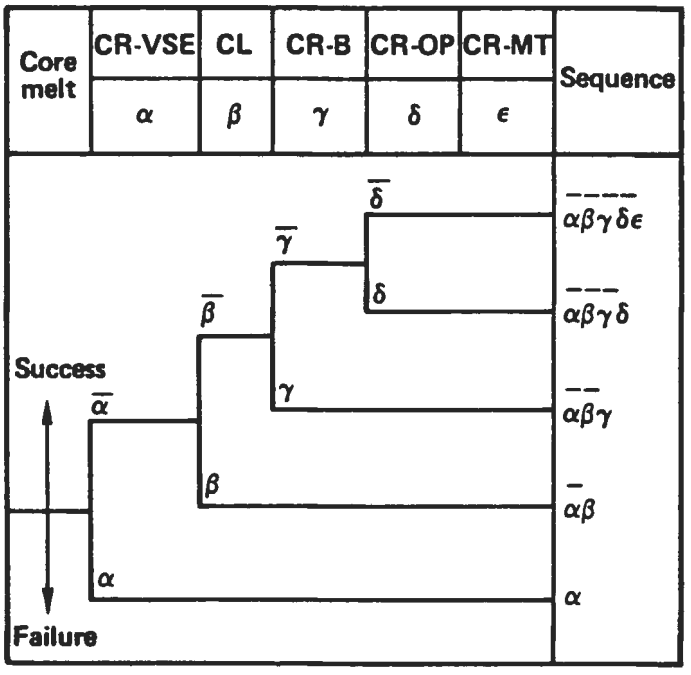

Fig. 6.14. Containment event tree.

(4) Containment failure due to melt-through of the containment basemat by the molten core.

(5) Failure of the containment to isolate--i.e., containment "leakage."

Definitions of the events used on the tree are compiled in Table 6.2.

The prime concern of containment analysis is the identification of the physical processes which can result in containment failure. An understanding of those physical processes is, in itself, of great importance in determining the consequences of a nuclear accident, because the consequences are dependent upon the timing of the radioactive release, the energy present in the containment at the time of containment failure, and the particular containment failure mode which occurs. This information is developed from evaluations of the accident sequences which are individually coupled to the containment event tree. The containment event tree thus provides the basic focal point for translation of an accident sequence probability into its associated environmental consequences. The containment failure mode probabilities and release category assignments are listed in Appendix C.

6.3 Uncertainty Analysis: Methodology and Design

A probabilistic risk assessment (PRA) involves estimation of the risk (i.e., frequency of radioactive release, core melt, etc.) associated with a damaging event such as an earthquake. The fact that the parameter of interest in a PRA is a probability recognizes that the damaging event (e.g., earthquake) as well

Table 6.2 Definition of events used on the containment event tree.

Event	Name	Description
α	CR-VSE	Containment Rupture--Vessel Steam Explosion. Steam flashing caused by the interaction of the molten core with water in the bottom of the reactor vessel causes vessel overpressure and subsequent shattering of the vessel. Missiles from the shattered vessel rupture the containment.
β	CL	Containment Leakage. Failure of the containment to completely isolate.
γ	CR-B	Containment Rupture--Burning. Hydrogen accumulated in the containment ignites, causing instantaneous overpressure, which ruptures the containment.
δ	CR-OP	Containment Rupture--Overpressure. Steam created in the core and released to the containment is not condensed by the containment ESF systems. The result is a slow buildup of containment pressure until overpressure occurs, which ruptures the containment.
ϵ	CR-MT	Containment Rupture--Melt-through. The molten core melts through the bottom of the reactor vessel and the containment basemat, thereby breaching the containment.

as the consequence event (e.g., core melt) are uncertain. Thus, the occurrence of these events must be expressed in terms of probability.

Strictly speaking, perhaps, an estimate of the probability or likelihood of an earthquake and a subsequent core melt and radioactive release should be based on actual experience. However, this is an unacceptable method, because the occurrence of such events as damaging earthquakes are rare and because a core melt occurrence would not be accepted by the general public. Thus, analytic and computer-based modeling methods must be used in a PRA. Their use introduces a second source of uncertainty.

In seismic risk analysis, it is important to recognize two types of uncertainty--random uncertainty and modeling uncertainty. The first, random uncertainty, is the inherent randomness associated with the occurrence of the events of interest. It is fundamental to the phenomenon being represented. The second type, modeling uncertainty, reflects incomplete knowledge of the models and calculational techniques used to estimate risk. Modeling uncertainty, in many cases, can be reduced within present limits of the state of the art by improved analytical models, tests, etc. Although general agreement exists that separating and identifying the two types of uncertainty is essential to a practical seismic risk analysis, judgment plays a paramount role in the process.

The importance of separating random and modeling uncertainty in a seismic risk analysis relates to their effect on the result--random uncertainty leads to a point estimate of the end items of interest (e.g., core melt frequency), whereas modeling uncertainty leads to a probability distribution on this frequency from which uncertainty intervals may be established.

In the SSMRP analysis, uncertainty in the seismic hazard characterization, seismic response of structures and components, and descriptions of structure and component failure was separated into random and modeling uncertainties; their combination reflects total uncertainty. Three sets of analyses were performed:

- Random variability, which may only be denoted best-estimate analysis.
- Total variability, which may be interpreted as an extreme case.
- Random/modeling uncertainty propagated separately, which yields uncertainty intervals on end items of interest.

The methodology to calculate the random variability only and the total uncertainty cases was described in Sec. 2.1. The separation of random and modeling uncertainty and the methodology that we used to propagate the two types of uncertainties through the probabilistic calculations is described here and is denoted "uncertainty analysis."

6.3.1 Methodology

The goal of the SSMRP uncertainty analysis was to describe the variation in the estimator of the frequency of radioactive release due to the uncertainties associated with the risk analysis techniques. Perhaps the optimal method for assessing the effect of analysis uncertainties on the estimator of risk would be to analytically propagate the uncertainties through the analysis. Because of the complexity of our analysis, this method was not practical. Instead, a Monte-Carlo simulation procedure was selected to assess the variation in the output probabilities due to modeling uncertainties. The procedure to propagate random and modeling uncertainties separately was a two-loop process--the outer loop treats modeling uncertainty and the inner loop treats random uncertainty. Several steps comprise the process. First, identify sources of modeling uncertainty in the seismic hazard characterization, seismic response and fragility descriptions, and systems models. Next, identify mechanisms to incorporate modeling uncertainty into the risk analysis and assign quantitative estimates of random and modeling uncertainty. Devise numerical experiments to perform the analysis--in our two-loop process, two experimental designs were constructed, one for the outer loop and one for the inner loop. Finally, perform the analyses. Each of these aspects is described.

6.3.1.1. Random and Modeling Uncertainty

To implement the computational procedure, the uncertainty in the seismic hazard characterization, seismic responses of structures and components, fragilities of structures and components, and systems models must be separated into random and modeling components.

Random uncertainty. Random uncertainty exists in each element of the seismic risk analysis.

- For the seismic hazard, random uncertainty is described by the seismic hazard curve itself, i.e., the probability per year that the Zion site experiences at least one earthquake of peak acceleration a. Also, random uncertainty is described by the ensemble of free-field acceleration time histories used in the SMACS analysis.
- For the seismic response step, many sources of random uncertainty exist--e.g., the properties of the soil, structures, and subsystems. For SMACS analyses, all sources of random uncertainty were assumed to be represented by a limited number of parameters of the models. For SSI, uncertainty was described by variability in soil shear modulus and material damping; in the structures and subsystems, variations in modal frequencies and modal damping were the mechanisms to describe uncertainty. The independent random variables in our SMACS analysis numbered 52--2 soil parameters, 2 structure parameters in each of the 5 structures analyzed (Zion unit 1 containment shell and internal structure, Zion unit 2 containment shell and internal structure, and the Zion AFT complex), and 2 each in the 20 piping systems analyzed. These parameters were assumed to be lognormally distributed and were varied by multiplying a nominal value, e.g., the nominal soil shear modulus, by a value selected from a lognormal distribution with median zero and coefficient of variation β_R. Table 4.5 itemizes the random variables in the seismic response calculations and their assumed random uncertainty (β_R). Additional detail concerning the values is contained in Chapter 4. The modus operandi of SMACS is simulation of earthquakes.
  Each simulation is for a sampled set of earthquake time histories and sampled values of the 52 input parameters. The values of the input parameters were sampled by a Latin hypercube procedure.
  The results of the SMACS analysis were estimates of the mean and variance-covariance of the responses of structures and components for the systems analysis.

- For the fragility phase of the analysis, random uncertainty is represented by the fragility function itself; i.e., the capacity of the component was assumed to be a random variable. For our analyses, lognormal distributions were assumed. The total number of fragilities in our analysis was 37.

Combining the seismic hazard, responses of structure and components, and fragility functions with the plant logic models permits calculation of a point estimate of risk with SEISIM.

Modeling uncertainty. Modeling uncertainty arises from our inability to precisely model all aspects of the phenomena. It exists in each element of the seismic risk analysis:

- The models used in the analysis, e.g., linear response models, lognormal distribution for capacities, system models, etc.

- Calculational methods, e.g., mathematical methods used for calculating responses, methods for combining probabilities, etc.

- Assessment of the model parameters, e.g., value of soil/structure/subsystem parameters, median capacities.

The principal source of modeling uncertainty is the use of expert opinion and engineering judgment. Some examples follow.

- The elicitation of expert opinions about zonation, seismicity and ground motion models in the region surrounding Zion. These opinions were used to estimate the hazard curves.

- The use of expert opinion and test data to estimate the medians and coefficients of variation for the fragility curves.

- The use of engineering judgment to estimate the medians and coefficients of variation of the soil/structure/piping parameters.

- The use of engineering judgment to estimate the probabilities of failures of unmodeled basic events.

One method to treat modeling uncertainty is to consider the estimates of the inputs to SEISIM as random variables--specifically the seismic hazard curve, the median values of the seismic responses of structures and components, the median values of the fragility functions, and the probability of failure of unmodeled systems. Two commonly used ways of doing this are:

- To consider a finite number of values for each parameter and associate a discrete probability distribution to the finite set to describe the uncertainty.

- To consider a continuum of values for each parameter and describe the uncertainty in terms of a cumulative distribution or probability density function.

Each area of modeling uncertainty is discussed here.

- For the seismic hazard, two major sources of modeling uncertainty can be identified--the phenomenon of local site amplification and development of the seismic hazard curve. Amplification of the free-field ground motion by a shallow soil site such as Zion (110 ft. of soil over bedrock) can have a profound effect on the seismic hazard curve and on the free-field acceleration time histories. Modeling of site amplification is discussed in Chap. 3. For our analyses, local site amplification was modeled explicitly in the seismic response calculations (SMACS) and in generation of the seismic hazard curve. This represented our best estimate of the effects of local site amplification. However, we recognize the large modeling uncertainty in all such models for the present state of the art. To assess the effect of local site amplification on seismic responses and seismic risk, two analyses were compared--our best-estimate analysis and a second analysis performed with free-field acceleration time histories uncorrected for local site effects and for a seismic hazard curve developed for a generic site condition. Details of the seismic input are contained in Chap. 3. Comparisons of seismic responses and risk are contained in Chaps. 4 and 7 respectively. The second principal source of modeling uncertainty in

the description of the seismic hazard at the Zion site was the differences of experts' opinions about the zonation and seismicity of the region surrounding the site. The variation in the seismic hazard due to different zonations and different levels of seismicity were incorporated into the uncertainty analysis by using the hazard curves based on the zonation and seismicity given by a subset of the experts used in the hazard analysis for the Zion site. Hence, this form of modeling uncertainty was represented by a family of equally probable seismic hazard curves used in our outer-loop calculation.

- For the seismic response step, recall that our end item of interest is variation in the median values of the seismic responses. To estimate this variation, SMACS analyses were performed as part of the two-loop computational procedure. Sources of modeling uncertainty were identified and quantified at the input phase to SMACS. In the same manner as for random uncertainty, a limited number of parameters was used to represent modeling uncertainty--soil shear modulus and material damping, structure frequencies and modal damping, and subsystem frequencies and modal damping. One major difference in the treatment of random and modeling uncertainty is the number of independent random variables--52 vs 8. Modeling uncertainty was associated with structure and subsystem type. Hence, modeling uncertainty was represented by: two soil parameters for SSI; two structure parameters for reinforced concrete structures; two structure parameters for prestressed concrete structures; and two subsystem parameters for piping systems. The variations introduced by these parameters was to represent uncertainty due to using engineering or expert opinions about the nominal value, and the biases that may be introduced by the models and analysis methods used in making the response calculations. These parameters were assumed to be lognormally distributed, on the general ground that uncertainty is usually well represented by this type of function. The mechanism to introduce this uncertainty was the application of a multiplication factor to the nominal value of the input parameter, e.g., soil shear modulus. This factor was selected from a lognormal distribution with zero median and coefficient of variation β_U. Table 4.5 itemizes these random variables and their assumed modeling uncertainty (β_U).

- For the fragility phase, modeling uncertainty was described by treating the median as a lognormal random variable. Again, this uncertainty was introduced in the analysis by multiplying the median capacity by a value chosen from a lognormal distribution with zero median and coefficient of variation β_U.

- Response calculations for certain subsystems were not performed and some components were not modeled. Thus, the probability of failure for these events was not assessed from a comparison of the responses and strengths of these units. Instead, the probability of failure was input directly into the systems analysis probability calculations. Because engineering judgment was used to assess these failure probabilities, the uncertainties associated with these assessments were included in the uncertainty analysis by treating the probability of failure for each unmodeled system as a uniform random variable.

6.3.2 Experimental Design

Recall that our computational procedure is a two-loop process--the outer loop treats modeling uncertainty and the inner loop treats random uncertainty. The parameters varied on the outer loop are the seismic hazard curve, the medians of the seismic responses (which results from the SMACS analyses), the medians of the fragilities, and the probability of failure of unmodeled systems. Usually, a simulation analysis such as the outer loop involves a large number of iterations of the basic risk analysis. However, the number of iterations can be reduced by appropriately choosing the sets of inputs to be used for each iteration. The basis of one such method is to choose the values for each input such that the entire range of values for the input is represented in the sample of inputs used. The designs of our outer and inner loops are based on such a method. Because of budget and other constraints, it was determined that the entire risk analysis could be replicated only a limited number of times. The number of iterations was limited to 14 assessments of risk. This, of course, involved many more runs of SMACS and SEISIM since, as you recall, SMACS and SEISIM analyses are made for a number of discretizations of the seismic hazard curve. In all of our cases, the seismic hazard curve was discretized into six acceleration levels (Chap. 3).

We used a Latin hypercube sampling procedure to select the parameter values for the inputs in the Zion risk analysis for the uncertainty study. Since the uncertainty study was limited to 14 assessments of the risk, the range of each of the parameters (e.g., the median of the fragility curve of a component) was partitioned into 14 non-overlapping subintervals spanning the parameter's range and having equal probability (based on the uncertainty distribution on that parameter) associated with them. A value was chosen, at random, from each subinterval, thus giving 14 equi-probable values for each parameter. By randomly combining values from the different subintervals for all parameters, 14 sets of values for the parameters are specified. These are the design points used for the uncertainty study. Combining the parameter values in this way assures that the entire range for each parameter is represented and each subinterval of the range is included only once in the sample. Each of the 14 design points represents a subregion of equal probability in the space of possible values for the parameters of the inputs into the risk analysis.

For the outer loop, a Latin hypercube sampling procedure was constructed for 8 response parameters and 37 fragility parameters, assuming 14 subintervals. Uncertainty in the seismic hazard was introduced by selecting hazard curves based on the opinions of 14 different experts. Uncertainty in the probability of failure for the unmodeled basic events is incorporated into the uncertainty analysis by randomly choosing 14 values from the appropriate uniform distribution. Each combination of values for the response parameters, fragility curves, probability of failure of unmodeled basic events, and a hazard curve represent one of the 14 design points in the uncertainty study.

One additional point should be made concerning the SMACS analyses. Section 6.3 described three sets of analyses:

- Random variability only.
- Total variability.
- Random/modeling uncertainty propagated separately.

In the first two sets, 30 earthquake simulations were performed for each interval of the seismic hazard curve. For the third set of analyses, 20 earthquake simulations were performed for each interval of the seismic hazard curve--i.e., the inner loop contained 20 earthquake simulations for each interval.

6.3.3 Flow Chart of Analysis

Graphical outline and flow diagrams of the SSMRP PRA methdology and the uncertainty analysis are presented in Figs. 6.15 and 6.16. Sequentially, the analysis involved

- A selection of design points, i, consisting of multipliers (δ_{il}:l = 1, 2, ..., 8) for the 8 response parameters (for soil shear modulus and soil material damping, frequency and damping for two structure types, and piping system frequency and damping) and multipliers (γ_{il}:l = 1,2, ...) for all fragility curves; a set of probabilities [$P_i(BE_q)$:q = 1, ... Q] for all unmodeled basic events; and a hazard curve, $HC_i = P_i(A > a)$.

- Given a hazard curve, a random sample of J = 20 earthquake time histories at each of K = 6 acceleration levels used as inputs into the SMACS response calculations.
  Note: Because of time and budget constraints, all 6 acceleration levels involving the 20 time histories were not analyzed. For 12 design points 2 acceleration levels were analyzed, each involving 20 time histories, and for the other 2 design points 3 acceleration levels were analyzed, each also involving 20 time histories. Thus, the total number of SMACS runs was 30 (12 x 2 + 2 x 3), each involving 20 time histories.

- To compute the frequency of core melt (radioactive release) using SEISIM, it is necessary to assess the probability of failure of basic events at all six acceleration levels. Thus, it was necessary to estimate the response parameters (i.e., the mean vector R and variance-covariance matrix $[\Sigma]_R$) at the acceleration levels for which these paramters are not determined directly in SMACS. A method to do this was developed. It is discussed in Appendix D.

- For a specific design point, the SMACS calculations were used to estimate the mean vector R and the variance-covariance matrix for the multi-dimensional distribution of responses. This input, along with the parameters of the fragility curve, is used in SEISIM to estimate the probability of failure for the modeled basic events.

- The probabilities of failure of the modeled and unmodeled basic events are combined to estimate the probability of initiating events and cut sets associated with the failure of safety systems.

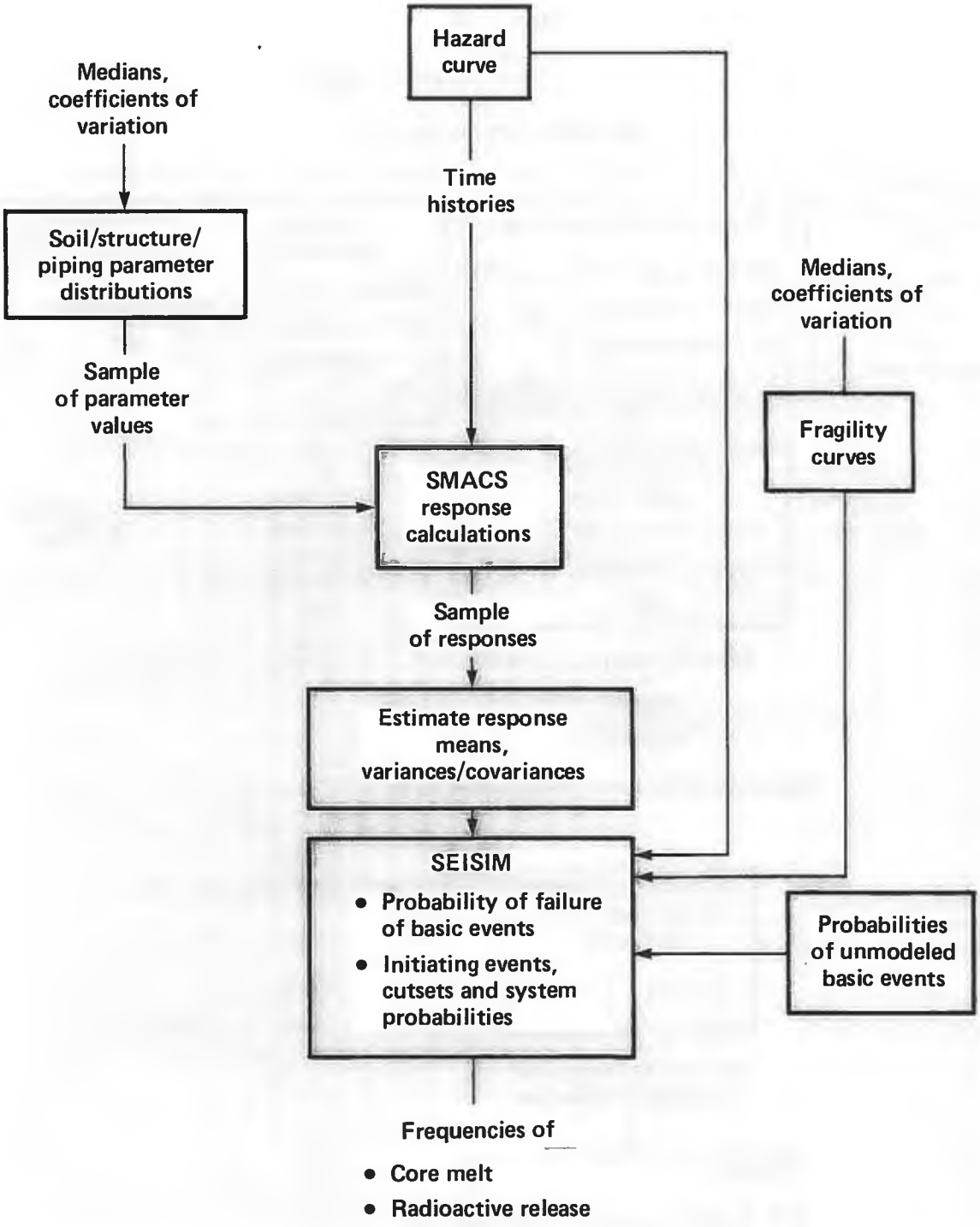

Fig. 6.15. SSMRP PRA methodology

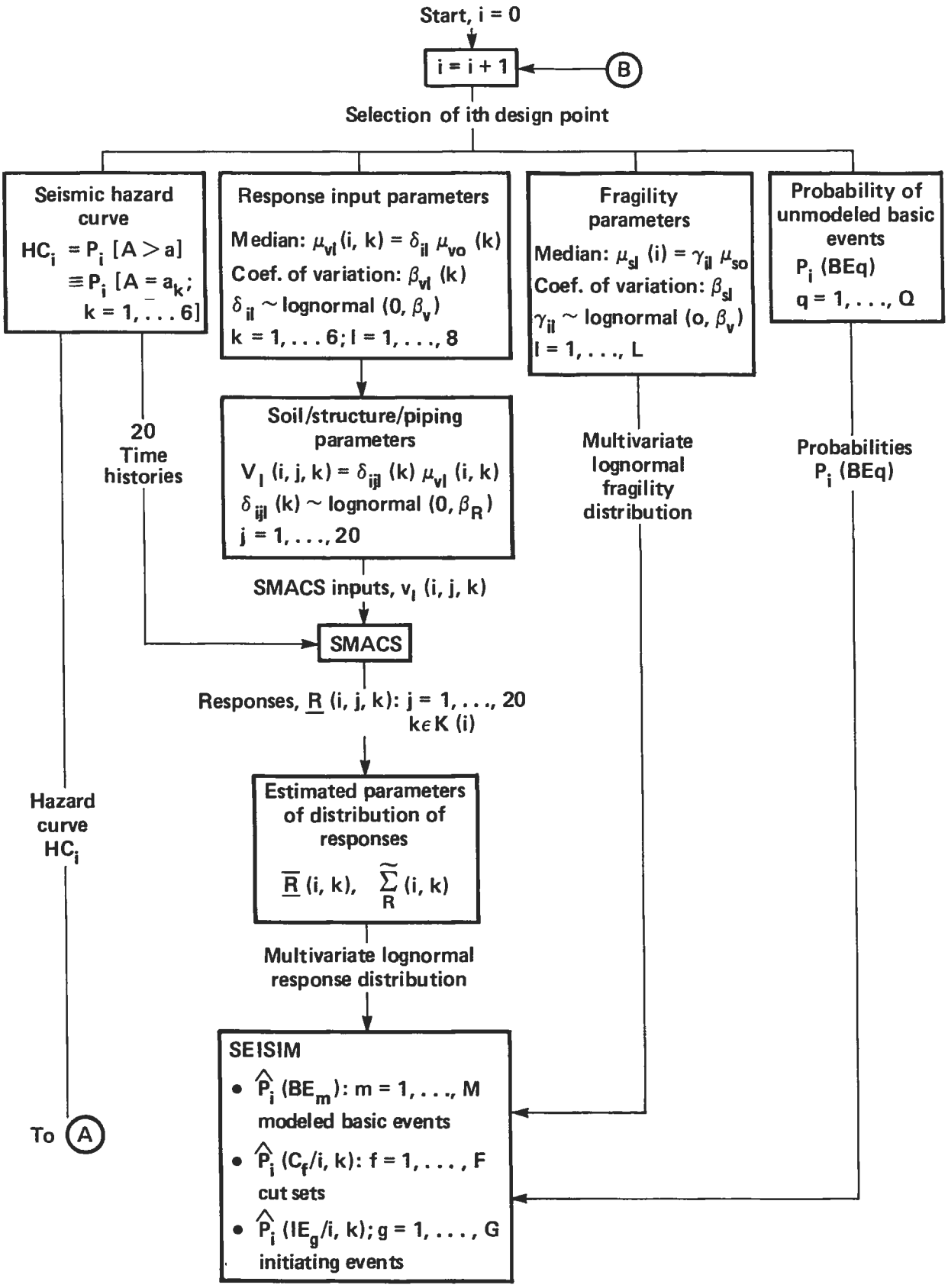

Fig. 6.16. Uncertainty analysis flow diagram

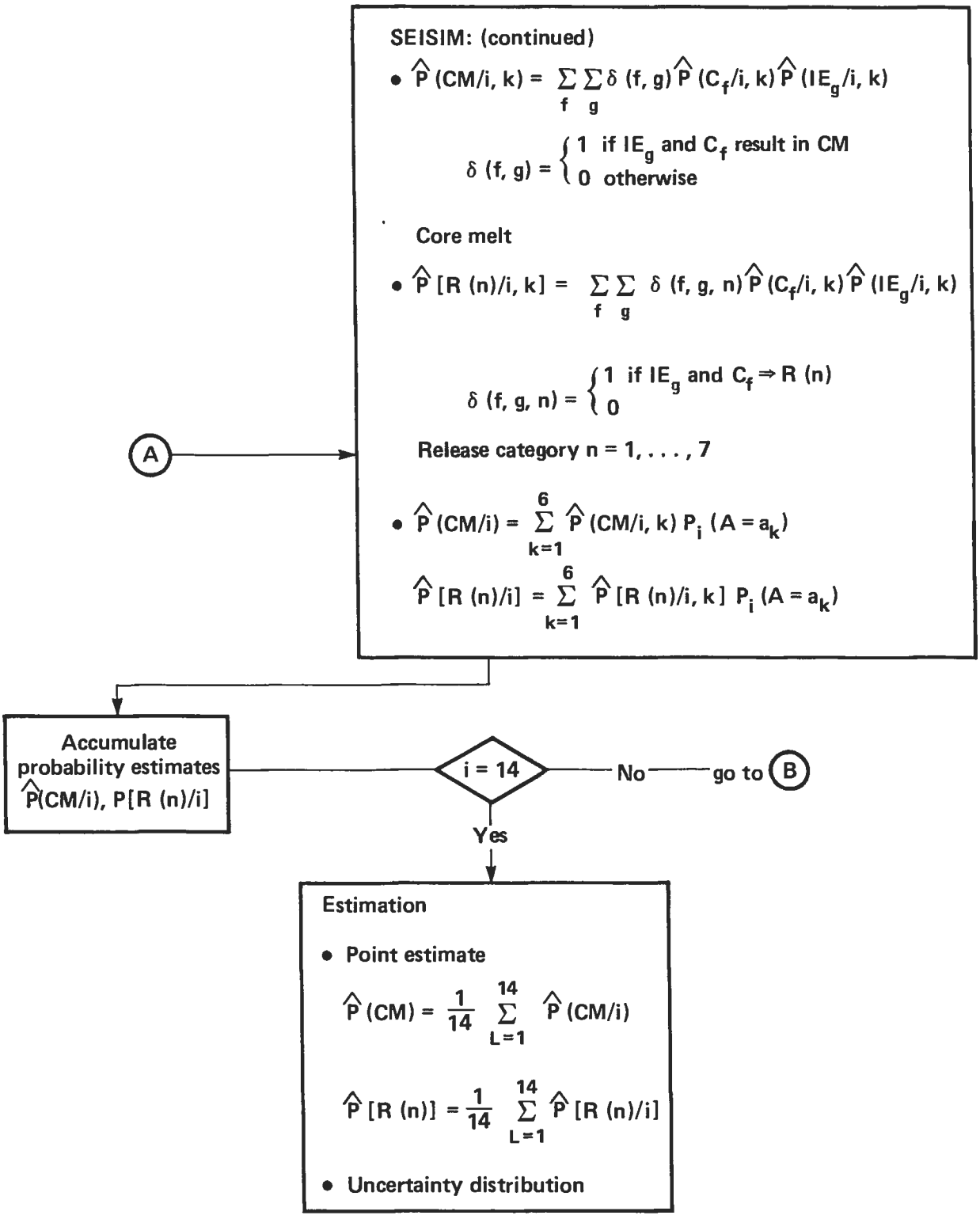

Fig. 6-16. (Continued).

- The probabilities of failure of the modeled and unmodeled basic events are combined to estimate the probability of initiating events and cut sets associated with the failure of safety systems.

- The probabilities of initiating events and cut sets are further combined in SEISIM to estimate the frequency of core melt and radioactive release for the seven release categories. These frequencies are estimated for six acceleration levels.

- Finally, the probabilities at the six acceleration levels are combined with the hazard curve to estimate the release frequencies.

- The analysis is looped through the I = 14 design points. Thus, there are 14 estimated values for P_r [Release (n)], n = 1, ... 7, which represent the variation in the estimated probabilities due to the uncertainties associated with the input parameters and the risk analysis methodology.

- The 14 accumulated probabilities can then be combined to:

  1. Evaluate a point estimate median of each probability.

  2. Estimate the cumulative distribution function for the uncertainty distribution of each probability. A plot of the estimated cumulative distribution function for release frequency is presented in Fig. 7.1. From this distribution the median and other percentiles (e.g., the 10th and 90th percentiles) can be determined.

PART II: RESULTS

CHAPTER 7: RESULTS OF ZION RISK ANALYSIS AND UNCERTAINTY INTERVALS

This chapter presents the results of the base-case calculations for the seismic risk analysis of the Zion nuclear power plant. Calculations to estimate the median core melt frequency and the uncertainty bounds are also described.

The base case described in this chapter is our best estimate of the configuration of the Zion plant and its emergency procedures. A number of important assumptions are described below.

1. It is assumed that "feed-and-bleed" emergency core cooling can be performed after an earthquake. In this procedure, which is employed if the auxiliary feedwater system has failed, the operator makes use of the emergency safety pumps to pump cooling water to the core. The resulting steam is bled off through the pressurizer relief valves.

2. The identified structural failure modes are assumed to have the most serious consequences. Two structural failure modes play crucial roles.

   (i) The failure of the roof of the service-water pump enclosure in the crib house is assumed to fail all six service-water pumps. This results in loss of the emergency AC power diesel generators, due to lack of cooling water.

   (ii) The failure of the wall between the turbine building and the auxiliary building is assumed to cause loss of all electrical power and control circuits between the auxiliary building and the containment.

   Both of these failures are assumed to fail the SIS, CHG, CSIS, and CSRS safety systems.

3. Soil failure under the toe of the containment is assumed to result in rocking motions large enough to to fail the SIS, CHG, RHR, CSIS, and CSRS piping between the AFT building and the reactor building.

4. Failure of the vertical column supports under the steam generators and reactor coolant pumps is assumed to result in a double-ended guillotine break of the primary coolant piping equivalent to a large LOCA. Two support failures in different loops are equivalent to a RVR.

These assumptions all play crucial roles in the base-case results. In Chapter 8, the results of cases selectively varying these assumptions are presented.

In the base case, it was also assumed that the reactor coolant pump seals do not fail due to failure of the crib house pump enclosure. This failure scenario would be: (1) earthquake occurs, (2) roof of the crib house pump enclosure falls on the service-water pumps, disabling them, (3) loss of AC power, (4) diesels start, but shut down because they lack cooling from the service water, (5) loss of offsite power has tripped the reactor coolant pumps, and (6) Zion is therefore in a station blackout. At this point in the

scenario the reactor coolant pump seals are of concern. They may be cooled either by the component-cooling water system (CCWS) or the high-pressure injection charging pumps. The CCWS has failed because of failure of the service water. The charging pumps are disabled due to the station blackout. Therefore, the seals are not cooled. It is our understanding that the pump manufacturer would not guarantee the seals for more than 30 minutes without cooling, even if the pumps were in a static condition. In that case, failure of a seal on a pump will result in a 300-gpm LOCA after 30 minutes. With four pumps, the total leakage rate is 1200 gpm, and all safety systems are disabled by the station blackout. We feel that the leak rate of 300 gpm and the time to failure of 30 minutes are conservative estimates. The effect of this seal failure assumption on the Zion analysis may be significant. In the current analysis, if a station blackout and uplift occurs, then the core cannot be cooled. This has the same effect as a coolant pump seal rupture.

This chapter is divided into two sections. The first section gives the results of a single calculation of the base case in which all random input variables have variance due only to random uncertainty. (The definitions of random and modeling uncertainty were presented in Chapter 2 of this report.) In effect, this random uncertainty case represents the risk at Zion computed with all specified random input variables having their medians set equal to their best-estimate values.

In the second section, the results of the uncertainty bound calculations are presented. In each of these runs, the effects of modeling uncertainty have been incorporated in a systematic way, so as to allow the estimation of uncertainty bounds on the risk results.

7.1 Release Category Frequency--Random Uncertainty Only

Table 7.1 summarizes the results of the risk calculations for the base case. This table presents the frequencies per year of occurrence of the seven release categories and the man-rem per year associated with each release category. As can be seen from this table, the release categories having the highest frequency of occurrence are release categories 2 (containment failure due to steam explosion with failure of CSIS and CSRS) and 7 (melt-through the basemat) with frequencies of occurrence of 1.4E-6 and 1.5E-6 per year, respectively. The released radiation comes from release categories 2 and 3 (containment failure due to overpressure). (The conversion of release category frequencies to man-rem/year released is based on averaged values for a PWR taken from NUREG/CR-2800 and are not specific to Zion.) The total frequency of core melt is seen to be 3.6E-6 per year and the total release is 9.6 man-rem/year. As will be seen below, these release category frequencies are due primarily to the failures of certain local structural elements and inter-building piping that result in common-cause failures of the safety systems.

Table 7.2 provides more detail as to how the frequencies are distributed among the six earthquake levels. In terms of both release and dose, it is noted that earthquake levels 2, 3, and 4 are dominant. We notice that the frequencies of occurrence and the man-rem appear to drop off in earthquake levels 1 and 6. This indicates that we have captured the bulk of the risk in the middle earthquake level categories, and that the range of earthquakes considered is adequate.

Table 7.1 Summary of release frequency and dose for the base case (with feed-and-bleed and structural failures).

Release category	Release frequency/yr	man-rem/yr
1	2.9E-8	0.2
2	1.4E-6	6.5
3	5.4E-7	2.9
4	0	0
5	8.3E-10	0
6	1.7E-7	0
7	1.5E-6	0
Total	3.6E-6	9.6

Table 7.2 Release categories and frequencies of release per year for the base case (with feed-and-bleed and structural failures).

Release category	Earthquake level 1	2	3	4	5	6	Total	man-rem/yr
1	3.08E-13	4.16E-11	3.09E-9	1.27E-8	7.62E-9	5.92E-9	2.94E-8	0.16
2	1.38E-8	2.77E-7	6.13E-7	2.61E-7	1.06E-7	8.29E-8	1.35E-6	6.50
3	3.74E-10	3.62E-9	1.18E-8	4.27E-7	8.09E-8	1.49E-8	5.39E-7	2.91
4	0	0	0	3.73E-11	4.87E-11	6.25E-12	9.22E-11	0
5	3.81E-12	1.41E-11	9.34E-12	2.91E-10	4.51E-10	6.26E-11	8.32E-10	0
6	7.24E-16	1.11E-13	4.32E-12	1.19E-7	3.96E-8	5.92E-9	1.65E-7	0.025
7	4.40E-9	8.44E-8	7.68E-7	3.80E-7	1.73E-7	5.19E-8	1.48E-6	0.03
						Grand total	3.57E-6	9.63

It will be recalled from Chapter 2 that the release category frequencies are computed from the sums of all the terminal event sequences which contribute to that category, and that each terminal event sequence is computed from the product of an initiating event probability, an accident sequence probability, a containment failure mode probability, and an earthquake probability. We can identify the dominant initiating events, dominant component failures and dominant accident sequences by examining these three elements separately.

For example, Table 7.3 shows the probabilities of the seven initiating events for each of the six earthquake levels. It can be seen from this table that, at the three lower earthquake levels, the initiating events are dominated by the transients T1 and T2. At earthquake level 4, it is primarily the small and small-small LOCAs and T2 which are important. At earthquake level 5 the

Table 7.3. Conditional probabilities per year of initiating events for the base case (with feed-and-bleed and structural failures).

Initiating event	Earthquake acceleration level					
	1	2	3	4	5	6
RVR	0	7.4E-7	7.7E-3	9.7E-3	1.7E-1	5.3E-1
LLOCA	0	2.2E-5	1.8E-2	3.8E-2	1.9E-1	2.5E-1
MLOCA	1.1E-4	6.0E-5	1.1E-2	3.6E-2	5.5E-2	3.4E-2
SLOCA	2.0E-4	6.5E-4	8.7E-2	2.6E-1	3.0E-1	1.6E-1
SSLOCA	1.4E-3	1.1E-2	1.5E-1	2.8E-1	1.9E-1	2.4E-2
T2	2.7E-1	8.1E-1	7.3E-1	3.7E-1	9.2E-2	2.8E-3
T1	7.3E-1	1.8E-1	6.0E-4	1.1E-6	3.5E-8	0

initiating event probabilities are fairly evenly spread over the initiating events, and the LLOCA and RVR initiating events have become a significant factor in the analysis. Finally, at level 6 it is seen that the RVR and LLOCA are the dominant initiating events. Thus, we see that as we increase the level of earthquake excitation the contribution of the more severe initiating events increases.

The initiating event for the two transients is primarily the loss of offsite power by failure of the ceramic insulators at the point where offsite power is brought into the switch yard. (This is considered an initiating event only if none of the four LOCAs has occurred.) The component failures which cause the LLOCA and the RVR initiating events are the failure of the primary coolant piping due to the failure of the supports of the steam generators and reactor coolant pumps. Without these two failures the initiating events for the LLOCA and RVR would be significantly smaller. Thus, it can be seen that it is not failure of the piping which results in a LLOCA or RVR, but rather the possibility of failure of the supports of the major components.

Table 7.4 presents the dominant accident sequences. This table shows the dominant accident sequences, the associated initiating event, and the resulting terminal event sequence frequency. The dominant component failures are indicated on this table, and the key to the dominant failures is given on Table 7.5. The terminal event sequence frequency is that number which is added directly into the release categories. The terminal event frequencies, therefore, determine which accident sequences are dominant. At the lower three earthquake levels, both the release category frequencies and the exposure are dominated by release categories 2 and 7. At levels 1 and 2, the release is due almost entirely to the transient accident sequences T2-4 and T1-7. Both are caused by failure of the auxiliary feedwater system due to structural failures. The uplift of the containment basemat causes failure of the AFWS pipes, and is also assumed to fail the containment sprays and the containment fan coolers. Since the containment sprays fail, the release in

Table 7.4. Characteristics of dominant accident sequences of the base case (with feed-and-bleed and structural failures).

	Initiating event	Accident sequence	Containment failure mode	Terminal event seq. probability per yr	man-rem/yr	Dominant components
Release category 2:						
Acceleration level 1	T2	4	Gamma	1.13E-9	0.01	Uplift, roof
	T2	4	Delta	2.65E-9	0.01	Uplift, roof
	T1	7	Gamma	3.03E-9	0.01	Uplift, roof
	T1	7	Delta	7.06E-9	0.03	Uplift, roof
Acceleration level 2	T2	4	Gamma	6.84E-8	0.33	Uplift, roof
	T2	4	Delta	1.60E-7	0.77	Uplift, roof
	T1	7	Gamma	1.48E-8	0.07	Uplift, roof
	T1	7	Delta	3.44E-8	0.17	Uplift, roof
Acceleration level 3	T2	4	Gamma	1.75E-7	0.84	Uplift, roof
	T2	4	Delta	4.08E-7	1.96	Uplift, roof
	SSLOCA	35	Gamma	1.8E-8	0.09	Uplift, roof
	RVR	7	Gamma	6.6E-9	0.03	Uplift, roof
	SSLOCA	35	Delta	5.9E-9	0.03	Uplift, roof
Acceleration level 4	T2	4	Delta	1.4E-7	0.67	Uplift, roof
	T2	4	Gamma	6.0E-8	0.29	Uplift, roof
	RVR	7	Gamma	1.0E-8	0.05	Uplift, roof
	SSLOCA	35	Delta	7.9E-9	0.04	
Acceleration level 5	RVR	7	Gamma	5.7E-8	0.27	Uplift, roof
	T2	4	Delta	1.6E-8	0.07	Uplift, roof
	RVR	6	Gamma	8.95E-9	0.04	CSIS & CFIS(I) CSRS
	T2	4	Gamma	6.7E-9	0.03	Uplift, roof
	SSLOCA	35	Gamma	6.5E-9	0.03	Uplift, roof
Acceleration level 6	RVR	7	Gamma	7.6E-8	0.36	Uplift, roof

Table 7.4. (continued)

	Initiating event	Accident sequence	Containment failure mode	Terminal event seq. probability per yr	man-rem/yr	Dominant components
Release category 3:						
Acceleration level 4	SLOCA	21	Delta	2.6E-7	1.40	Pipe doubles
	SSLOCA	21	Delta	1.45-7	0.78	Pipe doubles
	MLOCA	21	Delta	2.4E-8	0.13	Pipe doubles
Acceleration level 5	SLOCA	21	Delta	6.6E-8	0.35	Pipe doubles
	SSLOCA	21	Delta	9.3E-9	0.05	Pipe doubles
Release category 5:						
Acceleration level 4	SSLOCA	C	Gamma	2.9E-10	0	None
Acceleration level 5	SSLOCA	C	Gamma	4.5E-10	0	None
Acceleration level 6	SSLOCA	C	Gamma	6.3E-11	0	None
Release category 6:						
Acceleration level 4	T2	4	Epsilon	4.8E-8	0.01	Uplift, roof
	SSLOCA	34	Epsilon	3.7E-8	0.005	Uplift, roof
	LLOCA	27	Epsilon	2.6E-8	0.004	Single pipe
	MLOCA	27	Epsilon	5.7E-9	0.001	
Acceleration level 5	LLOCA	27	Epsilon	2.35E-8	0.004	Single pipe
	SSLOCA	34	Epsilon	5.52E-9	0.001	Uplift, roof
	T2	4	Epsilon	5.31E-9	0.001	Uplift, roof
	SSLOCA	D	Epsilon	3.12E-9	0	

Table 7.4. (continued)

	Initiating event	Accident sequence	Containment failure mode	Terminal event seq. probability per yr	man-rem/yr	Dominant components
Release category 7:						
Acceleration level 1	T2	4	Epsilon	9.00E-10	0	Uplift, roof
	T1	7	Epsilon	2.40E-9	0	Uplift, roof
Acceleration level 2	T2	4	Epsilon	5.3E-8	0	Uplift, roof
	T1	7	Epsilon	1.17E-8	0	Uplift, roof
Acceleration level 3	T2	4	Epsilon	1.4E-7	0	Uplift, roof
	LLOCA	13	Epsilon	2.2E-7	0	Single pipe
	SSLOCA	35	Epsilon	1.2E-7	0	Uplift, roof
	SLOCA	28	Delta	4.4E-8	0	Uplift, roof
	SLOCA	28	Epsilon	4.3E-8	0	Uplift, roof
	RVR	1	Epsilon	9.4E-8	0	ECRL supports
	MLOCA	13	Epsilon	4.8E-8	0	ECI
Acceleration level 4	SSLOCA	35	Epsilon	1.6E-7	0	Uplift, roof
	SLOCA	28	Epsilon	7.9E-8	0	Uplift, roof
	SLOCA	28	Delta	7.8E-8	0	Uplift, roof
Acceleration level 5	SSLOCA	35	Epsilon	4.5E-8	0	Uplift, roof
	SLOCA	28	Epsilon	2.9E-8	0	Uplift, roof
	SLOCA	28	Delta	2.8E-8	0	Uplift, roof
	LLOCA	28	Epsilon	2.7E-8	0	Uplift, roof
	LLOCA	28	Delta	2.6E-8	0	Uplift, roof
	MLOCA	28	Epsilon	7.5E-9	0	Uplift, roof
	MLOCA	28	Delta	7.4E-9	0	Uplift, roof

Table 7.5. Key to dominant component failure groups.

Key	Components failing
Uplift	Relative motion between AFT and reactor buildings failing all pipes in ECCS, RHR, AFWS, CSIS and CSRS.
Roof	Failure of the roof of the crib house service-water pump enclosure.
Shear wall	Failure of shear wall between auxiliary building and turbine building.
Single pipe 1	Pipe 6OH1005A in RHR system failing between AFT and reactor building.
Single pipe 2	Pipe ZOI1006A in RHR system failing between AFT and reactor building.
Single pipe 3	Pipe of the auxiliary steam supply line to the turbine-driven auxiliary freedwater pump.
Pipe pairs	These are 3 pairs of pipes running between the AFT and reactor buildings. Failure of any pair fails the RHR system. The pairs are defined by pipe numbers: 6OH1005A and 6OH1004A 6OH1005A and ZOH1001B 6OH1005A and ZOH1001C
Electrical pairs	These are 15 pairs of electrical bus and relay failures in the ESF power trains. Failure of any pair cuts off power to lube oil pumps in the AFWS.
Valve out/CST	This is a double consisting of the lockout of valve TVD1-OA and failure of the condensate storage tank.

T2-4 and T1-7 is assigned to release category 2 (80%) and release category 7 (19%). A second contributor to sequences T2-4 and T1-7 is failure of the crib house service-water pump enclosure room roof slab. This is assumed to fail the six service-water pumps, which in turn fails the diesel generators due to lack of cooling water. This, in conjunction with loss of off-site power, results in loss of all AC power, and hence loss of both the AFWS[a] and, again, the containment sprays.

[a] When the Zion AFW System was modeled, the turbine-driven AFW pump required AC power for its lube oil pump. Loss of AC power would therefore fail the turbine-driven AFW pump. It is our understanding that this situation has changed and that the turbine-driven AFW pump no longer requires AC power for its lube oil pump.

These two failures (uplift and roof) determine the release in categories 2 and 7 at earthquake levels 1 and 2. At earthquake level 3, accident sequence T2-4 is a dominant contributor to release categories 2 and 7, but now other sequences also become important. Sequence SSLOCA-35 occurs, due to the same two structural failures caused by T2-4. There is a small contribution of sequences RPV-1 and RPV-7 from failure of the supports of the steam generator and reactor coolant pump. In addition, for category 7 there are significant contributions from SLOCA-28 (which is caused by the uplift and pump room roof failures) and from LLOCA-13. The large LOCA initiating event is again failure of supports of the steam generator or reactor coolant pumps, and the sequence occurs due to failure of emergency coolant injection because of failure of a single pipe in the ECCS. This pipe failure occurs between the reactor and AFT buildings due to relative motion of the two buildings.

For earthquake levels 4, 5 and 6, significant contributions are found from release category 3 as well as from 2 and 7. For the upper three earthquake levels, the containment sprays are assumed to have failed from ground shaking alone. (For levels 1, 2 and 3, the containment sprays were assumed to have failed only in those accident sequences caused by the structural failures.) Release category 2 is dominated by the same sequences as discussed for level 2 (for the same reasons) except that at levels 5 and 6 the RVR sequence is the largest contributor. Release category 3 is due almost entirely to accident sequences SSLOCA-21, SLOCA-21 and MLOCA-21, which all occur due to the failure of pairs of pipes between the reactor and AFT buildings. These pairs of pipes are failing because the movement of the buildings is not the same. Failure of any one of these pipe pair combinations causes failure of both emergency core injection and the RHR system. The release in category 7 at the upper earthquake levels is due to accident sequences SLOCA-28 and SSLOCA-35. These are both the result of loss of emergency core cooling due to uplift and service-water pump enclosure roof failures.

In summary, it can be seen that of the total 9.6 man-rem/year, approximately 6.1 man-rem/year is due to accident sequences caused directly by the uplift and crib house pump room roof failures, and 2.7 man-rem/year is due to failures of pairs of pipes between the reactor and AFT buildings. At the three lower earthquake levels, transient accident sequences predominate, while at the upper three earthquake levels the smaller LOCAs predominate. Thus it is seen that, for the base-case computations of the seismic risk at Zion, the structural failures and the assumptions as to their consequences play an overriding role.

7.2 Uncertainty Interval Calculations

The procedure used to develop uncertainty intervals was presented in Chapter 2. This procedure involved running SEISIM by selecting values of uncertain parameters based on their probability distributions. The two-loop procedure was described in Chapter 6. Values of the medians of all input parameters were selected in the outer loop, and then SMACS and SEISIM calculations were used in the inner loop to compute point estimate probabilities (conditional on the parameter values). This procedure provided not only the median frequencies of release, but also a measure of uncertainty in the probability values. The release category frequencies are shown in Fig. 7.1. Also shown in Fig. 7.1 are bounds for the frequency of release, which

represent the 10th and 90th percentile limits on the release frequencies for a given release category. Figure 7.2 provides a measure of the core melt frequency per year. This curve was obtained using the 14 runs described in Chapter 2. The curve indicates that the frequency of radioactive release (per year) has a median value of 1E-5. The upper 90% and lower 10% limits are approximately three order of magnitude apart.

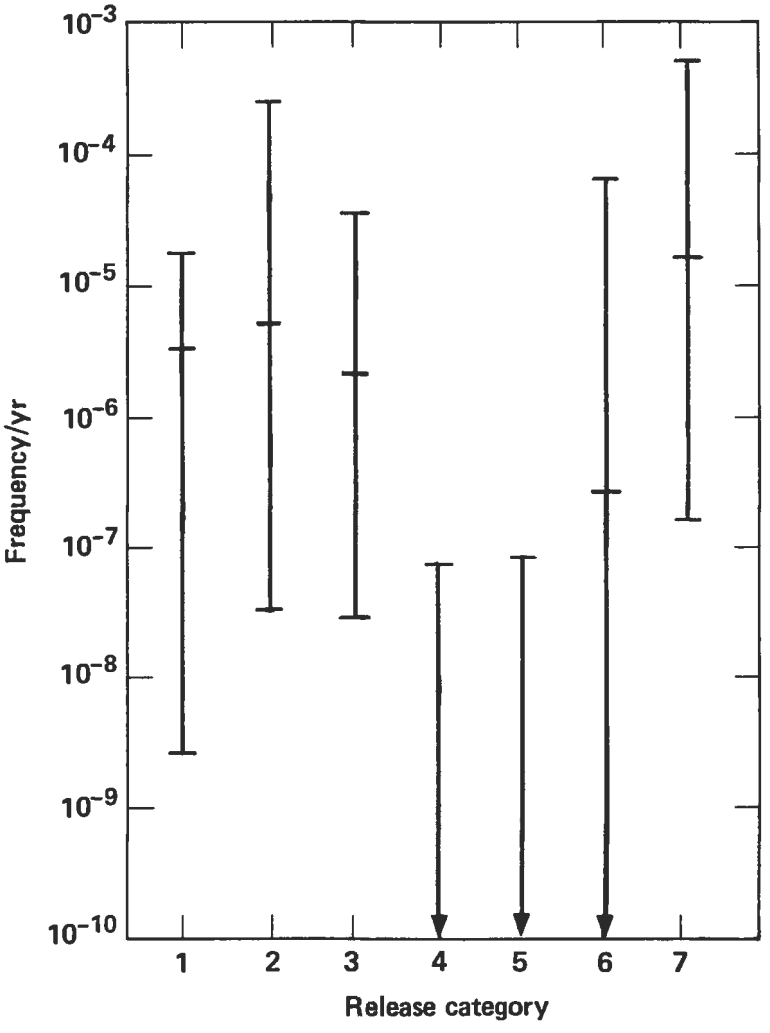

Fig. 7.1. Uncertainty intervals on release categories.

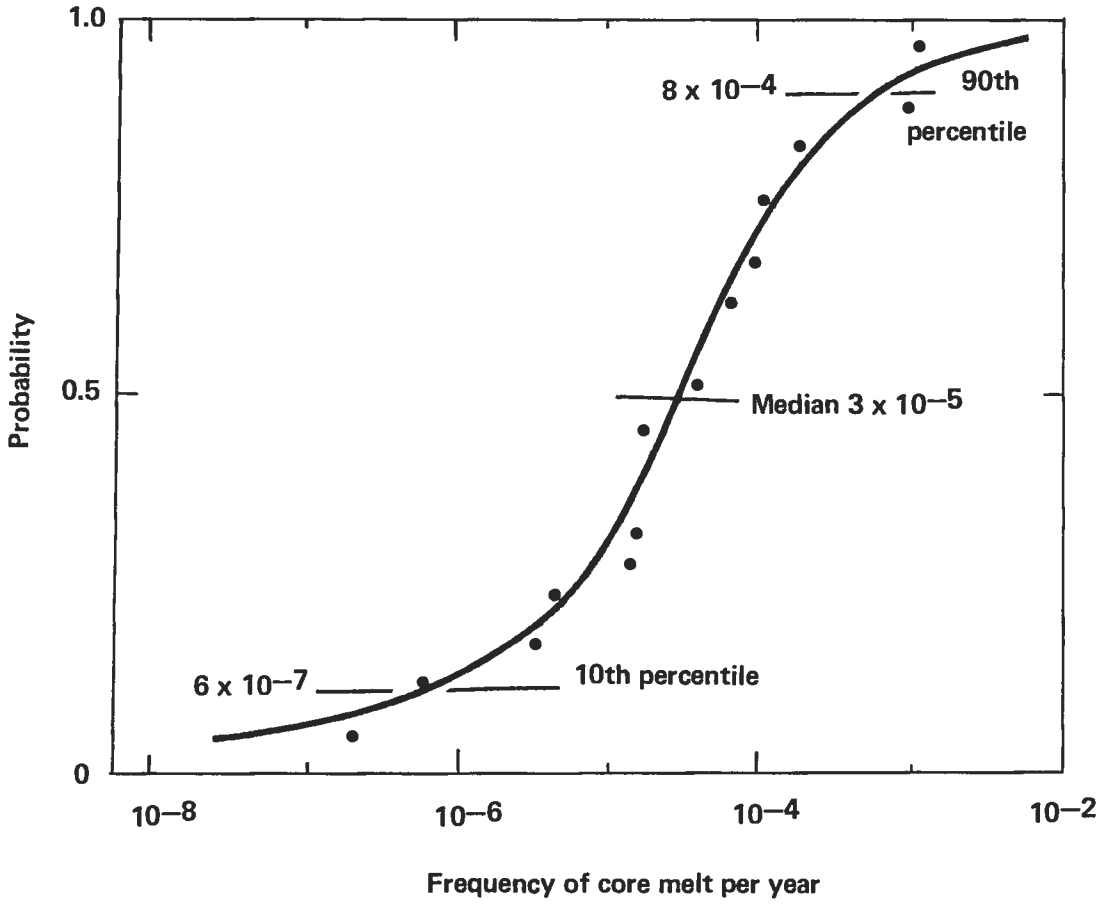

Fig. 7.2. Uncertainty intervals on frequency of core melt (best estimate). The data points are from the 14 runs described in Section 2.

CHAPTER 8: EFFECTS OF ASSUMPTIONS

This chapter presents the results of several calculations made to show the effects of the base case assumptions. The assumptions include consequences of structural failures, feed-and-bleed capability, and loss of AFWS due to severe steam environment. Table 8.1 provides a comparison of the cases we analyzed. This table provides five basic categories. Those cases include (1) base case (with feed-and-bleed, with structural failures), (2) Case 1 (with feed-and-bleed, without structural failures), (3) Case 2 (without feed-and-bleed, without structural failures), (4) Case 3 (without feed-and-bleed, with structural failures), and (5) Case 4 (without feed-and-bleed, with structural failures, with failure of AFWS pumps due to severe steam environment). This section describes the results for each one of these cases and determines what effect these changes have. Before making the comparisons, we define these assumptions.

The first assumption is the feed-and-bleed capability. Feed and bleed is an operation to cool the core in case the AFWS is not available during either a transient or small-small-LOCA event. If the AFWS fails, then the operator must detect this fact and take appropriate action. Appropriate action may include starting up either the charging or the safety injection pumps and realigning valves as necessary. The procedures for this operation are plant-specific. The cases with feed-and-bleed assume that this option is available to the operator. Cases without feed-and-bleed assume that this option is not available to the operator.

The next fundamental assumption, structural failures, includes several items. The three most important structural failures have been identified as: (1) uplift, (2) failure of the roof of the enclosure for the crib house pump, and (3) failure of the auxiliary building shear wall.

Uplift is defined as soil failure under the containment building. In the cases "with structural failures," uplift is assumed to result in sufficiently large rocking motions to fail the safety system piping between the AFT building and the containment building.

Collapse of the crib house pump enclosure roof could fail the service-water pumps beneath them. There are six pumps, three associated with each of the two Zion units. In the with-structural-failure case it is assumed that all six pumps will fail.

The third structural failure assumption concerns failure of the auxiliary building shear wall. Failure of this shear wall is assumed to cause loss of electrical power and control circuits between the auxiliary building and the containment building. The shear wall is assumed to fail the electrical and control circuits in the with-structural-failure case.

The last fundamental assumption analyzed in this chapter is the steam-environment assumption. This assumption is that failure of the steam line which powers the turbine-driven AFWS pump will allow steam to be released into the room or area where all the AFWS pumps are situated, causing these pumps to fail. This failure assumes that there is not proper segregation between the auxiliary feedwater pumps and that the steam environment is severe enough to make these pumps ineffective. Note that this assumption was not made for the base case. The base case assumed that, given failure of the steam line, the

Table 8.1. Comparison of cases analyzed to test effects of fundamental assumptions.

	Release	Frequency/yr	man-rem/yr
Base case (with feed-and-bleed and with structural failures)	1	2.9E-8	0.2
	2	1.4E-6	6.5
	3	5.4E-7	2.9
	4	0	0
	5	8.3E-10	0
	6	1.7E-7	0
	7	1.5E-6	0
	Total	3.6E-6	9.6
Case 1 (with feed-and-bleed and no structural failures)	1	1.9E-8	0.1
	2	1.9E-7	0.9
	3	6.1E-7	3.3
	4	0	0
	5	8.8E-10	0
	6	1.2E-7	0
	7	5.3E-7	0
	Total	1.5E-6	4.3
Case 2 (with no feed-and-bleed and no structural failures)	1	2.4E-8	0.1
	2	5.7E-7	2.7
	3	6.6E-7	3.6
	4	0	0
	5	0	0
	6	2.8E-7	0
	7	7.6E-6	0.2
	Total	9.1E-6	6.6
Case 3 (with no feed-and-bleed and with structural failures)	1	3.3E-8	0.2
	2	1.5E-6	7.2
	3	6.0E-7	3.2
	4	0	0
	5	0	0
	6	2.9E-7	0
	7	8.6E-6	0.2
	Total	1.1E-5	10.8
Case 4 (with no feed-and-bleed, with structural failures, and with steam environment)	1	3.3E-8	0.2
	2	1.5E-6	7.2
	3	6.0E-7	3.2
	4	1.9E-12	0
	5	2.7E-11	0
	6	2.8E-7	0
	7	8.6E-6	0.2
	Total	1.1E-5	10.9

other two pumps would be able to function properly. Case 4 shows the effect of this assumption.

Case 1

Case 1 (with feed-and-bleed, without structural failures) release frequencies and man-rem/year are shown in Table 8.2. Release categories 3 and 7 are dominant in terms of release frequency, while release categories 2 and 3 are dominant in terms of man-rem/year. We see that 77% of the released radioactive material comes from release category 3 and 21% comes from release category 2. A more detailed breakdown of this case is given in Table 8.3, which lists the release category frequencies for each earthquake level and the dominant contributors to release frequencies and man-rem/year. Table 8.3 shows that for release category 7, which is dominant in terms of release frequency, earthquake levels 2 and 3 dominate the risk. In terms of man-rem/year, the dominance is in release category 2 at earthquake levels 4, 5, and 6 and release category 3 at earthquake levels 4 and 5. It should be noted that the SSE is defined between our earthquake levels 1 and 2. Therefore, we find that the release frequencies and man-rem/year have their greatest risk in the >1-SSE range. Note the values in Table 8.3. We will later see how these earthquake levels change when we change assumptions.

In Table 8.4, we summarize a closer examination of those contributors that were found to be significant. This table lists the dominant terminal event sequences with their associated containment failure modes, accident sequence, acceleration range, and release category contributions. Also indicated are the dominant components that contribute most to the release sequence frequencies given in the table. Table 8.4 reveals that certain accident sequences appear regularly. These accident sequences are defined in the event trees shown in Chapter 6. We note first that SLOCA, SSLOCA, and MLOCA accident sequence 21 are considered dominant. All of these accident sequences include failure of the CSIS & CFCS(I) and RHRS. The dominant component in this case is pair of pipes which appears in the RHRS. The particular pipes in

Table 8.2. Summary of release frequencies and dose for Case 1 (with feed-and-bleed and no structural failures).

Release category	Release frequency/yr	man-rem/yr
1	1.9E-8	0.1
2	1.9E-7	0.9
3	6.1E-7	3.3
4	9.6E-11	0
5	8.8E-10	0
6	1.2E-7	0
7	5.3E-7	0
Total	1.5E-6	4.3

Table 8.3. Release frequencies and dose with different earthquake levels for Case 1 (with feed-and-bleed and no structural failures).

Release category	Earthquake level 1	2	3	4	5	6	Total	man-rem/yr
1	0	0	5.7E-12	6.8E-9	6.4E-9	5.7E-9	1.9E-8	0.1
2	0	0	1.1E-11	3.1E-8[a]	7.7E-8[a]	8.2E-8	1.9E-7	0.9[a]
3	2.9E-10	1.2E-10	4.6E-9	4.6E-7[a,b]	1.2E-7[a,b]	2.7E-8	6.1E-7[b]	3.3[a]
4	0	0	0	3.7E-11	5.1E-11	8.1E-12	9.6E-11	0
5	3.8E-12	1.4E-11	9.3E-12	2.9E-10	4.8E-10	8.2E-11	8.8E-10	0
6	0	0	0	7.5E-8	4.1E-8	6.7E-9	1.2E-7	0
7	2.0E-8	1.2E-7[b]	4.0E-7[b]	3.4E-8	4.1E-8	2.3E-8	5.3E-7	0
Grand Total							1.5E-6	4.3

[a] Dominant contributor to release frequency.
[b] Dominant contributor to man-rem/year.

Table 8.4. Characteristics of dominant accident sequences of Case 1 (with feed-and-bleed and without structural failures).

	Initiating event	Accident sequence	Containment failure mode	Terminal event seq. frequency per yr	man-rem/yr	Dominant components
Release category 2:						
Acceleration level 4	RVR	7	Gamma	9.9E-9	0.05	Single pipe 2, pipe pairs
	SSLOCA	34	Gamma	5.3E-9	0.03	Electrical pairs
	RVR	6	Gamma	4.4E-9	0.02	CSIS & CFCS(I), CSRS
	LLOCA	27[a]	Gamma	4.2E-9	0.02	Single pipe 2
Acceleration level 5	RVR	7	Gamma	5.6E-8	0.27	Single pipe 2, pipe pairs
Acceleration level 6	RVR	7	Gamma	7.6E-8	0.36	Single pipe 2, pipe pairs
	RVR	6	Gamma	9.9E-9	0.5	CSIS & CFCS(I), CSRS
Release category 3:						
Acceleration level 4	SLOCA[b]	21	Delta	2.9E-7	1.60	Pipe pairs
	SSLOCA	21	Delta	1.4E-7	0.76	Pipe pairs
	MLOCA	21	Delta	2.7E-8	0.15	Pipe pairs
Acceleration level 5	SLOCA	21	Delta	1.0E-7	0.54	Pipe pairs
Acceleration level 6	SLOCA	21	Delta	2.4E-8	0.13	Pipe pairs
	MLOCA	21	Delta	2.5E-9	0.01	Pipe pairs
Release category 6:						
Acceleration level 4	SSLOCA	34	Epsilon	3.7E-8	0.1	Electrical pairs
	LLOCA	27	Epsilon	2.9E-8	0	Single pipe 2
	MLOCA	27	Epsilon	6.3E-9	0	RCL break
Acceleration level 5	LLOCA	27	Epsilon	3.0E-8	0	Single pipe 2
	SSLOCA	34	Epsilon	5.8E-9	0	Electrical pairs
Acceleration level 6	LLOCA	27	Epsilon	5.8E-9	0	Single pipe 2

Table 8.4. (continued)

	Initiating event	Accident sequence	Containment failure mode	Terminal event seq. frequency per yr	man-rem/yr	Dominant components
Release category 7:						
Acceleration level 1	MLOCA	13	Epsilon	1.9E-8	0	RCL break
Acceleration level 2	MLOCA	13	Epsilon	5.2E-9	0	RCL break
	LLOCA	13	Epsilon	4.1E-9	0	Single pipe 1
Acceleration level 3	LLOCA	13	Epsilon	2.3E-7	0.01	Single pipe 1
	RVR	1	Epsilon	1.0E-7	0	RCL supports
	MLOCA	13	Epsilon	4.8E-8	0	RCL break
Acceleration level 4	SSLOCA	35	Epsilon	8.2E-9	0	RCL break
	LLOCA	28	Epsilon	8.2E-9	0	Single pipe 1
	LLOCA	28	Delta	6.1E-9	0	Single pipe 1
	MLOCA	28	Epsilon	6.1E-9	0	RCL break
	MLOCA	28	Delta	5.2E-9	0	RCL break
	SSLOCA	C	Epsilon	2.0E-9	0	Electrical pair
Acceleration level 5	LLOCA	28	Epsilon	1.4E-8	0	Single pipe 1
	LLOCA	28	Delta	1.4E-8	0	Single pipe 1
	SSLOCA	C	Epsilon	3.3E-9	0	Electrical pair
	MLOCA	28	Epsilon	3.1E-9	0	RCL break
	MLOCA	28	Delta	3.0E-9	0	RCL break
	SSLOCA	35	Epsilon	2.7E-9	0	RCL break
Acceleration level 6	LLOCA	28	Epsilon	1.0E-8	0	Single pipe 1
	LLOCA	28	Delta	1.0E-8	0	Single pipe 1

question are failing, not from the structural failures, but from high earthquake-generated stress in the pipes. The pipes in question run between the auxiliary building and the containment building. Another accident sequence shown as being dominant is LLOCA 13. The failure in this case is dominated by a single pipe. This pipe, part of the ECCS system, runs between the auxiliary building and the containment building. Proceeding down the list of dominant accident sequences, we also find similarity between LLOCA 28 and MLOCA 28. These involve failure of the same piping between the auxiliary building and containment building.

Case 2

Case 2 (without feed-and-bleed, without structural failures) release frequencies and man-rem/year are shown in Table 8.5. Release category 7 is dominant in terms of release frequency, while release categories 2 and 3 are dominant in terms of man-rem/year. We see that 55% of the released radioactive material comes from release category 3 and 41% comes from release category 2. A more detailed breakdown of this case is given in Table 8.6, which lists the release category frequencies for each earthquake level and the dominant contributors to release frequencies and man-rem/year. Table 8.6 shows that for release category 7, which is dominant in terms of release frequency, earthquake levels 2 and 3 dominate the risk. In terms of man-rem/year, the dominance is at earthquake levels 4 and 5 in both release categories 2 and 3. Note the values in Table 8.6 to see how these earthquake levels change when various assumptions are changed. Table 8.7 lists the Case 2 dominant terminal event sequences with their associated containment failure modes, accident sequence, acceleration range, and release category contributions. Also indicated in this table are the dominant components that contribute most to the release sequence frequencies given in the table. Table 8.7 reveals that certain accident sequences appear regularly. These accident sequences are defined in the event trees shown in Chapter 6.

Table 8.5. Summary of release frequencies and dose for Case 2 (without feed-and-bleed and with no structural failures).

Release category	Release frequency per yr	man-rem/yr
1	2.4E-8	0.1
2	5.6E-7	2.7
3	6.6E-7	3.6
4	1.9E-12	0
5	2.7E-11	0
6	2.8E-7	0
7	7.6E-6	0.2
Total	9.1E-6	6.6

Table 8.6. Release frequencies and dose with different earthquake levels for Case 2 (without feed-and-bleed and with no structural failures).

Release category	Earthquake level 1	2	3	4	5	6	Total	man-rem/yr
1	0	0	5.7E-12	1.2E-8	6.9E-9	5.8E-9	2.4E-8	0.1
2	0	0	1.1E-11	3.7E-7[a]	1.1E-7[a]	8.3E-8	5.6E-7	2.7[a]
3	2.7E-10	4.7E-8	2.9E-8	4.4E-7[a]	1.2E-7[a]	2.7E-8	6.6E-7	3.6[a]
4	0	0	1.9E-12	0	0	0	1.9E-12	0
5	3.8E-12	1.4E-11	9.3E-12	0 0	0	2.7E-11	0	
6	0	0	0	2.2E-7	5.9E-8	6.6E-9	2.8E-7	0
7	2.7E-8	4.6E-6[b]	2.8E-6[b]	3.2E-8	3.7E-8	2.3E-8	7.6E-6[b]	0.2
Grand Total							9.1E-6	6.6

[a] Dominant contributor to release frequency.
[b] Dominant contributor to man-rem/year.

Table 8.7. Characteristics of dominant accident sequences of Case 2 (without feed-and-bleed and with no structural failures).

	Initiating event	Accident sequence	Containment failure mode	Terminal event seq. frequency per yr	man-rem/yr	Dominant components
Release category 2:						
Acceleration level 4	T2	4	Delta	2.2E-7	1.1	Electrical pairs
	T2	4	Gamma	9.4E-8	0.5	Electrical pairs
	SSLOCA	21	Gamma	1.8E-8	0.1	Pipe pairs
	SSLOCA	34	Gamma	1.5E-8	0.1	Electrical pairs
Acceleration level 5	RVR	7	Gamma	5.6E-8	0.3	Single pipe 2, pairs
	T2	4	Delta	2.0E-8	0.1	Electrical pairs
	RVR	6	Gamma	9.9E-9	0.1	CSIS & CFCS(I), CSRS
	T2	4	Gamma	8.5E-9	0.1	Electrical pairs
Release category 3:						
Acceleration level 2	T2	4	Alpha	4.6E-8	0.3	Electrical pairs
Acceleration level 3	T2	4	Alpha	2.0E-8	0.1	Electrical pairs
	SSLOCA	29	Alpha	4.1E-9	0	Electrical pairs
	LLOCA	13	Alpha	2.3E-9	0	Single pipe 1
Acceleration level 4	SLOCA	21	Delta	2.9E-7	1.6	Pipe pairs
	SSLOCA	21	Delta	1.3E-7	0.7	Pipe pairs
	MLOCA	21	Delta	2.7E-8	0.2	Pipe pairs
Acceleration level 5	SLOCA	21	Delta	1.0E-7	0.5	Electrical pairs
Release category 6:						
Acceleration level 4	SSLOCA	34	Epsilon	1.0E-7	0	Electrical pairs
	T2	4	Epsilon	7.4E-8	0	Electrical pairs
	LLOCA	27	Epsilon	2.9E-8	0	Single pipe 2
Acceleration level 5	LLOCA	27	Epsilon	2.9E-8	0	Single pipe 2
	SSLOCA	34	Epsilon	1.9E-9	0	Electrical pairs
	T2	4	Epsilon	6.7E-9	0	Electrical pairs

Table 8.7. (continued)

	Initiating event	Accident sequence	Containment failure mode	Terminal event seq. frequency per yr	man-rem/yr	Dominant components
Release category 7:						
Acceleration level 2	T2	4	Epsilon	4.6E-6	0.1	Electrical pairs
	SSLOCA	29	Epsilon	6.2E-8	0	Electrical pairs
Acceleration level 3	T2	4	Epsilon	2.0E-8	0.1	Electrical pairs
	SSLOCA	29	Epsilon	4.1E-7	0	Electrical pairs
	LLOCA	13	Epsilon	2.3E-7	0	Single pipe 1
	RVR	1	Epsilon	1.0E-8	0	RCL supports
Release category 7:						
Acceleration level 2	T2	4	Epsilon	4.6E-6	0.1	Electrical pairs
	SSLOCA	29	Epsilon	6.2E-8	0	Electrical pairs
Acceleration level 3	T2	4	Epsilon	2.0E-8	0.1	Electrical pairs
	SSLOCA	29	Epsilon	4.1E-7	0	Electrical pairs
	LLOCA	13	Epsilon	2.3E-7	0	Single pipe 1
	RVR	1	Epsilon	1.0E-8	0	RCL supports

Case 3

Case 3 (without feed-and-bleed and with structural failures) release frequencies and man-rem/year are shown in Table 8.8. Release category 7 is dominant in terms of release frequency, while release categories 2 and 3 are dominant in terms of man-rem/year. We see that 67% of the released radioactive material comes from release category 2 and 30% comes from release category 3. A more detailed breakdown of this case is given in Table 8.9, which lists the release category frequencies for each earthquake level and the dominant contributors to release frequencies and man-rem/year. Table 8.9 shows that for release category 7, which is dominant in terms of release frequency, earthquake levels 2 and 3 dominate the risk. In terms of man-rem/year, the dominance is in release category 2 at earthquake levels 2, 3, and 4 and release category 3 at earthquake level 4. In Table 8.10 we look more closely into the contribution to risk. This table lists the dominant terminal event sequences with their associated containment failure modes, accident sequence, acceleration range, and release category contributions. Also indicated are the dominant components that contribute most to the release sequence frequency given in this table. Table 8.10 reveals that certain accident sequences appear regularly. These accident sequences are defined in the event trees shown in Chapter 6. Table 8.10 shows that T2-4 is a dominant sequence. This accident sequence involves failure of the AFWS. Case 3 assumes no feed-and-bleed capability, and without such backup the importance of the AFWS is enhanced. The cause of failure of T2-4 is being dominated by the structural failures of uplift and failure of the crib house service-water pump enclosure roof. Numerous other accident sequences are found to be important, as noted earlier in the section. Some of these are repeated here. For example, the SSLOCA, SLOCA, and MLOCA accident sequence 21 turns out to be dominant for release category 3, earthquakes levels 4 and 5. The only other accident sequence contributing significantly in terms of man-rem/year is the RVR-7. The dominant failure modes are failure of the crib house service-water pump enclosure roof and uplift.

Table 8.8. Summary of release frequency and dose for Case 3 (without feed and bleed and with structural failures).

Release category	Release frequency/yr	man-rem/yr
1	3.3E-8	0.2
2	1.5E-6	7.2
3	6.0E-7	3.2
4	1.9E-12	0
5	2.7E-11	0
6	2.9E-7	0
7	8.6E-6	0.2
Total	1.1E-5	10.8

Table 8.9. Release frequencies and dose with different earthquake levels for Case 3 (without feed-and-bleed and with structural failures).

Release category	Earthquake level						Total	man-rem/yr
	1	2	3	4	5	6		
1	3.1E-13	4.2E-11	3.1E-9	1.6E-8	7.8E-9	5.9E-9	3.3E-8	0.2
2	4.1E-12	2.3E-7[a]	6.1E-7[a]	4.6E-7[a]	1.1E-7	8.3E-8	1.5E-6	7.2[a]
3	4.5E-10	5.0E-8	3.5E-8	4.2E-7[a]	8.0E-8	1.5E-8	6.0E-7	3.2[a]
4	0	0	1.9E-12	0	0	0	1.9E-12	0
5	3.8E-12	1.4E-11	9.3E-12	0	0	0	2.7E-11	0
6	0	1.1E-13	4.3E-12	2.3E-7	5.0E-8	5.9E-9	2.9E-7	0
7	4.4E-8	4.8E-6[b]	3.2E-6[b]	3.7E-7	1.7E-7	5.2E-8	8.6E-6[b]	0.2
Grand Total							1.1E-5	10.8

[a] Dominant contributor to release frequency.
[b] Dominant contributor to man-rem/year.

Table 8.10. Characteristics of dominant accident sequences of Case 3 (without feed-and-bleed and with structural failures).

	Initiating event	Accident sequence	Containment failure mode	Terminal event seq. frequency per yr	man-rem/yr	Dominant components
Release category 1:						
Acceleration level 4	T2	4	Alpha	4.8E-9	0.03	Uplift, roof
Acceleration level 5	RVR	7	Alpha	3.8E-9	0.02	Uplift, roof
Acceleration level 6	RVR	7	Alpha	5.0E-9	0.03	Uplift, roof
Release category 2:						
Acceleration level 2	T2	4[a]	Delta/Gamma	2.3E-7	1.1	Uplift, roof
Acceleration level 3	T2	4[a]	Delta/Gamma	5.8E-7	2.8	Uplift, roof
	SSLOCA	35	Gamma	1.8E-8	0.08	Uplift, roof
Acceleration level 4	T2	4	Delta	2.7E-7	1.3	Uplift, roof
	T2	4	Gamma	1.1E-7	0.5	Uplift, roof
Acceleration level 5	RVR	7	Gamma	5.7E-8	0.3	Uplift, roof
	T2	4	Delta	2.1E-8	0.1	Uplift, roof
	T2	4	Gamma	9.1E-9	0.04	Uplift, roof
	RVR	6	Gamma	9.0E-9	0.04	CRIS & CFCS(I), CSRS
Acceleration level 6	RVR	7	Gamma	7.6E-8	0.40	Uplift, roof
Release category 3:						
Acceleration level 2	T2	4	Alpha	4.9E-8	0.26	Uplift, roof
Acceleration level 3	T2	4	Alpha	2.6E-8	0.14	Uplift, roof
Acceleration level 4	SLOCA	21	Delta	2.6E-7	1.40	Pipe pairs
	SSLOCA	21	Delta	1.4E-7	0.76	Pipe pairs
	MLOCA	21	Delta	2.4E-8	0.13	Pipe pairs
Acceleration level 5	SLOCA	21	Delta	6.6E-8	0.36	Pipe pairs
	SSLOCA	21	Delta	8.4E-9	0.05	Pipe pairs
	MLOCA	21	Delta	5.8E-9	0.03	Pipe pairs
Acceleration level 6	SLOCA	21	Delta	1.3E-8	0.07	Pipe pairs

Table 8.10. (continued)

	Initiating event	Accident sequence	Containment failure mode	Terminal event seq. frequency per yr	man-rem/yr	Dominant components
Release category 6:						
Acceleration level 4	SSLOCA	34	Epsilon	1.0E-7	0.02	Uplift, roof
	T2	4	Epsilon	9.1E-8	0.01	Uplift, roof
	LLOCA	27	Epsilon	2.6E-8	0	Single pipe 2
Acceleration level 5	LLOCA	7	Epsilon	2.3E-8	0	Single pipe 2
	SSLOCA	34	Epsilon	1.7E-8	0	Uplift, roof
	T2	4	Epsilon	7.2E-9	0	Uplift, roof
Release category 7:						
Acceleration level 2	T2	4	Epsilon	4.5E-6	0.1	Uplift, roof
Acceleration level 3	T2	4	Epsilon	2.0E-6	0.05	Uplift, roof
	SSLOCA	29	Epsilon	4.1E-7	0.01	Electrical pairs
	LLOCA	13	Epsilon	2.2E-7	0.01	Single pipe 1
	T2	4	Epsilon	1.5E-7	0	Uplift, roof
	SSLOCA	35	Epsilon	1.2E-7	0	Uplift, roof
	RVR	1	Epsilon	9.4E-8	0	RCL supports
	MLOCA	13	Epsilon	4.8E-8	0	RCL break
	SLOCA	28	Epsilon	4.4E-8	0	Uplift, roof
	SSLOCA	28	Delta	4.3E-8	0	Uplift, roof
Acceleration level 4	SSLOCA	35	Epsilon	1.6E-7	0	Uplift, roof
	SLOCA	28	Epsilon	7.9E-8	0	Uplift, roof
	SLOCA	28	Delta	7.8E-8	0	Uplift, roof

Case 4

Case 4 (without feed-and-bleed, with structural failures, and with a steam environment in AFWS) release frequencies and man-rem/year are shown in Table 8.11. Release category 7 is dominant in terms of release frequency, while release categories 2 and 3 are dominant in terms of man-rem/year. We see that 66% of the released radioactive material comes from release category 2 and 30% comes from release category 3. Note that this is essentially the same as we found in Case 3. A more detailed breakdown of this case is given in Table 8.12, which lists the release category frequencies for each earthquake level and the dominant contributors to release frequencies and man-rem/year. Table 8.12 shows that for release category 7, which is dominant in terms of release frequency, earthquake levels 2 and 3 dominate the risk. In terms of man-rem/year, the dominance is in release category 2 at earthquake levels 2, 3, and 4 and release category 3 at earthquake level 4. Table 8.10 provides a list of the dominant contributions. Refer to the previous discussion of Case 3 for a description of these contributors.

8.1 Feed-and-Bleed Assumption

Table 8.1 provides a comparison of the cases analyzed to show the effects of the fundamental assumptions. Availability of a feed-and-bleed operation is one fundamental assumption, as noted earlier. To determine the effect of this assumption we compare the base case with Case 3, which includes structural failures but no feed-and-bleed capability. We note that while the frequency of release increases from 3.6E-6 to 1.1E-5, the man-rem/yr contribution increases from 9.6 to 10.8. This implies that feed-and-bleed capability makes little difference to man-rem/year when structural failures are dominant. Another relevant comparison can be made between Case 1 and Case 2. Both cases are without structural failures, whereas Case 1 has feed-and-bleed and Case 2 does not. Here we see a more significant change, since the structural failures are no longer dominating. The release frequencies change from 1.5E-6

Table 8.11 Summary of release frequency and dose for Case 4 (case with feed-and-bleed, with structural failures, and with steam environment in the AFWS.)

Release category	Release frequency/yr	man-rem/yr
1	3.3E-8	0.2
2	1.5E-7	7.2
3	6.0E-7	3.3
4	1.9E-12	0
5	2.7E-11	0
6	2.8E-7	0
7	8.6E-6	0.2
Total	1.1E-5	10.9

Table 8.12 Release category frequencies and dose with different earthquake levels for Case 4 (case without feed-and-bleed, with structural failure, and with steam environment in AFWS.)

Release category	Earthquake level 1	2	3	4	5	6	Total	man-rem/yr
1	3.1E-13	4.2E-11	3.1E-9	1.6E-8	7.8E-9	5.9E-9	3.3E-8	0.2
2	4.1E-12	2.4E-7	6.1E-7[a]	4.6E-7[a]	1.2E-7	8.3E-8	1.5E-6	7.2[a]
3	4.6E-10	5.1E-8	3.5E-8	4.2E-7[a]	8.0E-8	1.5E-8	6.0E-7	3.3[a]
4	0	0	1.9E-12	0	0	0	1.9E-12	0
5	3.8E-12	1.4E-11	9.3E-12	0	0	0	2.7E-11	0
6	0	1.1E-13	4.3E-12	2.3E-7	5.0E-8	5.9E-9	2.8E-7	0
7	4.6E-8	4.8E-6[b]	3.2E-6[b]	3.8E-7	1.7E-7	5.2E-8	8.6E-6[b]	0.2
Grand Total							1.1E-5	10.9

[a] Dominant contributor to release frequency.
[b] Dominant contributor to man-rem/year.

to 9.1E-6 when feed-and-bleed is no longer available, and the man-rem/year values increase from 4.3 to 6.6. Thus, the decrease in release frequency attributable to the feed-and-bleed capability can be significant when structural failures are not dominant.

In examining the differences between Case 1 and Case 2, we note that the largest difference in terms of man-rem/year comes in release category 2, with some changes being noted in categories 3 and 7. A similar situation is found when comparing the case assuming structural failures, i.e., base case vs Case 3.

8.2 Structural Failure Assumptions

The second fundamental set of assumptions noted earlier are the structural failure assumptions. To determine the effect of these assumptions we compare several cases from Table 8.1. One comparison is between the base case and Case 1. In the base case we have both feed-and-bleed capability and structural failure, whereas in Case 1 we have feed-and-bleed capability but no structural failures. Thus we can examine the effect of structural failures, given that feed-and-bleed is available. The frequency per year decreases from 3.6E-6 to 1.5E-6 when the structural failure consequence assumptions are not used. We see, of course, a similar reduction in the numbers of man-rem/year, from 9.6 in the base case to 4.3 man-rem/year in Case 1. Another relevant comparison can be made between Case 2 and Case 3. Case 2 is without structural failures and Case 3 includes structural failures. In Case 3 we have a frequency of 1.1E-5, whereas this value is reduced to 9.1E-6 when structural failures are removed. Radiation contribution decreases from 10.8 to 6.6 man-rem/year. Thus, the assumptions as to the consequences of structural failures are significant. In comparing the base case with Case 1 we find that, while there are some changes in release categories 1 and 3, the bulk of the change again comes from release category 2. A similar situation is found when Case 2 is compared with Case 3. Again, only small changes occur in release categories 1 and 3, and the largest change comes from release category 2.

To identify contributions to the change in release category 2, we compare the dominant accident sequences from Table 7.4 (base case) with Case 1, which contains no structural failures. Note that for release category 2 the dominant accident sequences are T2-4, RVR-6, RVR-7 and SSLOCA-35. These are dominant when structural failures are included. In the case of no structural failures we find that the dominant sequences are RVR-6, RVR-7, and SSLOCA-35. Thus, in the absence of structural failure, the importance of T2-4 becomes less, since the dominant failures contributing to T2-4 were the structural failures. We note that the reactor vessel rupture, RVR-6 and RVR-7, are basically unchanged between the two cases, since the structural failures being considered do not have any effect on the RVR event. SSLOCA-35, as with T2-4, has structural failure as its dominant contribution. Once the structural failure probabilities have been removed, SSLOCA-35's probability becomes small, and, therefore, does not appear to be a dominant accident sequence in the case without structural failures. The same comparison can be made between Case 1 and Case 3. Both of these cases are without feed-and-bleed; Case 2 has no structural failures and Case 3 has structural failures. In these two cases T2-4 again is a dominant contributor, along with RVR-7 and SSLOCA-21. For

T2-4 the frequencies are increased when structural failures are added. We note that RVR-7 is not affected in this case. It still remains important because the accident sequence is not changed significantly by the inclusion of structural failures.

8.3 Steam Environment Assumption

The third assumption noted in this chapter was the steam environment assumption. This assumption is that the rooms containing the auxiliary feedwater pumps will become engulfed in steam if the steam line to the turbine-driven auxiliary feedwater pump should fail. This steam environment is assumed to fail all the auxiliary feedwater pumps. Previous to this case, the assumption was made that there was sufficient segregation among the pumps and the steam environment would not be severe enough to cause failure of all pumps simultaneously. We will examine what effect that assumption has on the overall risk.

In comparing Case 3 with Case 4 we find very little difference in the results. The release frequency rounded to one decimal point is the same (1.1E-5). We note a slight increase in man-rem/year from 10.8 to 10.9. The risk in this case due to the failure of the pipe leading to the turbine drive auxiliary feedwater pump could be a major contributor that is being masked by the structural failures. However, further studies running a case "without feed-and-bleed, without structural failure, and with the failure of the steam line" have shown that the difference is small. We can, therefore, state that, even though the steam line is an important component by itself, changes to that assumption show very little changes in the final outcome. To understand the reason for this phenomenon we look to see what effect the steam line has. Failure of the steam line to the auxiliary feedwater pump only becomes effective on those accident sequences which contain failure of the AFWS. This affects only the SSLOCA, T2, and T1 accident sequences. We note that at low earthquake levels, the initiating events are dominated by the T2 and T1 accident sequences and that the larger LOCAs and rupture are dominant at the higher earthquake levels. Therefore, at the lower levels where the SSLOCA, T2, and T1 accident sequences have a dominant effect, the probability of failure of the steam line is small. At earthquake levels where the probability of failure of the steam line is sufficiently large, the probabilities of T2, T1, and SSLOCA are small. So we have balancing effects that render the assumption of little significance.

8.4 Conclusions

Several important conclusions follow from these comparisons. The first is that the assumptions concerning feed-and-bleed and structural failures can have a very significant effect on the final results. The assumption of structural failures is found to have the larger effect on the final results. The fact that the structural failures are site-specific indicates that any seismic PRA analysis must carefully examine site-specific structural details. Based on this analysis, further examination of these assumptions is warranted. This work would include analysis of the actual probability of losing all six service-water pumps, given failure of the crib house pump enclosure roof, and analysis of the actual probability of rupturing all the pipes between the containment and auxiliary building, given the predicted values of basemat uplift.

Another important conclusion is that failure of the AFWS turbine-driven pump due to a break in the steam line feeding that pump would not have severe consequences for the overall analysis. If, however, the initiating event probabilities were to change significantly, then this conclusion should be reconsidered.

CHAPTER 9: CORRELATION EFFECTS ON SEISMIC RISK

The significance of the effects of correlation on seismic risk has been an open question ever since the WASH-1400 study was completed. In fact, one of the goals of the SSMRP was to investigate seismically induced correlation effects, and this was one of the reasons for the detailed level of structural modeling used in the SSMRP. In the following, we first discuss the sources of seismically induced correlation. We then present the results of two sets of calculations which show that correlation has little effect if the total risk is due primarily to single failures, while in contrast, correlation can change the final risk result by an order of magnitude if the risk is dominated by pairs of failures.

9.1 Aspects of Correlation

Recall from Chapter 6 that, to compute the frequency of release, we evaluate accident sequences which have the form

$$P(\text{ACC SEQ}) = P\,(C_1C_2C_3 \cup C_4C_5 \cup \ldots \cup C_iC_jC_k) \quad , \tag{9-1}$$

in which the C_i are basic events, and the terms $C_iC_jC_k$ are the minimal cutsets. (For the Zion risk assessment, each min cutset could consist of up to 10 correlated component failures.) The presence of correlation affects the evaluation of both the union of the cutsets and the evaluation of the cutsets themselves. In general, the largest effect is found in the evaluation of the cutsets themselves.

The basic ideas behind correlation are illustrated in Fig. 9-1, which considers the failure of two components. The lower curve shows the probability of both components failing together, that is, the intersection of the failures of the two components. For zero correlation ($\rho = 0$) the probability of both components failing is just a product of their probabilities, P_aP_b. When the failures of the two components are fully correlated ($\rho = 1$) then the probability of both components failing reduces to the minimum of the probabilities P_a and P_b. Thus it can be seen that when the failures are fully correlated, the probability of simultaneous failure of both components is just the same as the probability of failure of the strongest component. Hence if the two components were installed to provide redundancy, the redundancy is lost when the failures are fully correlated. The difference between the zero correlation limit and the fully correlated limit can be several orders of magnitude, depending on the magnitude of the probabilities P_a and P_b.

The upper curve in Fig. 9-1 shows the probability of failure of at least one of components a or b, that is, the probability of the union of the events a fails, b fails. For the uncorrelated case ($\rho = 0$) the probability of at least one failure is given by $P_a + P_b - P_aP_b$. For the fully correlated limit, the probability of at least one failure occurring is given by the maximum of the two probabilities P_a and P_b. This curve is usually much flatter than the curve for the union of the two failures, and in fact, for this simple case it is not hard to show that the probability of the union of the two failures does not vary by more than a factor of two regardless of the value of the correlation coefficient. In a simplified from, this result

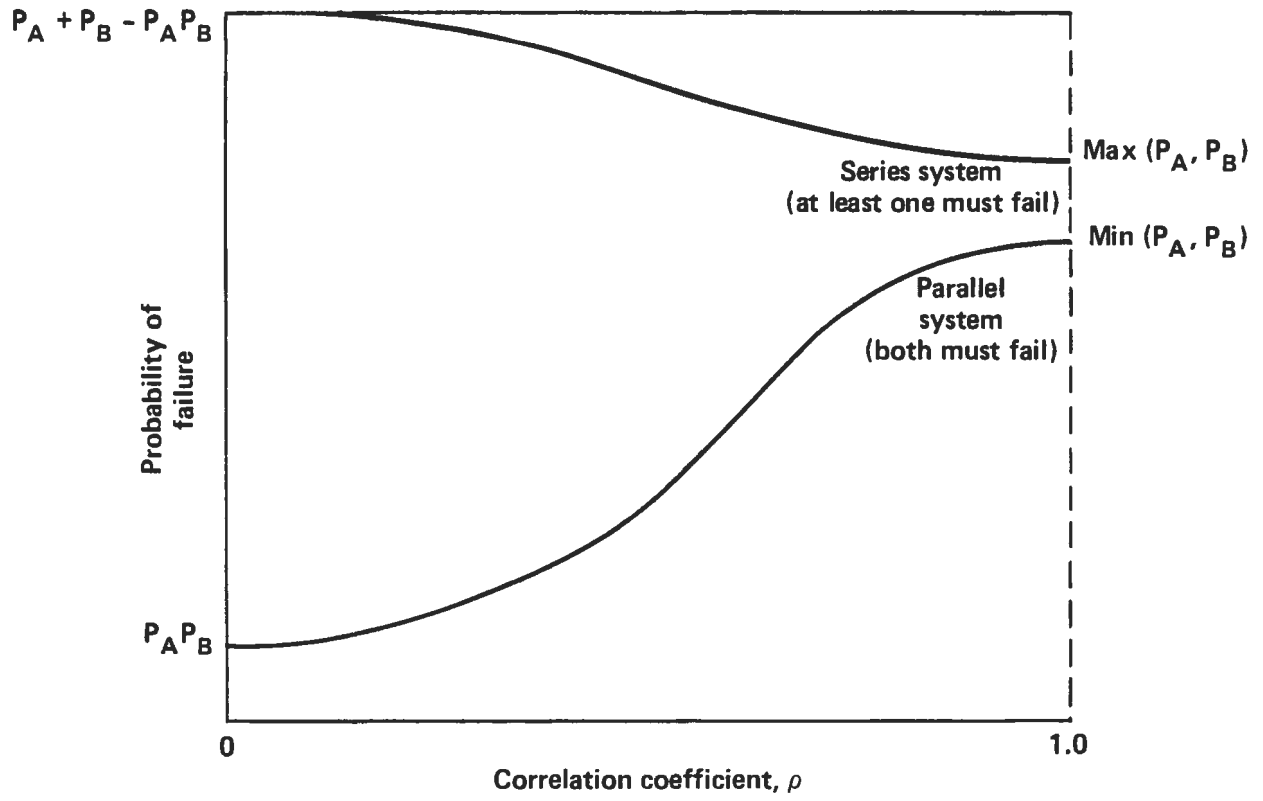

Fig. 9.1. Probability of failure of two component parallel and series systems as a function of correlation.

illustrates why the effects of correlation are more pronounced in the evaluation of the cutsets than in evaluation of the union of the cutsets.

When dealing with accident sequences such as in Eq. (9-1), which involve cutsets consisting of two or more component failures, the situation is not so clear cut. For the uncorrelated case, the probability of a cutset equals the product of the probabilities of the individual component failures. For the fully correlated case, the probability of the cutset equals the minimum of the failure probabilities occurring in the cutset. However, the evaluation of the union of the cutsets that have a number of different component failures is more complex. In this case, the uncorrelated ($\rho = 0$) limit for Eq. (9-1) is given by

$$P(\text{ACC SEQ}) = 1 - [1 - P(C_1C_2C_3)]\ [1 - P(C_4C_5)]\ \ldots\ [1 - P(C_iC_jC_k)] \quad , \quad (9\text{-}2)$$

provided the C_i, $i = 1, \ldots, n$, are all distinct.

The fully correlated limit is equal to the maximum of the minimum failure probabilities found in each cutset. Thus in Eq. (9-1) if it is assumed that the cutset failure probabilities were such that

$$P(C_1) > P(C_2) > P(C_3) > P(C_4)$$

then the fully correlated limit for the probability of the accident sequence would be just the probability $P(C_1)$. It can also be proved that if only positive correlations are present and if there are no repeated basic events in the accident sequence, then Eq. (9-2) is always an upper bound to the accident sequence probability. If the same basic event occurs in more than one cutset, it can no longer be guaranteed that Eq. (9-2) provides an upper bound. However, it will be close to being an upper bound, and is thus an acceptable approximation to an upper bound for the accident sequence.

These ideas enable one to get a heuristic explanation for the results obtained in the Zion risk analysis. For the cases where structural failures are included and where these structural failures dominate the total calculated risk, one is dealing with a situation in which the most important terms in the accident sequences are single failures, and hence the dominant cutsets in the accident sequences consist of a single component failure only. Since correlation then has no effect on the most important cutsets, the only effect of correlation comes in computing the union of the cutsets. As has been qualitatively indicated above, the effects of correlation on the union of cutsets are usually relatively small, with the result that whether or not correlation is considered for those cases dominated by single structural failures, the final risk numbers vary by only a small amount.

By contrast, however, in those cases in which the risk is dominated by failures of pairs of equipment, one finds correlation to have a large effect because correlation affects the probability of the component pairs which constitute the most important cutsets in the accident sequences. Thus, for these cases we find that correlation plays a very important role in evaluating the total risk of the plant.

9.2 Sources of Correlation

The correlations discussed above are correlations between failures of components. Correlation of the component failures arises from (a) correlation between the responses the two components experience and (b) correlation between the fragilities of the two components. Specifically, it may be shown that the correlation coefficient for two component failures may be expressed as

$$\rho = \frac{\beta_{R1}\,\beta_{R2}}{\sqrt{\beta_{R1}^2 + \beta_{F1}^2}\,\sqrt{\beta_{R2}^2 + \beta_{F2}^2}}\,\rho_{R1R2} + \frac{\beta_{F1}\beta_{F2}}{\sqrt{\beta_{R1}^2 + \beta_{F1}^2}\,\sqrt{\beta_{R2}^2 + \beta_{F2}^2}}\,\rho_{F1F2} ,$$

in which

ρ	=	correlation coefficient between the failures of components 1 and 2.
R1,R2	=	responses of components 1 and 2.
β_{R1}, β_{R2}	=	standard deviation of the logarithms of the responses R1 and R2.
β_{F1}, β_{F2}	=	standard deviations of the logarithms of the fragilities of components 1 and 2.

ρ_{R1R2} = correlation coefficient between responses R1 and R2.
ρ_{F1F2} = correlation coefficient between the fragilities of components 1 and 2.

This relation shows that the correlation between the failures of components 1 and 2 depends not only on the correlations between the respective responses and the respective fragilities, but also on the variances in these responses and fragilities.

Correlation between responses arises from the common ground shaking which occurs during an earthquake. Figure 9-2 shows a cross-section of the AFT complex, and the inset on the figure lists correlations between the accelerations of the five floor slabs. A high degree of correlation between the floor slab accelerations is evident, even between the top floor and grade level floor. Correlations between all pairs of the 315 responses (input to SEISIM code) were computed from the structural response calculations performed by the SMACS code. It will be recalled that, at each earthquake level, 30 deterministic time history building (and piping) response calculations are performed. From these 30 calculations, means and variances for each response and correlations for each pair of responses are computed. Thus, in the SSMRP analysis of Zion, the correlations between all responses are computed exactly.

Correlations between fragilities cannot be computed, but must be determined by experiment. No experimental data on fragilities correlation were found during the course of developing the SSMRP fragilities, so fragility correlation was treated as a sensitivity parameter. For the base case (Chapter 7) and cases analyzing the influence of the feed-and-bleed and structural failure assumptions (Chapter 8), the correlation between the fragilities was taken to be zero. This is the appropriate assumption if one is dealing with many like items of equipment which are manufactured en masse and are obtained (possibly from a variety of manufacturers) as off-the-shelf items. Under such circumstances, one would not expect a high degree of correlation between component fragilities. However, it should be reiterated that the choice of zero fragility correlation is an assumption unsupported by data. The potential influence of correlation between fragilities is shown in the sensitivity calculations described below.

9.3 Correlation Effects for the Base Case

The base case analyzed for the risk assessment of Zion was discussed in Chapter 7. For this base case, the structural failures and their most severe hypothesized consequences were included, and, furthermore, a capability to perform "feed-and-bleed" cooling was assumed. As was discussed in Chapter 7, the dominant failures contributing to the risk of the base case consisted of single structural failures, notably uplift of the containment basemat and failure of the crib house service-water pump enclosure roof. Thus, the accident sequences which dominated the risk for the base case were dominated by cutsets consisting of single structural failures. For the base case, it will be recalled that the response correlations were as calculated by the SMACS code and the fragility correlations were taken to be zero.

To determine the effect of including full correlation between the fragilities, an additional risk assessment was performed. For this assessment it was

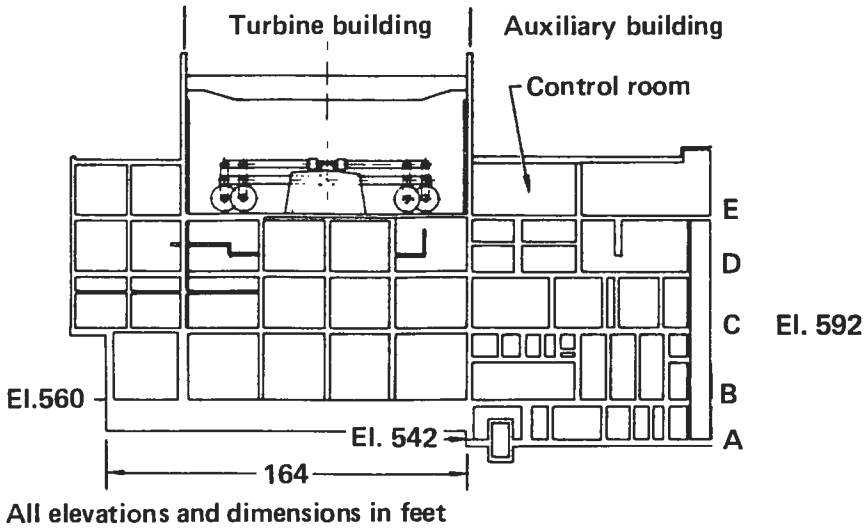

	Median Accel. (ft/s^2)	COV
A	3.0	0.195
B	3.0	0.19
C	3.2	0.23
D	3.98	0.23
E	4.0	0.26

	Correlation coefficients				
	A	B	C	D	E
A	1.00	0.99	0.91	0.81	0.71
B		1.00	0.90	0.82	0.72
C			1.00	0.75	0.65
D				1.00	0.97
E					1.00

Fig. 9.2. Computed response correlation coefficients for various floor slabs in the AFT building. Free-field acceleration was 5 ft/s^2.

assumed that the fragilities of all components in a generic fragility category were fully correlated, but that the fragilities of components in different generic fragility categories were uncorrelated. The results of this calculation showed that the total core melt frequency changed from 3.57E-6 per year to 3.62E-6 per year. Thus, the effect of including the fragility correlation of the base case was found to be minimal and there was very little change in the probabilities of the accident sequences themselves. The only noticeable effect occurred in the evaluation of the initiating event probabilities. Table 9.1 shows the initiating event probabilities for the case in which there is full fragility correlation and the correlation between responses is as calculated in SMACS. Comparison with Table 7.2, which gives the initiating event probabilities for the base case, shows that the main differences occur for the RVR initiating event at the higher earthquake acceleration levels. This follows since the RVR initiating event consists primarily of doubles which were failures of the supports of either the steam generator or the reactor coolant pumps in different loops. (There were also some single-failure events corresponding to primary coolant piping failure near the reactor pressure vessel nozzles, but these had a much smaller probability of occurrence per year.) Thus, including the effects of full fragility correlation is expected to have some effect on the RVR initiating event probability. However, the differences are only at the higher earthquake levels, and, as seen in Chapter 7, the dominant portion of the risk comes from the intermediate earthquake levels. The smaller LOCAs show little effect of correlation because, in general, they are dominated by single piping failures. Thus it can be seen for the base case, the primary effect of including fragility correlation is found in the computation of the initiating events, and the accident sequences themselves are changed very little because of the importance of the single structural failures. As a result, there is very little change in the total core melt frequency for this case.

Table 9.1 Summary of initiating event probabilities for case with calculated response correlation and fragility correlations set to 1.0.

Initiating event	Earthquake acceleration level					
	1	2	3	4	5	6
RVR	0	3.2439E-5	2.7791E-2	5.7012E-2	3.6397E-1	7.5514E-1
LLOCA	0	2.1618E-5	1.8043E-2	3.5780E-2	1.4976E-1	1.2915E-1
MLOCA	1.0565E-4	5.9867E-5	1.0567E-2	3.4657E-2	4.2112E-2	1.7648E-2
SLOCA	2.0893E-4	7.2951E-4	8.6615E-2	2.5389E-1	2.3740E-1	8.5350E-2
SSLOCA	1.4495E-3	1.1019E-2	1.4400E-1	2.6846E-1	1.3832E-1	1.1427E-2
T2	2.7213E-1	8.1286E-1	7.1289E-1	3.5020E-1	6.8448E-2	1.2941E-3
T1	7.2611E-1	1.7527E-1	5.8565E-4	1.0457E-6	2.5746E-8	0

9.4 Correlation Effects for the Case with No Structural Failure Consequences and No Feed-and-Bleed Capability

The largest effects of correlation are expected to be found in those cases in which dominant cutsets consist of more than one component failure. This would include the case analyzed in Chapter 8 in which no structural failure consequences were considered, and feed-and-bleed cooling capability was not assumed. In this case, as shown in Chapter 8, the dominant component failures consisted of pairs of electrical equipment associated with the emergency power system. It will be recalled that a total of 15 pairs of electrical gear contributed significantly to the core melt frequencies. In addition, in this case there was also a number of pipe failure doubles contributing to the core melt frequency that were due to relative motion between the auxiliary building and the reactor containment building. To determine the effect of correlation for this case, two additional analyses were performed. In the first analysis the fragility correlations were taken to be 1.0 for components in the same generic category, and the response correlations were as calculated in the SMACS code. This is denoted as Case 1 in Table 9.2. Case 2 in Table 9.2 was calculated with response correlations as computed by SMACS but fragility correlations set equal to zero. This is the case that was discussed in Chapter 8. The final calculation consisted of assuming zero correlations for the fragilities and for correlations between structural responses. This is shown as Case 3 in Table 9.2. From Table 9.2 it can be seen that the inclusion of fragility correlation increases the total core melt frequency to 2.0E-5 per year, whereas setting both the response and fragility correlations to zero gave a total core melt frequency of 2.5E-6 per year. Thus, these two limiting cases differ by an order of magnitude. The intermediate case in which the fragility correlations are assumed to be zero and the response correlations are as calculated gave a core melt frequency of 9.1E-6 per year, as discussed in Chapter 8. It should be recalled that there is no experimental evidence to determine whether or not the fragilities of equipment in the same categories should be considered correlated or uncorrelated, and until there are such data these cases must be considered equally likely. The conclusion from Table 9.2 is that if one neglects all correlation (in both responses and in fragilities), then one is likely to underestimate the core melt frequency by at least a factor of five and by as much as a factor of ten. The conclusion is based on our calculations for the risk at Zion when singles do not dominate.

Also shown in Table 9.2 is the associated dose expressed in terms of man-rem/year. The fully correlated case (which gives a value of 7.8 man-rem/year) and the uncorrelated case (which shows a dose of 5.3 man-rem/year) differ only by a factor of 50%. This difference is less pronounced than for the core melt frequencies because of the fact that the man-rem/year dosage is affected to a large extent by the terminal event sequences coinciding with the LOCAs, whereas it is the terminal events sequences coinciding with the transient events which are most affected by the correlation. Thus, if one examines the frequencies per year for the seven release categories shown in Table 9.2, one finds that the primary difference between the fully correlated and the uncorrelated case occurs in release category 7, and this release category is due almost entirely to the transient T2 terminal event sequences.

Table 9.2. The effects of correlations of structure responses and fragility functions on release frequencies and dose, with the assumption of no structure failures and no feed-and-bleed.

	Release category	Frequency/yr	man-rem/yr
Case 1	1	3.1E-8	0.2
(with full correlation for	2	7.4E-7	3.6
fragility functions and	3	6.5E-7	3.5
calculated correlations	4	0	0
for structure responses)	5	2.5E-11	0
	6	3.3E-7	0.1
	7	1.8E-5	0.4
	Total	2.0E-5	7.8
Case 2	1	2.4E-8	0.1
(with no correlation for fragility	2	5.7E-7	2.7
functions and with calculated	3	6.6E-7	3.6
correlations for structure	4	0	0
responses)	5	8.8E-10	0
	6	2.8E-7	0
	7	7.6E-6	0.2
	Total	9.1E-6	6.6
Case 3	1	1.5E-8	0.1
(with no correlation for fragility	2	2.5E-7	1.2
functions or structure responses)	3	7.4E-7	4.0
	4	4.5E-13	0
	5	2.5E-11	0
	6	1.8E-7	0
	7	1.3E-6	0
	Total	2.5E-6	5.3

Table 9.3 shows the initiating event probabilities for the uncorrelated case, that is, Case 3 of Table 9.2. These probabilities may be compared directly with the initiating event probabilities of Table 9.1 that correspond to the case of full correlation, that is, Case 1 of Table 9.2. Comparison of these tables show that it is only for the RVR and the large LOCA accident sequences that there are any significant differences in the initiating event probabilities. The reasons for this finding were discussed in Section 9.2. Here again the differences between the initiating event probabilities are only significant at earthquake levels 5 and 6. Tables 9.4 and 9.5 present the release category probabilities as a function of earthquake level for Case 1 and Case 3 (the fully correlated case and the uncorrelated case of Table 9.1). Tables 9.6 and 9.7 present the terminal event sequences that dominate the risk results in the seven release c

Table 9.3 Summary of initiating event probabilities for case with zero response and fragility correlation.

Initiating event	Earthquake acceleration level					
	1	2	3	4	5	6
RVR	0	1.753E-10	1.310E-4	5.580E-4	2.578E-2	1.755E-1
LLOCA	0	2.162E-5	1.856E-2	3.792E-2	2.294E-1	4.349E-1
MLOCA	1.056E-4	5.987E-5	1.087E-2	3.673E-2	6.450E-2	5.942E-2
SLOCA	1.886E-4	5.373E-4	8.057E-2	2.447E-1	3.111E-1	2.643E-1
SSLOCA	1.450E-3	1.102E-2	1.495E-1	2.951E-1	2.470E-1	5.922E-2
T2	2.721E-1	8.130E-1	7.397E-1	3.850E-1	1.222E-1	6.707E-3
T1	7.261E-1	1.753E-1	6.081E-4	1.150E-6	4.600E-8	0

Table 9.4 Summary of release frequencies for case with full correlation for fragility functions and calculated correlations for structures responses, without feed-and-bleed and without structural failures.

Release category	Earthquake acceleration level					
	1	2	3	4	5	6
1	0	0	1.1E-12	1.6E-08	1.1E-08	3.6E-09
2	0	0	9.1E-12	5.1E-07	1.7E-07	5.7E-08
3	8.7E-10	1.3E-07	5.3E-08	3.7E-07	9.2E-08	2.5E-09
4	0	0	4.7E-13	0	0	0
5	3.2E-12	1.3E-11	8.8E-12	0	0	0
6	0	0	0	2.8E-07	5.0E-08	1.4E-09
7	8.6E-08	1.3E-05	5.2E-06	2.8E-08	2.8E-08	9.8E-08

Table 9.5 Summary of release frequencies for case with no correlation for fragility functions and structure responses, without feed-and-bleed and without structural failure.

Release category	Earthquake acceleration level					
	1	2	3	4	5	6
1	0	0	4.8E-12	8.4E-09	3.6E-09	2.6E-09
2	0	0	1.1E-13	1.7E-07	4.8E-08	2.9E-08
3	1.9E-10	3.6E-09	8.4E-09	5.2E-07	1.6E-07	4.7E-08
4	0	0	3.6E-13	0	0	0
5	3.2E-12	1.3E-11	9.1E-12	0	0	0
6	0	0	0	1.1E-07	5.9E-08	1.3E-08
7	1.9E-08	3.6E-07	7.9E-07	2.5E-08	4.0E-08	3.9E-08

the risk results in the seven release categories and at the dominant earthquake acceleration levels, again for the fully uncorrelated and the fully correlated cases of Table 9.2. Comparison of these tables shows that the primary difference occurs in release category 7 at earthquake levels 2 and 3. Some differences are noted for release category 3. However, the dominant contributors to release category 3 are found to be SLOCA 21 and SSLOCA 21 at earthquake level 4. These two terminal event sequences are dominated by pipe singles and thus show very little change between the uncorrelated and fully correlated cases. As a result of this, release category 3 is less affected by correlation than release category 7.

9.5 Conclusions on Correlation Effects

As seen above, effects of correlation on a risk analysis which is dominated by single failures, especially structural failures, are relatively minor and are due primarily to the evaluation of the initiating events. For the cases wherein the dominant risk contributors are pairs of component failures, such as electrical components, correlation is found to have a significant effect on the core melt frequency and may vary the final result by up to an order of magnitude. Furthermore, the difference between including correlation in responses only, or including correlation in both responses and in fragilities, resulted in a factor of five difference in the total core melt frequency. Thus it can be concluded that the effects of correlation are significant and that it would be worthwhile to perform some experimental determination of the type of fragility correlation most appropriate for typical components in nuclear reactors. Results computed for Zion would tend to indicate that electrical gear should be examined for correlation.

Finally, it should be noted that in computing the accident sequence probabilities (in the evaluation of the union of cutsets) Eq. (9.2) is used. This is an approximation to the upper bound of the accident sequence probability and it is possible when dealing with high levels of correlation

Table 9.6 Characterstics of dominant accident sequences with full correlation for fragility functions and calculated correlations for structure responses, without feed-and-bleed and without structural failures.

	Initiating event	Accident sequence	Containment failure mode	Terminal event seq. frequency per yr	man-rem/yr	Dominant components
Release category 1:						
Acceleration level 4	T2	4	Alpha	4.9E-9	0	
	RVR	7	Alpha	3.6E-9	0	3 pipe pairs 2 single pipes
	SLOCA	21	Alpha	2.8E-9	0	2 pipe pairs, LOCA pair, 2 single pipes
	SSLOCA	34	Alpha	1.8E-9	0	6 relay bus pairs
	RVR	6	Alpha	1.6E-9	0	
	SSLOCA	21	Alpha	6.9E-9	0	3 pipe pairs single pipe
Acceleration level 5	RVR	7	Alpha	7.4E-9	0	
	RVR	6	Alpha	1.3E-9	0	
	SLOCA	21	Alpha	8.5E-10	0	
	T2	4	Alpha	3.1E-10	0	
	LLOCA	27	Alpha	2.7E-10	0	
	SSLOCA	34	Alpha	2.4E-10	0	
	LLOCA	28	Alpha	2.1E-10	0	
Release category 2:						
Acceleration level 4	T2	4	Delta	2.8E-7	1.3	
	T2	4	Gamma	1.2E-7	0.6	
	RVR	7	Gamma	5.4E-8	0.3	3 pipe pairs 2 single pipes
	RVR	6	Gamma	2.4E-8	0.1	
	SSLOCA	34	Gamma	2.2E-8	0.1	6 relay bus pairs

Table 9.6. (continued)

	Initiating event	Accident sequence	Containment failure mode	Terminal event seq. frequency per yr	man-rem/yr	Dominant components
Acceleration level 5	RVR	7	Gamma	1.1E-7	0.5	
	RVR	6	Gamma	2.0E-8	0.1	
	T2	4	Delta	1.7E-8	0.1	
	T2	4	Gamma	7.3E-9	0	
Acceleration level 6	RVR	7	Gamma	5.0E-8	0.2	
	RVR	4	Delta	4.4E-9	0	3 pipe pairs 2 pipe pairs 2 single pipes
	RVR	7	Delta	1.6E-9	0	
Release category 3:						
Acceleration level 2	T2	4	Alpha	1.3E-7	0.7	
	SSLOCA	29	Alpha	1.5E-9	0	
Acceleration level 3	T2	4	Alpha	3.9E-8	0.2	
	SSLOCA	29	Alpha	7.5E-9	0	
	RVR	1	Alpha	3.3E-9	0	None
	LLOCA	13	Alpha	2.1E-9	0	2 single pipes
Acceleration level 4	SLOCA	21	Delta	2.7E-7	1.5	2 pipe pairs 2 single pipes
	SSLOCA	21	Delta	6.9E-8	0.4	3 pipe pairs single pipe
	MLOCA	21	Delta	2.4E-8	0.1	
Acceleration level 5	SLOCA	21	Delta	8.4E-8	0.5	
	MLOCA	21	Delta	5.3E-9	0	
	SSLOCA	21	Delta	2.5E-9	0	

Table 9.6. (continued)

	Initiating event	Accident sequence	Containment failure mode	Terminal event seq. frequency per yr	man-rem/yr	Dominant components
Release category 6:						
Acceleration level 4	SSLOCA	34	Epsilon	1.5E-7	0	6 relay bus pairs
	T2	4	Epsilon	9.4E-8	0	
	LLOCA	27	Epsilon	2.6E-8	0	2 single pipes 3 pipe pairs
	MLOCA	27	Epsilon	5.6E-9	0	
Acceleration level 5	LLOCA	27	Epsilon	2.2E-8	0	
	SSLOCA	34	Epsilon	2.0E-8	0	
	T2	4	Epsilon	5.8E-9	0	
	MLOCA	27	Epsilon	1.6E-9	0	
Release category 7:						
Acceleration level 1	T2	4	Epsilon	7.0E-8	0	
	MLOCA	13	Epsilon	1.5E-8	0	
Acceleration level 2	T2	4	Epsilon	1.3E-5	0.3	
	SSLOCA	29	Epsilon	1.5E-7	0	
Acceleration level 3	T2	4	Epsilon	3.9E-6	0.1	
	SSLOCA	29	Epsilon	7.4E-7	0	
	RVR	1	Epsilon	3.3E-7	0	
	LLOCA	13	Epsilon	2.1E-7	0	2 single pipes 3 pipe pairs
	MLOCA	13	Epsilon	4.3E-8	0	
Acceleration level 6	RVR	1	Epsilon	5.7E-8	0	
	LLOCA	13	Epsilon	1.1E-8	0	2 single pipes 3 pipe pairs single pipe 2 single pipes

Table 9.7. Characterstics of dominant accident sequences with no correlation for fragility functions and calculated correlations for structure responses, without feed-and-bleed and without structural failures.

	Initiating event	Accident sequence	Containment failure mode	Terminal event seq. frequency per yr	man-rem/yr	Dominant components
Release category 1:						
Acceleration level 4	SLOCA	21	Alpha	2.5E-9	0.01	3 pipe pairs 2 single pipes
	SSLOCA	21	Alpha	2.4E-9	0.01	3 pipe pairs 2 single pipes
	T2	4	Alpha	1.9E-9	0	
	SSLOCA	34	Alpha	5.1E-10	0	relay and bus
	LLOCA	27	Alpha	3.4E-10	0	2 single pipes 3 pipe pairs
	MLOCA	21	Alpha	2.5E-10	0	3 pipe pairs 1 single pipe
Acceleration level 5	SLOCA	21	Alpha	1.1E-9	0	3 pipe pairs 2 single pipes
	RVR	7	Alpha	4.9E-10	0	3 pipe pairs 2 single pipes
	SSLOCA	21	Alpha	4.5E-10	0	3 pipe pairs 2 single pipes
	LLOCA	27	Alpha	4.2E-10	0	2 single pipes 3 pipe pairs 2 single pipes
	T2	4	Alpha	3.5E-10	0	
Acceleration level 5	LLOCA	28	Alpha	3.2E-10	0	2 single pipes
	SSLOCA	34	Alpha	1.6E-10	0	relay & bus
Acceleration level 6	RVR	7	Alpha	1.6E-9	0	2 pipe pairs 1 single pipe
	SLOCA	21	Alpha	4.2E-10	0	3 pipe pairs 2 single pipes 2 pipe pairs
	LLOCA	28	Alpha	3.6E-10	0	1 single pipe

Table 9.7. (continued)

	Initiating event	Accident sequence	Containment failure mode	Terminal event seq. frequency per yr	man-rem/yr	Dominant components
Release category 2:						
Acceleration level 4	T2	4	Delta	1.1E-7	0.5	
	T2	4	Gamma	4.6E-8	0.2	
Acceleration level 5	T2	4	Delta	2.0E-8	0.1	
	T2	4	Gamma	8.4E-9	0	
	RVR	7	Gamma	7.4E-9	0	3 pipe pairs 2 single pipes
	LLOCA	27	Gamma	5.1E-9	0	2 single pipes 3 pipe pairs 2 single pipes
Acceleration level 6	RVR	7	Gamma	2.4E-8	0.1	2 pipe pairs 1 single pipe
	LLOCA	27	Gamma	1.6E-9	0	2 single pipes 3 single pipes
Release category 3:						
Acceleration level 2	T2	4	Alpha	3.5E-9	0	
Acceleration level 3	T2	4	Alpha	4.4E-9	0.02	
	LLOCA	13	Alpha	2.1E-9	0.01	2 single pipes
	SSLOCA	29	Alpha	8.4E-10	0	
	MLOCA	13	Alpha	4.4E-10	0	4 single pipes
	SSLOCA	7	Delta	3.0E-10	0	2 pipe pairs 2 single pipes

Table 9.7. (continued)

	Initiating event	Accident sequence	Containment failure mode	Terminal event seq. frequency per yr	man-rem/yr	Dominant components
Acceleration level 4	SLOCA	21	Delta	2.6E-7	1.38	3 pipe pairs 2 single pipes
	SSLOCA	21	Delta	2.4E-7	1.28	3 pipe pairs 2 single pipes
	MLOCA	21	Delta	2.4E-8	0.13	3 pipe pairs 1 single pipe
Acceleration level 5	SLOCA	21	Delta	1.1E-7	0.57	3 pipe pairs 2 single pipes
	SLOCA	21	Delta	4.5E-8	0.24	3 pipe pairs 2 single pipes
Acceleration level 6	SLOCA	21	Delta	4.1E-8	0.22	3 pipe pairs 2 single pipes 2 pipe pairs
	MLOCA	21	Delta	4.4E-9	0.02	2 pipe pairs 1 single pipe 3 pipe pairs
Release category 6:						
Acceleration level 4	SSLOCA	34	Epsilon	4.2E-8	0	relay & bus
	T2	4	Epsilon	3.6E-8	0	
	LLOCA	27	Epsilon	2.8E-8	0	2 single pipes 3 pipe pairs
	MLOCA	27	Epsilon	6.2E-9	0	
Acceleration level 5	LLOCA	27	Epsilon	3.5E-8	0	2 single pipes 3 pipe pairs 2 single pipes
	SSLOCA	34	Epsilon	1.4E-8	0	relay & bus
	T2	4	Epsilon	6.6E-9	0	
	MLOCA	27	Epsilon	2.5E-9	0	

Table 9.7. (continued)

	Initiating event	Accident sequence	Containment failure mode	Terminal event seq. frequency per yr	man-rem/yr	Dominant components
Acceleration level 6	LLOCA	27	Epsilon	1.1E-8	0	2 single pipes 3 pipe pairs 3 single pipes
Release category 7:						
Acceleration level 1	MLOCA	13	Epsilon	1.5E-8	0	
	T2	4	Epsilon	3.2E-9	0	
Acceleration level 2	T2	4	Epsilon	3.5E-7	0	
Acceleration level 3	T2	4	Epsilon	4.4E-7	0	
	LLOCA	13	Epsilon	2.1E-7	0	2 single pipes
	SSLOCA	29	Epsilon	8.3E-8	0	
	MLOCA	13	Epsilon	4.4E-8	0	4 single pipes
Release category 7:						
Acceleration level 4	LLOCA	28	Epsilon	5.7E-9	0	
	LLOCA	28	Delta	5.6E-9	0	
	MLOCA	28	Epsilon	4.9E-9	0	1 single pipe
	MLOCA	28	Delta	4.8E-9	0	1 single pipe
	SSLOCA	35	Epsilon	3.3E-9	0	
Acceleration level 5	LLOCA	28	Epsilon	1.6E-8	0	2 single pipes
	LLOCA	28	Delta	1.6E-8	0	2 single pipes
	MLOCA	28	Epsilon	3.5E-9	0	1 single pipe
	MLOCA	28	Delta	3.4E-9	0	1 single pipe
	SSLOCA	35	Epsilon	1.8E-9	0	
Acceleration level 6	LLOCA	28	Epsilon	1.8E-8	0	1 single pipe
	LLOCA	28	Delta	1.7E-8	0	1 single pipe
	MLOCA	28	Epsilon	1.9E-9	0	
	MLOCA	28	Delta	1.8E-9	0	3 pipe pairs

that this approximation may overestimate the effects of correlation. Use of Eq. (9.2) is currently standard within the industry, and although there are certain promising techniques on the horizon which may provide more accurate estimates, the use of Eq. (9.2) is the best technique available today. As discussed in Chapter 11, a task in the verification program of the SSMRP will address the question of the possible over-conservatisms induced by the use of Eq. (9.2) to determine accident sequence probabilities.

CHAPTER 10: SENSITIVITY TO LOCAL SITE EFFECTS AND SOIL-STRUCTURE INTERACTION ASSUMPTIONS

Computations of structure and subsystem responses included effects of local site conditions and structure-to-structure interaction. These effects are not routinely included in nuclear power plant design calculations. The significance of these effects was closely examined through their effects on responses and radioactive release frequency. Both the containment building and the Auxiliary Fuel-Handling Turbine Building (AFT) were assumed to have a rigid foundation. For the containment building, the assumption is easily justifiable, considering the thickness of the foundation and the stiffening effects of the containment shell and internal structure. For the AFT complex, the assumption was validated by making response comparisons of a single rigid-foundation model with a flexible-foundation model composed of a series of 11 rigid segments.

10.1 Local Site Effects

10.1.1 Response Results

One major source of modeling uncertainty that was not treated with the inner/outer loop computational procedure (Chap. 2) was the phenomenon of local site amplification for the Zion site. Amplification of free-field ground motion by a shallow soil site such as Zion (110 ft. of soil over bedrock) can have a profound effect on the seismic hazard curve and on the free-field acceleration time histories. Modeling of site amplification was discussed in detail in Chap. 3. For the Zion risk analysis calculations (random variability only, total uncertainty, and uncertainty intervals), local site amplification was modeled explicitly in generating the seismic hazard curve and in the seismic response calculations. This represented our best estimate of the effects of local site amplification; however, we recognize the large uncertainty in all such models, given the present state of the art.

To assess the effect of local site amplification on seismic responses and seismic risk, a second analysis was performed with free-field acceleration for a seismic hazard curve developed for a generic soil site. Chapter 3 described the process and results. The seismic hazard curves of Fig. 3.5 are reproduced here in Fig. 10.1. Two comparisons are made to assess the effects of local site amplification--seismic responses and seismic risk.

To compare seismic responses, a common basis must be established. Recall that the seismic hazard curve is discretized into intervals of peak free-field acceleration for which seismic response calculations and systems analyses are performed. The common basis for comparison of seismic responses was selected to be intervals of peak free-field acceleration with equal probabilities of occurrence. For the two differing seismic hazard curves, intervals of equal probability of occurrence lead to earthquakes with different peak accelerations. Figure 10.1 shows two ranges of earthquakes for which responses are compared--acceleration ranges 2 and 4. Acceleration range 2 has peak rock outcrop accelerations of 0.10-0.20 g and corresponding peak soil surface accelerations of 0.17-0.48 g, which result from explicit modeling of

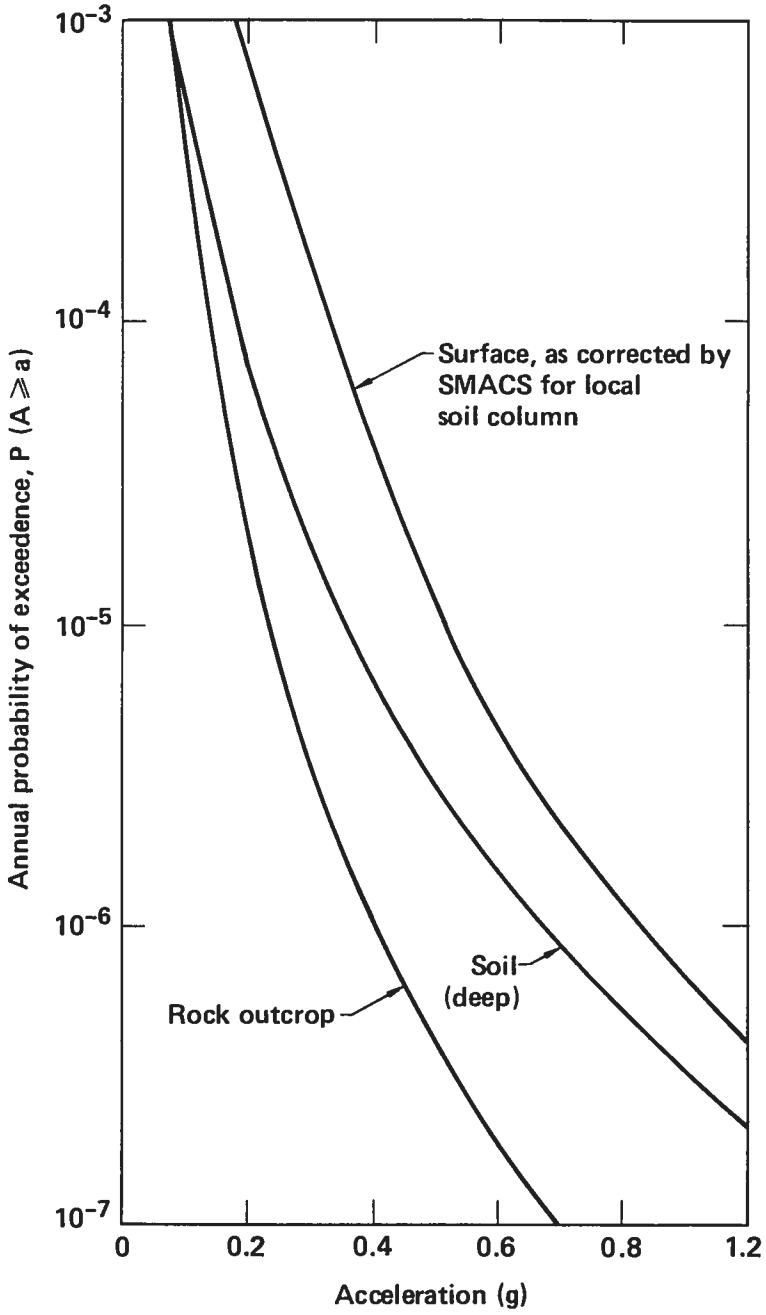

Fig. 10.1. Zion hazard curves compared. Hazard curves with and without effects of local soil column. For reference, the "rock outcrop" hazard curve is also shown.

local site amplification at the Zion site. Note that an interval of peak acceleration on the rock outcrop generates a wider interval of peak acceleration on the soil surface; i.e., uncertainty in soil properties increases variability of the earthquake time histories. Acceleration range 2 for the case without local site amplification contains earthquakes with peak accelerations of 0.11-0.22 g. Figure 10.2a shows a comparison of median responses for acceleration range 2, with local site amplification and without. The average ratio is 0.54 for foundation horizontal accelerations, 0.80 for foundation vertical acceleration, 0.54 for structure horizontal response, 0.75 for structure vertical response, 0.58 for piping system accelerations, and 0.60 for piping system resultant moments. Hence, for equal-probability earthquakes, the modeling uncertainty attributable to local site amplification is itemized. Note that vertical free-field motion and, consequently, vertical response is less affected by local site amplification. In general, a comparison of beta values shows up to 10% effect, but the majority of response beta values are the same.

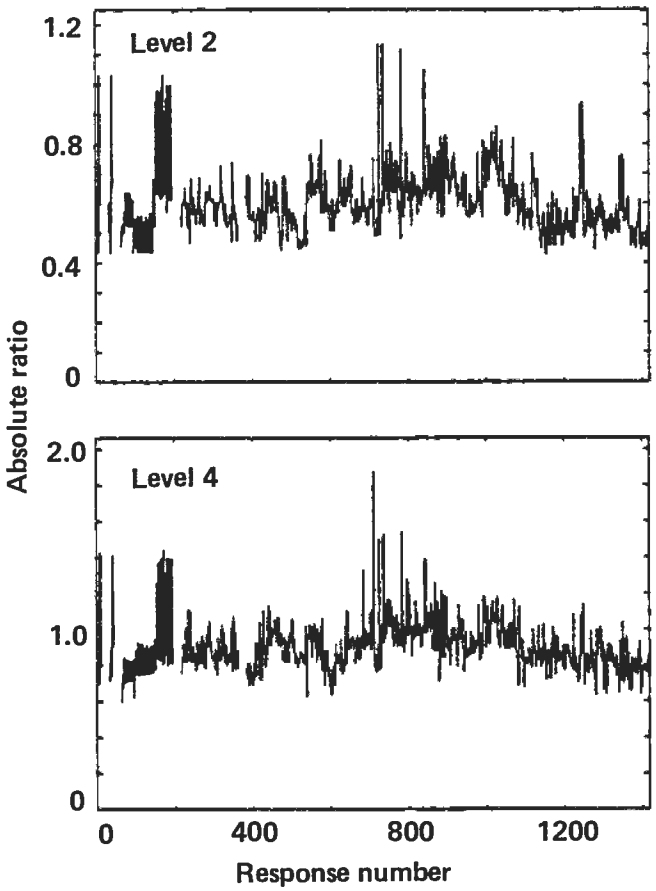

Fig. 10.2a. Comparison of median responses with and without local site effects for earthquake acceleration levels 2 and 4.

Acceleration range 4 has peak rock outcrop accelerations of 0.32-0.48 g and corresponding peak soil surface accelerations of 0.49-1.1 g, which, again, result from explicit modeling of local site amplification. For the case without local site amplification, acceleration range 4 contains earthquakes with peak accelerations of 0.53-0.69 g. For this case, median responses are closer (Fig. 10.2). The average ratio is 0.82 for foundation horizontal response, 1.14 for foundation vertical response, 0.81 for structure horizontal response, 1.04 for structure vertical response, 0.88 for piping system accelerations, and 0.91 for piping system resultant moments. Modeling uncertainty of local site amplification for this acceleration range is not as significant as for lower acceleration ranges. Beta values are similar. Hence, at high probabilities of occurrence, large differences in response are observed, whereas, for rarer events, the differences are less pronounced. One method of assimilating this information is by examining seismic risk, which is discussed next.

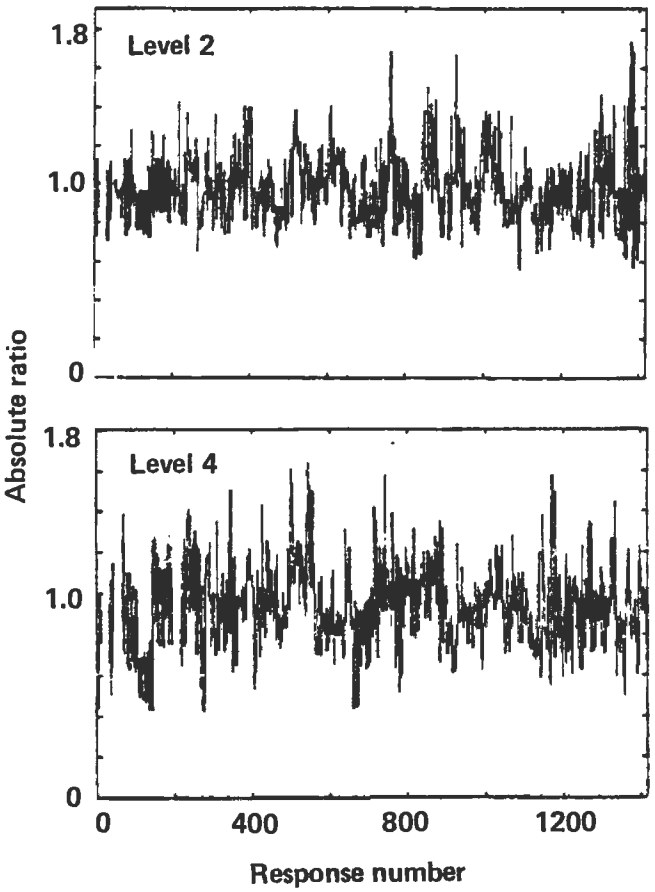

Fig. 10.2b. Comparison of betas with and without local site effects for earthquake acceleration levels 2 and 4.

10.1.2 System Results

As pointed out in the preceding section, effect of local site amplification is pronounced at the lower earthquake levels. As the excitation level increases, the differences in response decrease. In this section, system results are presented.

Table 10.1 is a direct comparison of release frequency and dose per year for the two cases. Release frequencies in each category show higher values with local site effects than without, as expected. The core melt frequency with local site effects is larger by a factor of four than the core melt frequency without, (3.56×10^{-6} vs 9.26×10^{-7}). Dose release shows a similar magnitude of effect, (9.62 vs 2.72). Table 10.2 lists release frequencies in each category. The release frequencies are higher with local site effect included than without, with few exceptions. For example, for release category 3 of earthquake level 3, it is 8.09E-8 vs 1.07E-7 (with vs without). The major contributors are from small LOCA-21 and small-small LOCA-21, which are due to the failure of three pairs of inter-building pipes (as shown in Table 10.3). The major difference comes from small-small LOCA-21. The cut set for this accident sequence is the success of the reactor protection system (RPS), the auxiliary feedwater systems (AFWS), the emergency cooling injection (ECI) for the small-small LOCA, the emergency cooling recirculation system (ECR) for the small-small LOCA, the failure of the containment spray injection system (SIS), and the residual heat removal systems (RHR). Success probabilities for the AFWS, the ECI, and the ECR are much lower with local site effect than without. The component failures which cause the large LOCA and reactor pressure vessel rupture initiating events are the failure of the

Table 10.1. Release frequency and dose per year computed with and without the effect of local site conditions.

	With local site effect		Without local site effect	
Release category	Release frequency per yr	man-rem/yr	Release frequency per yr	man-rem/yr
1	2.94E-8	0.16	6.54E-9	0.04
2	1.35E-6	6.50	3.87E-7	1.86
3	5.39E-7	2.91	1.48E-7	0.80
4	9.22E-11	0	0	0
5	8.32E-10	0	6.58E-11	0
6	1.65E-7	0.02	6.90E-8	0.002
7	1.48E-6	0.03	3.15E-7	0.007
Total	3.57E-6	9.6	9.26E-7	2.72

Table 10.2. Release frequencies per year at different earthquake levels for base case responses computed without local site effects.

Release Category	Earthquake level 2	3	4	5	6	Total	man-rem/yr
1	*	2.72E-10	4.58E-10	3.65E-9	2.16E-9	6.54E-9	0.04
2	9.78E-10	1.36E-7	1.30E-7	8.7E-8	2.81E-8	3.87E-7	1.86
3	1.51E-11	1.74E-9	1.84E-9	1.07E-7	3.72E-8	1.48E-7	0.80
4	*	*	0	*	*	0	0
5	*	*	*	3.21E-11	3.27E-11	6.48E-11	0
6	*	*	3.2E-8	2.34E-8	1.36E-8	6.90E-8	0.02
7	1.74E-9	6.62E-8	5.70E-8	1.12E-7	7.82E-8	3.15E-7	0.007
				Grand Total	9.26E-7	2.72	

* Indicates numerical values less than 10^{-11}.

Table 10.3. Dominant accident sequences for the base case computed without local site effects

	Initiating event	Accident sequence	Containment failure mode	Terminal event seq. frequency per yr	man-rem/yr	Dominant components
Release category 1:						
Acceleration level 3	SSLOCA	35	Alpha	2.07E-10	0	Uplift, roof
	SLOCA	28	Alpha	6.41E-11	0	Uplift, roof
Acceleration level 4	SSLOCA	35	Alpha	2.73E-10	0	Uplift, roof
	SLOCA	28	Alpha	1.44E-10	0	Uplift, roof
	RVR	7	Alpha	1.62E-11	0	Uplift, roof
	LLOCA	28	Alpha	1.56E-11	0	Uplift, roof
Acceleration level 5	T2	4	Alpha	8.69E-10	0.01	Uplift, roof
	SSLOCA	35	Alpha	6.18E-10	0	Uplift, roof
	SSLOCA	21	Alpha	5.94E-10	0	Pipe pairs
	SLOCA	21	Alpha	4.48E-10	0	Pipe pairs
	SLOCA	28	Alpha	3.76E-10	0	Uplift, roof
	RVR	7	Alpha	3.49E-10	0	Uplift, roof
	LLOCA	28	Alpha	1.45E-10	0	Uplift, roof
	MLOCA	28	Alpha	8.53E-11	0	Uplift, roof
Acceleration level 6	RVR	7	Alpha	5.85E-10	0	Uplift, roof
	SLOCA	28	Alpha	3.01E-10	0	Uplift, roof
	SLOCA	21	Alpha	2.91E-10	0	Pipe pairs
	SSLOCA	35	Alpha	2.85E-10	0	Uplift, roof
	LLOCA	28	Alpha	1.71E-10	0	Uplift, roof
	T2	4	Alpha	1.31E-10	0	Uplift, roof
	RVR	6	Alpha	1.06E-10	0	CSIS & CFCS(I),CSRS
	LLOCA	27	Alpha	9.61E-11	0	Single pipe
	MLOCA	28	Alpha	7.57E-11	0	Uplift, roof
Release category 2:						
Acceleration level 3	T2	4	Delta/Gamma	1.31E-7	0.63	Uplift, roof
Acceleration level 4	T2	4	Delta/Gamma	1.30E-7	0.62	Uplift, roof

Table 10.3. (continued)

	Initiating event	Accident sequence	Containment failure mode	Terminal event seq. frequency per yr	man-rem/yr	Dominant components
Acceleration level 5	T2	4	Delta	4.87E-8	0.23	Uplift, roof
	T2	4	Gamma	2.09E-8	0.10	Uplift, roof
	SSLOCA	35	Gamma	7.42E-9	0.04	Uplift, roof
	RVR	7	Gamma	5.30E-9	0.03	Uplift, roof
Acceleration level 6	RVR	7	Gamma	8.88E-9	0.04	Uplift, roof
	T2	4	Delta	7.34E-9	0.04	Uplift, roof
	SSLOCA	35	Gamma	3.42E-9	0.02	Uplift, roof
	T2	4	Gamma	3.15E-9	0.02	Uplift, roof
	RVR	6	Gamma	1.60E-9	0.01	CSIS & CFCS(I), CSRS
	LLOCA	27	Gamma	1.15E-9	0.01	Single pipe
	SSLOCA	35	Delta	1.14E-9	0.01	Uplift, roof
Release category 3:						
Acceleration level 5	SSLOCA	21	Delta	5.88E-8	0.32	Pipe pairs
	SLOCA	21	Delta	4.43E-8	0.24	Pipe pairs
	MLOCA	21	Delta	4.33E-9	0.02	Pipe pairs
Acceleration level 6	SLOCA	21	Delta	2.88E-8	0.16	Pipe pairs
	SSLOCA	21	Delta	4.88E-9	0.03	Pipe pairs
	MLOCA	21	Delta	3.54E-9	0.02	Pipe pairs
Release category 6:						
Acceleration level 5	T2	4	Epsilon	1.65E-8	0	Uplift, roof
	LLOCA	27	Epsilon	4.80E-9	0	Single pipe
Acceleration level 6	LLOCA	27	Epsilon	7.97E-9	0	Single pipe
	T2	4	Epsilon	2.49E-9	0	Uplift, roof
	SSLOCA	34	Epsilon	1.54E-9	0	Uplift, roof
	MLOCA	27	Epsilon	1.17E-9	0	Uplift, roof
Acceleration level 4	T2	4	Epsilon	3.2E-8		Uplift, roof
Release category 7:						
Acceleration level 3	T2	4	Epsilon	1.63E-7	0	Uplift, roof
	SSLOCA	35	Epsilon	1.72E-8	0	Uplift, roof

Table 10.3. (continued)

	Initiating event	Accident sequence	Containment failure mode	Terminal event seq. frequency per yr	man-rem/yr	Dominant components
Acceleration level 4	SSLOCA	35	Epsilon	2.27E-8	0	Single pipe
	LLOCA	13	Epsilon	1.16E-8	0	Uplift, roof
Acceleration level 5	SSLOCA	35	Epsilon	5.13E-8	0	Uplift, roof
	SLOCA	28	Epsilon	1.88E-8	0	Uplift, roof
	SLOCA	28	Delta	1.84E-8	0	Uplift, roof
	LLOCA	28	Epsilon	7.26E-9	0	Uplift, roof
	LLOCA	28	Delta	7.11E-9	0	Uplift, roof
	MLOCA	28	Epsilon	4.27E-9	0	Uplift, roof
	MLOCA	28	Delta	4.18E-9	0	Uplift, roof
Acceleration level 6	SSLOCA	35	Epsilon	2.37E-8	0	Uplift, roof
	SLOCA	28	Epsilon	1.50E-8	0	Uplift, roof
	SLOCA	28	Delta	1.47E-8	0	Uplift, roof
	LLOCA	28	Epsilon	8.55E-9	0	Uplift, roof
	LLOCA	28	Delta	8.38E-9	0	Uplift, roof
	MLOCA	28	Epsilon	3.79E-9	0	Uplift, roof
	MLOCA	28	Epsilon	3.71E-9	0	Uplift, roof

primary coolant piping due to the failure of the supports of the steam generators and reactor coolant pumps. The component failures which cause the medium LOCA and small LOCA initiating events are the failure of the primary coolant piping, equivalent to break of a single pipe whose diameter is 3 to 6 inches, and of 1.5 to 3 inches, respectively. Higher responses were observed from the effects of local site conditions, making reactor pressure vessel rupture, large LOCA, medium LOCA, and small LOCA initiating events more probable. This, in turn, causes the lower initiating event probability for small-small LOCA event (see Tables 10.4 and 7.3). Recall that the terminal event sequence probability is defined as the product of the earthquake occurrence, initiating event, accident sequence and containment failure probabilities. The common basis for the comparison of seismic risk was selected to be intervals of peak free-field acceleration with equal probabilities of earthquake occurrence. The difference of containment failure probability is minimal between these two cases. The remaining initiating event and accident sequence probabilities are lower with the effects of local soil conditions. This explains why some release category frequencies are lower even though the effects of local site conditions are included.

10.2 Effects of Structure-to-Structure Interaction

10.2.1 Response Results

As discussed in Sec. 4.2.2, the major difference between the SSI models of SSMRP Phases I and II was the inclusion of structure-to-structure interaction effects in the latter case. "Structure-to-structure interaction" refers to an effect that earthquake-induced vibration of a structure has on an adjacent structure. Interaction is of potential significance for nuclear power plants because of the small distances which often separate adjacent structure and the large massive structure-foundation systems involved. Two characteristics of the structures and foundations affect structure-to-structure interaction--the relative size of the foundations and the relative mass of the structures. In

Table 10.4. Initiating event conditional probabilites for the base case computed without local site effects.

Initiating events	Earthquake acceleration levels					
	1	2	3	4	5	6
RVR		0	9.66E-9	1.46E-3	1.70E-2	7.12E-2
LLOCA		0	3.50E-6	8.31E-3	5.68E-2	1.65E-1
MLOCA		0	6.60E-4	3.98E-3	3.43E-2	7.77E-2
SLOCA		1.30E-4	3.29E-2	6.92E-2	1.97E-1	3.67E-1
SSLOCA		3.68E-4	1.06E-1	1.31E-1	2.94E-1	2.22E-1
T2		1.35E-1	8.47E-1	7.86E-1	4.00E-1	9.64E-2
T1		8.65E-1	1.30E-2	3.10E-6	0	

both cases, the larger of the two affects the smaller. For the Zion nuclear power plant, three foundations were considered--two containment building foundations and the AFT complex. The AFT complex foundation is significantly larger than either containment building foundation. In addition, the mass of the AFT complex is approximately five times the mass of either containment building. Hence, both important characteristics of the structure-foundation system indicate that structure-to-structure interaction will have a greater effect on response of the containment building than on the AFT complex. Indeed, this was shown to be the case for deterministic analyses (Vol. 4 of Ref. 1). Response results for our systems analyses are compared here.

Table 10.5 itemizes a comparison of responses of the foundation (peak and spectral acceleration), in the structures (peak and spectral acceleration), and in piping systems (peak accelerations and resultant moments). Comparisons of median values and betas are included and discussed below. In general, when structure-to-structure interaction was included, all median responses tended to remain the same or increase. Exceptions were horizontal response in the AFT complex and peak accelerations in four piping systems, which decreased slightly. Table 10.5 shows results for acceleration range 2, which are typical of all acceleration ranges.

Table 10.5. Median responses and beta values with and without structure-to-structure interaction for acceleration range 2.

(a) FOUNDATION AND STRUCTURE RESPONSE (PEAK AND SPECTRAL ACCELERATIONS)

	Ratio of medians		Ratio of betas		No. of response points
	Mean	COV	Mean	COV	
Containment building foundation					
NS	0.999	0.035	0.947	0.088	4
EW	1.01	.018	1.01	0.106	4
Vertical	1.56	0.108	0.909	0.045	4
Top of containment shell					
NS	1.11		0.775		1
EW	1.23		1.07		1
Vertical	1.64		0.898		1
Internal structure					
NS	1.02	0.074	0.848	0.053	10
EW	1.06	0.043	1.03	0.086	10
Vertical	1.55	0.079	0.952	0.078	8
AFT complex					
NS	0.945	0.015	0.982	0.025	40
EW	0.976	0.027	0.997	0.031	20
Vertical	1.09	0.069	0.993	0.037	40

Table 10.5. (Continued)

(b) PIPING SYSTEM RESPONSE (ACCELERATIONS AND MOMENTS)

	Ratio of medians		Ratios of betas		No. of	Supporting
	Mean	COV	Mean	COV	responses	structures[a]
SW to AFW pump						
Accel.	0.995	0.014	1.04	0.060	13	3
Mom.	1.01	0.033	1.02	0.053	132	
RHR pump discharge						
Accel.	0.964	0.016	1.05	0.017	9	3
Mom.	1.02	0.037	1.07	0.069	34	
RHR pump suction						
Accel.	1.05	0.086	1.09	0.118	8	5
Mom.	1.14	0.163	1.01	0.049	50	
RHR and SI-1						
Accel.	1.01	0.008	0.948	0.015	2	4
Mom.	1.10	0.158	0.975	0.049	22	
RHR and SI-2						
Accel.	0.978	0.034	1.02	0.051	21	4
Mom.	1.02	0.127	0.998	0.066	69	
Boron inj. tank to containment						
Accel.	1.05	0.022	1.00	0.005	2	4
Mom.	1.17	0.071	1.01	0.019	15	
Charging pump discharge						
Accel	0.976	0.030	0.992	0.159	18	3
Mom.	1.01	0.070	0.972	0.125	107	
Pressurizer relief lines						
Accel	1.09	0.046	0.921	0.048	7	1
Mom.	1.20	0.154	0.929	0.075	26	
AFW SG-1A to containment						
Accel.	1.01		0.974		1	2
Mom.	1.08	0.147	0.933	0.079	23	
AFW Outside containment						
Accel.	1.02	0.45	1.03	0.083	25	4
Mom.	1.12	0.168	0.981	0.096	116	
RCL and branch Lines						
Accel.	1.11	0.043	0.976	0.049	17	1
Mom.	1.27	0.172	0.909	0.115	118	

Table 10.5. (Continued)

(b) PIPING SYSTEM RESPONSE (ACCELERATIONS AND MOMENTS)

	Ratio of Medians		Ratios of betas		No. of	Supporting
	Mean	COV	Mean	COV	responses	structures[a]
Pressurizer relief lines						
Accel.	1.09	0.046	0.921	0.048	7	1
Mom.	1.20	0.154	0.929	0.075	26	
AFW SG-1B to cont.						
Accel.	1.05	--	0.983	--	1	2
Mom.	1.14	0.101	1.01	0.110	27	
AFW SG-1C to cont.						
Accel.	1.17	--	1.12	--	1	2
Mom.	1.25	0.173	1.20	0.136	28	
AFW SG-1D to cont.						
Accel.	1.11	--	1.05	--	1	2
Mom.	1.19	0.159	1.13	0.105	27	
MS lines inside cont.						
Accel.	1.09	0.005	0.924	0.015	2	2
Mom.	1.65	0.185	1.06	0.202	8	
MS lines outside cont.						
Accel.	1.08	0.005	1.04	0.064	2	4
Mom.	1.44	0.176	1.05	0.043	12	
Aux. MS outside cont.						
Accel.	1.12	0.068	0.929	0.097	4	4
Mom.	1.37	0.132	1.41	0.204	12	
Aux. MS inside cont.						
Accel.	--	--	--	--	0	2
Mom.	1.27	0.187	1.15	0.210	52	

Supporting Structures

[a] 1. Inside containment--internal structure alone.
2. Inside containment--internal structure and containment shell.
3. AFT complex alone.
4. AFT complex to containment shell.
5. AFT complex to internal structure.

- Foundation response. Response of the containment building foundation only has been saved for input to the systems analysis. Horizontal response of the containment building foundation is minimally affected by structure-to-structure interaction. Vertical response, however, is increased by 56%. Note that increases in vertical response are observed throughout the containment building structures (containment shell and internal structure). This effect is due principally to additional induced vertical motion resulting from rocking of the AFT complex. Betas of response change up to 10%, as shown.

- Structure response. Table 10.5 shows response in three structures--containment shell, internal structure, and AFT complex. In the containment shell, response at only one point was saved for input to the systems analysis. Horizontal and vertical accelerations are both increased when structure-to-structure interaction is included. Vertical response increase most (64%), as discussed above. The greater flexibility of the containment shell than the internal structure accounts for the enhanced structure-to-structure interaction. Note that responses at several additional points on the containment shell were calculated and used as input to piping systems. Hence, changes in response of the containment shell manifest themselves in piping system response. Horizontal response in the internal structure changes by up to 11%, with the average increases being 2% and 6% in each direction. Vertical response again changes the most, with an average of 55% and a maximum increase of 78%. As expected, the AFT complex is least affected by structure-to-structure interaction (shown by the ratios of Table 4.5).

- Piping system response. Two forms of response are calculated for piping systems--peak accelerations and resultant moments. Table 4.5 tabulates results for both. Piping systems may be categorized by location within the Zion Unit 1 structures as follows:

  - Outside the containment and the AFT complex, e.g., in the crib house or underground. Two piping systems fall in this category. Their responses are unaffected by structure-to-structure interaction and are not included in Table 10.5.
  - Inside the containment, supported on the internal structure alone or on the internal structure and containment shell. Eight piping systems fall in this category.
  - Supported entirely in the AFT complex. Three piping systems are in this category.
  - Supported in the AFT complex and one support on the containment shell or internal structure. Seven piping systems fit this category.

  Some observations can be made concerning piping system responses.

  - In general, accelerations in piping systems were affected least by structure-to-structure interaction--median responses varied -4% to +17%.

- Responses (accelerations and moments) were minimally affected for piping systems supported entirely in the AFT complex, as expected.

- For piping systems supported inside the containment and running between the containment and the AFT complex, increases in piping moments occur. Average values are shown in Table 4.5. It appears that increased accelerations in the internal structure produce increased piping moments. Also, all piping system elements connected to the containment shell experienced large increases (up to 110%) due to structure-to-structure interaction. The average statistics do not explicitly show this fact.

Hence, structure-to-structure interaction has an important effect on response. Following sections interpret these increases from a systems viewpoint, determining how they affect risk.

10.2.2 System Results

As discussed in the preceding section, responses are affected by structure-to-structure interaction. In this section, we present the effect of structure-to-structure interaction on the system analysis. Table 10.6 shows the comparison of core melt frequency and dose. As shown in the table, the core melt frequency is increased by 20% (3.57E-6 vs 2.94E-6) and the dose is increased by 10% (9.63 vs 8.7 man-rem/year). The base case, which included the effects of structure-to-structure interaction in the response calculations, was described in Section 7.1. Table 10.7 compares release frequencies and doses per year in each category. In general, the release category frequencies are higher with structure-to-structure interaction than without. Table 10.8 shows release category frequencies per year in each earthquake level without the effect. The major contribution to release frequencies are found from earthquake levels 2, 3 and 4. Table 10.8 shows initiating event conditional probabilities for the seven initiators. Closely examining Tables 10.8 and 7.3 (base case) we find that, at level 2, initiating event probabilities do not differ. As the earthquake acceleration level increases, initiating event probabilities due to LOCAs increase more rapidly with the interaction effects than without. The reasoning is that the initiating probabilities are the joint failure probabilities contributed from pipe breaks in the primary coolant system and the associated branch lines inside the containment building. These structure and subsystem responses are generally affected by the interaction effects. In addition, because of the hierarchy in the calculation of initiating event probabilities, the probabilities for transients T2 and T1 decrease at a faster rate with the effects than without. Table 10.9 represents dominant accident sequences. This table and Table 7.4 reveal that the dominant accident sequences generally remain the same with and without the interaction effects.

As discussed in the previous section, the structure and subsystem responses tend to remain the same or increase for the containment building and the subsystem housed inside the containment and running between the containment and AFT building. Table 10.10 shows the comparison of structure responses at selected structure locations for acceleration level 4. If the accident sequences are primarily due to the failure of the structures (e.g., basemat uplift or service-water pumps enclosure roof) then the terminal event

Table 10.6. Release frequencies and dose with and without the effect of structure-to-structure interaction.

Release category	With structure-to-structure interaction: Release frequency per yr	With structure-to-structure interaction: man-rem/yr	Without structure-to-structure interaction: Release frequency per yr	Without structure-to-structure interaction: man-rem/yr
1	2.94E-8	.16	2.09E-08	0.113
2	1.35E-6	6.50	1.70E-06	8.16
3	5.39E-7	2.91	6.77E-08	0.365
4	9.22E-11	0	3.19E-11	8.6E-05
5	8.32E-10	0	2.49E-10	2.5E-04
6	1.65E-7	.02	2.46E-07	0.037
7	1.48E-6	.03	9.06E-07	0.02
TOTAL	3.57E-6	9.63	2.94E-6	8.7

Table 10.7. Frequencies of release per year at different earthquake levels for the base case computed without structure-to-structure interaction.

Release category	Earthquake acceleration levels: 1	2	3	4	5
1		2.05E-11	1.33E-09	9.70E-09	9.81-09
2		2.89E-07	7.48E-07	4.65E-07	1.93E-07
3		4.06E-09	1.18E-08	3.96E-08	1.22E-08
4		0	0	0	3.17E-11
5		0	0	2.99E-11	2.19E-10
6		0	0	1.83E-07	6.30E-08
7		1.15E-07	5.30E-07	1.51E-07	1.09E-07

Table 10.8. Initiating event conditional probabilities for the base case computed without structure-to-structure interaction.

Initiating events	Earthquake acceleration levels 1	2	3	4	5
RVR		3.21E-5	5.42E-3	1.51E-2	2.86E-1
LLOCA		2.06E-4	1.59E-2	4.32E-2	2.20E-1
MLOCA		3.21E-5	1.04E-3	5.14E-2	3.01E-2
SLOCA		2.02E-5	1.51E-2	4.84E-2	5.65E-2
SSLOCA		5.15E-3	6.67E-2	1.45E-1	1.40E-1
T2		8.18E-1	8.95E-1	7.43E-1	2.68E-1
T1		1.76E-1	7.65E-4	2.30E-6	1.07E-7

frequencies are determined by initiating events. Recall that the terminal event frequency is the product of four parameters, namely, the earthquake occurrence probability, the containment failure probability, the accident sequence probability, and the initiating event probability. If the accident sequences are primarily due to the failure of pipes, then the terminal event frequencies are determined by both initiating event and accident pipe sequence probabilities. The dominant components contributing to the failure are those which run between the AFW complex and containment building, such as the safety injection piping from the RHR heat exchanger to the cold injection leg.

10.3 AFT Complex Foundation Model

Foundation modeling for the response calculations was discussed in Sec. 4.2.2 for the reactor buildings and the AFT complex. In both cases, rigid foundations were assumed. For the reactor building, a rigid foundation is easily justifiable, considering the thickness of the foundation and the stiffening effects of the containment shell and internal structure. However, modeling the AFT complex foundation as rigid required additional study and justification. Foundation modeling is another example of modeling uncertainty.

To evaluate the rigid foundation assumption, we analyzed the AFT complex for two conditions--a single rigid foundation and a series of 11 rigid segments (Fig. 10.3). Coupling between the 11 segments was treated in two ways: (1) coupling through the super-structure and foundations themselves was modeled by the structure model, (2) through-soil coupling was included in the generation of the impedances for the 11 rigid segments. Note that the rigid segments were selected according to structure and foundation layout conditions.

The flexible foundation analysis was an extended application of the substructure approach. Recall that the key elements of the substructure approach are specifying the free-field ground motion, determining the foundation input motion, determining foundation impedances, modeling the structure, and the SSI analysis itself. In our investigation, the first three

Table 10.9. Dominant accident sequences for the base case computed without structure-to-structure interaction.

	Initiating event	Accident sequence	Containment failure mode	Terminal event seq. frequency per yr	man-rem/yr	Dominant components
Release category 2:						
Acceleration level 2	T2	4	Delta/Gamma	2.37E-7		Pump encl. roof, uplift
	T1	7	Delta/Gamma	5.11E-8		Pump encl. roof, uplift
Acceleration level 4	T2	4	Delta	2.86E-7	1.37	Pump encl. roof, uplift
			Gamma	1.23E-7	0.59	Pump encl. roof, uplift
Acceleration level 3	T2	4	Delta/Gamma	7.31E-7		Pump encl. roof, uplift
	T1	7	Delta/Gamma	6.24E-10		Pump encl. roof, uplift
Acceleration level 5	RVR	7	Gamma	7.53E-8	0.36	Pump encl. roof, uplift
	T2	4	Delta	4.57E-8	0.22	Pump encl. roof, uplift
			Gamma	1.96E-8	0.10	
	RVR	6	Gamma	3.34E-8	0.16	CFCS & CSIS
Release category 3:						
Acceleration level 4	SLOCA	21	Delta	2.09E-8	0.11	CSIS & CFCS(I), CSRS
	SLOCA	21	Delta	1.73E-8	0.09	6OH1005A ZOH1001CMJ
ZOH1001BMJ 6OH1004A						
Acceleration level 3	T2	4	Alpha	9.22E-9	0.05	Uplift, roof
	SLOCA	13	Alpha	1.75E-9	0.01	
Acceleration level 5	SLOCA	21	Delta	8.80E-9	0.05	3 pipe pairs
	MLOCA	21	Delta	2.05E-9	0.01	3 pipe pairs
	SSLOCA	21	Delta	1.32E-9	0.01	3 pipe pairs
Release category 6:						
Acceleration level 4	T2	4	Epsilon	9.71E-8	0.01	Crib house roof, uplift
	SSLOCA	34	Epsilon	4.91E-8	0.01	MRA1LUBBMG REC1393CMJ REC1393BMJ REC1393AMJ

Table 10.9. (continued)

	Initiating event	Accident sequence	Containment failure mode	Terminal event seq. frequency per yr	man-rem/yr	Dominant components
						MRA11B--MG REC1393CMJ REC1393BMJ REC1393AMJ
	LLOCA	27	Epsilon	3.43E-8	0.01	2 single pipes 3 pipe pairs
Acceleration level 5	LLOCA	27	Epsilon	3.23E-8	0.01	3 single pipes
	T2	4	Epsilon	1.55E-8	0	Crib house roof, uplift
	SSLOCA	34	Epsilon	1.13E-8	0	MRA1LUBBMG MRA11B--MG REC1393CMJ REC1393BMJ REC1393AMJ
Release category 7:						
Acceleration level 2	T2	4	Epsilon	5.93E-8	0	Pump encl. roof, uplift
	T1	7	Epsilon	1.28E-8	0	Pump encl. roof, uplift
	LLOCA	13	Epsilon	2.92E-8	0	6OH1005AMJ
Acceleration level 3	T2	4	Epsilon	1.83E-7	0	Pump encl. roof, uplift
	T1	7	Epsilon	1.56E-10	0	Pump encl. roof, uplift
	LLOCA	13	Epsilon	1.74E-7	0	6OH1005AMJ
Acceleration level 4	SSLOCA	35	Epsilon	8.58E-8	0	Pump encl. roof, uplift
	SLOCA	28	Epsilon	1.66E-8	0	Pump encl. roof, uplift
			Delta	1.63E-8	0	Pump encl. roof, uplift
	LLOCA	28	Epsilon	1.38E-8	0	Pump encl. roof, uplift
			Delta	1.35E-8	0	Pump encl. roof, uplift
Acceleration level 5	SSLOCA	35	Epsilon	3.28E-8	0	Pump encl. roof, uplift
	LLOCA	28	Epsilon	2.61E-8	0	Pump encl. roof, uplift
			Delta	2.56E-8	0	Pump encl. roof, uplift

Table 10.10. Structure responses at selected structure locations at Level 4 with and without structure-to-structure interaction.

Structure location	With structure-to-structure interaction		Without structure-to-structure interaction	
	Median	Beta	Median	Beta
SG	30 (ft/s^2)	0.25	28	0.30
RCP	31 (ft/s^2)	0.32	33	0.30
60H1005A	740,000 (ft-lb)	0.65	427,000	0.58
Z0I1006A	79,000 (ft-lb)	0.54	53,000	0.52
Z0H1001A	3,200 (ft-lb)	0.26	3,400	0.26
Free Field	23,000 (ft/s^2)	0.20	23,000	0.20
Foundation	14,000 (ft/s^2)	0.19	14,000	0.22

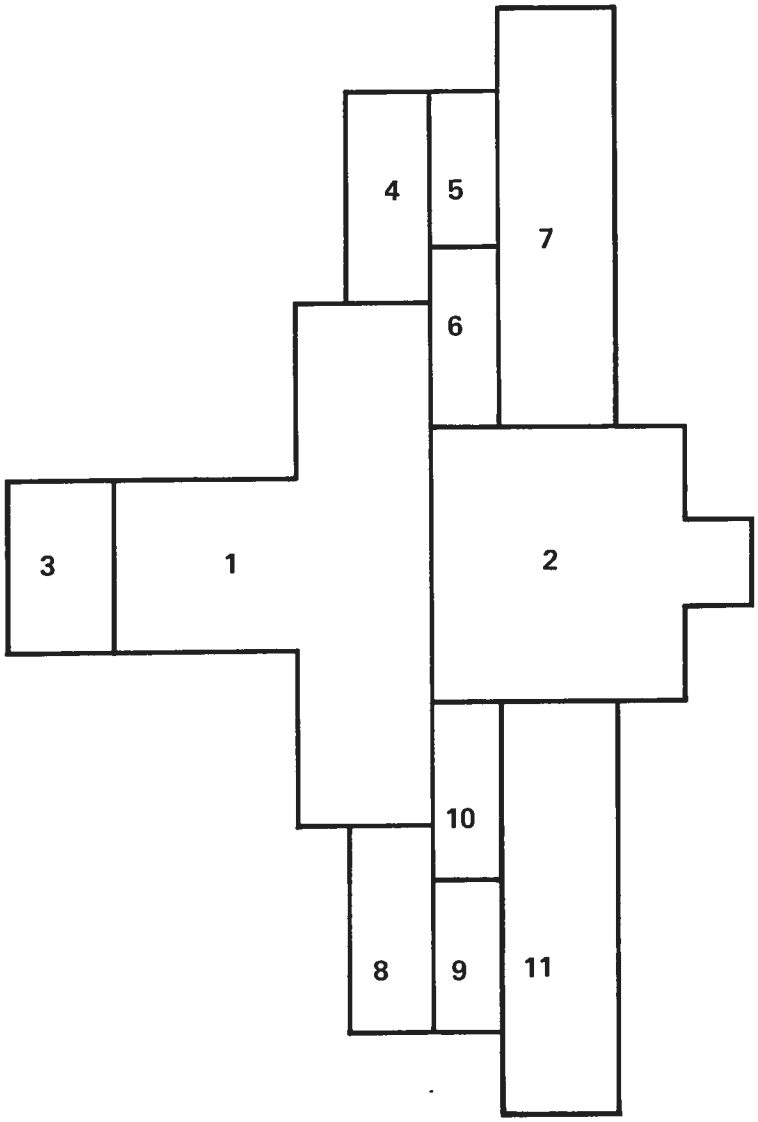

Fig. 10.3. Discretization of the Zion AFT Complex foundation.

steps remained unchanged. Also, we assumed the AFT complex to be surface founded, and no embedment effects were included. The major modifications to the substructure approach were in the final two steps--modeling the structure and SSI analysis. The analysis procedure is based on the pseudostatic mode method and is exact in its representation of coupling between foundation degrees-of-freedom through the foundation itself and the structure. In the implementation, the behavior of the structure is modeled by its fixed-base and pseudostatic modes. In addition, the coupling stiffness matrices between structure and foundation degrees of freedom and foundation degrees of freedom themselves are explicitly generated and used. The SSI analysis itself can be considered in two stages: (1) Calculate the motion of each foundation segment as a result of interaction. (2) Given these foundation motions, calculate in-structure response. The full three-dimensional finite-element model of the Zion AFT complex was used in the assessment.

Figure 10.4 shows a comparison of in-structure response spectra at node 3005, which represents response at the control room. Note the minimal effect of assuming a flexible foundation representation for the AFT complex. Other locations within the structure were investigated and similar results obtained. The principal reason for this result is the significant stiffening effect of the structural elements connecting the foundation segments--a phenomenon which requires a three-dimensional treatment and the explicit generation of coupling stiffnesses to capture. Simpler approximate procedures significantly underestimate this effect.

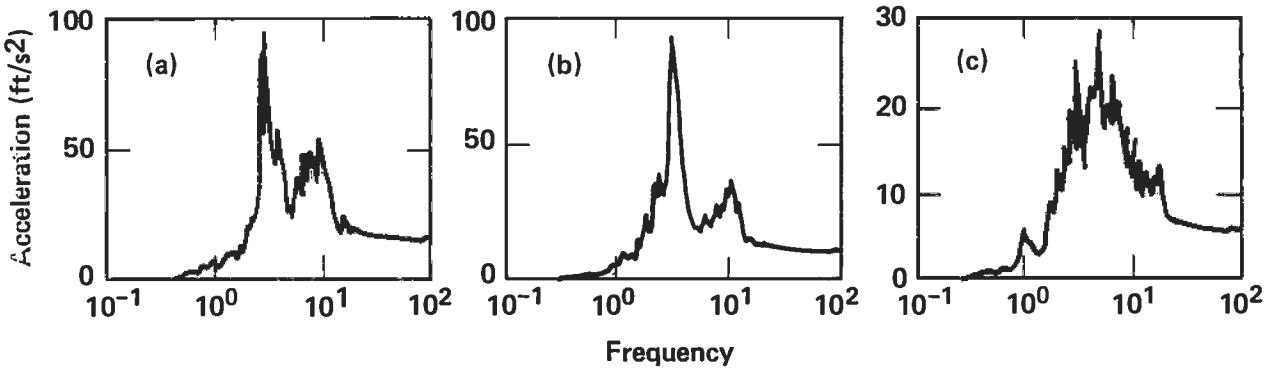

Fig. 10.4. Comparison of response spectra for single rigid foundation vs flexible foundation, at the control room. (a) X direction, (b) Y direction, (c) Z direction. The spectra in one panel can not be distinguished with the magnitudes of ordinates in this figure.

CHAPTER 11: SUMMARY AND RECOMMENDATIONS FOR FUTURE WORK

11.1 Specific Recommendations

As outlined in Chapter 7, the median core melt frequency for the base case was 3×10^{-5} per year and the uncertainty intervals on the core melt frequency spanned approximately three orders of magnitude. The median frequency of core melt was dominated by certain structural failures and the assumption that feed-and-bleed cooling could be performed after an earthquake if the auxiliary feedwater system had been lost. Further, the assumptions as to the consequences of the structural failures and the assumption as to the feed-and-bleed capability could make an order-of-magnitude difference in the final median frequency of core melt. Clearly, some further investigation into these assumptions is warranted.

The most important of these failures was the possibility of soil failure and uplift of the foundation of the containment, with resulting failure of pipes between the containment and the auxiliary building. Our evaluation of uplift of the foundation was very limited and was based on linear calculations and extrapolation of these linear calculations, using two limited studies that had been performed by outside investigators. Soil failure and uplift is a highly nonlinear phenomenon and it is recommended that nonlinear analysis of the uplift be made and compared with the extrapolated values used in the final Zion calculations. A task along these lines has already been identified for the verification studies for the SSMRP.

The question of pipe failure between buildings needs further consideration. Failure of pipes between buildings is due to relative motion and is thus a strain-controlled phenomenon. The maximum strain and, hence, stress is limited by the relative movement of the structures. Conventional wisdom would hold that the pipes themselves would not break but rather failure would first occur at the supports. The nature of the failure would be a function of the exact configuration of the penetrations and the nearest anchor points in the buildings. Two aspects need further investigation. First, analyses should be made in which the possiblity of failing nearby supports should be allowed. This was not done for the analyses presented in this report. Secondly, the calculated moments should be compared with nonlinear stress-strain behavior in the piping. Tasks to examine these aspects have been proposed for the SSMRP Verification Project. It may also be that proper estimation of the strain-induced failure of piping is amenable to experiment, using appropriately sized pipes and appropriate support configurations.

The other structural failures of importance were the failure of the poured reinforced concrete roof of the crib house service-water pump enclosure, and the failure of the wall between the auxiliary building and the turbine building (a composite wall consisting of poured concrete panels and vertical steel columns). In each case, in predicting the failure of these elements, consideration is taken of the ductility available to absorb the ground shaking energy. This ductility factor was used in all the fragilities of the structures as well as the fragilities of the major components and pipes to account for nonlinear energy absorption. Examination of the fragilities shows that the ductility factor has a strong effect on the final median value of failure in each case. Thus, the failure probabilities are quite sensitive to the assumed value of ductility. Although ductility is a widely used concept

in failure-prediction methodologies, its background is based on a limited number of studies by Newmark and his co-workers. Most of these studies dealt with single-degree-of-freedom systems. We recommend examination of typical multi-degree-of-freedom structures and components to evaluate the appropriate ductility factors in a nonlinear fashion. Here again, for the smaller components, it may be possible to determine ductility limits by experiment. Examination of the ductility factor for multi-degree-of-freedom structures or components has already been identified for the SSMRP Verification Project.

The importance of including local site effects in both the hazard curve and in calculation of the building and subsystem responses was shown in Chapters 3 and 10. As part of the Zion analysis, only limited evaluations of this effect could be performed. Clearly, additional studies (currently planned in the SSMRP Verification Project) are necessary to understand the conditions in which inclusion of local site effects is necessary.

Correlation between fragilities of components in the same generic category have been shown to be quite important. To the best of our knowledge, there are no existing data concerning the question of correlated fragilities. Indeed, this is an area that can only be examined experimentally and we recommend that an experimental program be considered. A second area of importance concerning fragility correlation is the possibility that fragilities developed from design analysis using the Newmark approach could be correlated by virtue of the fact that they were all developed using the same method. For example, if we tend to under-estimate median values of strength for one component, we are likely to under-estimate them for all components. This would imply a degree of correlation that may not exist. This question needs further investigation.

As seen in Chapter 8 for the cases in which failures of electrical components were found to be quite important, the failure of electrical buses, relays and circuit breakers were predominant. In the SSMRP analysis of Zion we considered relays and circuit breakers to be governed by the fragility corresponding to that of inadvertent trip of circuit breakers, and failure due to relay chatter was not considered. Existing data show that relay chatter is to be expected at very low levels of seismic excitation. In general, it is not considered likely that such relay chatter can cause problems, because most important circuits containing relays are protected by time-delay circuits. However, a possibility remains that intermittent chatter of a relay could affect locking circuits, inducing changes in state of a system and causing downstream consequences. No detailed examination of the electrical circuitry at Zion was performed. Informal discussions with electrical engineers indicate that this is not a major problem but that such locking circuits can exist. We recommend that circuitry typical of the control and safety systems in reactors be examined to determine whether or not such locking circuits exist and whether they could cause problems during seismic excitation.

The reactor protection system at Zion was not examined in detail; nor was a fault tree developed for this system. The values used for the failure of the reactor protection system were based on the Diablo Canyon seismic study. Failure of the reactor protection system was treated as a random event having a relatively low probability of failure. No accident sequences which involved failure of the reactor protection system were found to be important in our

final results. However, if the reactor protection system were to have a significantly higher probability of failure, then a significant number of additional accident sequences would result.

11.2 General Comments and Limitations

There are a number of general limitations on the results that have been presented here. The first limitation, one of the most important, is our use of the WASH-1400 containment failure modes to specify radioactive release. The WASH-1400 release categories and containment failure modes were based on scenarios in which failure occurred due to random events; the possiblities of extensive common-cause failures were not addressed. The WASH-1400 containment failure modes may not be appropriate for the seismic situation. In particular, they do not distinguish between the consequences of a reactor-vessel-rupture accident involving the failure of the primary coolant piping alone and the case involving failure of both the primary coolant piping and the secondary steam piping. In the latter case, considerably more energy would be released into the containment, and the probability of failure of the containment could perhaps be higher. Tasks have been identified in the SSMRP Verification Project to address the issue of containment failure modes and to include the recent research that has been performed in this area both by NRC and its contractors.

Another limitation is that we have not considered aging effects. Aging effects on fragilities would be most significant. We are not aware of any data on aging effects on the fragility of nuclear components due to seismic excitation. This is an area that can only be examined by testing. We recommend that such testing be performed on those important components affected by aging.

Another area not addressed is the possiblity of the effects of earthquake-induced fires and flooding inside the plant. These are secondary failure effects that were outside the scope of the SSMRP as originally planned. However, fires and flooding are important potential consequences of large earthquakes. If fires were to occur inside a plant, there is the possiblity that the seismic ground shaking could damage the fire-detection and protection systems, in which case the potential consequences of these fires would be greatly enhanced.

All our risk analysis results presented in this report were based on the use of lognormal distributions to represent the statistics of the responses and the fragilities. The lognormal distribution was found to provide a reasonable fit to the calculated responses and the limited fragilities data available seem to be relatively well represented by lognormal distributions. So, in general, we have no reason to believe that such distributions are not appropriate for this type of risk analysis. However, we have not tested this assumption by employing different types of distributions or using pure Monte Carlo approaches to generate risk numbers without specification of a particular form of distribution. Tasks in the SSMRP verification Project have been planned to address this issue.

Finally, all the risk results in this report are based on our use of an upper-bound approximation in computing the unions of cut sets for the accident sequences. Recent developments at LLNL show promise of a means of replacing

those upper bounds with more realistic estimates. We recommend that further evaluations of the upper-bound calculations be made.

In spite of the limitations and omissions noted in this chapter, the risk results presented in this report represent a most extensive effort to examine the seismically induced risk of radioactive release at a nuclear power plant. The identification of system failure in terms of failures of individual components, the methodology to calculate failure of correlated components, the extensive calculations of responses of structures and components using state-of-the-art methods, and the development of fragilities of individual components provide a data base of results which can be used by both the U.S. NRC and the general nuclear community to examine seismic safety questions at an unprecedented level of resolution.

REFERENCES

1. Smith, P. D., Chuang, T. Y, Bernreuter, D. L., Shieh, L. C., Bohn, M. P., Wells, J. E., Johnson, J. J., "Seismic Safety Margins Research Program - Phase I Final Report," UCRL-53021, also NUREG/CR-2015, 10 Volumes, September, 1981.

2. U.S. Nuclear Regulatory Commission, "Reactor Safety Study: An Assessment of Accident Risks in U.S. Commercial Nuclear Power Plants, WASH-1400," NUREG-75/014, October, 1975.

3. Bernreuter, D. L., Chung, D. H. and Mortgat, C. P., "Seismic Safety Margins Research Program Phase I Final Report - Development of Seismic Input (Project II)," NUREG/CR-2015, Vol. 3, (1983).

4. Trifunac, M. D. and Brady, A. G., "A Study on the Duration of Strong Earthquake Ground Motion," Bull, Seism. Soc. Am., 65, 581-626, 1975.

5. Gasparini, D. and Vanmarke, E. H., "Simulated Earthquake Motions Compatible with Prescribed response Spectra," Report 2 of Evaluation of Seismic Safety of Buildings, Department of Civil Engineering, Massachusetts Institute of Technology, Cambridge, Mass., Publ. No. R76-4, January 1976.

6. Bernreuter, D. L, "Seismic Hazard Analysis: Application of Methodlogy, Results and Sensitivity Studies," Lawrence Livermore National Laboratory, Livermore, Calif., UCRL/CR-1582, Vol. 4, 1981; also published as U.S. Nuclear Regulatory Commission NUREG/CR-1582, Vol. 4, 1981.

7. Nuttli, O. W., "The Relation of Sustained Maximum Ground Acceleration and Velocity to Earthquake Intensity and Magnitude, " Report 16 of State-of-the-Art for Assessing Earthquake Hazards in the United States, U.S. Army Corps of Engineers Waterways Experiment Stations, Vicksburg, Miss., Misc. Paper S-73-1, November 1979.

8. Chung, D. H. and Bernreuter, D. L., "The Effect of Regional Variation of Seismic Wave Attenuation on the Strong Ground Motion from Earthquake," Lawrence Livermore National Laboratory, Livermore, Calif., UCRL-53004, 1981, also published as U.S. Nuclear Regulatory Commission NUREG/CR-1655.

9. Nuttli, O. W., "Similarities and Differences Between Western and Eastern U.S. Earthquakes, and Their Consequences for Earthquake Engineering," to be published in Earthquake and Earthquake Engineering: The Eastern U.S., Knoxville, Tenn., 1981.

10. Campbell, K. W. (1981) "Near-Source Attentuation of Peak Horizontal Acceleration" Bull. Seism. Soc. Am., 71, 2039-2070.

11. Joyner, W. B. and Boore, D. M. (1981) "Peak Horizontal Acceleration and Velocity from Strong-Motion Records Including Records from the 1979 Imperial Valley, California, Earthquake", Bull. Seism. Soc. Am., 71, 2011-2038.

12. Nuttli, O. W., (1982), "Advances in Seismicity and Tectonics" Proc. of Third Intnl. Earthquake Micorzonation Conf., 1, 3-24.

13. Nuttli, O. W. (1983a) Empirical Mangitude and Scaling Relations for Mid-Plate and Plate-Margin Earthquakes (to be published in Techonophysics).

14. Nuttli, O. W. (1983) "Average Seimsic Source-Parameter Relations for Mid-Plate Earthquakes" (to be published in the Bull. Seism. Soc. Am.).

15. Bernreuter, D. L., (1979), "Site, Soil Column Considerations in Seismic Hazard Analysis" Proc. of the Third ASCE Specialty Conf. on Structural Design of Nuclear Power Plants, Boston, Mass., April 3-5, 1979.

16. McCann, M. W. and Boore, D. M., "Variability in Ground Motions: Root Mean Square Acceleration and Peak Acceleration for the 1971 San Fernando Earthquake" Bull. Seism. Soc. Am., 1982.

17. Cornell, C. A., Bannon, H. and Shakal, A. F., "Seismic Motion and Response Prediction Alternatives," Earthquake Eng. and Struc. Dynam., 7, 295-315, 1979.

18. Trifunac, M. D. and Brady, A. G., "On the Correlation of Seismic Intensity Scales with the Peaks of Recorded Strong Ground Motion," Bull, Seism. Soc. Am., 65, 139-162, 1975.

19. Apsel, R. J., Frazier, G. A., Jurkevics, A., and Fried, J. C., "Application of Earthquake Source Modeling to Assess the Relative Differences Between Seismic Ground Motion in the Eastern and Western Regions of the United States and to Characterize the Type and Direction of Incoming Seismic Waves: Final Report." Del Mar Technical Associates, Del Mar, CA, DELTA-R-80-043, September 1980.

20. Johnson, J. J., Maslenikov, O. R., Chen, J. C., and Chun, R., "Seismic Safety Margins Research Program Phase I Final Report -- Soil Structure Interaction (Project III)," Lawrence Livermore National Laboratory, Livermore, Calif., UCRL-53021, Vol. 4, 1981 (also published as U.S. Nuclear Regulatory Commission NUREG/CR-2015, Vol. 4.)

21. Johnson, J. J., "Soil-Structure Interaction: The Status of Current Analysis Methods and Research," Lawrence Livermore National Laboratory, Livermore, Calif., UCRL-53011, October 1980 (also published as U.S. Nuclear Regulatory Commission NUREG/CR-1780).

22. Luco, J. E., "Linear Soil Structure Interaction," Lawrence Livermore National Laboratory, Livermore, Calif., UCRL-15272, July, 1980 (included in Ref. 1).

23. Wong, H. L. and Luco, J. E., "Soil-Structure Interaction: A Linear Continum Mechanics Approach (CLASSI)," Report CE, Dept. of Civil Engineering, University of Southern California, Los Angleles, 1980.

24. Wesley, D. A., Hashimoto, P. S., and Narver, R. B., "Variability of Dynamic Characteristics of Nuclear Power Plant Structures," Lawrence Livermore National Laboratory, Livermore, Calif., UCRL-15267, July 1980 (prepared by Structural Mechanics Associates; also published as U.S. Nuclear Regulatory Commission NUREG/CR-1661).

25. ASCE Committee on Reliability of Offshore Structures, Subcommittee on Foundation Materials, Probability Theory and Reliability Analysis Applied to Geotechnical Engineering of Offshore Structure Foundations, 1979.

26. Seed, H. B., Idriss, I. M., "Soil Moduli and Damping Factors for Dynamic Response Analysis," University of California, Earthquake Engineering Research Center, EERC 70-10, 1970.

27. Shibata, H., "On the Reliability Analysis for Structural Design Including Pipings and Equipment," presented at the Seminar on Probabilistic Seismic Analysis of Nuclear Power Plants, January 16-19, 1978, Berlin.

28. Kennedy, R. P., Campbell, R. D., Hardy, G, and Banon, H., "Subsystem Fragility - Seismic Safety Margins Research Program (Phase I)," Lawrence Livermore National Laboratory, Livermore, Calif., UCRL-15407, NUREG/CR-2405,(1981).

29. Cover, L. E., "Equipment Fragility Data Base," Seismic Safety Margins Research Program (Phase I), Lawrence Livermore National Laboratory, Livermore, Calif., UCRL-53038, NUREG/CR-2680, March 1982.

30. Pacific Gas and Electric Co., (August 1977), Department of Engineering, Analysis of the Risk to the Public from Possible Damage to the Diablo Canyon Nuclear Power Station from Seismic Events, Dockets 50-275-OL and 50-323-OL (P G and E, San Francisco, CA).

31. Wells, J. E., "SEISIM: A Probabilistic Risk Assessment Tool Used in Evaluating Sciesmic Risk", Proceedings of the Conference on Seismic Risk and Heavy Industrial Facilities, (Lawrence Livermore National Laboratory, Livermore, Calif.), 1983.

32. Garcia, A. A., J. E. Kelly, P. J. Amico, W. J. Parkinson, and F. L. Leverenz (August 1979), Seismic Safety Margins Research Program (Phase I), Interim Report, Project VII Systems Analysis, Event Tree Development and Construction, Report No. SAI-003-79-BE, (Science Applications, Inc., Bethesda, MD 20014).

33. Barlow, R. E., and H. E. Lambert (1975), "Introduction to Fault Tree Analysis," Reliability and Fault Tree Analysis (SIAM, Philadelpha, PA).

34. George, L. L., and J. E. Wells (May 1981), "The Reliability of Systems of Dependent Components," Proceedings of the ASQC Quality Congress (American Society of Quality Control, San Francisco, CA).

35. Johnson, N. L., and S. Kotz (1972), Distributions in Statistica: Continuous Multivariate Distributions (Wiley, New York, NY).

36. Lambert, H. E. (1975), "Measures of Importance of Events and Cut Sets in Fault Trees," Reliability and Fault Tree Analysis, pp. 83-84 (SIAM, Philadelphia, PA).

37. Worrell, R. B., and D. W. Stack, A Sets User's Manual for the Fault Tree Analyst, Sandia National Laboratories, Albuquerque, NM, SAND77-20-51, 1978 (also published as NUREG/CR-0465).

38. Worrell, R. B. (1981), "Notes on Changes to SETS Program," informal publication of Sandia National Laboratories, Albuquerque, NM.

39. Willie, R. R., "Computer-Aided Fault Tree Analysis," Operations Research Center, University of California, Berkeley, CA, ORC 78-14A, August 1978.

40. Wells, J. E., and D. A. Lappa, "Probabilistic Culling in Fault Tree Evaluation," Proceedings of the 1983 Reliability and Maintainability Symposium, IEEE, New York, NY, 1983.

41. Dames and Moore, Report of Geological and Seismological Environmental Studies, Proposed Nuclear Power Plant, Zion, Illinois, for the Commonwealth Edison Company, June 1967.

42. Kenney, R. P., S. A. Short, D. A. Wesley, and T. H. Lee, "Effect on Nonlinear Soil Structure Interaction due to Base Slab Uplift on the Seismic Response of a High Temperature Gas Cooled Reactor (HTGR)," Nuclear Engineering and Design, 38, 1976.

43. Wolf, J. P. and Skrikerud, P. E., "Seismic Excitation with Large Overturning Moments: Tensile Capacity, Projecting Basemat, or Lifting-Off?," Nuclear Engineering and Design, 50, 305-321, 1978.

APPENDIX A

JUSTIFICATION OF THE EFFECTS OF LOCAL SITE CORRECTIONS

APPENDIX A
JUSTIFICATION OF THE EFFECTS OF LOCAL SITE CORRECTIONS

A1.0 INTRODUCTION

One of the key steps in the assessment of seismic hazard is the development of a ground motion model, which requires sufficient instrumented earthquake data. The ground motion model used in Phase 1 was based on the ground motion data from the Western United States (WUS). The effect of local site conditions at Zion were accounted for by use of a simple soil classification procedure. The ground motion models so developed are valid only at what could be loosely termed "average" soil sites. Since the site conditions at Zion are significantly different from WUS sites, such an approach can introduce significant modeling errors in the analysis. In Phase 2 an attempt was made to explicitly include the effects of Zion local site conditions on the seismic hazard curve and frequency characteristics of the seismic input motions.

The ideal way to develop the seismic hazard at the Zion site would be to use a ground motion model based on regression analysis of data from sites similar to the Zion site. However, this was not possible because there were no data available from Zion, and there are few data from sites like Zion. An alternative approach would be to use the current site response procedure, such as equivalent linear techniques, assuming a vertical incident wave to correct a set of time histories appropriate for a rock outcrop for the local soil column at Zion. The site amplification factors at the site were computed using equivalent linear techniques and accounting for the uncertainty in dynamic soil properties with a numerical experimental design scheme.

One important step in the approach was to validate the computed amplifications for the Zion site to assure that they are reasonable and consistent with recorded data. To show this we examined some recently available data recorded at both soil sites and at nearby rock outcrops from a number of earthquakes. In particular, we used data from soil/rock station pairs recorded from Friuli and Oroville earthquakes. In addition, some published data of observed site amplifications at sites in three sediment-filled valleys in the Garm region of the USSR were also ultilized in our data base. Site amplifications were developed from the real records. These data, along with the previously available results from underground nuclear explosions, provide an empirical data base to justify results of our Zion analyses.

The following sections show the results of data analysis illustrating the magnitude of site amplifications and variations as recorded from several earthquakes. The computed site amplification factors for the Zion site, using the same level of rock outcrop motion, were compared with those derived from real data. One of the sites, Cornino-Forgaria, was modeled and analyzed by the computer program SHAKE (Ref. A-1) to calculate the response. The computed responses were compared to the recorded results. These comparisons served as an additional validation of the procedure employed.

A2.0 OBSERVATION OF SITE AMPLIFICATION BASED ON REAL RECORDS

The approach used for this study was to analyze real motions recorded at sites where both surface soil motions and nearby rock motions were available. The response spectra (or the Fourier spectra) of recorded motions between the soil

and the nearby rock station for the same component were computed to develop the spectral ratio for a given site. For engineering purposes, the representative site amplification is defined as the mean spectral ratio computed from the same component of soil/rock motion pair for a set of selected earthquakes. The mean spectral ratios in two horizontal directions are often different due to the complicated nature of geologic properties and wave characteristics. This aspect of the phenomenon cannot be represented by a one-dimensional model and assumed material behavior. For the purpose of validation in this study, results of two horizontal components were combined into one data set.

To compute site amplifications using earthquake records, it is necessary to have data recorded simultaneously at a soil station and a nearby rock station. The distance between the soil and the rock station should be relatively small in comparison with the epicentral distance of the earthquake. Furthermore, for justification purposes, it is essential that site characteristics such as soil layering, soil/rock type and impedance ratio between soil/rock system be somehow similar to the Zion site. However, such records are limited, and there are only a few cases in the existing data base. A summary of site conditions, earthquake location parameters, and average peak acceleration data of rock outcrops are shown in Table A-1. Detailed descriptions of earthquake parameters and soil conditions are described in each subsection. Results shown do not include very low frequencies, since such data are not base-line-corrected and large spectral ratios could result. This exclusion is not critical because it is out of our frequency range of interest.

A2.1 SOIL/ROCK STATION PAIRS FROM THE OROVILLE EARTHQUAKES

Following the Oroville, California, earthquake (August 1, 1975; $M_L = 5.7$), a number of strong accelerograms were obtained simultaneously at many of the stations for each of the 12 well-recorded aftershocks. These records cover a wide range of magnitude ($2.8 \leq M_L \leq 5.2$), focal depth ($2.6 \leq h \leq 12$ km), and site conditions. Most of these records are at epicentral distances less than 16 km. Figure A-1 shows the earthquakes and the site locations together with the generalized surface geology, as given by Bucholz (Ref. A-2). All sites west of Earl Broadbeck Health (EBH) are located on several hundred feet of alluvial soil deposit, while the sites east of EBH are situated either on thin tertiary gravel deposits overlying crystalline bedrock or directly on crystalline rock. The thickness of alluvium decreases gradually from the west to the east of the region shown in Fig. A-1. The data set provides reliable information for studying the effect of local site condition on free-field earthquake motion.

D. Johnson Ranch (DJR), and Oroville Medical Center (OMC) stations, both located on a shallow soil site, were of primary interest for investigating site amplification from the Oroville earthquakes. However, as noted by Seekins and Hanks (Ref. A-2), the data recorded at the nearby rock station (Department of Water Resource (DWR)) are not reliable because the recording instrument was not properly mounted. Thus, site amplification investigations were limited to the DJR station. This site consists of about 35 to 40 ft (10.7 to 12.2 m) of Pleistocene gravel and alluvium, having an average shear wave velocity of 1100 ft/s (335 m/s), overlying the bedrock with an average shear wave velocity about 5400 ft/s (1646 m/s). (See Ref. A-3.)

Table A-1. Summary of site conditions, earthquake location parameters and average horizontal peak ground accelerations at rock outcrops.

Sites	Site conditions: Soil layer (ft)	Site conditions: Soil/rock	Names	No. of records	Earthquakes: M_L range	Earthquakes: Epicenter distance (km)	Rock outcrop average PGA (g)
Forgaria	116	Partially overconsolidated alluvium/limestone and sandstone	Friuli (1976)	5	4.4-6.1	5-20	0.095
Buia	Deep soil	Recent alluvium/limestone and sandstone	Friuli (1976)	4	4.4-6.1	10-20	0.107
DJR	33	Pleistocene gravel and alluvium/mesozoic greenstone	Oroville (1975)	5	4.0-4.9	6-20	0.082

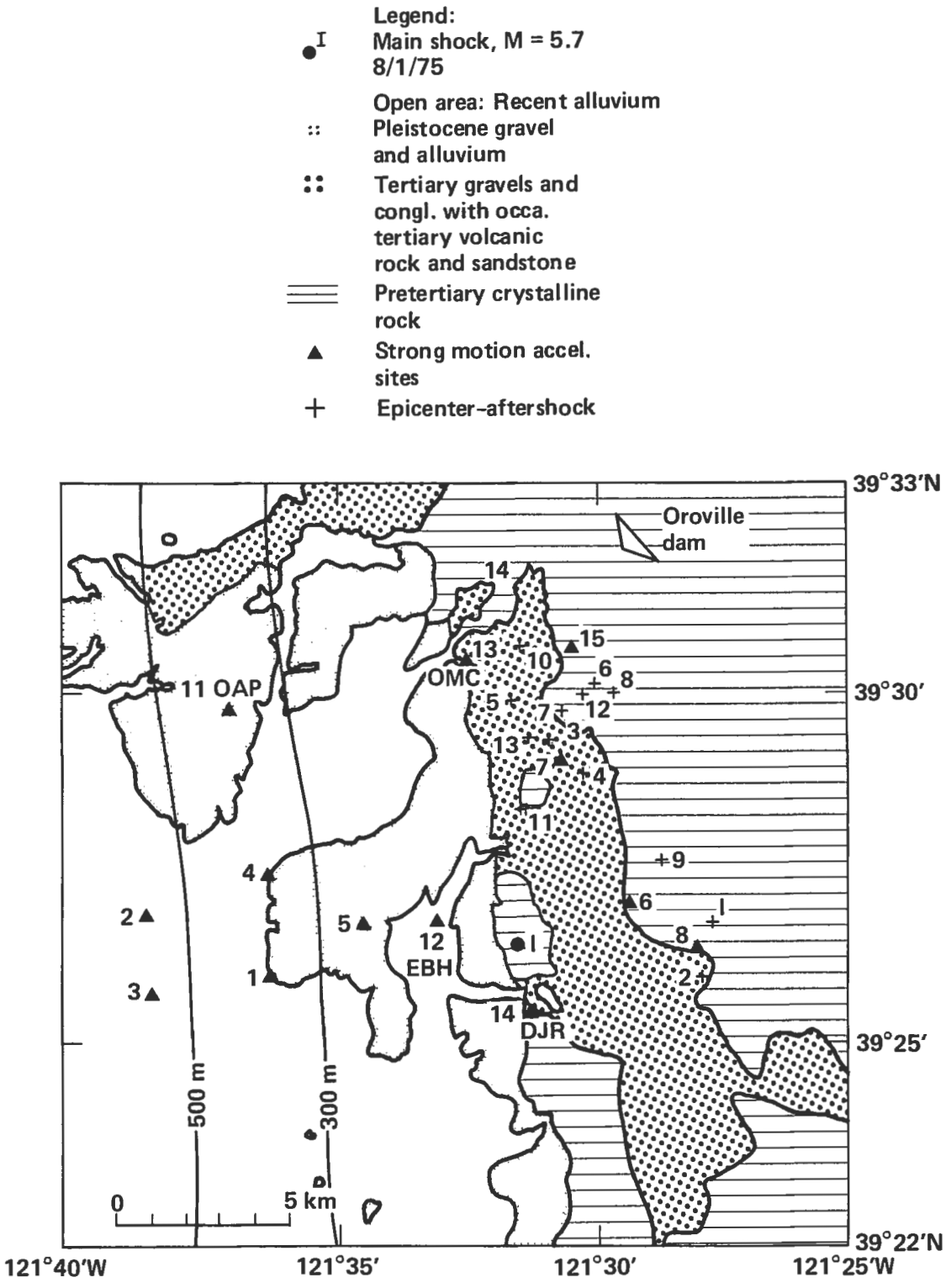

Fig. A-1. Epicentral region of the 1975 Oroville earthquakes.

Table A-2 summarizes the earthquake location parameters and peak acceleration data for 14 major aftershocks of the 1975 Oroville earthquakes. Inspecting the peak ground acceleration (PGA), one immediately sees that the PGA in the western part of the region is consistently lower than those in the eastern part, and the PGAs at DJR for most of the aftershocks are much higher than at the other stations. This fact strongly suggests local site amplification at this site.

To investigate the effects of the local site conditions for the entire frequency range, two rock stations (Numbers 6 and 8), were used as station pairs to DJR. Five good records from four earthquakes, with local magnitudes ranging from 4.0 to 4.9, were used for the evaluation of site amplification at DJR. The earthquakes and the soil/rock station pairs used for this investigation are shown in Table A-3. Note that the focal depths of the four earthquakes are fairly close (9.2 to 12.0 km), and the epicenters of all aftershocks are confined to a small region. Since the distance variation between soil/rock pairs and the epicenters of the aftershocks is small, the site distance and site azimuth effects may be insignificant.

Recorded time histories and their response spectra for both components of each soil/rock station pairs were examined. Since the orientation of the records at station number 6 (S6) is 35 degrees off from DJR (S55E vs N90E), the coordinates of S6 were transformed to the uniform orientation. It is understood that this is an approximation, since the real accelorogram would not likely follow a simple relationship of a transformation of the coordinates. Comparisons of time histories and response spectra before and after the transformation of the coordinate reveal no significant effect of such transformation. To illustrate the site effect, Figs. A-2, 3, and 4 show time histories and their response spectra, with 5% damping, for three components of the DJR/S6 station pair from earthquake 13. Some interesting features are observed: 1) The strongest resonant phenomena are clearly noticable at a frequency range near 7 Hz for both horizontal components. Using an average shear wave velocity of 1100 ft/s (335 m/s) and 35 to 40 ft (10.7 to 12.2 m) of soil, the site frequency of the simple one-dimensional shear wave model varies from 6.9 to 7.8 Hz, which agrees quite well with the field data. 2) The magnitudes of site amplification in both components are quite different. In the EW direction, amplifications are about 3.5 at PGA and about 4.1 at peak frequency, while in the NS direction the corresponding amplifications are 1.9 and 2.6, respectively. Furthermore, second and third peak resonances appear in the NS but not in the EW component. 3) In the vertical component the peak frequency occurs around 14 Hz, which also agrees reasonably well with the simple one-dimensional p-wave model, assuming the Poisson's ratio of the soil to be about 0.25 to 0.30. The PGA and peak spectral accelerations were amplified about 1.7 and 3.0 times, respectively.

The mean spectral ratio for all five components in the NS and EW directions are shown in Figs. A-5 and 6. Notice that the three modes of peak resonances occur at the same frequency ranges in both directions, but the order of magnitude of site amplification is quite different in both directions. The mean spectral ratios of soil to rock for both horizontal components are shown in Fig. A-7. The mean spectral ratio for the vertical component is shown in Fig. A-8. As expected, the major peak frequency of the p-wave is higher than that of s-wave for material having Poisson's ratio of about 0.25 to 0.33.

Table A-2. Earthquake location parameters and peak acceleration data for 1975 Oroville Earthquake. Ref. A-2.

Eqk. No.	Date	Origin Hr Min	Lat. Min of 39°N	Long. Min of 121°W	Depth km	M_L	Accelerograph stations 2	3	OAP	1	4	5	EDH	OMC	DJR	7	DWR	6	8	9	10
1	Aug 2[a]	20 22	26.69	27.76	3.6	5.1		NR	5	4											
2	2[a]	20 59	25.93	27.97		5.2		(3)	3	7				8							
3	3	01 03	29.30	30.72	8.3	4.6		(4)	6	11	11	17	18	18			27				
4	3	02 47	28.84	30.11	6.3	4.1		(3)	11	6	(11)	(12)	16				10				
5	6	03 50	29.88	31.43	9.3	4.7	10	16	25	22	21	23	22	43[c]	70		47				
6	6[b]	03 51	30.00	29.93	9.3	~3	<	<	5	3	[d]	4	<	<	11		8				
7	6	16 41	29.64	31.49	9.6	3.6	3	7	5	(4)	[d]	6	5		16		15				
8	8	07 00	29.93	29.56	9.2	4.9			8	16	7	10	17		21	16	27	11			
9	11	06 11	27.57	28.75	2.6	4.3			NR	(<)	(<)	(<)	6	(6)	20	17	(6)	47	17		
10	11	15 59	30.54	31.26	9.8	3.6			8[c]	<	<	6	6	10[c]	(11)	6	15	(6)	(5)		
11	16	05 48	28.41	31.26	9.4	4.0			4	17	7	11	14	11	22	7	8	11	6		
12	16	12 23	29.90	30.06	6.8	2.8			(<)	5	3	6	(5)		(11)	8	23	(3)	3		
13	Sep 26	02 31	29.30	31.16	9.7	4.0				10	10	14	10	12	24	[e]	22	11	(6)	(6)	10
14	27	23 34	31.34	31.74	12.0	4.6			33	15	12	12	16	18[c]	58	[e]	16	[d]	17	7	50

[a] Location data of Morrison et al. (1976).

[b] Aftershock of 0350, located with P- and S-waves read from strong-motion accelerograms.

[c] In P-wave on vertical component.

[d] Out of film.

[e] Film advance malfunction.

Table A-3. Earthquakes and station pairs used at DJR.

Earthquake number	Local magnitude	Depth (km)	Epi distance to DJR (km)	Soil/rock station pair
8	4.9	9.2	9.3	DJR/S6
11	4.0	9.4	5.8	DJR/S8
11	4.0	9.4	5.8	DJR/S6
13	4.0	9.7	7.7	DJR/S6
14	4.6	12.0	11.7	DJR/S8

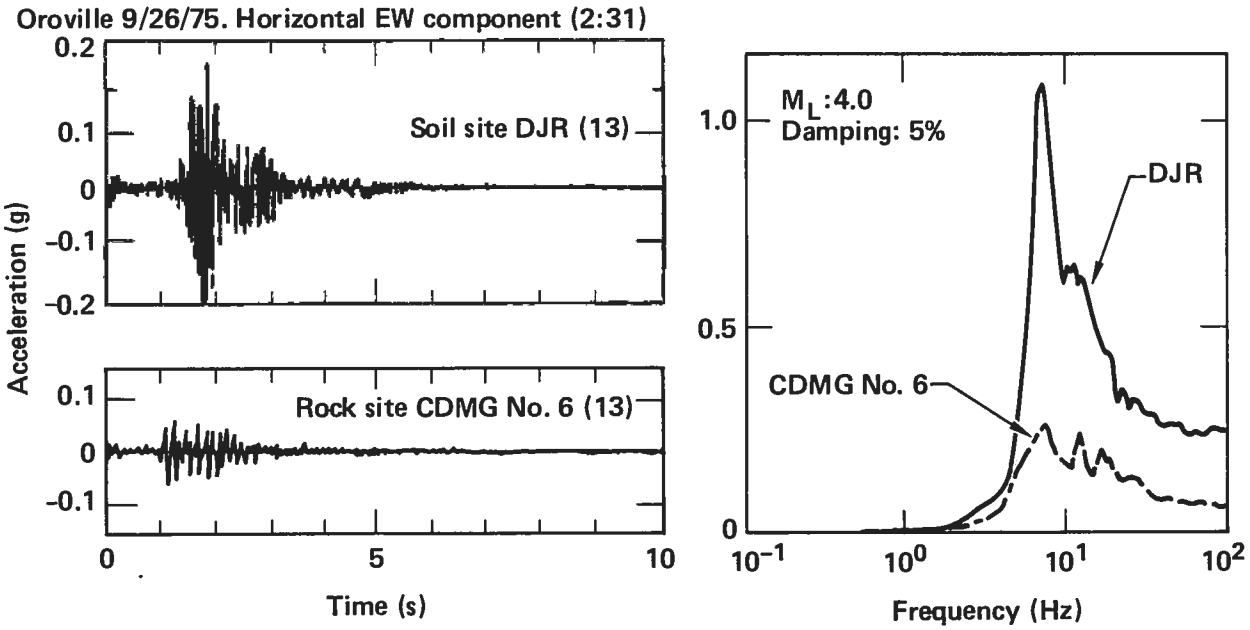

Fig. A-2. Acceleration time histories and the corresponding response spectra of the EW component of Earthquake #13, recorded at the DJR station and the CDMG #6 station.

Oroville 9/26/75 Horizontal NS component (2:31)

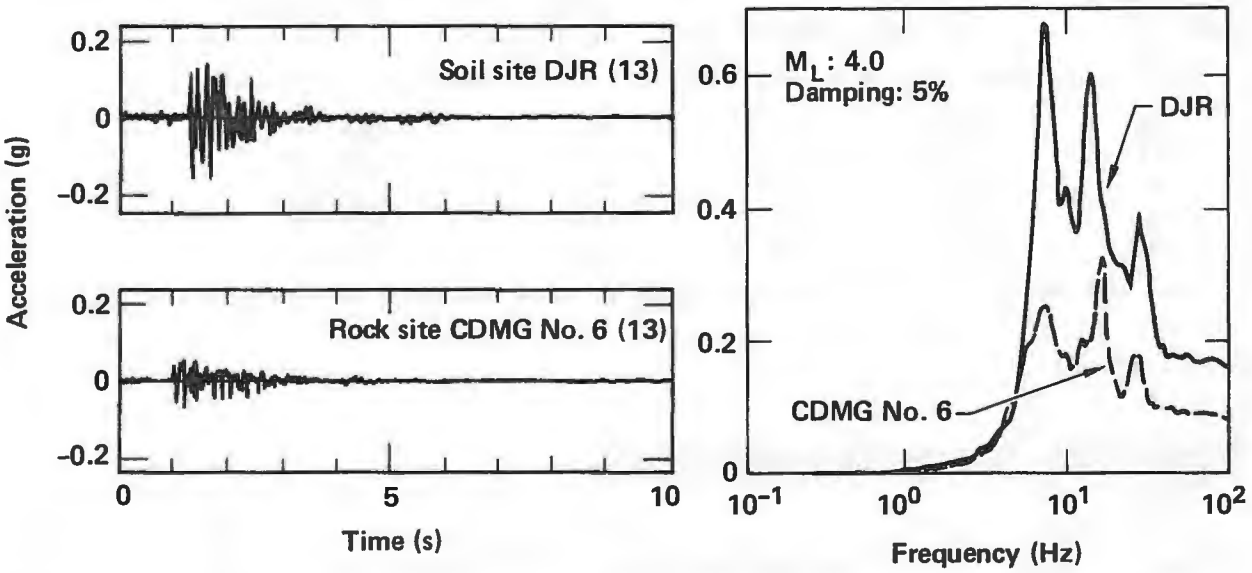

Fig. A-3. Acceleration time histories and the corresponding response spectra of the NS component of Earthquake #13, recorded at the DJR station and the CDMG #6 station.

Oroville 9/25/75. Vertical component (2:31)

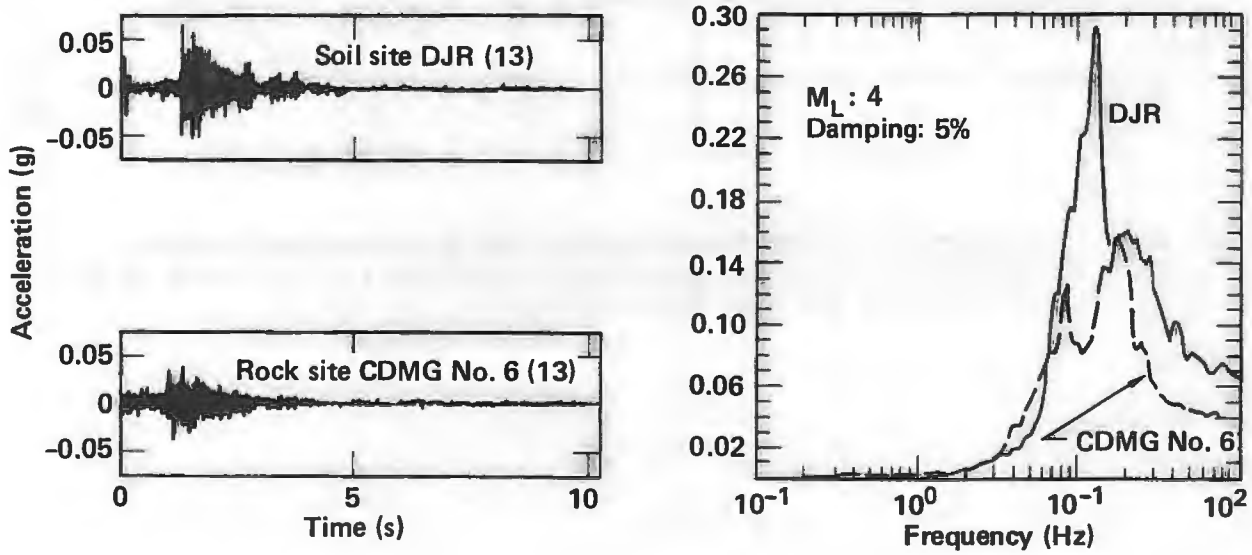

Fig. A-4. Acceleration time histories and the corresponding response spectra of the verical component of Earthquake #13, recorded at the DJR station and the CDMG #6 station.

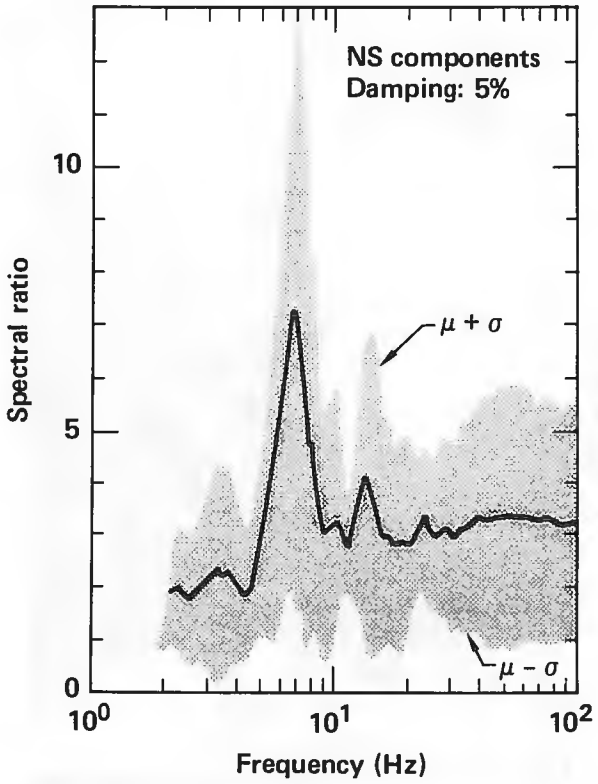

Fig. A-5. Spectral ratios of the NS component of the August and September 1975 Oroville earthquakes, recorded at the DJR soil site and the CDMG #6 and #8 rock sites. The solid line is the mean of 5 spectral ratios, and the shading marks the variation in the mean (±1 standard deviation).

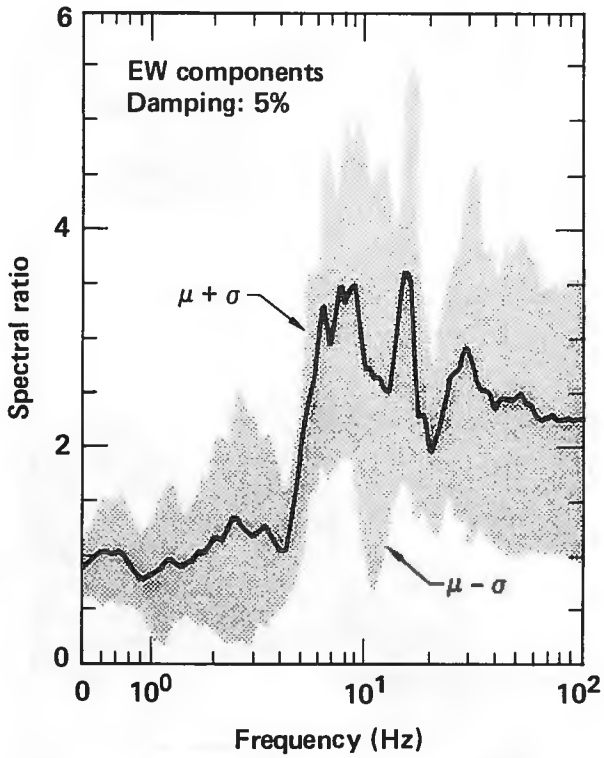

Fig. A-6. Spectral ratios of the EW component of the August and September 1975 Oroville earthquakes, recorded at the DJR soil site and the CDMG #6 and #8 rock sites. The solid line is the mean of 5 spectral ratios, and the shading marks the variation in the mean (±1 standard deviation).

Table A-4 shows the coefficients of variation (COV) of mean site amplification at DJR for both horizontal components and the vertical component. Large variability is observed.

A2.2 SOIL ROCK STATION PAIRS FROM THE 1976 FRIULI EARTHQUAKES

A large body of local data associated with the aftershocks of the 1976 Friuli earthquake (M_L > 5.9) has formed the data base for a linear regression analysis to study correlation of peak ground acceleration with magnitude and distance for this earthquake. Most of the data were obtained at a hypocentral distance less than 25 km. Values of horizontal PGA, for the uncorrected data, range between 0.013 g and 0.526 g. About 93% of the data above 0.031 g are associated with 14 different aftershocks, with the local magnitude between 3.7 and 6.3. Epicentral distances vary between 5 and 190 km, and focal depth between 6 and 11 km. The accelerograph stations were situated on rock or rock-like sites and soil sites. The rock sites include limestone, dolomite,

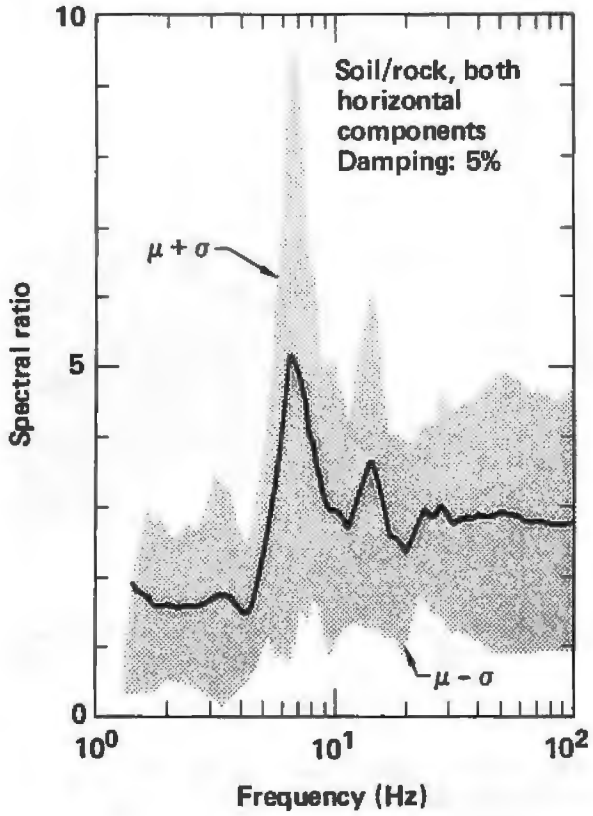

Fig. A-7. Spectral ratios of soil to rock for both horizontal components of the August and September 1975 Oroville earthquakes, recorded at the DJR soil site and the CDMG #6T and #8 rock sites. The solid line is the mean of 5 spectral ratios, and the shading marks the variation in the mean (±1 standard deviation).

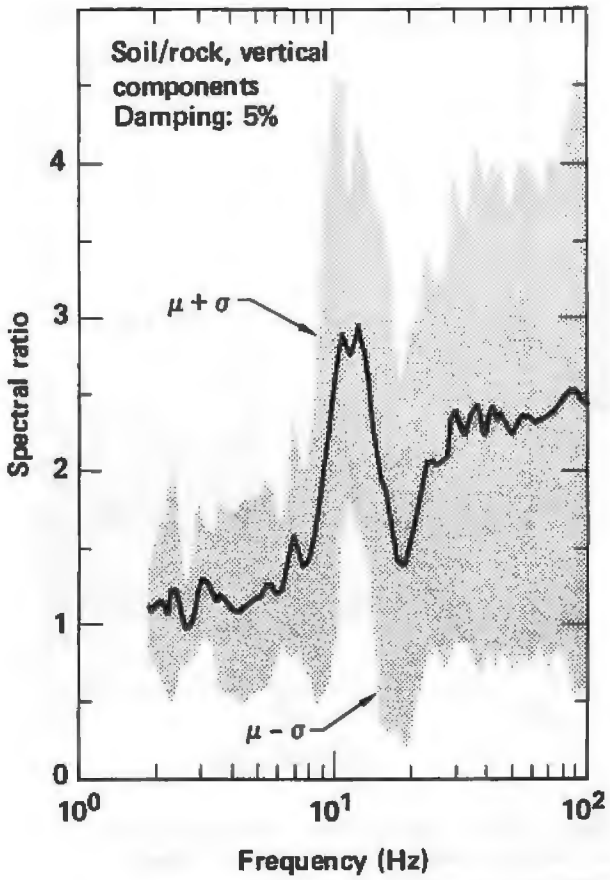

Fig. A-8. Spectral ratios of the vertical component of the August and September 1975 Oroville earthquakes, recorded at the DJR soil site and the CDMG #6T and #8 rock sites. The solid line is the mean of 5 spectral ratios, and the shading marks the variation in the mean (±1 standard deviation).

Table A-4. Coefficients of variation of site amplifications at DJR from the 1975 Oroville earthquakes.

	Horizontal component			
	NS	EW	Both	Vertical component
PGA	0.67	0.60	0.64	0.75
Peak spectral acceleration at 7 Hz	0.75	0.49	0.86	0.59

and cemented conglomerates overlain by about 15 feet (4.5 m) of alluvium. Soil sites consist of alluvium and moraine deposits of varying thickness and characteristics. Studies by Faccioli and Agalbato (Ref. 4) reported that although the Friuli earthquakes were characterized by relatively low peak ground motions, certain local site conditions can give rise to abnormally high accelerations under suitable combinations of source, magnitude, and distance. Furthermore, Chiaruttini and Siro (Ref. 5) reported that sites on thick consolidated alluvium and rocky sites do not show statistically significant differences in recorded data, but that thin alluvium sites exhibit stronger average accelerations and a significant difference in the magnitude coefficient.

Two accelerograph stations (S. Rocco and Cornino Forgaria) are separated by a distance of only 650 m. The S. Rocco station is on outcropping limestone, and Cornino-Forgaria is on an alluvial deposit underlain by sloping bedrock. Cross-section through these two accelerograph stations is shown in Fig. A-9. This cross-section is approximately parallel to the north-south direction, which is one of the components of recorded motion. At these stations a number of accelerograms were simultaneously recorded during the aftershock. These data are of considerable interest for a study of local site amplification. Since the two stations are so close, the effect of source mechanism and travel path may be minimized by taking the ratio of the Fourier amplitude spectrum or response spectrum from the recorded motions at the stations from the same earthquake. Table A-5 lists the five strongest aftershocks that gave a complete record at the two stations. The earthquake location parameters and the peak acceleration data are also shown in the table. The magnitude varies from 4.4 to 6.1, and the epicentral distance varies between 4.5 and 20 km. The deepest earthquake had a focal depth of 18 km and the shallowest about 6 km. As can be seen from the table, the accelerations at Cornino-Forgaria are greater than those of S. Rocco for the same component. Ratios of the peak ground acceleration of each component of records are also shown in Table A-5. The PGA at the alluvial deposit are 1.4 to 3.9 times larger than that at the nearby rock outcrop station. The spectral acceleration ratios between the soil and the rock stations for the entire frequency range were also computed for these five aftershocks.

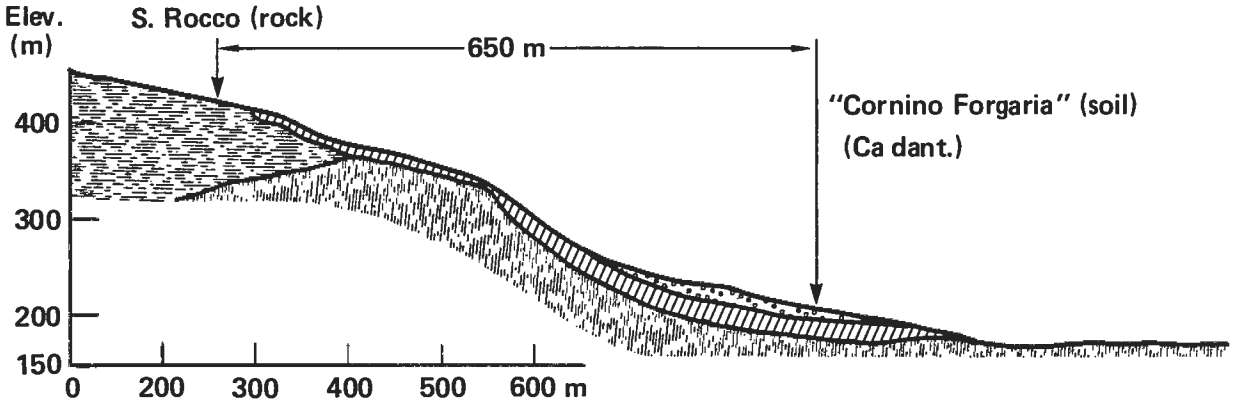

Fig. A-9. Site profile passing through the accelerographic stations of S. Rocco and Cornino-Forgaria.

Table A-5. Five earthquake location parameters and peak acceleration data, Friuli, Italy, 1976.

Eqk No.	Date & time	Mag.	EPI (KM)	Focal Depth (KM)	Cornino Forgaria				S. Rocco				Amp. (PGA)		
					Rec. No.	NS	Vert	EW	Rec. No.	NS	Vert	EW	NS	Vert	EW
1	June 11 17:16:37	4.4	4.5	17.8	F89	0.095	0.046	0.085	R98	0.065	0.031	0.031	1.46	1.48	2.74
2	Sept. 11 16:31:12	5.5	15.5	9.0	F131	0.095	0.049	0.111	R132	0.041	0.019	0.069	2.32	2.59	1.61
3	Sept. 11 16:35:00	5.9	14.0	6.0	F138	0.126	0.113	0.228	R139	0.089	0.045	0.091	1.42	2.51	2.51
4	Sept. 15 03:15:19	6.1	10.0	9.0	F152	0.262	0.095	0.217	R153	0.067	0.058	0.121	3.91	1.02	1.79
5	Sept. 15 09:21:28	6.0	20.0	11.7	F168	0.350	0.186	0.336	R169	0.142	0.082	0.234	2.46	2.27	1.44

The S. Rocco station, on an outcropping of hard limestone, is about 200 m higher than the Cornino-Forgaria station. The shear wave velocity profiles at both sites were measured by in-situ cross-hole seismic velocity surveys (Ref. 6). As shown in Fig. A-10, the shear wave velocity at Cornino-Forgaria varies from 600 ft/s (183 m/s) near the ground surface to about 1900 ft/s (579 m/s) at 50 ft (15 m), where a moderate rock layer about 12 ft (3.7 m) thick is encountered. Beneath this layer, the shear wave velocity decreases to 1400 ft/s (427 m/s) at a depth of 80 ft (24 m) and increases again to 2500 ft/s (762 m/s) between 90 ft (27 m) and 102 ft (31 m), where another rock layer may be inferred. The shear wave velocity below 116 ft (35 m) varies less, which suggests that the rock half space having an average shear wave velocity of 2855 ft/s (870 m) may be defined for site response analysis. The average shear wave velocity at S. Rocco site varies between 2000 and 3000 ft/s (610-915 m/s). The complicated topography and sloping soil/rock interface at Cornino-Forgaria stations clearly cannot be represented by simple one-dimensional wave propagation models, except for the out of plane direction, which may be closer to the horizontal layer condition assumed in the model.

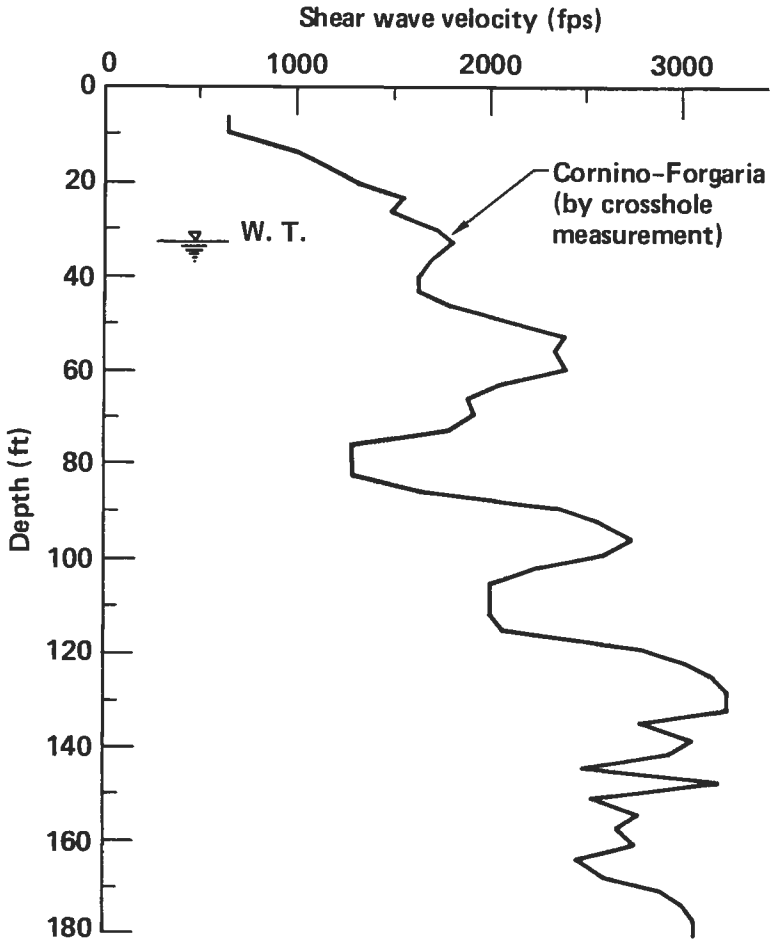

Fig. A-10. Shear wave velocity profile at the Cornino-Forgaria site.

Figures A-11, 12 and 13 show the acceleration time histories and their response spectra for 5% damping at the Cornino-Forgaria and S. Rocco stations for the three components from earthquake number 4, as shown in Table A-5. A much higher amplification through the highest frequency range is found in the north-south direction, which almost coincides with the cross-section passing through the accelerograph stations of S. Rocco and Cornino-Forgaria, as shown in Fig. A-9. The effect of irregular topography, site property heterogeneity, and wave contents in two directions may be the reason for the large difference in site amplification. In the vertical direction, motions were amplified for frequencies above 2.5 Hz. The dominant frequency is between 6 and 7 Hz. The spectral ratios for the remainder of the four earthquakes were computed. The spectral ratio of the Cornino-Forgaria and S. Rocco stations for the north-south component and the east-west component are shown in Figs. A-14 and 15. It can be seen that the dominant frequency was 3 Hz in both directions. A second resonant phenomenon appears between 5 and 6 Hz in the north-south component, but is not visible in the east-west component. The average spectral ratio for frequencies above 6 Hz is about 2.4 in the north-south direction and is about 2.0 in the east-west direction. Figures A-16 and 17 show the spectral ratio for both horizontal components and vertical components, respectively. The average spectral ratios are 2.2 on PGA and 4.2 on peak spectral acceleration. The same orders of spectral ratio on PGA and peak frequency are found in the vertical component. The peak frequency of 6 Hz for the vertical component leads to p-wave and s-wave velocity ratio of 2 which implies that the average Poisson's ratio is larger than one third. The coefficients of variation of the mean spectral ratio are shown in Table A-6. The coefficients of variation at PGA are smaller than those of the DJR site, (e.g., 0.32 vs 0.64).

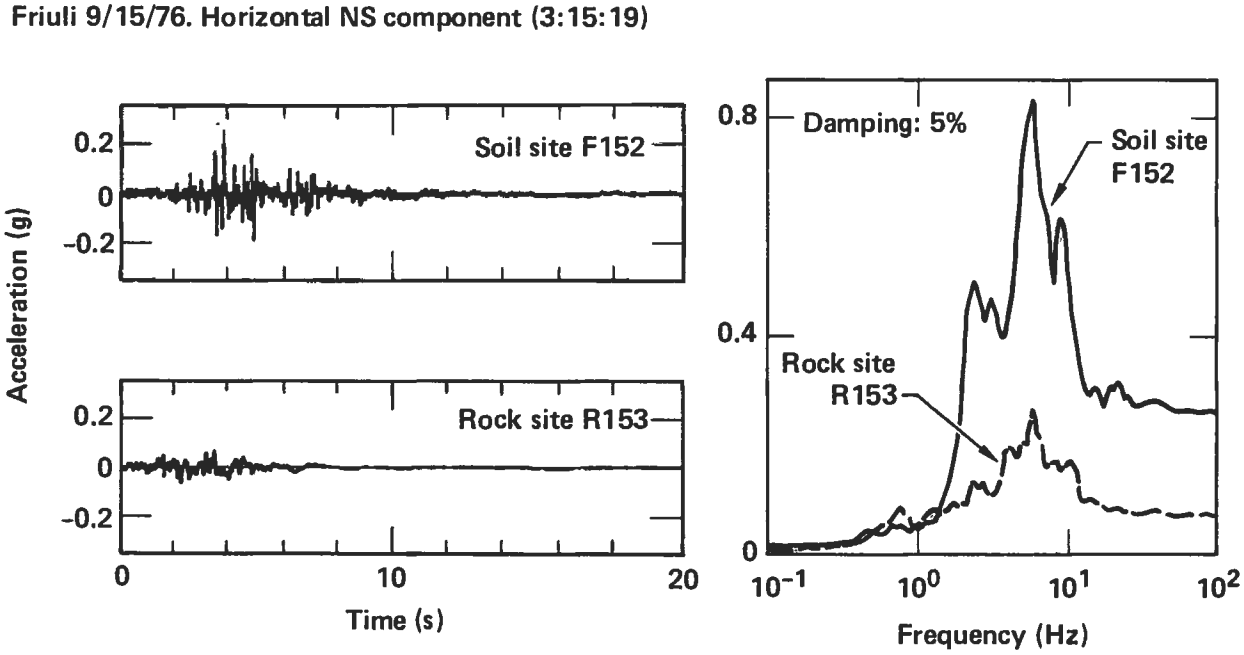

Fig. A-11. The recorded motion of soil and rock and its spectral analysis from the 9/15/76 Friuli earthquake. NS components.

Friuli 9/15/76. Horizontal EW component (3:15:19)

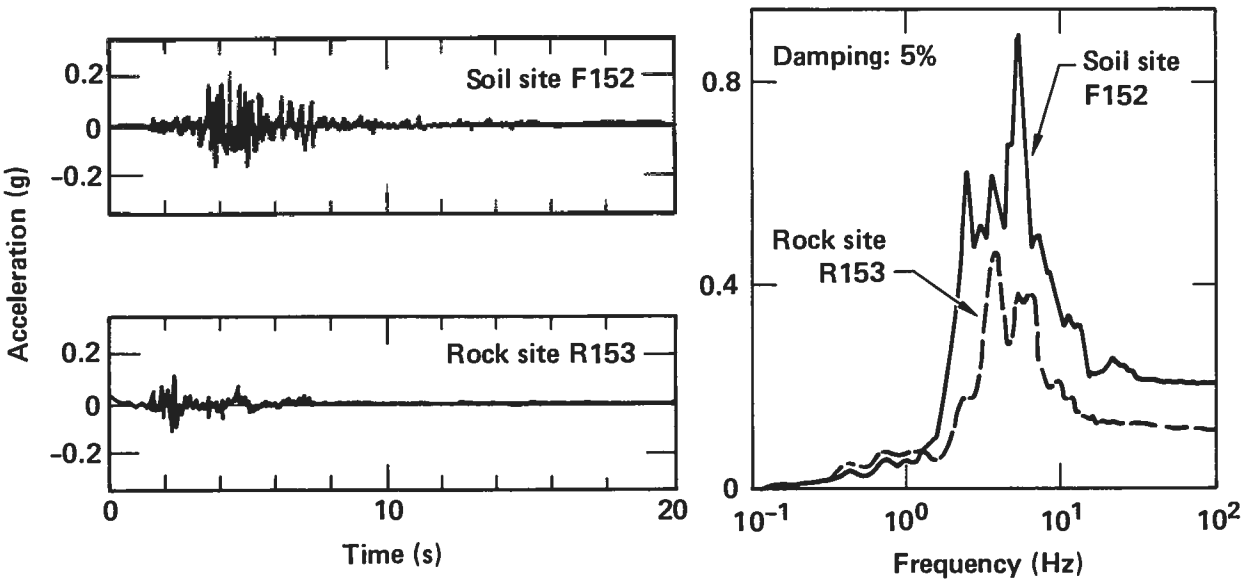

Fig. A-12. The recorded motion of soil and rock and its spectral analysis from the 9/15/76 Friuli earthquake. EW components.

Friuli 9/15/76. Vertical component (3:15:19)

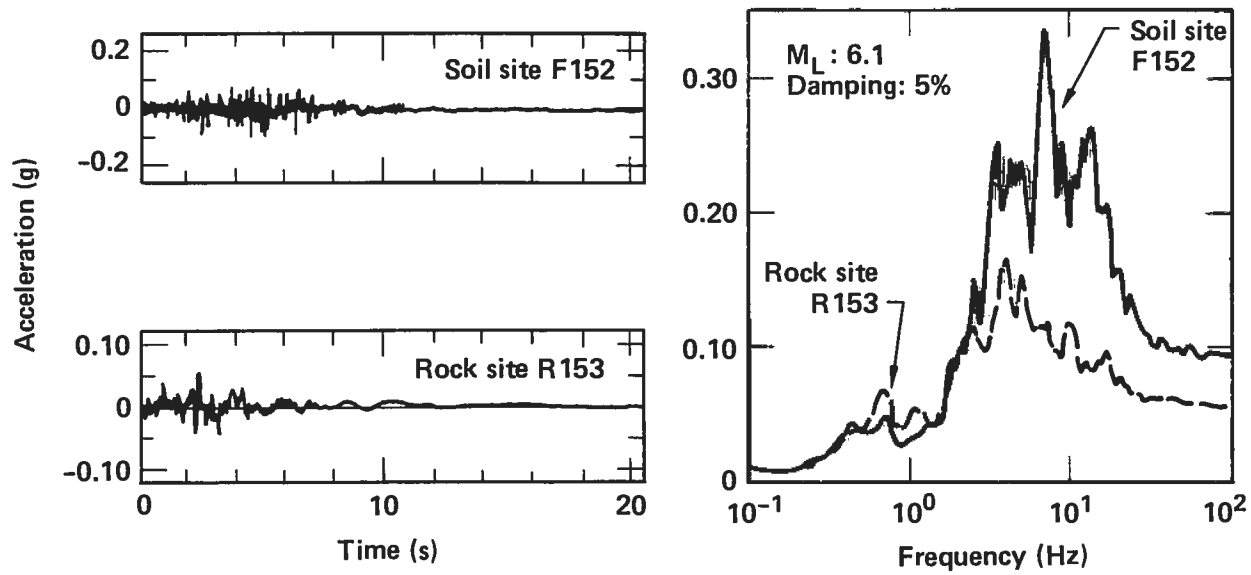

Fig. A-13. The recorded motion of soil and rock and its spectral analysis from the 9/15/76 Friuli earthquake. Vertical components.

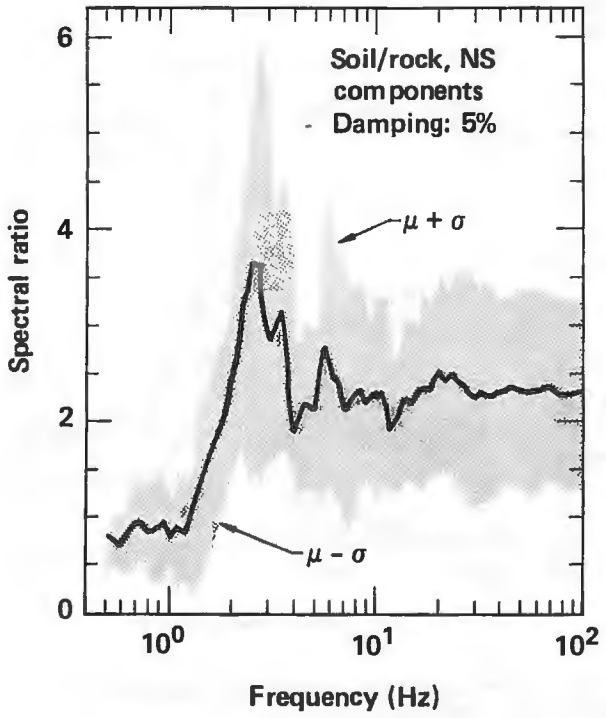

Fig. A-14. Spectral ratios of the NS component of the June and September 1976 Friuli earthquakes, recorded at Cornino-Forgaria and San Rocco. The solid line is the mean of 5 spectral ratios, and the shading marks the variation in the mean (±1 standard deviation).

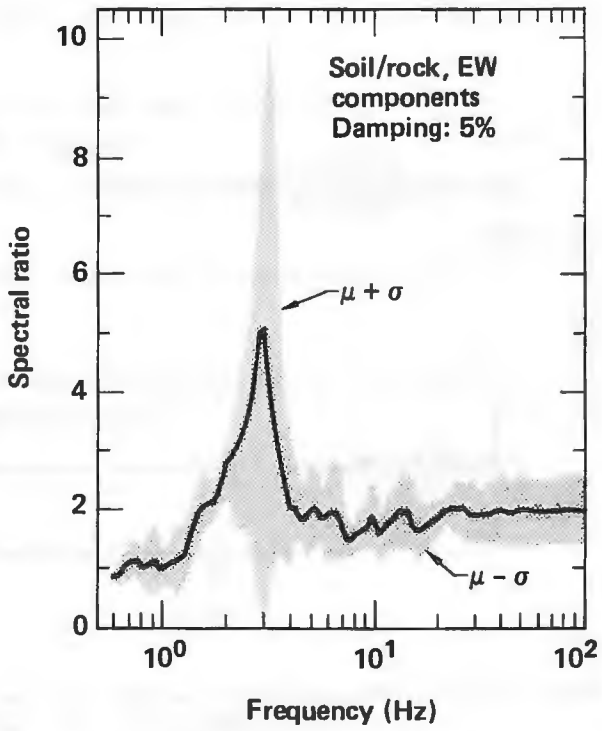

Fig. A-15. Spectral ratios of the EW component of the June and September 1976 Friuli earthquakes, recorded at Cornino-Forgaria and San Rocco. The solid line is the mean of 5 spectral ratios, and the shading marks the variation in the mean (±1 standard deviation).

Data recorded on the soil station at the Buia site were also compared to the corresponding component at the S. Rocco site. The Buia station is located on a deep deposit of alluvium overlying a rock formation of limestone and sandstone. Four earthquakes ($4.4 < M_L < 6.1$) with epicenters varying from 10 km to 20 km were used for this station pair. The average peak ground accelerations are 0.11 g at S. Rocco and 0.12 g at Buia station. The mean site spectral ratio and their plus/minus standard deviation for both horizontal and vertical components are shown in Figs. A-18 and 19. Note that for this deep, soft soil site, the PGA is not amplified, but appreciable amplification is observed in the low frequency range. In this case it is about 1.3 Hz, which is likely the fundamental frequency of the site. The coefficients of variation of the mean spectral ratio are shown in Table A-7.

A2.3 OBSERVATION OF THE RESPONSE OF SITES IN SEDIMENT-FILLED VALLEYS

Experimental studies of the response of sediment-filled valleys to earthquake motion were reported by Tucker et al. (Ref. A-7), King and Tucker (Ref. A-8), and Tucker and King (Ref. A-9). In the first paper, the variation of earthquake motion on and in hard rock (granite) was investigated. In their

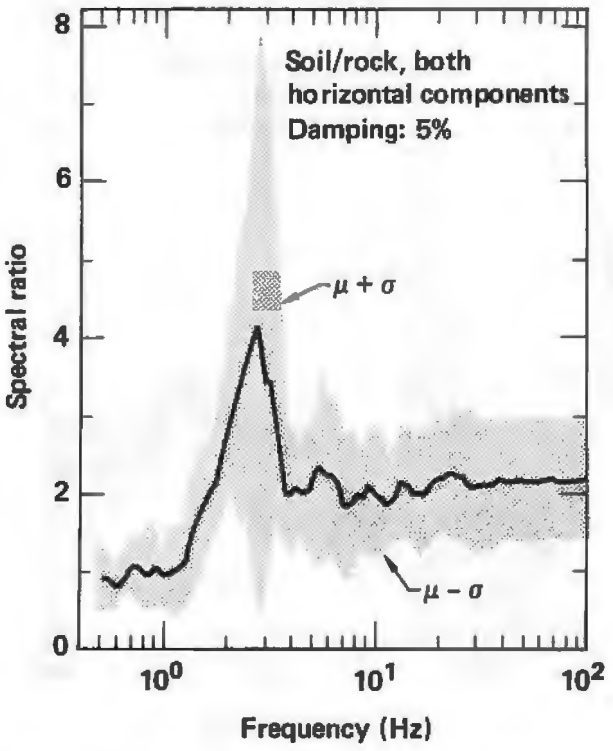

Fig. A-16. Spectral ratios of both horizontal components of the June and September 1976 Friuli earthquakes, recorded at Cornino-Forgaria and San Rocco. The solid line is the mean of 5 spectral ratios, and the shading marks the variation in the mean (±1 standard deviation).

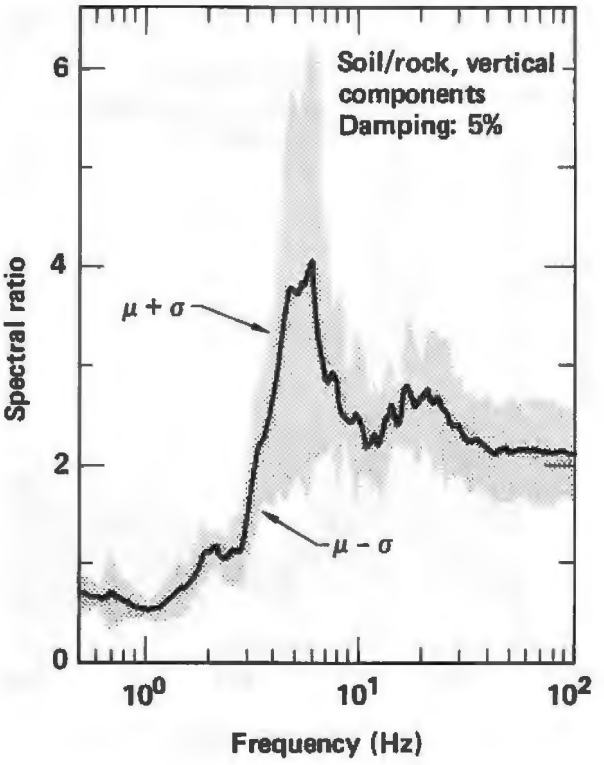

Fig. A-17. Spectral ratios of the vertical component of the June and September 1976 Friuli earthquakes, recorded at Cornino-Forgaria and San Rocco. The solid line is the mean of 5 spectral ratios, and the shading marks the variation in the mean (±1 standard deviation).

second and third papers, they reported the ratio of motion recorded at sites on the valley sediments to motion recorded at the nearby rock outcrop. They also studied the dependence of this ratio on frequency, the position of the sediment site within the valley, and the input signal's azimuth, incidence and wave type of strong and weak motions. Part of their results are briefly summarized as additional data to demonstrate the effects of local site conditions.

The ratio of motion is presented as the ratio of the smoothed Fourier amplitude spectrum, rather than the ratio of response spectrum. In fact, both ratios can be used to represent a transfer function (or amplification) of a site, since either a smoothed Fourier amplitude spectrum or a damped response spectrum represents the major characteristic of the entire motion time history. The conversion from Fourier to response spectra amplification depends on the bandwidth spectral window used in the smoothing Fourier amplitude spectrum and the damping ratio used in computing the response spectrum. Generally, a factor near 0.85 may be applied to convert from the Fourier to response spectra amplification (Ref. A-10).

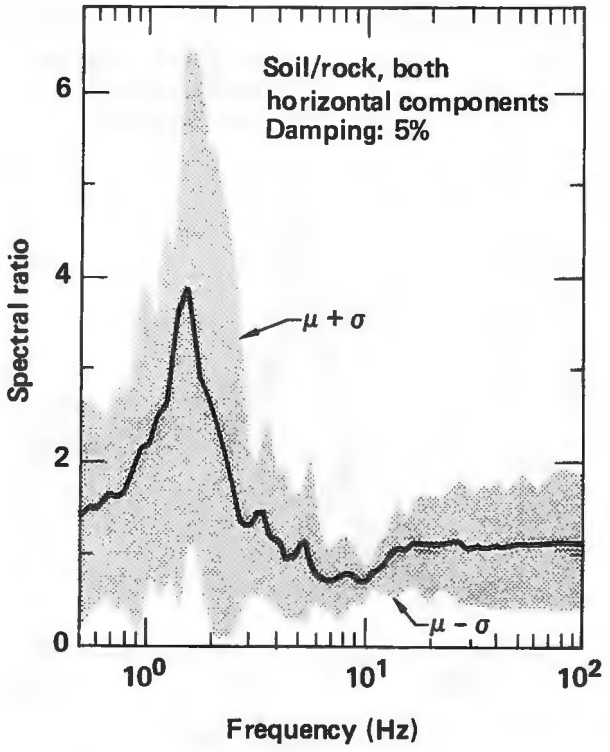

Fig. A-18. Spectral ratios of both horizontal components of the September 1976 Friuli earthquakes, recorded at Buja and San Rocco. The solid line is the mean of 8 spectral ratios, and the shading marks the variation in the mean (±1 standard deviation).

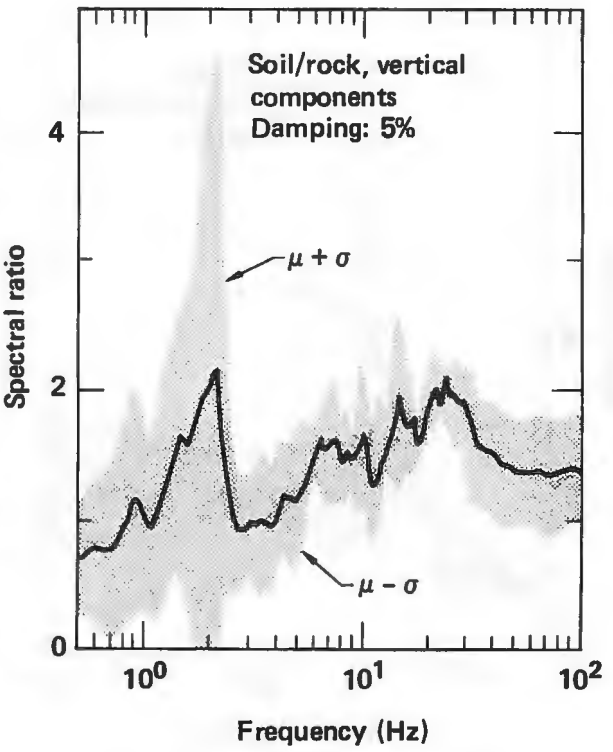

Fig. A-19. Spectral ratios of the vertical component of the September 1976 Friuli earthquakes, recorded at Buja and San Rocco. The solid line is the mean of 4 spectral ratios, and the shading marks the variation in the mean (±1 standard deviation).

Table A-6. Coefficients of variation of the mean spectral ratio at Forgaria-Cornino from the 1976 Friuli Earthquakes.

	Horizontal component			
	NS	EW	Both	Vertical component
PGA	0.41	0.25	0.32	0.23
Peak frequency (Hz)	0.57 2.80	0.92 2.80	0.81 2.80	0.52 6.00

Table A-7. Coefficients of variation of the mean spectral ratio at Forgaria-Cornino from the 1976 Friuli Earthquakes.

	Horizontal component			
	NS	EW	Both	Vertical component
PGA	0.60	0.47	0.59	0.33
Peak	0.71	0.55	0.71	1.14
frequency (Hz)	1.30	1.30	1.30	2.10

Table A-8. List of events used for site amplification study by Tucker et al. (Ref. A-7).

Event No.	Time (GMT)	Date	Latitude (N)	Longitude (E)	Depth (km)	M_L*
1	0311	10/12/76	37°06'	71°36'	160	3.0
2	0238	11/14/76	36°42'	71°00'	210	3.0
3	0827	11/14/76	39°15.9'	70°41.1'	10	1.9
4	0851	11/15/76	36°36'	71°00'	200	3.2
5	0831	11/18/76	38°59.7'	70°43.3'	4	1.2
6	2323	11/18/76	39°07.4'	70°32.7'	?	?
7	1008	11/20/76	(t_s-t_p 1 sec)		?	?
8	1008	09/11/77	39°22.4'	70°04.8'	8	3.3
9	1954	09/13/77	39°03.2'	71°28.4'	0	3.3
10	0900	09/14/77	(small Afghanistan event)		?	?
11	1751	09/14/77	36°12'	70°48'	110	3.7
12	1301	09/15/77	38°55.4'	70°50.9'	9	2.9
13	1339	09/21/77	38°54.8'	70°51.5'	10	1.4
14	0801	09/22/77	36°42'	71°12'	180	3.3
15	1017	09/25/77	36°42'	71°12'	200	3.8
16	1225	09/27/77	38°37.3'	70°18.6'	12	3.2
17	1539	10/04/77	38°46.6'	70°21.6'	2	2.5
18	2016	10/04/77	35°48'	69°24'	110	4.6
19	0230	10/11/77	36°30'	70°36'	210	4.0
20	1341	10/12/77	36°30'	70°24'	200	3.5
21	1151	10/13/77	38°59.6'	70°37.0'	8	1.5
22	1534	10/27/77	39°19.7'	70°41.6'	6	2.1
23	1948	11/01/78	39°30'	72°36	?	5.8
24	1229	05/20/79	39°25.2'	69°40.2'	53	4.2
25	1940	10/20/79	38°55.9'	70°36.4'	15	4.6
26	0810	09/21/80	39°07.9'	70°44.6'	6	3.2

* M_L is converted from energy class, K (= log E, where E is the radiated seismic energy in Joules), according to the relationship $M_L = 0.56\ K - 2.2$, which is valid for the Garm region but not necessarily other regions (Rautian, 1965).

As shown in Fig. A-20, three sediment-filled valleys (Chusal, Yasman and Runo located in the Garm region of the USSR) were selected as the experimental studies. During the experimental period, measurements of motion from hundreds of weak events and from four strong events (numbers 23 to 26 of Table A-8) were recorded. A number of events were selected for analysis on the basis of epicenter, magnitude and quality of recording. Table A-8 lists the events used in this study. The ground acceleration levels of these events range from 10^{-5} to 0.2 g. The epicenter of some of these events are shown in Fig. A-20.

- Chusal Valley
  Chusal Valley is a small (400 to 700 m), sediment-filled valley with a maximum depth, at the center, of 60 m. The sediments are composed of loess and gravel, and are underlain by low damping granite. The vertical cross section and the shear wave velocity profile are shown in Fig. A-21. The sediment depth and the average s-wave and p-wave velocities are known from refraction studies. The impedance ratio between rock and soil deposit was estimated to be near six. Four stations on the sediment and a station located in a tunnel of the hardrock were installed. King and Tucker (Ref. A-8) studied in detail the response of this valley to weak motions (10^{-5} to 10^{-3} g) and concluded that the response strongly depended on frequency and the position of the site within the valley, but depended, only

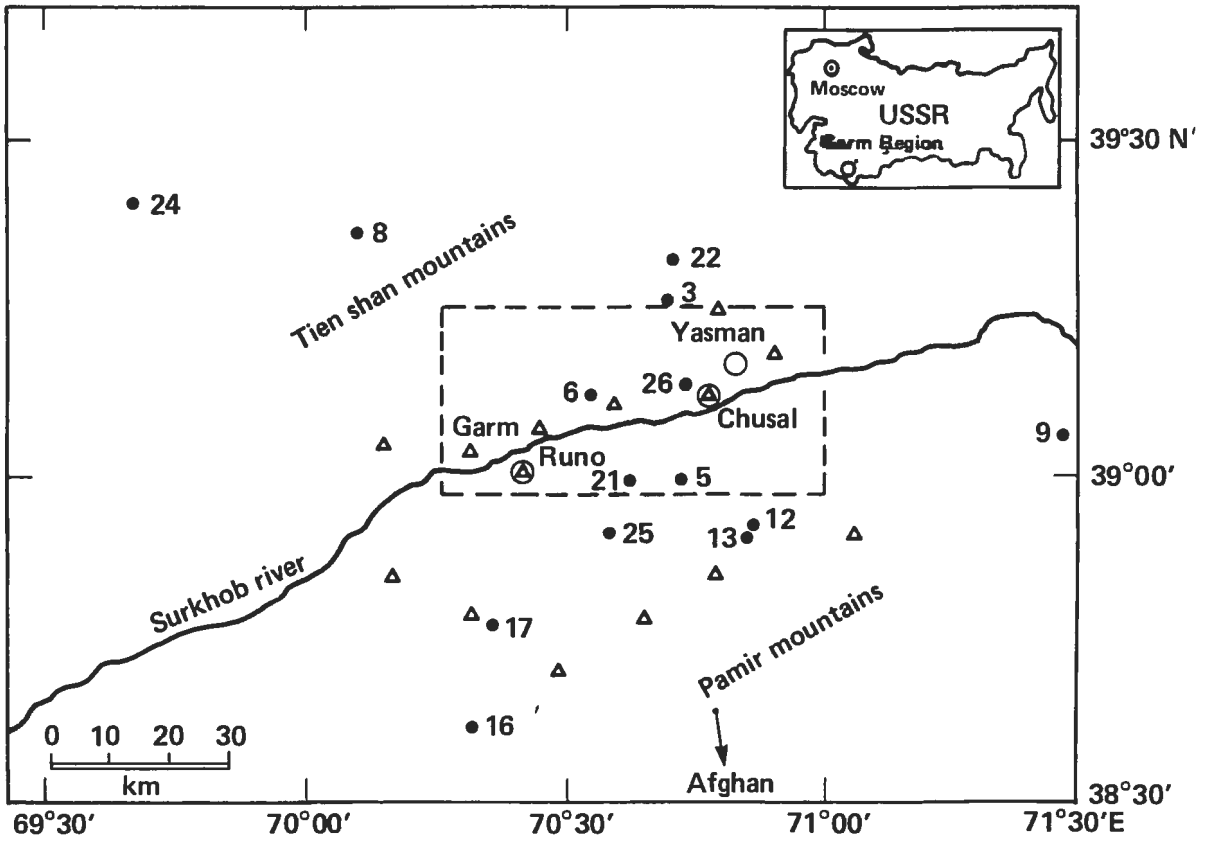

Fig. A-20. Locations of three sediment-filled valleys and parts of earthquake epicenters used for experimental amplification studies by Tucker et al. (Ref. A-7).

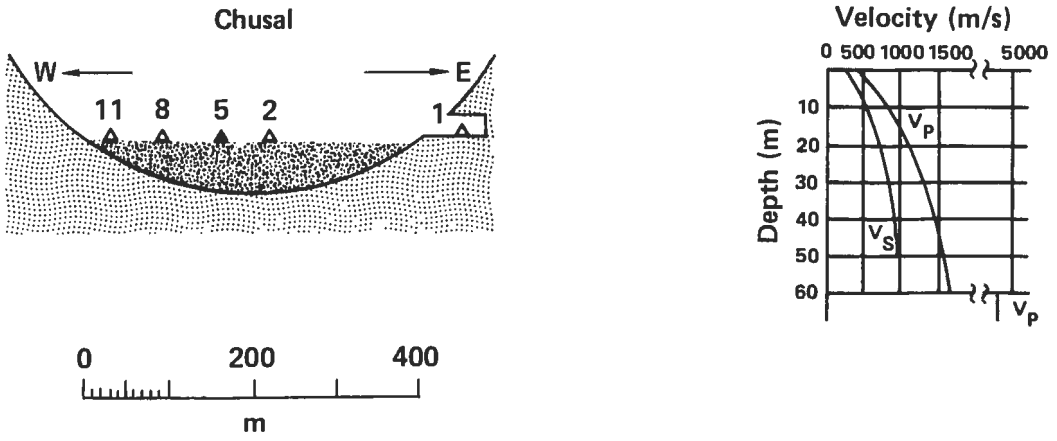

Fig. A-21. Diagrammatic cross-section and shear wave velocity profile of the Chusal site (Ref. A-7).

slightly, on wave-type, component of motion and the input signals azimuth and incidence angles. The Fourier spectral amplitude ratio of motions recorded between the soil stations and the nearby rock station was as high as 10. The ratio varied by only a factor of 2 to 3 from the events with different angles of azimuth and incidence. Figure A-22 shows the spectral ratios for each component of events recorded at the valley stations (numbers 2, 5, 8, and 11) and the tunnel site. Note the large difference between the valley site responses at the first peak near 2 to 4 Hz. Figure A-23 shows the comparison of spectral ratio for each component of four weak motions (3, 5, 6, and 7), and four strong motions 23, 24, 25, and 26). The PGA of the weak motion group ranges from 10^{-5} to 10^{-3} g and the strong motion group ranges from 0.04 to 0.2 g. There are no significant differences between the weak motion group and the strong motion group.

- Yasman Valley

Yasman Valley (about 10 km by 1.3 km and of unknown depth) is composed of alluvium sediment and is underlain by granite rocks. For this site the average soil-rock impedance contrast for s-waves is estimated to be around five. The diagrammatic cross section of the valley with the recorded stations in the valley (number 1, 2, 3, and 4) and the nearby rock outcrop station is shown in Fig. A-24. Spectral ratios of a distant Afghanistan and 3 local events (numbers 8, 9, and 16) are also shown in Fig. A-24. These four events have similar magnitude but very different azimuths with respect to the Yasman Valley. Considerable variation is observed at the middle station, where the average difference between curves is a factor of three. This implies that the ratio value due to the effect of azimuth can be $\pm$50% of the mean value. In the center of the valley, during one event, motions were amplified up to 10 times in the frequency band 1 to 4 Hz. The fundamental site frequency is expected to be within this range. At the edge of the valley, the motions were deamplified in the band between 1 to 4 Hz but were amplified at a frequency near 10 Hz. The factor of amplification was as high as 7. Site amplifications in the NS direction (perpendicular to the valley sides) are almost 2 times higher than those in the EW direction.

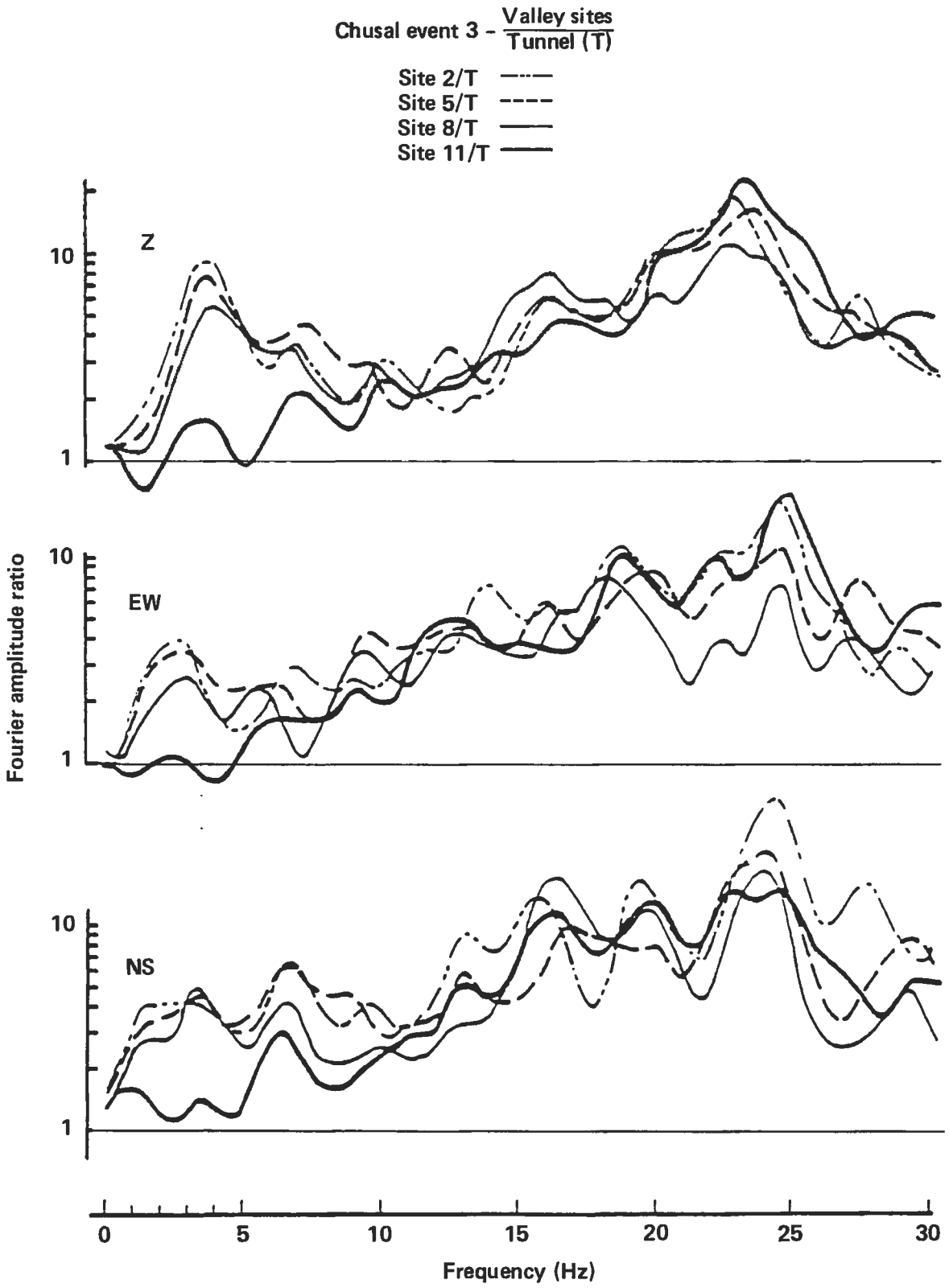

Fig. A-22. Soil/rock spectral ratios of the first 4 s of the S-wave of Event 3 for the three components of motion recorded at Chusal Valley stations 2, 5, 8, and 11 (Ref. A-7).

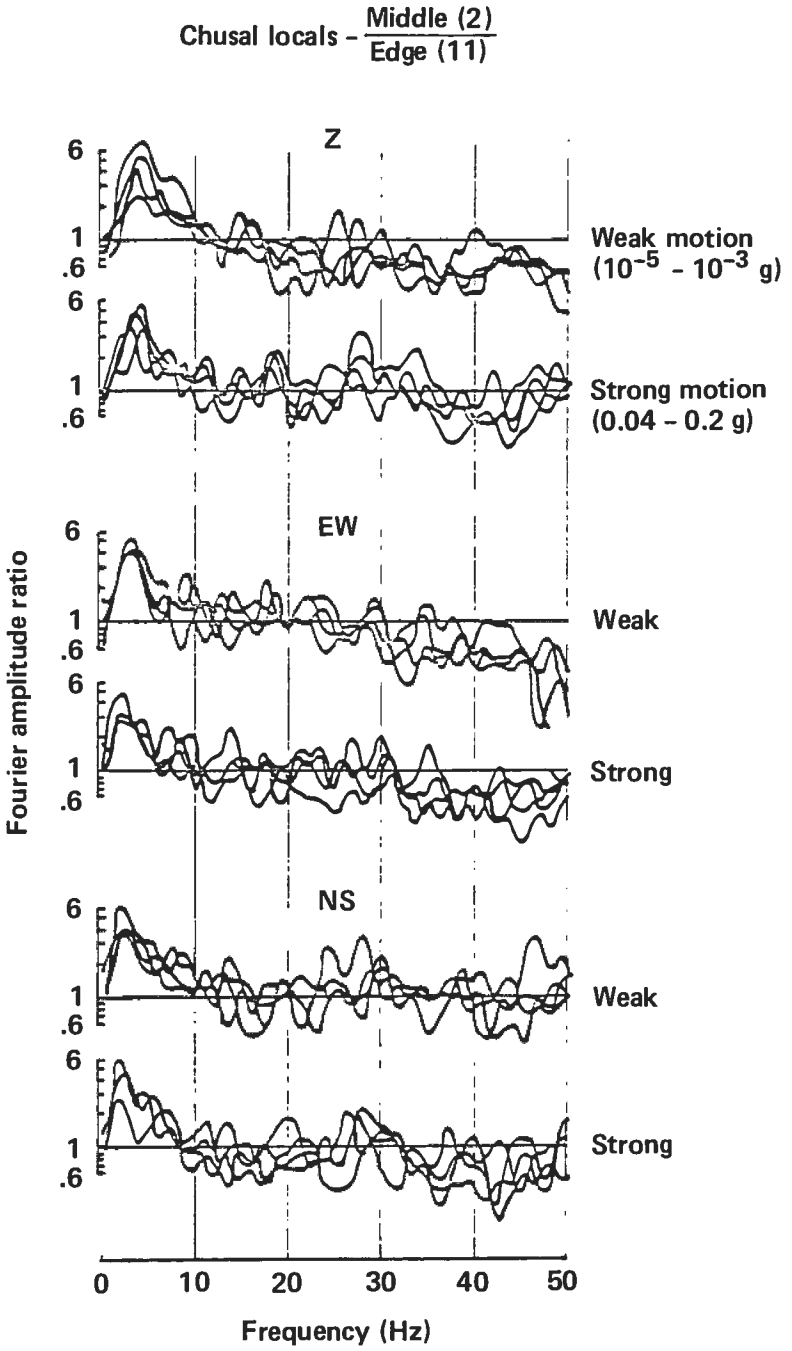

Fig. A-23. Valley-middle/valley-edge spectral ratios of four small events and four strong events for the three components of motion recorded at the Chusal site (Ref. A-7).

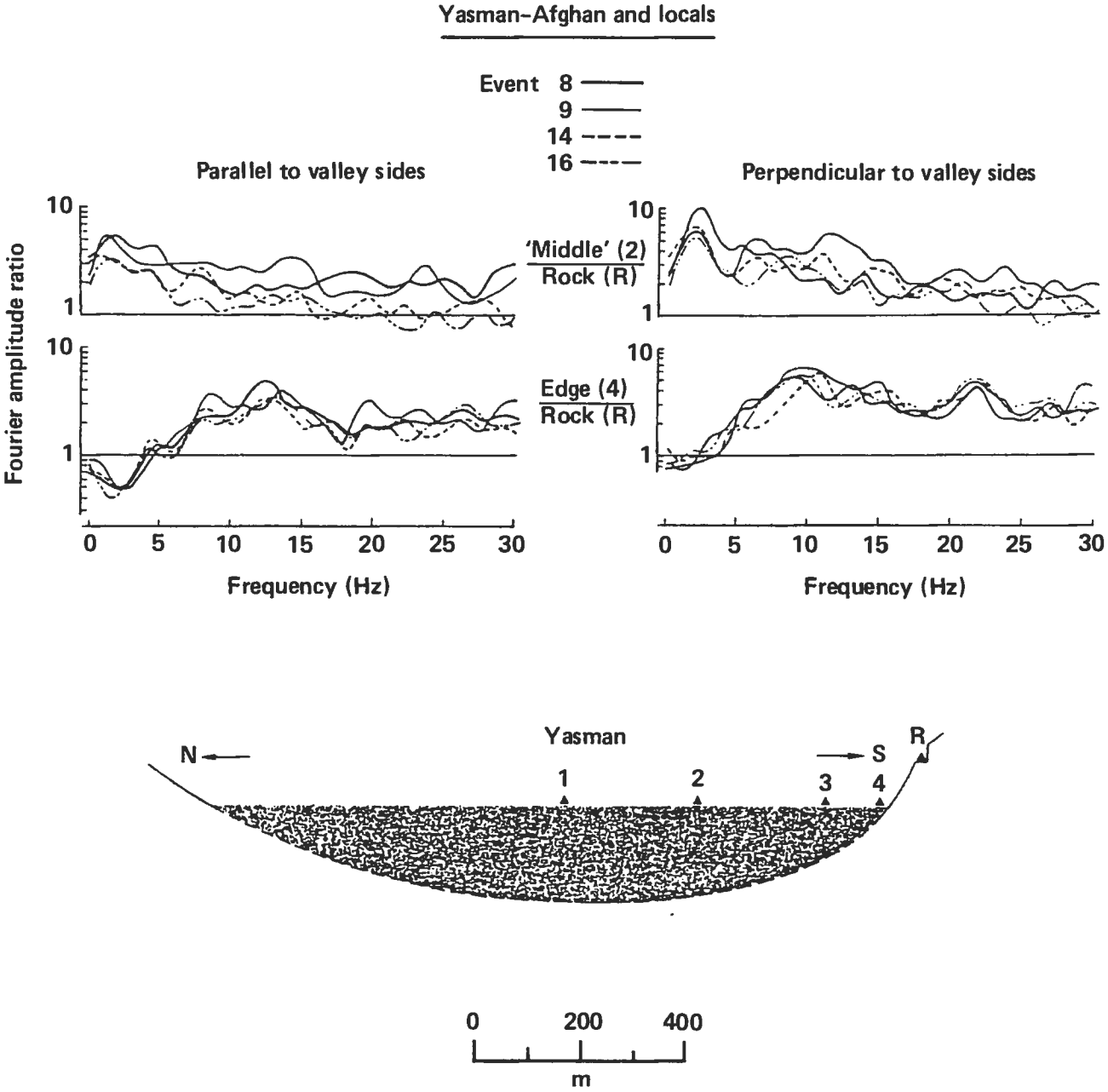

Fig. A-24. Soil/rock spectral ratios of Yasman Valley sites recorded for four events. The top two panels show mid-valley-soil/rock ratios; the bottom two panels show valley-edge-soil/rock ratios. The left panels show the results for the component of motion along the valley; the right panels show the results for the component of motion across the valley.

- Runo Valley
  Runo valley (about 5 km by 0.7 km and 100 m deep) consists of the high deformed Meso-Cenozoic marine and lagoon deposits. The valley is underlain by low damping granite. The impedance ratio between the soil and the rock is estimated to be about three. The cross section as well as the spectral ratio from three local events and one distant Afghanistan event are shown in Fig. A-25. At this particular site an amplification factor of two to three was observed from event to event. Considerable amplifications were observed at the edge of the valley for the frequency band from 1 to 30 Hz. At the valley center motion was amplified for low frequency band (<8 Hz), but the motion remained at the same level or was attenuated for frequencies greater than 10 Hz. This fact is attributed to the deep, soft soil deposit at the valley center.

On the basis of ground motion measurements at mid-valley and the nearby rock outcrop, Fig. A-26 shows the medians of the absolute mid-valley site amplifications. At Chusal and Yasman Valleys an average site amplification on the order of five was observed in the frequency band 1-5 Hz. Assuming a factor of 0.85 to convert from Fourier amplitude to response spectra, the average amplification in terms of response spectra ratio, as defined earlier, is 4.2, which is of the order found at other sites. Chusal's sediments amplify motion in the 10-30 Hz band by a factor of 5 to 6, while Yasman's sediments amplify motion in this band by a factor of 2 or less. Tucker reported that Chusal's higher amplification in this band may be due to soft sediments in the top few meters, or possibly to the underestimated deamplification effects of the tunnel rock station. The records from the deep, soft soil deposit at the Runo Valley show site amplification considerably smaller than average (about 2 to 5) and the absence of a sharp resonance peak.

A2.4 SITE AMPLIFICATION DATA FROM UNDERGROUND NUCLEAR EXPLOSIONS

Research on nuclear ground-motion data has established that ground motion response spectra of nuclear explosions and earthquakes are similar in the frequency range 0.2-100 Hz. Recordings have shown that ground motion from nuclear explosions could differ by up to a factor of 10 due to the effect of local site geology (Refs. A-11, A-12). Some published data are summarized herein to demonstrate local site amplification.

Ground motion data from a series of underground nuclear explosions at the Nevada Test Site (NTS) were used to provide experimental validation of analytical models of site response (Ref. A-11). Site amplification factors were derived from these data for a variety of record stations located at different geological configurations and a wide range of ground motion levels (0.01 to 0.75 g). The epicentral distances range from 17 km to 550 km. For engineering applications, the near field sites (R < 150 km) were selected for our data base. The diagrammatic, geological cross sections through station pairs used for computing site amplifications are shown in Fig. A-27. The major site characteristics represented by the thickness of soil layers, the density and the shear wave, as well as p-wave velocity of the soil layer and the underlying bedrock, are shown in this figure.

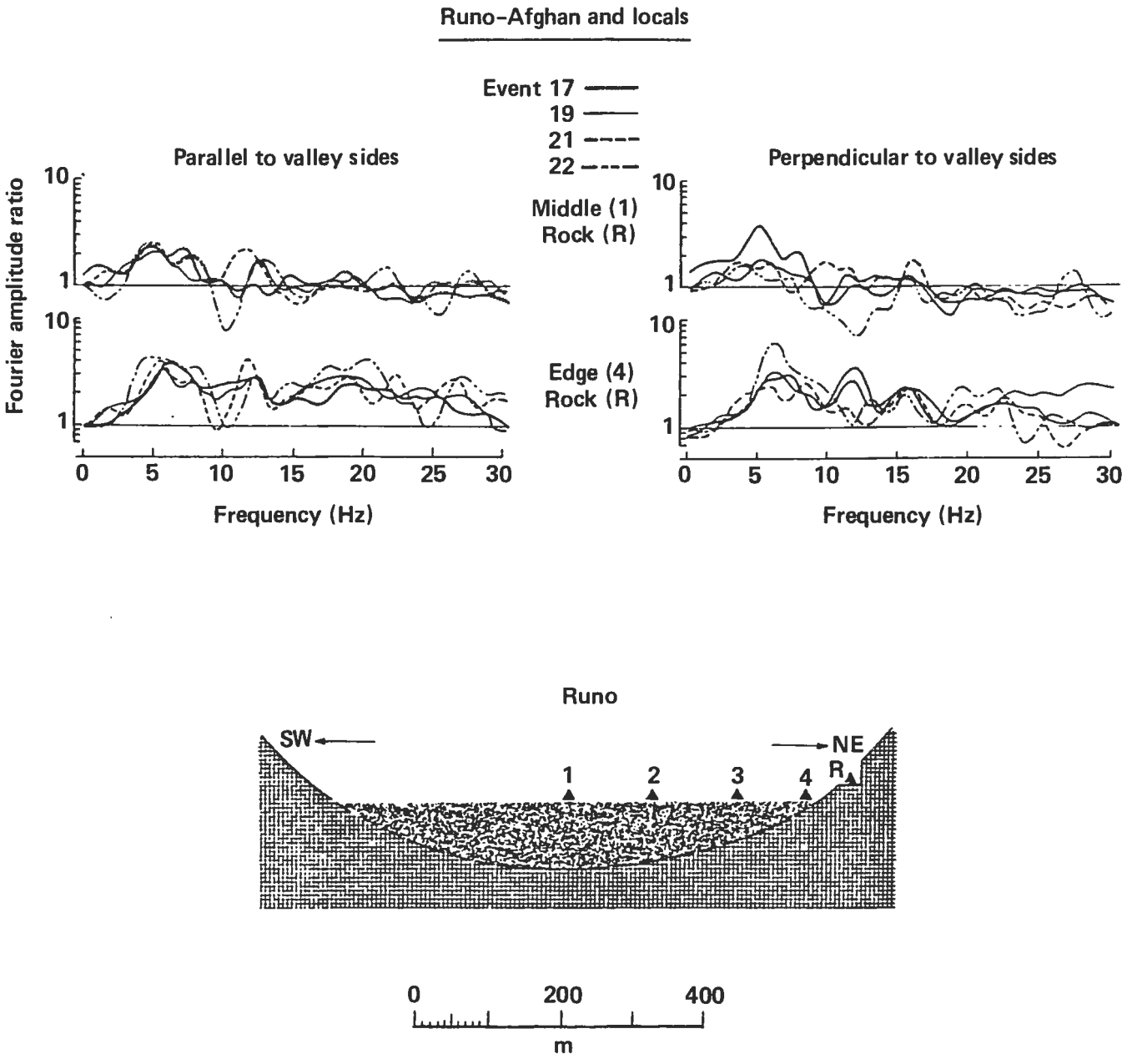

Fig. A-25. Soil/rock spectral ratios of Runo Valley sites recorded for four events. The top two panels show mid-valley-soil/rock ratios; the bottom two panels show valley-edge-soil/rock ratios. The left panels show the results for the component of motion along the valley; the right panels show the results for the component of motion across the valley.

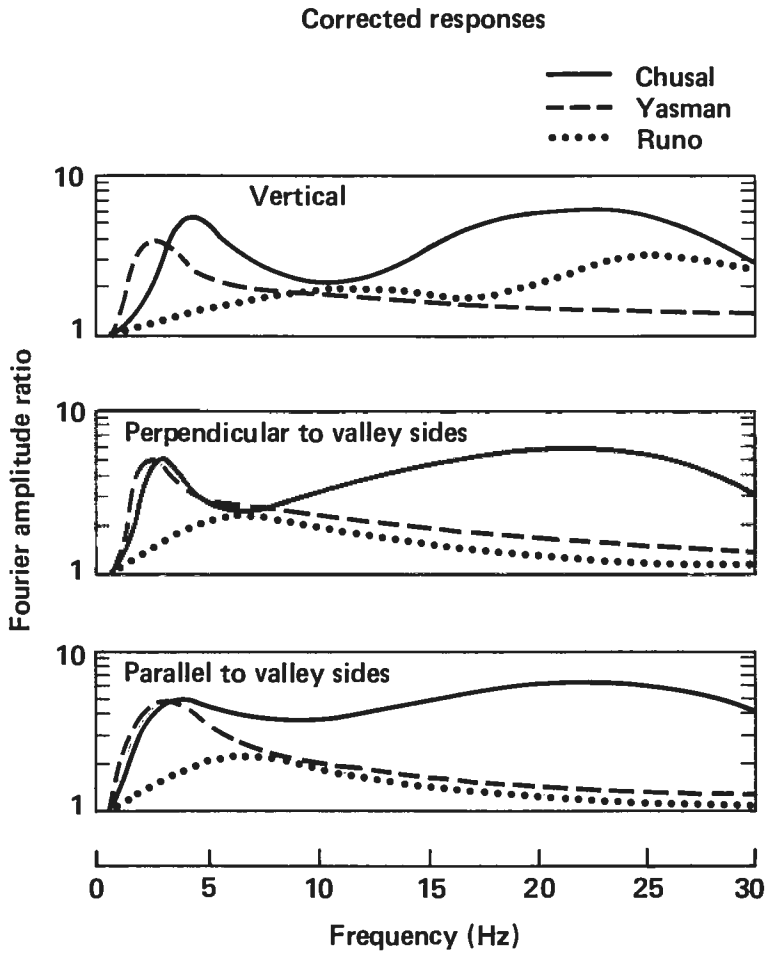

Fig. A-26. Corrected mid-valley spectral ratios of Chusal, Yasman, and Runo Valleys (Ref. A-7).

- Tonapah Site

  A pair of recording stations are located 183 m apart, on dacite (an igneous rock) and on 13 m of mine tailings fill. The impedance ratio between the fill and the bedrock is about 4.5. From more than 20 records obtained at this station pair, Murphy (Ref. A-11) has shown that the average site amplification near the fundamental period of the site is about 4.5 in radial components and about 3.1 in transverse components.

  The PGA was amplified more than 2.2 times. Figure A-28 shows the spectral ratio (mean and standard deviation) of the radial component for 30 NTS events, as published by Hays (Ref. A-12). The amplification occurs in a relatively narrow frequency range centered around 7 Hz. This frequency corresponds to the fundamental natural frequency of the fill layer. The PGA levels at this site were from 3.3×10^{-5} to 2.51×10^{-2} g, and the shear strain level was about 10^{-6} to 10^{-5}. The coefficient of variation of the mean spectral ratio near the dominant frequency is about 0.3-0.4.

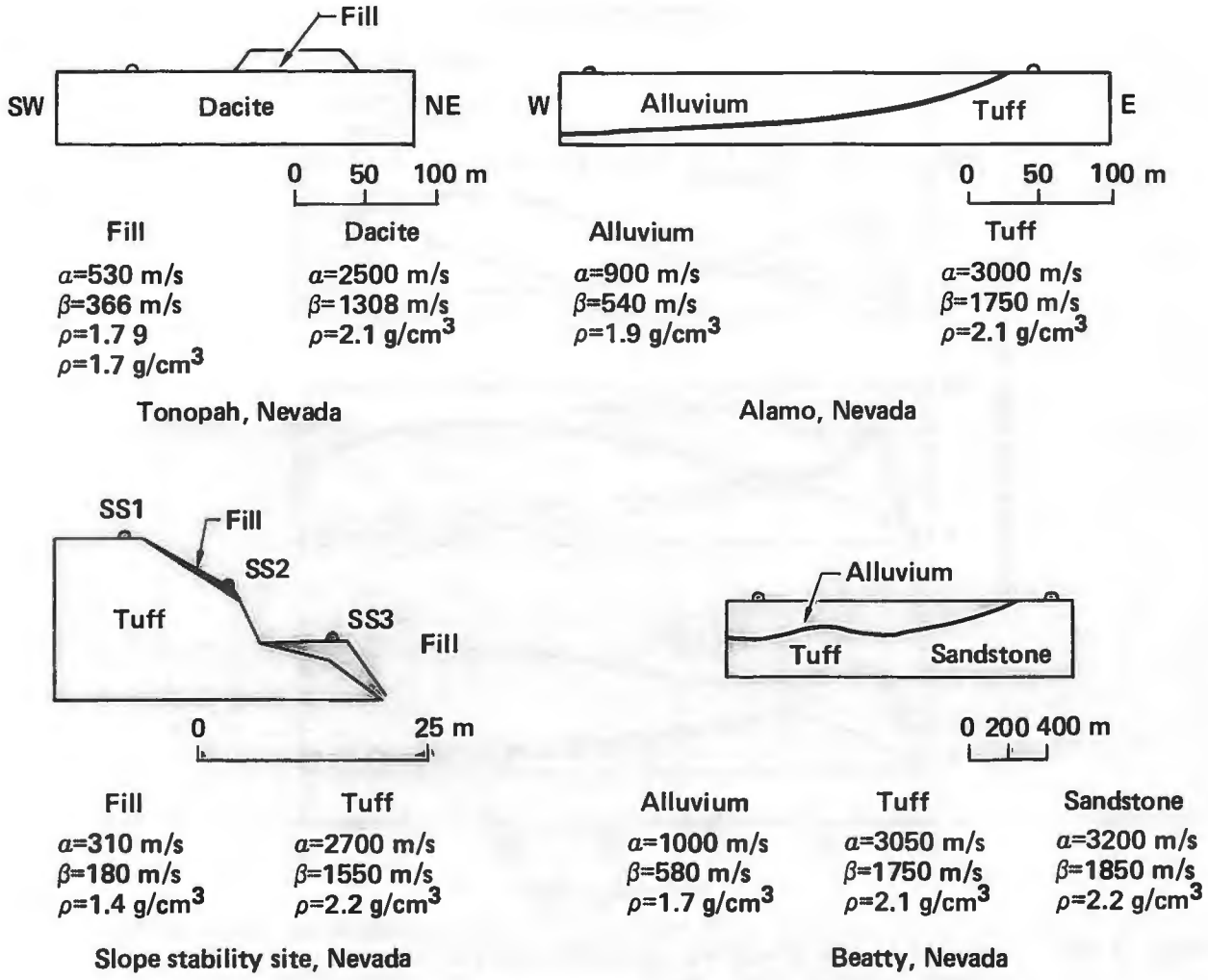

Fig. A-27. Diagrammatic geological cross-section through station pairs at NTS. After Ref. A-11.

- Beatty Site

  Seven records of NTS events recorded at two stations in the Beatty site were used to compute the average site amplifications for the radial and transverse components of motion. The average epicentral distance is closer to the source locations than the Tonopah site (57 km vs 126 km). As can be seen from Fig. A-27, the geology is complex, with the rock station situated on sandstone, while the nearby alluvium layer overlies a layer of tuff, which presumably overlies sandstone at an unknown depth. As the geological properties of the sandstone and the tuff are not significantly different, the effect of this complicated rock formation may be insignificant. The impedance ratio of rock to soil is about 4. The average PGA were amplified 2.5 times. The site amplification in radial components is 4.5 near 4.0 Hz, while the transverse component is 5.0 near 2.5 Hz. The amplification occurs at two different frequencies for two horizontal components, possibly due to the effect of the complicated geology. Nevertheless, appreciable amplification occurs for both components.

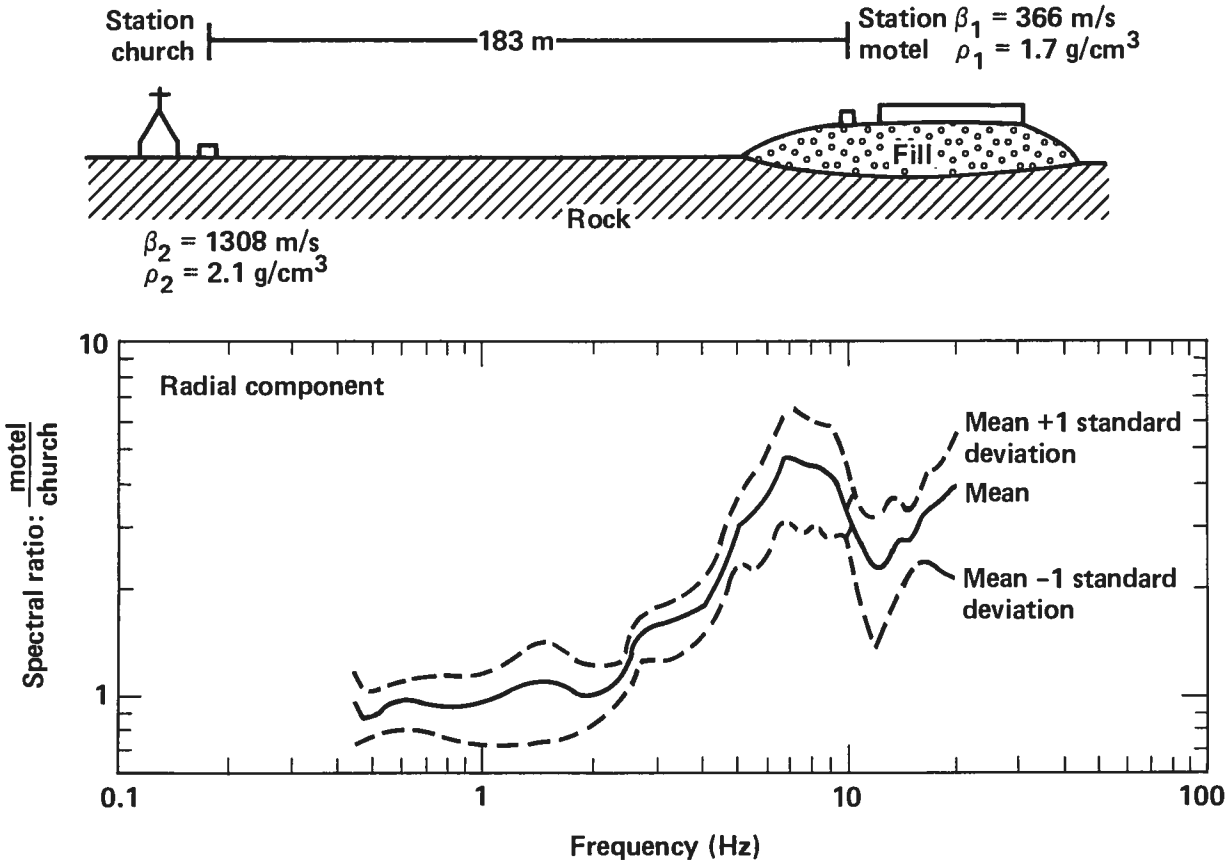

Fig. A-28. Variability of ground motion recorded at two sites in Tonopah, Nevada (Ref. A-12).

In 1974, instruments were placed in rock (tuff) in the bottom of a 41-m hole and at the surface on alluvium. The mean transfer function for 10 nuclear explosions is shown by Hays (Ref. A-13) and Murphy (Ref. A-11) et al. As seen in Fig. A-29, the average spectral amplitudes of the subsurface rock motions are one-tenth of the corresponding surface motion around 0.33 s, which is the fundamental period of the site. This means that the motion was amplified 10 times near 3 Hz.

- Alamo Site

  There are two stations at the Alamo site: one on a rock outcrop (tuff), and one on top of an alluvial deposit 40 m thick, overlying the tuff formation. The two stations are 300 m apart. The average shear wave velocity of the alluvium is 540 m/s and the impedance ratio between the soil layer and the baserock is estimated to be 3.6. Records of four NTS events were used to compute the average site amplification. The ratio at PGA is about 2.1. The spectral ratios at the dominant frequency of 3.5 Hz are 2.4 in the radial component and 3.4 in the transverse component.

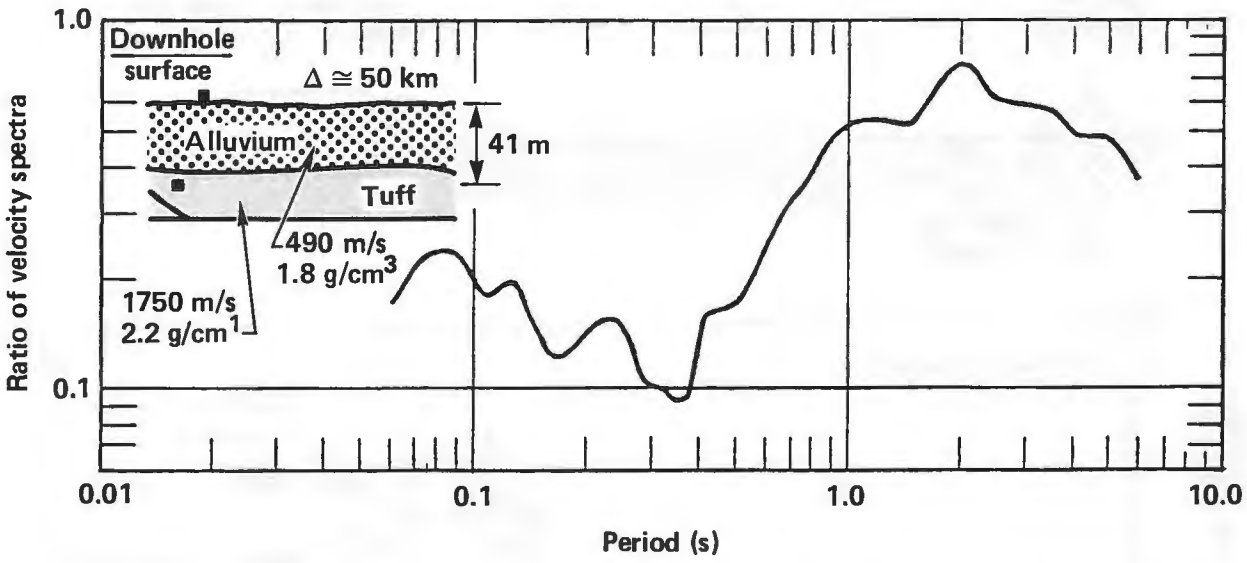

Fig. A-29. Variation of horizontal ground response with depth at Beatty, Nevada (Ref. A-13).

- Pahute Mesa Site
  Three stations located in the Pahute Mesa area of NTS were subjected to very strong shaking (maximum acceleration 7.55 x 10^{-1} g). The average epicentral distance from the source was estimated to be 17 km. Station 1 (SS1) is situated on the tuff rock outcrop. Station 2 (SS2) and Station 3 (SS3) are situated on 3 m and 6 m of fill, respectively. The distance between these three stations is less than 30 m. The average shear wave velocity, for these relatively soft deposits, is 180 m/s. There is little or no amplification at SS2 relative to SS1 at the observed frequency range, a result that we attribute to the thin fill at SS2. The amplifications at SS3 relative to SS1 are quite large, with an amplification factor averaging 6 in the radial component and 5.5 in the transverse component. The peak amplification occurs near 8 Hz.

Table A-9 is a summary of experimental site amplifications obtained from four sites subjected to underground nuclear explosions at the NTS. As shown earlier, the amplifications and coefficients of variation of the mean values at the PGA and the peak spectra are comparable to those of earthquake motion. Local site condition, especially thin soil deposit, can affect the dominant spectral components of the incident waves and, therefore, cause significant variation in the signature of the input ground motion.

A3.0 DEVELOPMENT OF SITE AMPLIFICATION FOR THE ZION SITE

The mean site amplification derived from records at DJR and Forgaria-Cornino provide useful information about site amplification that may be developed in shallow soil sites. Ideally, if this type of site response data exists for Zion or a site similar to Zion, such site amplification could apply directly to Zion. However, there are a number of differences in site conditions

Table A-9. Summary of average spectral ratios obtained from underground nuclear explosions.

Site	Soil layer (m)	No. of records	Component[a]	Max. accel. (g)	Ave. Epi distance (km)	Average spectral ratio & COV[b] PGA	COV	PEAK	COV	Freq. (Hz)
Tonopah	13	20	R	2.52×10^{-2}	126	2.4	0.38	4.5	0.36	7.0
Tonopah	13	20	T	2.52×10^{-2}	126	2.2	0.32	3.1	0.32	7.0
Beatty	52	7	R	1.90×10^{-2}	57	2.8	0.43	4.5	0.58	4.0
Beatty	52	7	T	1.90×10^{-2}	57	2.7	0.56	5.0	0.64	2.5
Alamo	40	4	R	3.10×10^{-3}	107	2.0	0.11	2.3	0.22	3.5
Alamo	40	4	T	3.10×10^{-3}	107	2.2	0.27	3.4	0.29	3.8
SS3/SS1	6	2	R	7.55×10^{-1}	16.6	3.0		5.8		8.0
SS3/SS1	6	2	T	7.55×10^{-1}	16.6	2.5		5.5		8.0

[a] R = Radial component
T = Transverse component
[b] PGA = Peak ground acceleration
COV = Coefficient of variation

between Zion and the DJR and Cornino sites. Consequently, it is not considered appropriate to apply the observed results to the Zion site. Therefore, it is necessary to use a theoretical model and current site response procedures to compute the expected amplification factors at Zion.

The characteristics of the Zion site, a relatively flat shallow soil layer over a very stiff bedrock, lead one to expect amplified motion in a narrow frequency range. This phenomenon must be considered in response calculations. The seismic hazard curve and the ensembles of acceleration time histories are defined for the rock outcrop. The free-field surface motion can be estimated or calculated by a theoretical model of the expected behavior of the Zion site. The model should be validated to the extent possible, and free-field surface motions can be calculated from rock outcrop motions.

The Zion site is on about 110 feet (33.5 m) of soil overlying Niagara dolomite bedrock. The bedrock has an average shear wave velocity of 9000 ft/s (2744 m/s). The soil deposit consists of three distinct sub-layers. The top layer, about 35 feet (10.7 m) thick, is formed by granular lake deposits of dense, fine-to-medium sand with variable amounts of gravel. The second layer, 30 feet (9.2 m) thick, is a cohesive firm-to-hard glacial fill. The remaining 65 feet (19.8 m) soil layer is a cohesionless, glacial deposit of dense sand and gravel. The soil deposit was discretized for the response computation as three sublayers underlain by a half space.

The soil column was modeled as a system of horizontal layers of infinite extent. Viscoelastic material models for each layer were assumed--shear modulus, density, Poisson's ratio, and material damping. One-dimensional wave propagation was also assumed--vertically propagating shear waves producing horizontal motion and dilatational waves producing vertical motion.

Modeling the soil properties at Zion entails estimating the nominal shear modulus and material damping to be expected for each discretization of the seismic hazard curve. Nominal values of these parameters for each layer and for each range of acceleration were determined by iterative, one-dimensional wave propagation analysis. The resulting equivalent linear properties approximately account for soil's nonlinear behavior during earthquake motion. A summary of nominal soil properties for each interval of the hazard curve was shown in Table A-4.2 of Section 4.22 of the main text. The average PGA level of rock outcrop for data analyses is about 0.1 g. Thus, we presented the Zion site amplification only for the comparable PGA level.

Because we lack knowledge of the nominal dynamic soil properties associated with excitation levels, the variability of nominal values should be considered. A set of numerical experiments was performed to investigate the effect of variation in three parameters on the resulting equivalent linear properties. The parameters were the low-strain shear modulus, the specified reduction in shear modulus with strain level, and the specified material damping with strain level. The assumed variability in these parameters was based on data from Zion and from sites with similar soil. The uncertainty due to input motion was also taken into account by selecting representative acceleration time histories in each box of the hazard curve. The coefficients of variation of the equivalent nominal shear modulus and damping ratio are about 0.4 and 0.5, respectively, for a rockcrop PGA level of 0.1 g .

For the Zion analysis, local site amplification was modeled explicitly in the seismic response calculations and in generation of the seismic hazard curve. As mentioned earlier, the procedure was to define the free-field ground motion and associated seismic hazard curve on a hypothetical rock outcrop. This seismic hazard curve was developed from a ground motion model with that uncertainty removed which was thought to be due to differences in site conditions where the ground motion data were recorded. The time histories were then propagated through a linear viscoelastic soil model with properties of the experimental design used in the SMACS analysis. Figures A-30 and 31 show spectral ratios for horizontal and vertical free-field ground motion. The mean and mean standard deviation are shown. Note that the uncertainty in these ratios is due to uncertainty in the rock outcrop time histories and in the soil properties. For this case, only sources of random uncertainty in the soil were treated. Thirty earthquake simulations were analyzed, with soil properties selected according to a Latin hypercube sampling procedure used in the SMACS analysis. The results show a mean PGA amplification of about 2, which corresponds well with recorded data. Mean simulated amplification in the amplified frequency range is 3 to 4, which is slightly less than the amplification exhibited by the recorded data. The average COV of the mean amplification is 0.2 at PGA and 0.3 at dominant frequency for the horizontal components, while the COV is approximately 0.2 both at PGA and dominant frequency for the vertical components. This model appears to be reasonable, considering most sources of uncertainty.

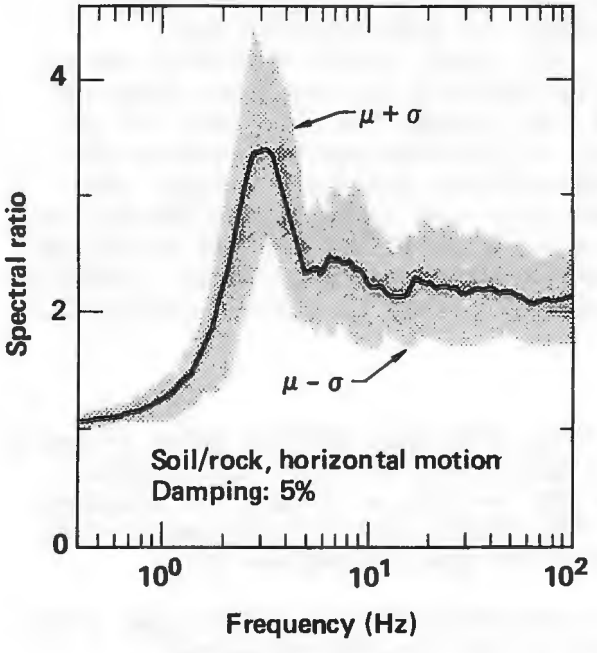

Fig. A-30. Computed soil/rock spectral ratios for horizontal motion at the Zion site. The solid line is the mean of 30 spectral ratios, and the shading marks the variation in the mean (±1 standard deviation).

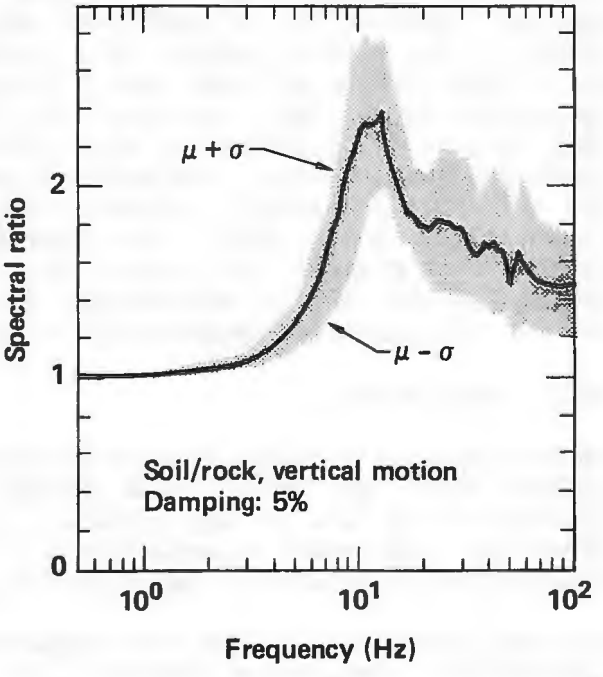

Fig. A-31. Computed soil/rock spectral ratios for vertical motion at the Zion site. The solid line is the mean of 30 spectral ratios, and the shading marks the variation in the mean (±1 standard deviation).

A4.0 SHAKE PROCEDURES APPLIED TO FORGARIA-CORNINO

To assist in validating the modeling procedure, models of the Forgaria-Cornino site were constructed, analyses performed, and the results compared to the recorded motions. Neglecting the topography effect, each horizontal component of recorded motion at S. Rocco was specified as rock outcrop motion and input to the soil model of the Cornino-Forgaria site. Surface motions were calculated by the computer code SHAKE. These calculated motions were compared to the corresponding recorded motions. At this site good agreement was found between calculated motion and recorded motion in the EW components. Figure A-32 shows the comparison of response spectra between the recorded motion and one of the calculated motions. In the NS direction, as shown in Fig. A-33, the analysis gives the correct peak frequency but underpredicts the response amplitudes for most of the frequencies. This may be due to the complicated effect of topography in the NS direction, while shaking in the EW direction is closer to the horizontal layer assumption made in the SHAKE procedure.

Site response calculations must consider the uncertainty contributed by the variation of the depth of the soil model, dynamic soil properties, and the impedance ratio between soil and bedrock. All of these factors could contribute significant uncertainty to calculated responses. Because the soil profile at Cornino was complex, we considered three models, with the bedrock assumed at depths of 49, 90 and 116 ft. The variation of soil properties was performed on the 116-ft model. We considered ±50% of nominal shear modulus and nominal damping ratio as the upper and lower limits. We analyzed five possible combinations of shear modulus and damping ratio in soil properties, including the case of nominal soil properties. We also included two variations of bedrock shear wave velocity. The lower limit of bedrock shear wave velocity was taken as 2020 ft/s (71% of nominal) and the upper limit as 3500 ft/s (122% of nominal). Only nominal soil properties were used for the 49-ft and 90-ft models. The mean, minimum, and maximum resonse spectra for all the cases considered, together with the recorded soil/rock motion, are shown in Fig. A-34. Due to the complicated site condition and the assumptions of the SHAKE program, it is understood that differences between the predicted motion and the recorded motion over the entire frequency range occur. However, the overall predicted responses by SHAKE are comparable to the recorded data.

A5.0 CONCLUSIONS

The analyses of recorded data at several sites show that shallow soils strongly amplify earthquake motions from bedrock to the ground surface. In general, site amplifications are approximately 2 at PGA and 3.5 or greater at dominant frequency. The order of amplification is consistent with results reported by investigators for underground explosion data and some earthquake data.

The amplifications at Zion were computed by equivalent linear techniques from site models in which the uncertainty of soil properties was simulated according to Latin hypercube sampling procedure. The shape and the magnitude of mean site amplification predicted by this technique are similar to those obtained from recorded data at similar sites. The coefficients of variation (COV) of the mean site amplification obtained from the recorded data are much higher than those of the calculated data. The higher COVs could be due to the effect of complicated irregular topography, inclined soil-rock interface and the contribution of the inclined body wave as well as horizontal surface wave propagation.

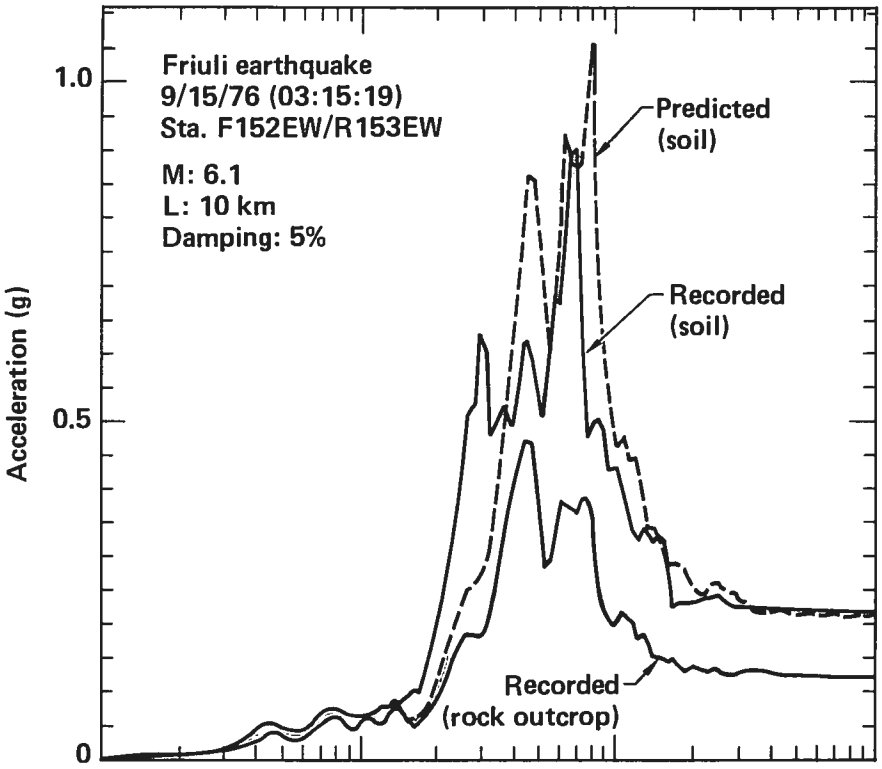

Fig. A-32. Response spectra of predicted motion and recorded motion at the Cornino-Forgaria station from the 9/15/76 Friuli earthquake. EW components.

A first step in the validation of the SHAKE code was taken by comparing the response spectra of the calculated and recorded motions at the Cornino-Forgaria site. In the EW direction, the response spectra of calculated motions are comparable, for engineering design purposes, to those of recorded motion. In the NS direction, the SHAKE code underestimates the response. The underestimation may be due to the effect of topography and to heterogeneity of the soil/rock formation.

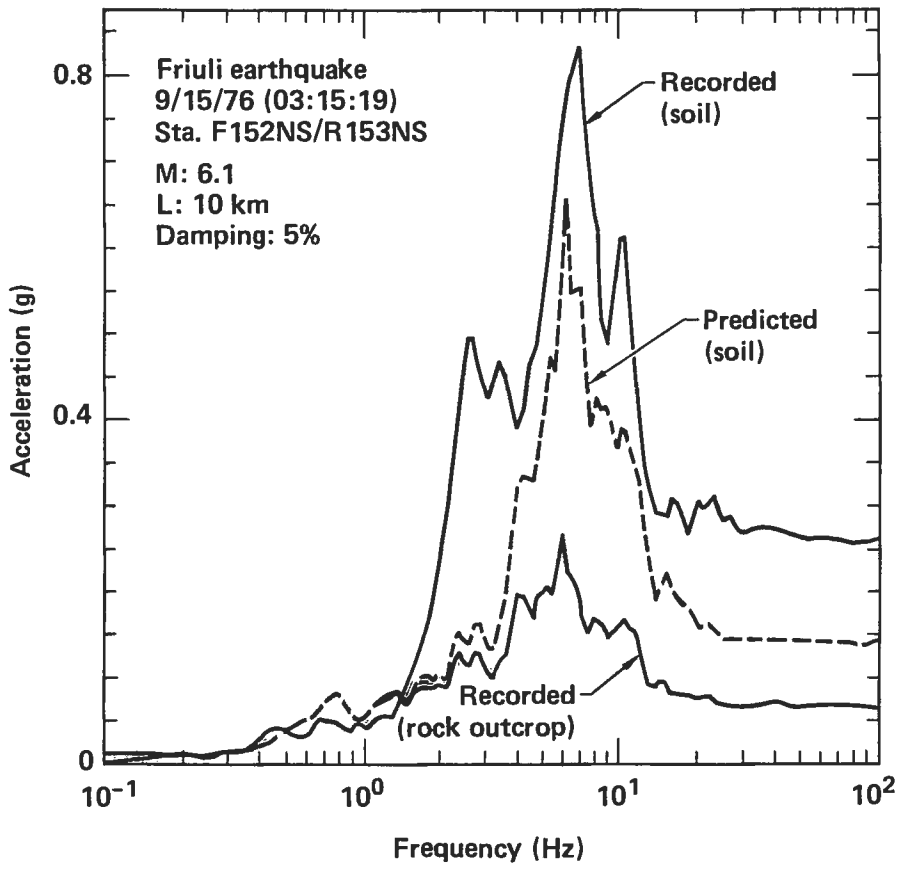

Fig. A-33. Response spectra of predicted motion and recorded motion at the Cornino-Forgaria station from the 9/15/76 Friuli earthquake. NS components.

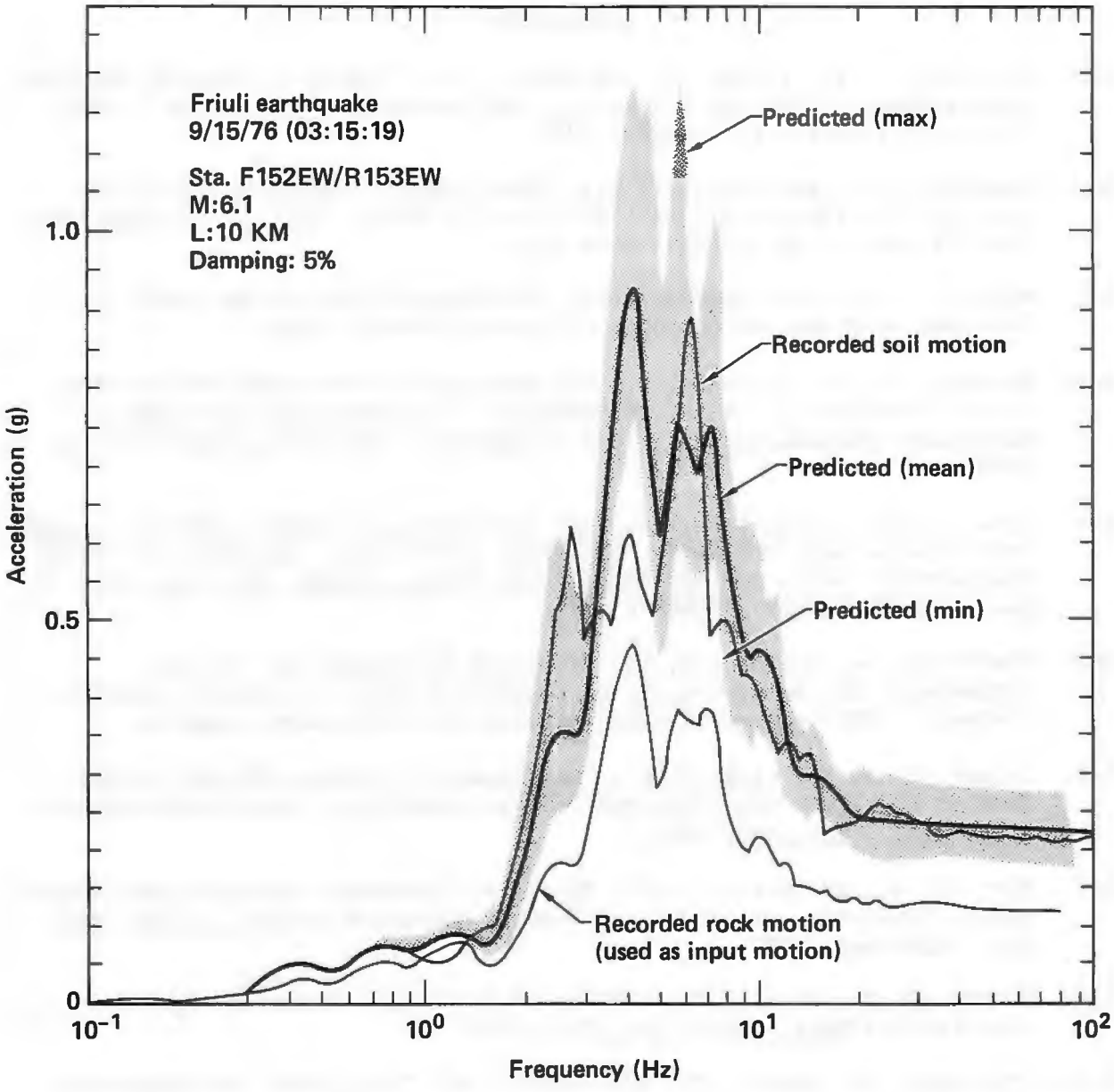

Fig. A-34. Response spectra of predicted motion (including maximum and minimum) and recorded motion at the Cornino-Forgaria station from the 9/15/76 Friuli earthquake. EW components.

REFERENCES

A-1. Schnable, P. D., Lysmer, J. and Seed, H. B., "SHAKE: A Computer Program for Earthquake Response Analysis of Horizontally Layered Sites," EERC 72-12, U.C. Berkeley, December 1972.

A-2. Seekins, L. C. and Hanks, T. C., "Strong-Motion Accelerograms of the Oroville Aftershocks and Peak Acceleration Data," Bull. Seism. Soc. Am., Vol. 68, No. 3, pp 677-689, June 1978.

A-3. Wooten, T., Private Communication, Office of Strong Motion Study, Division of Mines and Geology, California, August 1982.

A-4. Faccioli, E. and Agalbato, D., "Attenuation of Strong-Motion Parameter in the 1976 Friuli, Italy, Earthquakes," U.S. National Conference on Earthquake Engineering, Stanford University, California, August 22-24, 1979.

A-5. Chiaruttini, C. and Siro, L., "The Correlation of Peak Ground Horizontal Acceleration with Magnitude, Distance, and Seismic Intensity for Friuli and Ancona, Italy, and the Alpide Belt," Bull. Seism. Soc. Am., Vol. 71, No. 6, pp 1993-2009, December 1981.

A-6. Fontanive, A. and Gorelli, V., "Indagini Geofisiche Sui Terreni Sottostanti Gli Accelerografi Di Forgaris-S. Rocco E Forgaria-Cornino (Udine)," CNEN Laboratorio Ingegneria Sito RAD/RSI-CSN Casaccia.

A-7. Tucker, B. E. and King, J. L., "Dependence of Sediment-Filled Valley Response on Input Amplitude and Valley Properties," Draft submitted to Bull. Seism. Soc. Am., 1982.

A-8. King, J. L. and Tucker, B. E., "Observed Variations of Earthquake Motion Across a Sediment-Filled Valley," draft submitted to Bull. Seism. Soc. Am., September 1982.

A-9. Tucker, B. E., et al., "Variations of Earthquake Motion on Hard Rock," submitted to Bull. Seism. Soc. Am., 1982.

A-10. Vonmarcke, E., Kausel, E., and Bouchon, M., "Local Soil Amplification Effects at the Yankee Nuclear Plant Site, Rowe, Massachusetts," report prepared under the direction of Weston Geophysical Corp. for Yankee Atomic Electric Company, March 1982.

A-11. Murphy, J. R., Davis, A. H., and Weaver, N. L., "Amplification of Seismic Body Waves by Low-Velocity Surface Layers," Bull. Seism. Soc. Am. Vol. 61, No. 1, February 1971.

A-12. Hays, W. W., "Procedure for Estimating Earthquake Ground Motions," USGS prof. paper 1114, 1980.

A 13. Hays, W. W., Rogers, A. M., and King K. W., "Empirical Data About Local Ground Response," EERI 2nd National Conf. on Earthquake Eng., Stanford, California, proc., p 223-232.

APPENDIX B

DESCRIPTION OF SAFETY AND AUXILIARY SYSTEMS AT THE ZION NUCLEAR POWER PLANT

APPENDIX B
DESCRIPTION OF SAFETY AND AUXILIARY SYSTEMS AT THE ZION NUCLEAR POWER PLANT

This appendix discusses the systems in Zion 1 for which fault trees were generated. This work was based on the Zion Nuclear Power Stations FSAR and detailed drawings and written procedures for the Zion plant. More detailed descriptions were previously discussed (Vol. 8, Phase I report).

B.1 ECCS SYSTEM DESCRIPTION

In reponse to a LOCA, the ECCS is called upon to reflood the core if necessary and keep it covered. Before describing how the ECCS accomplishes this, we provide the success criteria defined for the ECCS in Table B.1. As shown in Table B.1, the ECCS is made up of three pumping systems and the accumulators. Different combinations of these systems can be used in responding to different break sizes. The following components are part of ECCS.

1. Two centrifugal charging pumps (CP)

2. Two high head safety injection pumps (SIP)

Table B.1. Definition of ECCS equipment success requirements for LOCA events at Zion Unit 1.

LOCA size (equivalent diam.)	Injection mode (ECI)	Recirculation mode (ECR)
Large Breaks > 6"	1/2 LPIS[a] + 3/4 ACC	1/2 LPIS
Medium 6" ≥ Breaks > 3"	1/2 CP + 1/2 SIP + 3/4 ACC or 2/2 SIP + 3/4 ACC	1/2 CP + 1/2 SIP or 2/2 SIP or 1/2 LPIS
Small 3" ≥ Breaks > 1.5"	1/2 CP + 1/2 SIP or 2/2 SIP	1/2 CP + 1/2 SIP or 2/2 SIP
Small-small 1.5" ≥ Breaks > 0.5"	1/2 CP + 1/2 SIP or 2/2 SIP or 2/2 CP	1/2 CP + 1/2 SIP or 2/2 SIP or 2/2 CP

[a]The RHR pumps are used for LPIS because there are no separate LPIS pumps.

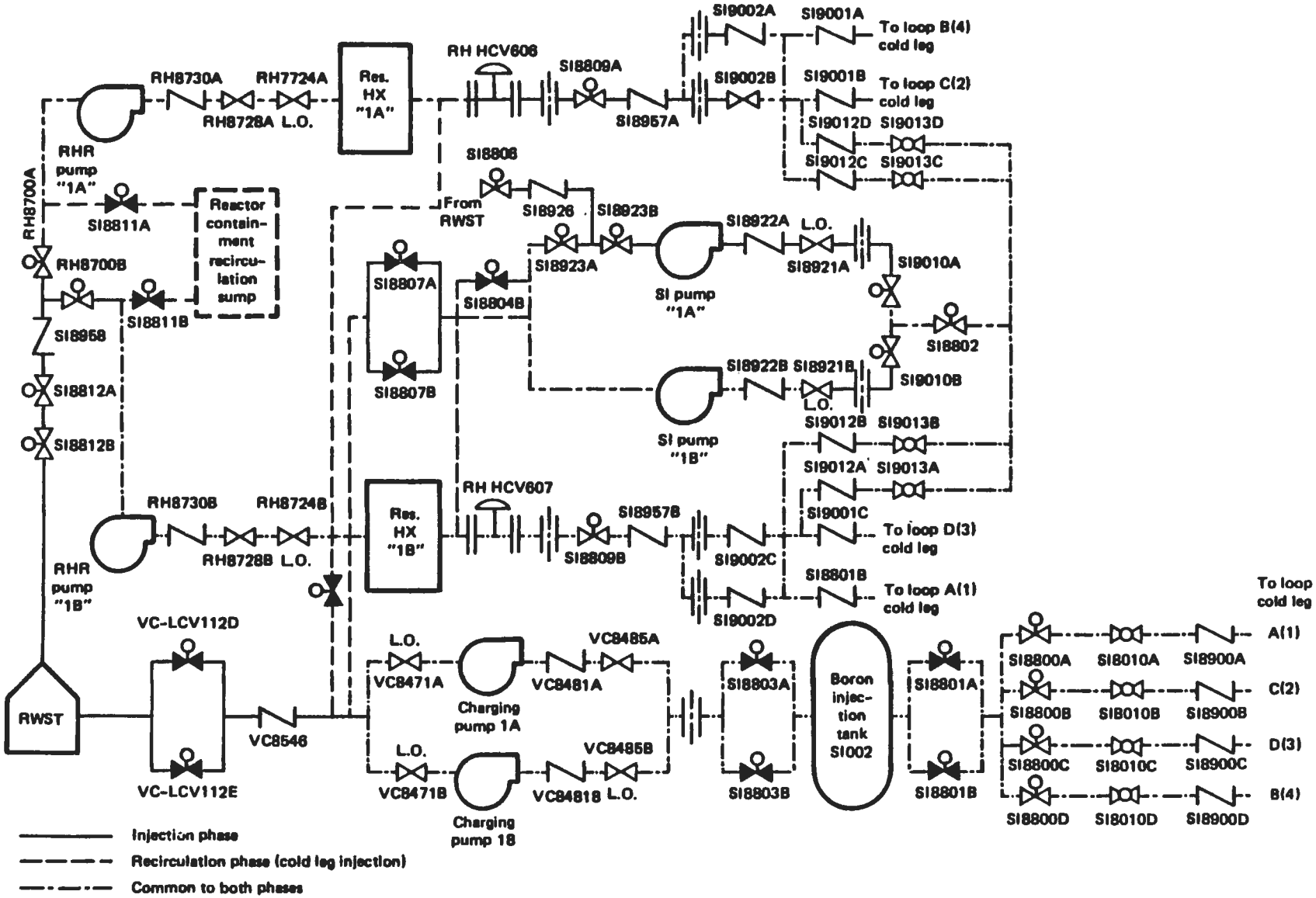

Fig. B-1. Description of ECCS.

3. Two residual heat removal pumps (RHR)

4. Two residual heat exchangers

5. Four accumulator tanks (one on each loop)

6. One boron injection tank (BIT)

7. Refueling water storage tank (RWST)

8. All related valves and piping

All of the systems which make up the ECCS are designed to the seismic Class 1 design code. The accumulator tanks are located inside containment but outside the missile barrier. The refueling-water storage tank is located between the auxiliary and containment buildings. All the pumping systems take suction in the injection phase from this storage tank. All the other system components are located in the auxiliary building. Figure B.1 is a single-line diagram showing the major components of the ECCS.

Accumulators

There are four accumulator tanks, one for each cold leg of the primary coolant system. The accumulator system is the only passive system in the ECCS. In the event of a large or medium LOCA, the borated water in the accumulators is injected into the primary system as soon as the pressure of the primary system drops below that of the accumulators (650 psig normal pressure). The accumulators are maintained at their pressure by compressed nitrogen gas. The only action required to inject the borated water into the primary system cold legs is the mechanical action of opening two swing-disc check valves in series. It should be noted that in a less than medium size break the primary system pressure will not drop below 650 psig as a result of the blow-down.

Centrifugal Charging Pumps

Two high-pressure centrifugal charging pumps are provided. These two pumps serve as part of the Chemical and Volume Control System (CVCS) during normal plant operation. In an accident, these pumps are isolated from the CVCS by a safety injection signal and used to supply high-pressure borated water to the primary system at a rate of 150 gpm each. During the injection phase operation of ECCS, these pumps take water from the refueling water storage tank (RWST) and inject the water into the primary coolant system via the boron injection tank.

The discharge pressure of 2670 psig for these pumps enables them to inject high boron concentrated water into the primary coolant in the event of a transient or small-small LOCA. In the transient event, the boron concentration aids in poisoning the reaction; however, in the small-small LOCA, it not only poisons the reaction, it also maintains the core water inventory. The charging pumps can pump water into the primary system at normal or above-normal operating pressures: this feature differentiates the charging pumps from the safety injection (SI) and residual heat removal (RHR) pumps.

During the recirculation phase of operation, the charging pumps take water from the containment sump via RHR Pump 1A. If this pump fails, but the

crosstie valves between the SI and charging pumps are opened, the charging pumps can take water from RHR Pump 1B.

Safety Injection Pumps

Two high-pressure safety injection pumps are part of the ECCS and provide water for the primary coolant system at the rate of 400 gpm each when the primary system pressure drops below 1520 psig. Above a pressure of 1520 psig, the SI pumps recirculate the water back to the RWST. During the injection phase, the SI pumps take water from the RWST to supply borated water to the four primary coolant cold legs. During recirculation, these pumps take water from the containment sump via RHR Pump 1B. If this pump fails, but the crosstie valves between the SI and charging pumps are opened, the SI pumps can also take water from RHR Pump 1A.

Residual Heat Removal Pumps

Two low pressure RHR pumps deliver large quantities of borated water (3000 gpm for each pump) when the primary system pressure drops below 170 psig. Before the primary system pressure drops below 170 psig, these pumps take water from the RWST during the injection phase and recirculate the water back to the RWST. The operator initiates the recirculation phase of the ECCS operation when the first low level alarm in the RWST has been reached or when the amount of water in the containment sump provided by containment spray pumps and leakage from the break is enough to provide the required Net Positive Suction Head (NPSH) for the RHR pumps. During the recirculation phase, the RHR pumps take water from the containment sump and recirculate the water back to the four cold legs through residual heat exchangers. In another mode of the recirculating phase, after approximately 19 hours into the accident and in order to complete the subcooling of the core, the recirculation water is injected into the hot legs.

B.2 AUXILIARY FEEDWATER SYSTEM DESCRIPTION

We now consider the response of the Auxiliary Feedwater System (AFWS) to a seismically initiated nuclear power plant accident. The event tree analysis discussed previously identified the AFWS as an important system in the event of a small-small LOCA or a transient-initiated accident. Such an accident requires removal of the decay heat from the core by the secondary side of the Nuclear Steam Supply System (NSSS). In order for the secondary side to successfully remove the heat, the steam generators must be adequately cooled by the associated active systems designed for that purpose. Both the AFWS and the Power Conversion System (PCS) can deliver cooling water to the steam generators. In the following pages we describe the analysis of the AFWS in light of the above considerations.

If the PCS is not available, the AFWS is required to provide adequate coolant to the steam generators. The design of the AFWS specifies that one of the three auxiliary feedwater pumps delivers water to two of the four steam generators at or below the pressure of the secondary steam relief safety valve set points. The system is composed of:

- Five secondary steam relief safety valves and one power-operated relief valve for each steam generator, any one of which will sufficiently depressurize the steam generator.

- Two motor-driven pumps requiring power from the 4160 KV emergency AC buses.
- One turbine-driven pump at twice the required rated capacity, requiring steam from either the main steam line A or D.
- Two headers connected by normally locked-closed manual isolation valves, each of which can deliver to all four steam generators through normally open valves.
- Eight normally open, air-operated throttling valves requiring instrument air, but failing open.
- One connection from each of the two headers to each main feedwater line leading to each of the steam generators.
- The preferred source of cooling water is from the secondary condensate storage tank which is not seismically qualified. It is located outside the auxiliary building.
- A secondary source from the service-water system which is automatically or manually activated on low pump suction pressure.
- One supply header for each pump, all interconnected by normally open AC-motor-operated valves.
- Associated check valves on the pump supply headers and the headers to the main feedwater line.
- Normally open manual valves for isolation of each pump for maintenance.
- Miniflow test lines from each pump to the secondary condensate storage tanks.

The equipment listed above is designed to Seismic Class 1 design codes, except for the secondary condensate storage tank and its supply header. The pumps, the discharge header piping up to the containment penetration, the supply header piping from the service-water system interface, and the supply header piping from the secondary condensate storage tank header interface are all located inside the auxiliary building. The main feedwater header, the steam generators, and the interconnecting AFWS piping are located inside the containment. Additionally, the service-water system and condensate system involve piping that is located on or under the turbine building, and also outside of it. Note the service-water system starts at the crib house. See Figure B.2 for a description of the AFWS.

When the auxiliary feedwater system is needed, it must operate to remove decay heat before boil-off of the primary system inventory causes sufficient uncovering of the core to result in an irreversible melting of the fuel rods. This time period is from 1 to 1-1/2 hours [based on calculations referred to in Appendix I, page 61, of the Reactor Safety Study (RSS)]. This includes 1/2 hour until the U-tube steam generators have boiled dry. After this time period, additional stresses are placed on the steam generator when it is

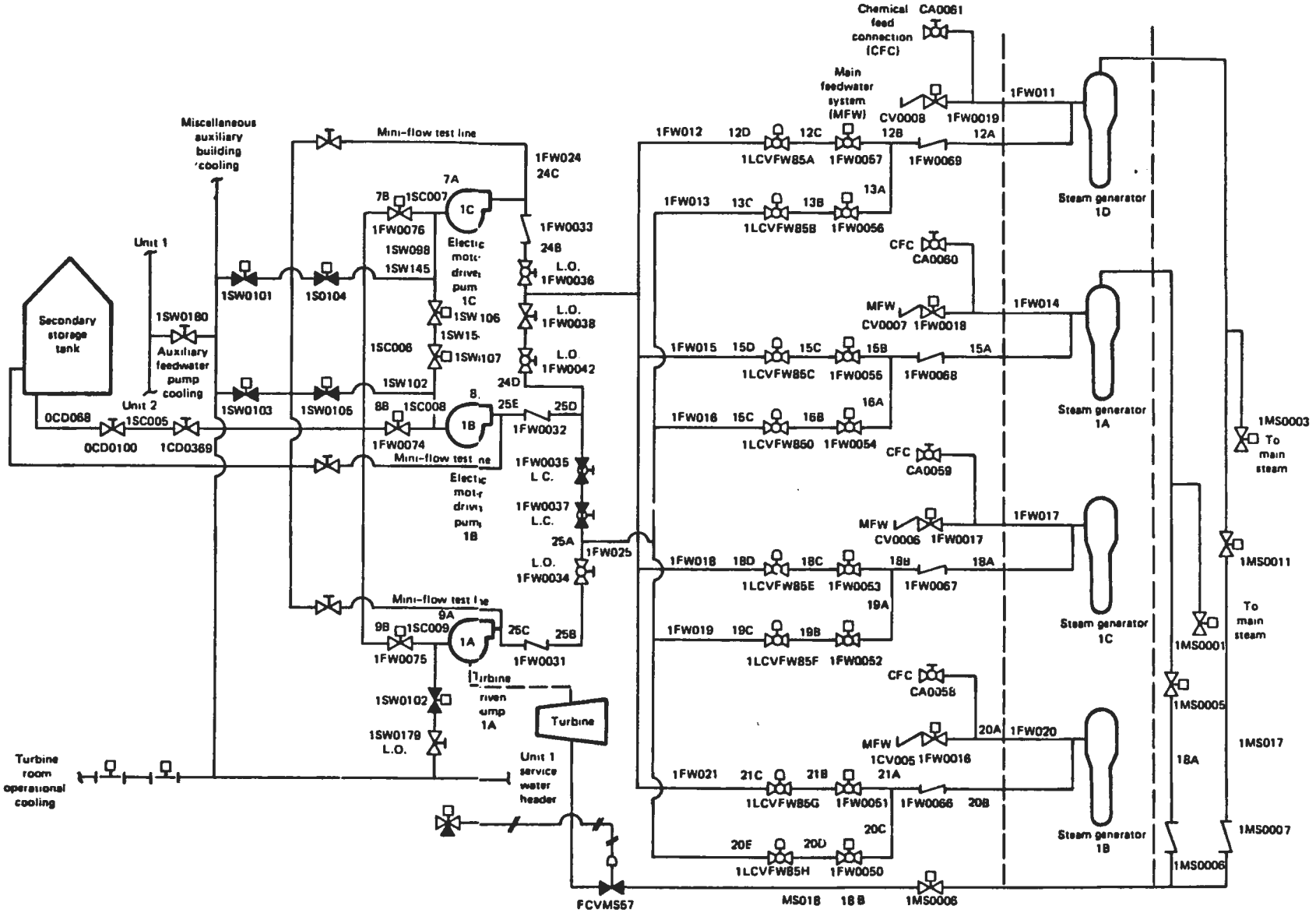

Fig. B-2. Description of AFWS.

refilled; however, this effect has been ignored in terms of causing further structural failures in the secondary system or primary/secondary interface.

Certain transient event initiators could result in simultaneous degradation of the AFWS operability. A main feedwater line rupture between the check valve inside the containment and the connection to the steam generator would disable one steam generator and would require isolation by the operator to avoid AFWS flow out of the rupture. Additionally, a loss of offsite power would mean that diesel power from one of the diesel generators would have to be available to supply electric power to run the AC motor-driven pumps and to provide lubrication for the steam-turbine-driven pump. Finally, a break in main steam lines A and/or D would eliminate or reduce redundancy in the steam supply to the turbine-driven AFWS pump. Steam generator tube ruptures also result in the loss of the associated steam generator for use in the cooldown process because the affected steam generator must be isolated to limit radiation releases out of the secondary steam-relief valves. Steam generator tube ruptures place additional burden on the operators, a factor which is discussed in this section.

When an accident occurs which requires heat transfer from the primary system to the secondary system, the heat transfer must take place until the residual heat removal system can cool the reactor from hot shutdown to cold shutdown. The length of time the heat transfer takes affects the likelihood of the pump's failure to run; the repairability of components; the adequacy of the secondary condensate storage tank cooling inventory; and the failure and repair of interfacing systems, such as the service-water system and the emergency electric power system. The secondary condensate storage tank has an alarm at the 170,000 gallon level (its capacity is 500,000 gallons). This would supply adequate coolant inventory for between 8 to 24 hours, assuming the nonseismic tank and header survived the initiating earthquake.

The AFWS naturally interfaces with the instrumentation and control system. The motor-driven pumps are activated by the following signals:

- Low water level on any steam generator.
- Safety injection control signal.
- Loss of offsite AC electric power.

The steam-turbine-driven pump is activated by either of two signals--low water level on any two steam generators or complete loss of AC electric power (offsite AC plus emergency AC). In addition, the cooling-water supply from the service-water system is activated automatically on low suction pressure to the pumps. Manual activation of the pumps and valves is possible if automatic signals do not initiate operation of the system.

The operators interface with the AFWS system by controlling the flow of coolant to the secondary side. The control is achieved by air-operated throttling valves in each of the two header legs to each steam generator. Backup-control is provided by AC motor-operated valves. The operators must allow enough coolant to the steam generators to avoid boil-off of the primary coolant. However, they must not cool the steam generators too rapidly . Too rapid a cooldown can result in additional structural effects on the primary system.

To determine these effects, the operator depends on the instrumentation associated with the steam generator water level and system flow indicators.

Further, if line breaks occur as a result of the earthquake initiator, the operator must isolate them and align the correct coolant flow path to the steam generators and/or the pumps and/or water supplies. Pump flow indicators and the pump suction line low-pressure annunciator also provide information to the operator.

Finally, a steam generator tube rupture accident, which is similar in most respects to a small-small LOCA, requires operator identification. It differs from the small-small LOCA in that radiation from the primary coolant is leaked into the secondary side and out the secondary steam relief valves. This results in the lighting up of a secondary side radiation-level annunciator. From this instrumentation, as well as the steam generator water level instrumentation, the operator must then isolate the affected steam generator to prevent it from releasing too much radiation into the atmosphere. This process is not trivial: according to the FSAR, it requires turning off the high-pressure injection pumps (charging pumps) within a certain time period. Given the new time limitations on turning off the high-pressure injection pumps resulting from the Three Mile Island accident and the difficulty in identifying the affected steam generator, it is possible that the water level in the steam generator can go high enough to fill the main steam line associated with that steam generator. This would result in a quenching of the steam flow from that steam generator.

In addition, if the steam generator water level instrumentation is lost, the operator is likely to err in the direction of overfilling the steam generator. Again, the result could be quenched steam flow in one or more steam generators. If the quenched steam flow occurs in either main steam line A or D, the redundancy of the steam supply to the steam turbine pump is compromised.

In an analysis concerning randomly initiated events, the operator-instrumentation interface can be ignored because the probability of instrumentation failure is low. However, in an earthquake-initiated event, the simultaneous occurrence of an accident initiator and instrumentation failures cannot be ruled out. In this situation, the operator response would be based on severely limited information and would therefore be less likely to succeed. The likelihood of the operator failing to correctly complete the required action is dependent on the state of the crucial instrumentation. For this reason, whenever operator action is required, the piece or pieces of instrumentation crucial to that action are identified. This identification made possible a better assessment of the instrumentation response to a seismic event.

Finally, the maintenance and test procedures for the AFWS affect the system availability. According to the Zion technical specifications, two of the three auxiliary feedwater pumps can be simultaneously out of service. The resulting degradation of system availability is modeled by the use of a three-component dependency model, which had been developed previously by SAI. In the SAI model, the probability is zero of Pump 1C being in maintenance when Pumps 1A and 1B are in maintenance. The probability of any other combination of maintained pumps being out for maintenance at the same time would be taken from Zion data on limiting conditions for operation (LCOs). This information

could also be obtained from another data source, such as the RSS. The AFWS is tested on a monthly basis.

In this section we have described the design basis and the framework under which the AFWS was examined. An earthquake-initiated event is unique in that it affects every component in the plant simultaneously. For this reason, a thorough analysis is required of every component and every interface of the AFWS. The continuing examination of other important safety systems may bring even more information to light. Therefore, a complete review of this analysis will be made on a continuing basis.

B.3 SERVICE-WATER SYSTEM DESCRIPTION

In this section we consider the response of the service-water system (SWS) and its associated safety-related functions to an earthquake-initiated LOCA or a transient event. During the course of the event-tree analysis, it became clear that since the service-water system interfaced with many of the important systems, it should be classified as a critical system for SSMRP analysis. We therefore include a description of the system and the definition of its design basis. We also discuss the service-water system relationship with possible transient initiators. In addition, we discuss the modeling of the system with respect to normal and emergency operation valving configurations, and also with respect to the requirements of Zion Unit 2 (Zion Unit 1 is the object of the SSMRP analysis).

The function of the service-water system is to provide the cooling water necessary for all plant equipment. The service-water system differs from the other important plant systems in two respects: it is interconnected with Zion Unit 2, and it is required for both normal and emergency operation. The design requirements for both LOCA and transient-initiated events are that one out of three pumps per unit must be operational. (In normal operation, two out of three service water pumps per unit are required.) It has been assumed that the one-out-of-three requirement will satisfy all emergency requirements consistent with the SSMRP systems analysis task only if the system can be brought from the normal configuration to emergency configuration. In addition, the water delivered from the crib house on Lake Michigan by the pump sets of both Unit 1 and Unit 2 must reach the equipment it is designed to service.

The following equipment-cooling functions were analyzed:

- Containment fan cooling system fan motors and heat exchangers.
- Component cooling-water heat exchangers.
- Diesel-generator-cooling heat exchangers.
- Auxiliary feedwater pump cooling.

The following emergency cooling functions were assumed to be less important to the systems analysis task:

- Auxiliary building HVAC.
- Emergency pump room coolers: RHR, SIS, etc.

- Penetration pressurizers for the containment.
- Computer room and control room HVAC.

The following assumptions were made: the HVAC and pump room coolers are not crucial for bringing the plant to hot shutdown, the penetration pressurizers do not have a critical effect on containment leakage paths, and equipment could run without room-cooling under emergency conditions. This may be modeled more accurately if one assumes that the equipment failure rates would be dependent on the temperature in the room.

In addition to its equipment cooling function, the service-water system can serve as a water supply for the auxiliary feedwater system and the fire water system. Figure B.3 provides a description of the service water pumps and supply.

The service-water system is designed to Seismic Category 1, with the exception of the return piping from the safety related equipment. Because the service-water system is required for normal operation, the loss of all or part of the system capabilities could result in a transient accident. This system is vital: the loss of service water required for emergency operations would result in a core melt. Therefore, a transient initiated by a pipe rupture in the common pipe between Unit 1 and Unit 2, and failure to isolate it, would result in the loss of both units. Also, transients caused by the loss of a service water pump could result in a degraded service-water system, and normal operation of this system is required to protect the plant. Because of this importance, the interfaces should be properly accounted for in the list of failures causing a transient with resulting loss of the power conversion system because related equipment is cooled by the operational mode of the service-water system. These types of failures could be important elements in the most likely cut sets of total plant failure, because they are common to both the initiator and the emergency safeguards.

A fault tree model of the service-water system must include consideration of the system's role in Unit 2 emergency requirements and in changing from normal operational status to emergency status. The SWS is a system which provides for both Zion units; however, it is generally considered as two independent systems with crossties, each with the capacity to provide for the emergency requirements of both units simultaneously. Because a correct model must consider the effects of this redundant capacity, it is conceivable that a particular unit's configuration of three service water pumps could provide the pumping flow for both Unit 1 and Unit 2 accident needs. The system also includes a redundant set of electric-motor-operated isolation valves, which can be closed automatically or manually, thereby cutting off the water flow to the parts of the system which provide for normal plant operation. This reduces the pumping requirements from the two out of three per plant required for the normal operation system configuration to the one out of three per plant required for the emergency operation system configuration. The requirement on one individual unit's service water pumps for pumping to the other unit (as a result of that unit's part of the SWS failing to operate in an emergency) would be equivalent to an extra pump load (one of three pumps but for two units). The requirement on that unit's service water pumps, if the isolation valves fail to close off the water flow to normal operational parts of the system, would also be equivalent to an extra pump load (two of three for that unit).

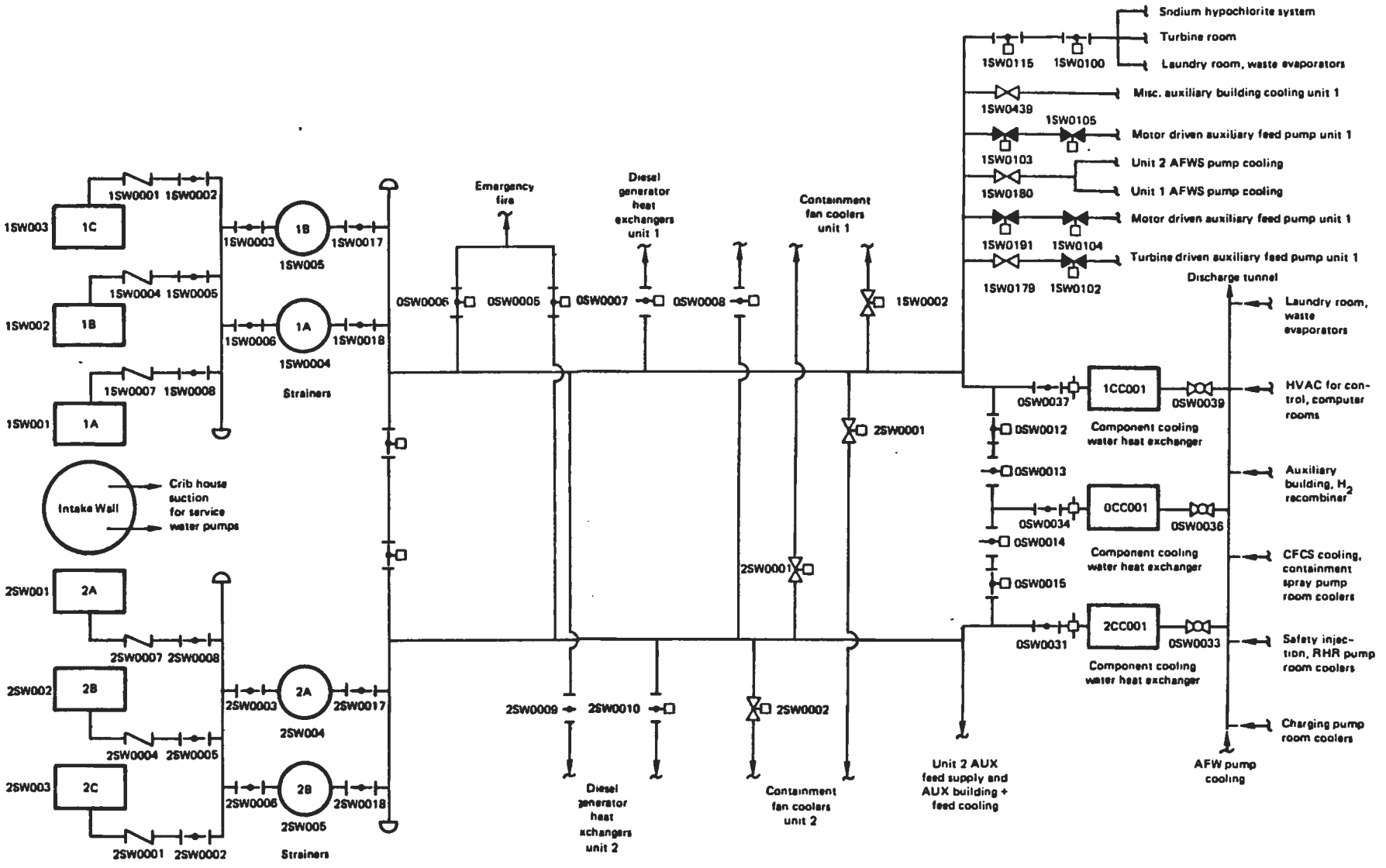

Fig. B-3. Service-water pumps and supply.

- Pump A, B, or C fails to provide flow to the system (failure of a positive flow).

- The other unit requires flow for its cooling requirements (existence of a negative flow).

- One of two isolation valves fails to close and isolate operational equipment (existence of a negative flow).

B.4 ELECTRICAL POWER DESCRIPTION

In this section, we consider the response of electric power to a seismically initiated nuclear power plant accident. The event tree analysis, discussed previously, did not identify electric power (EP) as a specific system on the event trees. However, most systems that would be considered as accident-mitigating systems require electric power.

Unit 1 of the Zion plant has three major electrical divisions--17, 18, and 19. These are illustrated in Figures B.4, B.5 and B.6 respectively. The system design satisfies the single-failure criteria in that any one of the three divisions, including its control power, can be lost and the system will still have enough safety features operating to safely control the plant in any operational mode.

A division consists of a 4160-VAC engineered safety feature bus, a 480-V engineered safety feature bus, a 480-VAC motor-control center, a 120-VAC instrumentation bus, and a 125-VDC control bus. Each division can be fed from a 4160-VAC bus supplied by the system auxiliary transformer. In Unit 1, Divisions 18 and 19 have a diesel generator dedicated to supplying them power in the event of offsite power loss. Division 17 has a swing diesel attached to it. The swing diesel can feed either Division 17 for Unit 1 or the equivalent division for Unit 2--it swings to the division first requiring power.

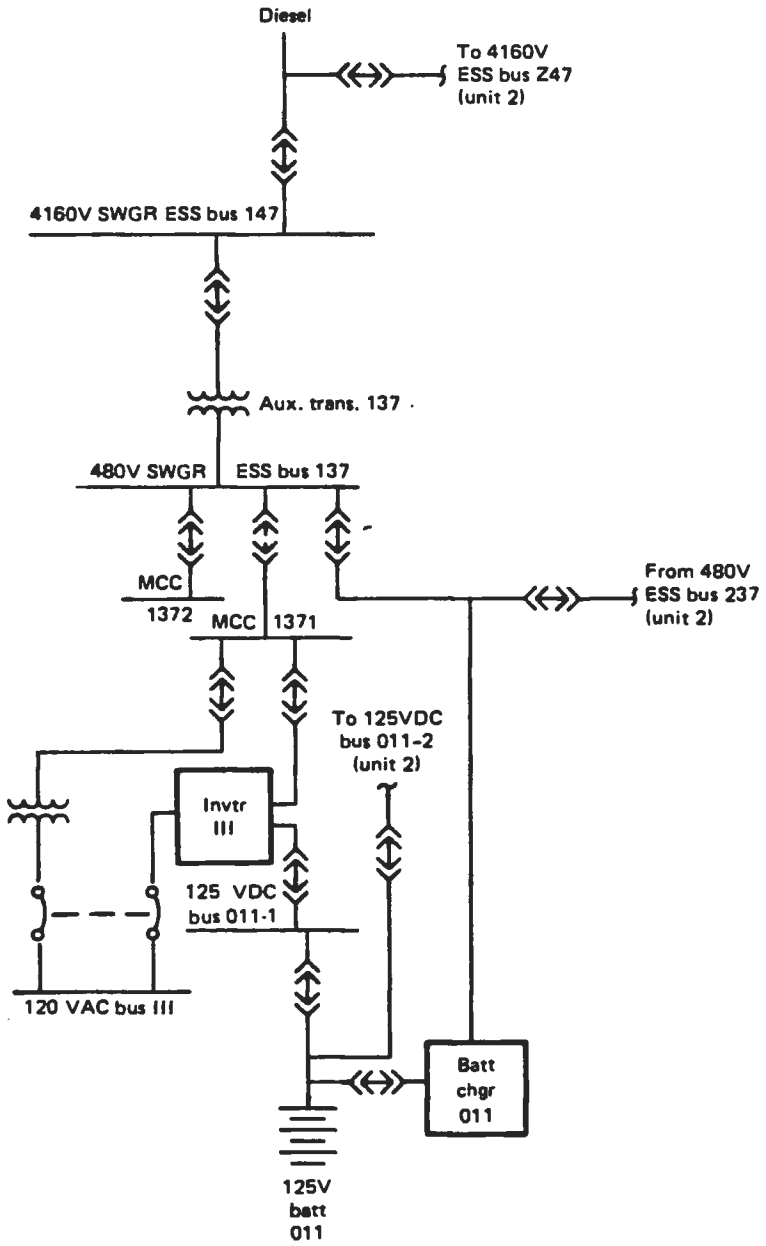

Fig. B-4. Electrical power--Division 17.

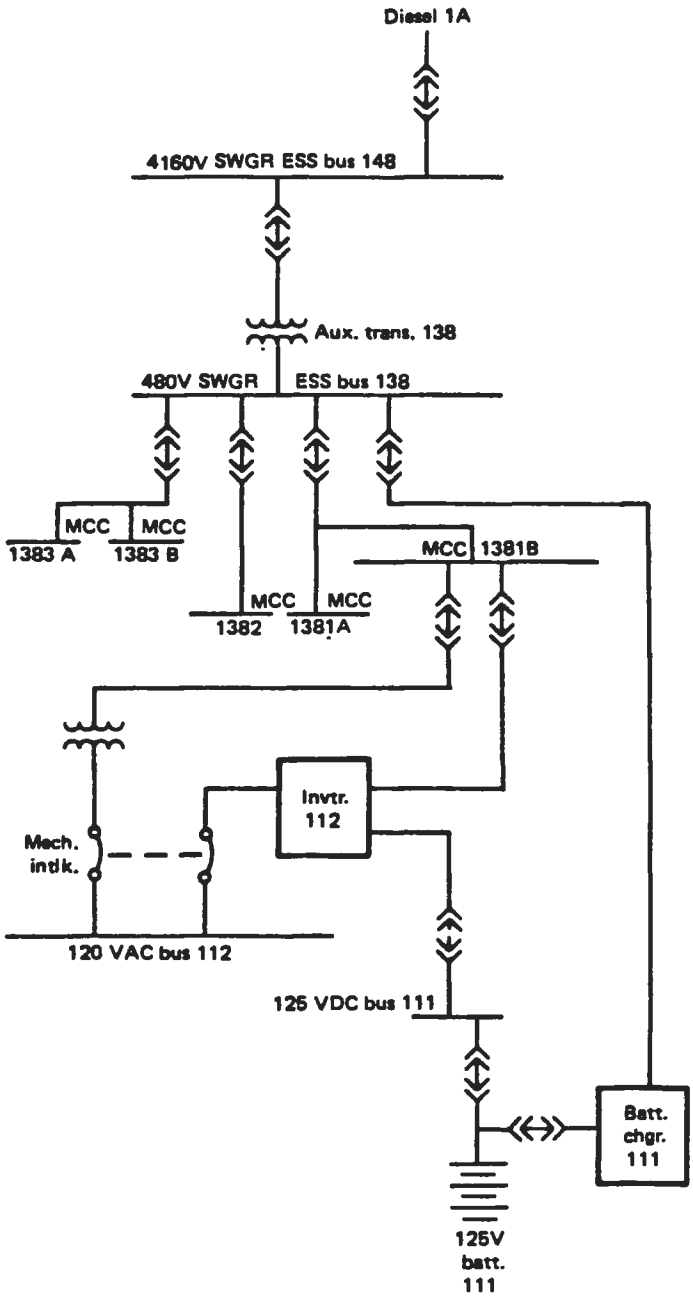

Fig. B-5. Electrical power--Division 18.

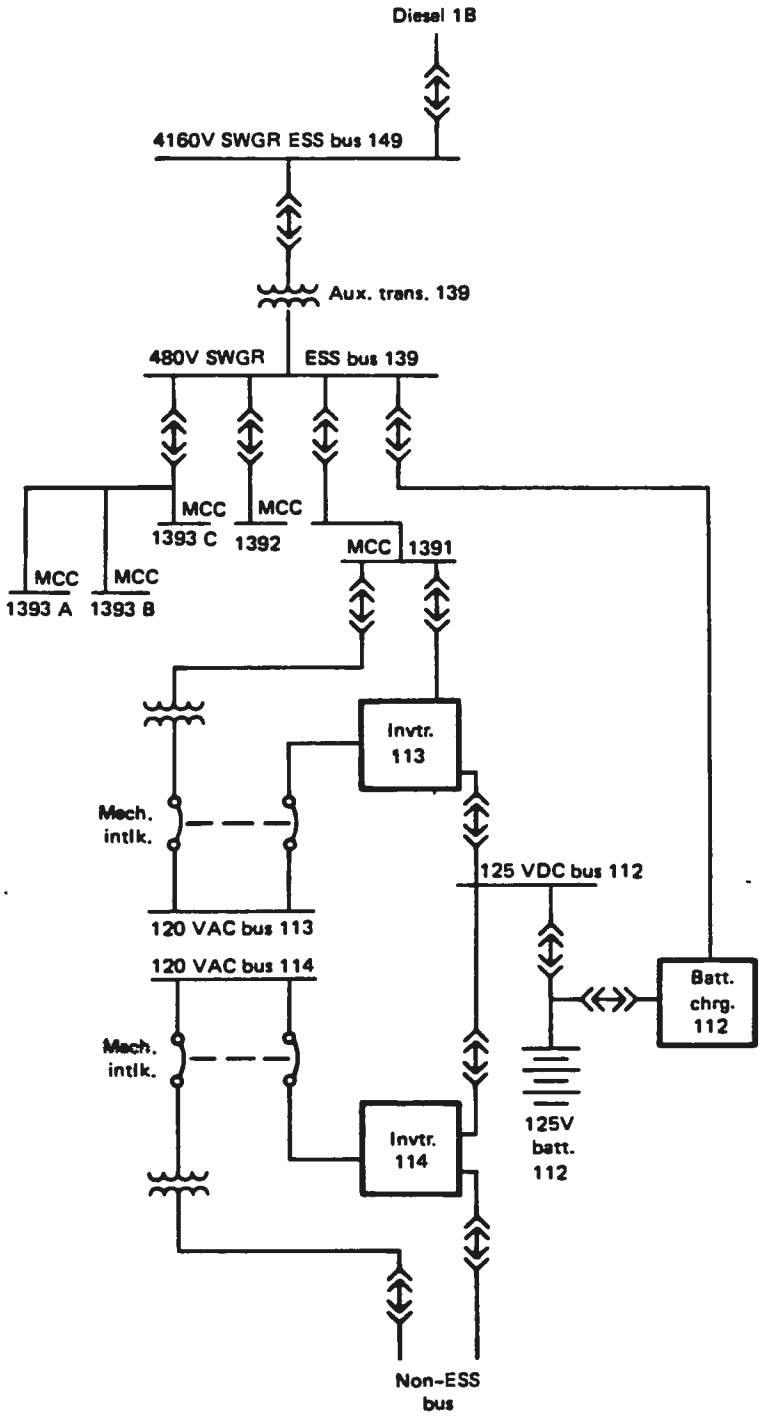

Fig. B-6. Electrical power--Division 19.

APPENDIX C

RELEASE CATEGORY ASSIGNMENTS

APPENDIX C
RELEASE CATEGORY ASSIGNMENTS

C1.0 INTRODUCTION

The tables provided in this appendix list the release categories and associated probabilities for the accident sequences used in our analysis. The accident sequence numbers in the first column of the tables relate to the event trees that are described in Chapter 6. The remaining columns indicate the status of the five containment failure modes used in the SSMRP. In each of these columns a number and a probability in parentheses are listed. The number represents the release category and the probability in parentheses is the probability of that release category occurring for the associated accident sequence. The omission of an entry indicates that the containment failure mode does not apply to that accident sequence.

It is assumed that the sum of all the failure probabilities for each of the containment release categories will be equal to 1.0. In the tables, all of the initiating event categories have been indicated. The tables for the T1 and T2 release category assignments have two parts. The first part, for Earthquake Levels 1, 2, and 3 (as noted in the table heading), assumes that the CSIS and CFCS(I) are functioning properly. The second part, for Earthquake Levels 4, 5, and 6 (again, as noted in the table heading), assume failure of the CSIS and CFCS(I).

Table C.1. RVR release category assignments

Seq. No.	α	β	γ	δ	ε
1	3(.01)				7(.99)
2	3(.01)				7(.99)
3	3(.01)			2(.49)	7(.50)
4	3(.01)			2(.49)	7(.50)
5	3(.06)				7(.94)
6	1(.06)	2(*)	2(.91)	2(.03)	
7	1(.06)	2(*)	2(.91)	2(.03)	

(*) Fraction determined by calculated isolation valve failure. Less than 0.01.

Table C.2. LLOCA release category assignments

Seq. No.	α	β	γ	δ	ε
2	3(.01)	5(*)			7(.99)
4	3(.01)	5(*)			7(.99)
6	1(.01)	2(*)	2(.12)	2(.08)	6(.78)
7	1(.01)			3(.99)	
8	3(.01)	5(*)		7(.49)	7(.50)
9	3(.01)	5(*)			7(.99)
10	3(.01)	5(*)			7(.99)
11	3(.01)	2(*)			6(.99)
12	3(.01)	4(*)		7(.39)	7(.60)
13	3(.01)	5(*)			7(.99)
14	3(.01)	5(*)			7(.99)
15	3(.01)	5(*)			6(.99)
16	3(.01)	4(*)		7(.39)	7(.60)
18	3(.01)	5(*)			7(.99)
20	1(.01)	5(*)	2(.24)	2(.56)	6(.19)
21	1(.01)			3(.99)	
22	3(.01)	5(*)		7(.60)	7(.39)
23	1(.01)	4(*)			7(.99)
24	1(.01)	4(*)	2(.12)	2(.04)	6(.82)
25	1(.01)	4(*)		7(.39)	7(.60)
26	1(.01)	4(*)			7(.99)
27	1(.01)	4(*)	2(.12)	2(.04)	6(.82)
28	1(.01)	4(*)		7(.49)	7(.50)

(*) Fraction determined by calculated isolation valve failure. Less than 0.01.

Table C.3. MLOCA release category assignments

Seq. No.	α	β	γ	δ	ε
2	3(.01)				7(.99)
4	3(.01)				7(.99)
6	1(.01)		2(.12)	2(.08)	6(.73)
7	1(.01)			3(.99)	
8	3(.01)	5(*)		7(.49)	7(.49)
9	3(.01)				7(.99)
10	3(.01)				7(.99)
11	3(.01)				6(.99)
12	3(.01)			3(.39)	7(.60)
13	3(.01)				7(.99)
14	3(.01)				7(.99)
15	3(.01)				6(.99)
16	3(.01)			3(.39)	7(.60)
18	3(.01)				7(.99)
20	1(.01)		2(.24)	2(.56)	6(.19)
21	1(.01)			3(.99)	
22	3(.01)			7(.60)	7(.39)
23	1(.01)			3(.39)	7(.60)
24	1(.01)		2(.12)	2(.04)	6(.83)
25	1(.01)			3(.39)	7(.60)
26	1(.01)			3(.39)	7(.60)
27	1(.01)		3(.12)	2(.04)	6(.83)
28	1(.01)			7(.49)	7(.50)
29	3(.01)				7(.99)
30	3(.01)				7(.99)
31	3(.01)	2(*)			6(.99)
32	3(.01)	4(*)			7(.99)
33	1(.01)				7(.99)
34	1(.01)	2(*)		2(.39)	7(.99)
35	1(.01)	4(*)		3(.39)	7(.99)

(*) Fraction determined by calculated isolation valve failure. Less than 0.01.

Table C.4. SLOCA release category assignments

Seq. No.	α	β	γ	δ	ε
2	3(.01)				7(.99)
4	3(.01)				7(.99)
6	1(.01)		2(.12)	2(.08)	6(.78)
7	1(.01)			3(.99)	
8	3(.01)	5(*)		7(.49)	7(.49)
9	3(.01)				7(.99)
10	3(.01)				7(.99)
11	3(.01)				6(.99)
12	3(.01)			3(.39)	7(.60)
13	3(.01)				7(.99)
14	3(.01)				7(.99)
15	3(.01)				6(.99)
16	3(.01)			3(.39)	7(.60)
18	3(.01)				7(.99)
20	1(.01)		2(.24)	2(.56)	6(.19)
21	1(.01)			3(.99)	
22	3(.01)			7(.60)	7(.39)
23	1(.01)			3(.39)	7(.60)
24	1(.01)		2(.12)	2(.04)	6(.82)
25	1(.01)			3(.39)	7(.60)
26	1(.01)			3(.39)	7(.60)
27	1(.01)		2(.12)	2(.04)	6(.82)
28	1(.01)			7(.49)	7(.49)
29	3(.01)				7(.99)
30	3(.01)				7(.99)
31	3(.01)	2(*)			6(.99)
32	3(.01)	4(*)			7(.99)
33	1(.01)				7(.99)
34	1(.01)	2(*)	3(.39)		6(.60)
35	1(.01)	4(*)			7(.99)

(*) Fraction determined by calculated isolation valve failure. Less than 0.01.

Table C.5. SSLOCA release category assignments.

Seq. No.	α	β	γ	δ	ε
2	3(.01)	5(*)			7(.99)
4	3(.01)	5(*)			7(.99)
6	1(.01)	2(*)	2(.12)	2(.08)	6(.78)
7	1(.01)			3(.99)	
8	3(.01)	5(*)		7(.04)	7(.95)
9	3(.01)	5(*)			7(.99)
10	3(.01)	5(*)			7(.99)
11	3(.01)	2(*)		3(.04)	6(.95)
12	3(.01)	4(*)		3(.39)	7(.60)
13	3(.01)	5(*)			7(.99)
14	3(.01)	5(*)			7(.99)
15	3(.01)	2(*)		3(.04)	6(.95)
16	3(.01)	4(*)		3(.39)	7(.60)
18	3(.01)	5(*)			7(.99)
20	1(.01)	6(*)	2(.24)	2(.56)	36(.19)
21	1(.01)	6(*)	2(.12)	3(.99)	
22	1(.01)			7(.60)	7(.39)
23	1(.01)	2(*)	2(.12)	2(.04)	6(.83)
24	1(.01)	2(*)	2(.12)	2(.04)	6(.83)
25	1(.01)	2(*)	2(.12)	2(.04)	6(.83)
26	1(.01)	2(*)	2(.12)	2(.04)	6(.83)
27	1(.01)	2(*)	2(.12)	2(.04)	6(.83)
28	1(.01)	2(*)	2(.12)	2(.04)	6(.83)
29	3(.01)	5(*)			7(.99)
30	3(.01)	5(*)			7(.99)
31	3(.01)	2(*)		2(.04)	6(.95)
32	3(.01)	4(*)		4(.39)	7(.60)
33	1(.01)	2(*)	2(.12)	2(.04)	6(.83)

(*)Fraction determined by calculated isolation valve failure. Less than 0.01.

Table C.5. SSLOCA release category assignments. (continued)

Seq. No.	α	β	γ	δ	ε
34	1(.01)	2(*)	2(.12)	2(.04)	6(.83)
35	1(.01)	2(*)	2(.12)	2(.04)	7(.83)
36	3(.01)	5(*)	5(.12)	5(.04)	7(.83)
37	3(.01)	5(*)	5(.12)	5(.04)	7(.83)
38	2(.01)	3(*)		3(.04)	6(.95)
39	3(.01)	4(*)			7(.99)
40	1(.01)	2(*)		2(.04)	6(.95)
41	1(.01)	2(*)		2(.04)	6(.95)
42	1(.01)	2(*)		2(.04)	6(.95)

(*)Fraction determined by calculated isolation valve failure. Less than 0.01.

Table C.6. T1 release category assignments for earthquake levels 1, 2, 3.

Seq. No.	α	β	γ	δ	ε
7	3(.01)	5(*)			7(.99)
8	3(.01)	5(*)			7(.99)
9	3(.01)	5(*)			7(.99)
10	3(.01)	5(*)			7(.99)
14	3(.01)	5(*)			7(.99)
15	3(.01)	5(*)			7(.99)
16	3(.01)	5(*)			7(.99)
20	3(.01)	5(*)			7(.99)
21	3(.01)	5(*)			7(.99)
22	3(.01)	5(*)			7(.99)
23	3(.01)	5(*)			7(.99)
24	3(.01)	5(*)			7(.99)

(*) Fraction determined by calculated isolation valve failure. Less than 0.01.

T1 release category assignments for earthquake levels 4, 5, 6.

Seq. No.	α	β	γ	δ	ε
7	1(.01)		2(.24)	2(.56)	6(.19)
8	1(.01)		2(.24)	2(.56)	6(.19)
9	1(.01)		2(.24)	2(.56)	6(.19)
10	1(.01)		2(.24)	2(.56)	6(.19)
14	1(.01)		2(.24)	2(.56)	6(.19)
15	1(.01)		2(.24)	2(.56)	6(.19)
16	1(.01)		2(.24)	2(.56)	6(.19)
20	1(.01)		2(.24)	2(.56)	6(.19)
21	1(.01)		2(.24)	2(.56)	6(.19)
22	1(.01)		2(.24)	2(.56)	6(.19)
23	1(.01)		2(.24)	2(.56)	6(.19)
24	1(.01)		2(.24)	2(.56)	6(.19)

Table C.7. T2 release category assignments for earthquake levels 1, 2, 3

Seq. No.	α	β	γ	δ	ε
4	3(.01)	5(*)			7(.99)
5	3(.01)	5(*)			7(.99)
6	3(.01)	5(*)			7(.99)
7	3(.01)	5(*)			7(.99)
11	3(.01)	5(*)			7(.99)
12	3(.01)	5(*)			7(.99)
13	3(.01)	5(*)			7(.99)
14	3(.01)	5(*)			7(.99)
15	3(.01)	5(*)			7(.99)

(*) Fraction determined by calculated isolation valve failure. Less than 0.01.

T2 release category assignments for earthquake levels 4, 5, 6.

Seq. No.	α	β	γ	δ	ε
4	1(.01)		2(.24)	2(.56)	6(.19)
5	1(.01)		2(.24)	2(.56)	6(.19)
6	1(.01)		2(.24)	2(.56)	6(.19)
7	1(.01)		2(.24)	2(.56)	6(.19)
11	1(.01)		2(.24)	2(.56)	6(.19)
12	1(.01)		2(.24)	2(.56)	6(.19)
13	1(.01)		2(.24)	2(.56)	6(.19)
14	1(.01)		2(.24)	2(.56)	6(.19)
15	1(.01)		2(.24)	2(.56)	6(.19)

APPENDIX D

REGRESSION MODELING OF RESPONSE PARAMETERS

APPENDIX D
REGRESSION MODELING OF RESPONSE PARAMETERS

D1.0 INTRODUCTION

The uncertainty study of the SSMRP Zion risk analysis was designed to assess the risk for 14 sets of values of the input parameters (i.e., hazard curve, fragility medians, response medians). To assess the risk at one of the 14 design points requires a complete run of the SSMRP Zion risk analysis. Each such run involved response calculations for 20 time histories using SMACS at 6 acceleration levels. Because of the time and cost to do all these SMACS runs, an alternative approach to estimating the means and variance-covariances of the responses at all acceleration levels was considered. This approach, an outline of which is the topic of this section, involved regression modeling of the response parameters.

A review of the results of the response calculations in which the only source of variation was random variation suggested that the response means and variance-covariances could be modeled by a polynomial function of acceleration level. Based on this observation, the following procedure was developed to estimate the response parameters at 6 acceleration levels:

1. Use the results of the response calculations including only random variation to estimate the coefficients of a polynomial model for each parameter.
2. Run SMACS to compute the responses at 2 or 3 acceleration levels for each of the 14 design points in the uncertainty study.
3. Use the results of these runs to adjust the polynomial model for the effects of the changes in input parameters.
4. Use the resulting polynomial equation to estimate the response parameters for all acceleration levles.

The details of this procedure are outlined in the following sections.

D2.0 MODELING AND ESTIMATION PROCEDURE

The modeling and estimation procedure is graphically summarized in Figure D.1.

D2.1 POLYNOMIAL MODELS FOR THE RESPONSE PARAMETERS

Since there are 333 responses calculated for the Zion risk analysis, there are 333 means, 333 standard deviations and (333 x 332)/2 correlation coefficients (or covariances) to be modeled. A review of the responses based on SMACS runs in which the only source of variation was random variation indicated that

- the means could be adequately modeled by a quadratic polynomial function of acceleration level.
- some standard deviations fit a linear model while others show a definit quadratic trend.
- the correlations were either constant over the acceleration levels or followed a linear model.

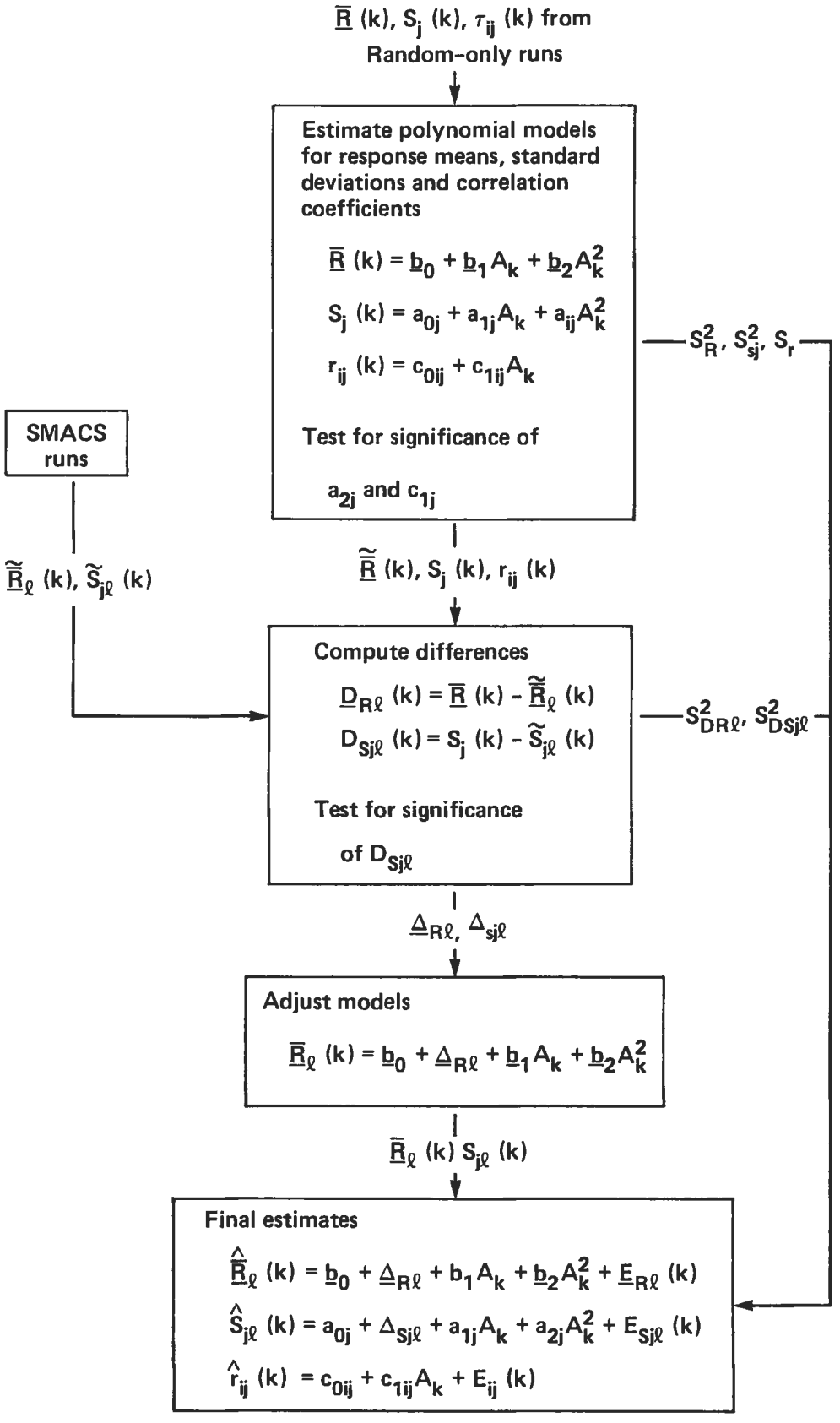

Figure D.1. Flow diagram of response parameter modeling procedure.

Using these models and the data in which only random variation was included in the respone calculations, estimates of the coefficients for the respective models were assessed. For the standard deviations, tests of significance of the quadratic and linear terms were made. Thus, models of the forms

- Vector of Means, $\underline{\bar{R}}$: $\underline{\bar{R}}(k) = \underline{b}_0 + \underline{b}_1 A_K + \underline{b}_2 A_K^2$ (D.1)

- jth Standard Deviaition S_j: $S_j(k) = a_{0j} + a_{1j} A_k + a_{2j} A_k^2$ (D.2)

  or

  $$S_j(k) = a_{0j} + a_{1j} A_k$$

- (i,j)th Correlation Coefficient, r_{ij}: $r_{ij}(k) = C_{0ij} + C_{1ij} A_k$ (D.3)

  or $r_{ij}(k) = C_{0ij}$

were developed for each of the response parameters.

D2.2 MODEL ADJUSTMENT DUE TO ANALYSIS UNCERTAINTIES

The models for the response parameters given in Eqs. (D.1) - (D.3) were based on the responses calculated when only random variation was associated with the inputs into SMACS. The uncertainty study was designed to describe the variation in the proability of core melt (release) due to uncertainties associated with the analysis methodology. The uncertainty study involved assessing the Zion risk when the input parameters (e.g., medians of the inputs into the response calculations) were varied. When the medians of the input parameters, e.g., soil shear modulus and damping, are changed it is likely that the responses would change also. Thus the response means, standard deviations and correlation coefficients would also change. This was introduced into the model by including a term which attempts to describe the expected change in response as the input parameters are varied, i.e., allows for the change due to analysis uncertainty. In terms of the model for the response means, Eq. (D.1), the adjusted model is

$$\underline{\tilde{\bar{R}}}_L(k) = \underline{b}_0 + \underline{\Delta}_{RL} + \underline{b}_1 A_k + \underline{b}_2 A_k^2 \quad (D.4)$$

where Δ_{RL} is the expected change in response mean when the medians of the input parameters are changed from the nominal value to the value for the L^{th} design point.

To estimate this change, response calculations were run at K = 2 or 3 acceleration levels for each of 14 design points. Based on these runs, the response means, $\underline{\tilde{\bar{R}}}_L(k)$ and standard deviations, $\tilde{S}_{jL}(k)$ for k = 1, .. , K were

evaluated. The differences between the calculated values and the estimated values based on Equations (D.1) and (D.4) were assessed, i.e.,

- Difference in Means

$$\underline{D}_{RL}(k) = \underline{\bar{R}}(k) - \underline{\tilde{\bar{R}}}_{L}(k) \qquad k=1,\ldots, K = 2 \text{ or } 3 \qquad (D.5)$$

- Difference in jth Standard Deviation

$$D_{sjL}(k) = S_{j}(k) - \tilde{S}_{jL}(k) \qquad k=1,\ldots, K \qquad (D.6)$$

For the means, the expected change, Δ_{RL} was estimated by the average difference at the K acceleration levels for which SMACS runs were made, i.e.

$$\underline{\Delta}_{RL} = \frac{1}{K} \sum_{k=1}^{K} \underline{D}_{RL}(k) \qquad (D.7)$$

For the standard deviations, the following procedure was followed:

- The difference of the jth calculated variance for the Lth design point and the jth estimated variance based on Eq. (D.2) was

$$D^2_{SjL}(k) = | S^2_j(k) - \tilde{S}^2_{jL}(k) | \qquad (D.8)$$

- an F-statistic was evaluated, i.e.,

$$F_{jL} = \frac{\sum_{k=1}^{K} D^2_{sjL}(k) / (K-1)}{S^2_{sj}} \qquad (D.9)$$

where S^2_{Sj} is the variance associated with modeling the standard deviations using Eq. (D.2).

If $F_{jL} \leq 7.0$, no adjustment in the regression equation was made.

If $F_{jL} > 7.0$, an adjustment Δ_{Sjl} was made in Eq. (D.2), where,

$$\Delta_{SjL} = \frac{1}{K} \sum_{k=1}^{K} D_{SjL}(k) \qquad (D.10)$$

Although it was felt that changing the medians of the input parameters would affect the response means, the same was not necessarily true for the standard deviations. Thus, an F-test, as described above, was made to determine if a significant change did occur. If so, adjustments would be necessary for the correlation coefficients. That is, changes in the medians of the input parameters were assumed not to affect correlations between the responses.

D2.3 UNCERTAINTIES

The procedure so far produces response means, standard deviations and correlation coefficients which satisfy the polynomial equations given in Eqs (D.4), (D.2) with possibly the adjustment in (D.10), and (D.3) respectively. The actual response parameters would not satisfy such a smooth relationship but would vary about that trend line. With this in mind, two sources of variations were identified and introduced into the interpolation procedure. These sources of variation are:

1. The variation of the responses, from the runs which included only random variation, which were used to estimate the initial polynomial models, Eqs. (D.1) and (D.2), denoted $\underline{S}_R$ and S_{Sj} for the means and standard deviations respectively.
2. The uncertainty in the estimated adjustments $\underline{\Delta}_R$ or $\underline{\Delta}_{Sj}$ due to the effect of analysis uncertainty. An estimate of this uncertainty is given by the variation in the differences $\underline{D}_R(k)$ and $D_{Sj}(k)$ observed at the acceleration levels at which SMACS runs were made. The estimated standard deviations were

   - Means:

$$S_{DRL} = \left[\frac{1}{K-1} \sum_{k=1}^{K} \left(\underline{D}_{RL}(k) - \Delta_{RL} \right)^2 \right]^{1/2}$$

   - Standard Deviations:

$$S_{DSjL} = \left[\frac{1}{K-1} \sum_{k=1}^{K} \left(D_{SjL}(k) - \Delta_{SjL} \right)^2 \right]^{1/2}$$

Since no adjustments were made on the correlation coefficients, only the former source of variation was included. The estimate of the variation in the correlations is given by

$$S_r = \left[\frac{1}{T} \sum_{k=1}^{K} \sum_{i=1}^{333} \sum_{\substack{j=1 \\ j<i}}^{332} \left(r^*_{ij}(k) - r_{ij}(k) \right)^2 \right]^{1/2}$$

where $r^*_{ij}(k)$ is the observed $(ij)^{th}$ correlation and $r_{ij}(k)$ is the predicted correlation based on Eq. (D.3) and $T = \frac{K \times 333 \times 332}{2} - 1$.

To introduce variation in the response parameters due to the indentified sources of variation, random samples were drawn from a normal distribution with the appropriate standard deviation. Thus, the final estimate of the response parameters at the unobserved acceleration levels were:

- Means:

$$\underline{\bar{R}}_L(k) = \underline{b}_0 + \Delta_{RL} + \underline{b}_L A_k + \underline{b}_2 A_k^2 + \underline{E}_{RL}(k) \qquad k=1,\ldots,6 \quad L=1,\ldots,14$$

$$\underline{E} \sim N\left(0, [S_R^2 + \underline{S}_{DR}^2]^{1/2}\right)$$

- Standard Deviations:

$$S_{jL}(k) = a_{0j} + \Delta_{SjL} + a_{1j}A_k + a_{2j}A_k^2 + E_{SjL}(k) \qquad k=1,\ldots,6 \quad L=1,\ldots,14$$

$$\underline{E} \sim N\left(0, [S_S^2 + S_{DS}^2]^{1/2}\right)$$

where Δ_{sjl} and $a_{2j}A_k^2$ may be eliminated, depending on the results of tests performed.

- Correlation Coefficients:

$$\hat{r}_{ij}(k) = C_{0ij} + C_{lij}A_k + E_{ij}(k) \qquad k=1,\ldots,6$$

or

$$= C_{0ij} + E_{ij}(k)$$

$$E \sim N(0, S_r)$$

APPENDIX E

GLOSSARY OF ACRONYMS

ACC	Accumulator(s)
AFW, AFWS	Auxiliary feedwater (system)
BOC	Bottom of core
CDF	Cumulative distribution function
CFC, CFCS	Containment fan cooler (system)
CFCS(I)	I = injection phase
CFCS(R)	R = recirculation phase
CHG	Charging pumps (system)
CL	(See listing following CR-VSE)
CP	Charging pump
CR	Containment rupture
CR-B	B = (hydrogen) burning
CR-MT	MT = melt-through
CR-OP	OP = overpressure
CR-VSE	VSE = vessel steam explosion
CL	Containment leakage
	L = leakage
CSS	Containment spray system
CSIS	Containment spray injection system
CSRS	Containment spray recirculation system
CVCS	Chemical and volume control system
ECC, ECCS	Emergency core cooling (system)
ECF	Emergency core functionability
ECI	Emergency coolant injection
ECR	Emergency coolant recirculation
EP, EPS	Electric power (system)
ESF	Engineered safety features(s)
ET	Event tree
FSAR	Final safety analysis report
HPIS	High pressure injection system
IE	Initiating event
LOCA	Loss-of-coolant accident
LLOCA	Large loss-of-coolant accident
MLOCA	Medium loss-of-coolant accident
SLOCA	Small loss-of-coolant accident
SSLOCA	Small-small loss-of-coolant accident
LPIS	Low pressure injection system
MSIV	Main steam isolation valve
MWe	Megawatt electrical
NPSH	Net positive suction head

PAHR	Post-accident heat removal
PARR	Post-accident radioactivity removal
PCS	Power conversion system
PDF	Probability density function
PWR	Pressurized water reactor
RCL	Reactor coolant loop
RCS	Reactor coolant system
RHR, RHRS	Residual heat removal (system)
RPS	Reactor protection system
RSS	Reactor safety study (WASH-1400)
RVR	Reactor vessel rupture
RWST	Refueling water storage tank
SAR	Safety analysis report
SEISIM	Seismic Evaluation of Important Safety Improvement Measures
SHA, SHAS	Sodium hydroxide addition (system)
SI, SIP, SIS	Safety injection [pums(s)] (system)
SSMRP	Seismic Safety Margins Research Program
SSR	Secondary steam relief
S/RV	Safety/reliev valve
S/RV-O	O = failure to open
S/RV-R	R = failure to reclose
SW	Service water (system)
TOC	Top of core

APPENDIX F

NUMBER, LOCATION, DIRECTION, AND TYPE OF RESPONSES REFERRED TO IN FIGS. 4.21 AND 4.22

FREE FIELD RESPONSES

RESPONSE NUMBER	DIRECTION	ACCELERATION TYPE
1	X	PEAK
2	X	SPEC 4 HZ
3	X	SPEC 8 HZ
4	X	SPEC 16 HZ
5	Y	PEAK
6	Y	SPEC 4 HZ
7	Y	SPEC 8 HZ
8	Y	SPEC 16 HZ
9	Z	PEAK
10	Z	SPEC 4 HZ
11	Z	SPEC 8 HZ
12	Z	SPEC 16 HZ

CONTAINMENT BASEMAT RESPONSES

RESPONSE NUMBER	DIRECTION	ACCELERATION TYPE
33	X	PEAK
34	X	SPEC 4 HZ
35	X	SPEC 8 HZ
36	X	SPEC 16 HZ
37	Y	PEAK
38	Y	SPEC 4 HZ
39	Y	SPEC 8 HZ
40	Y	SPEC 16 HZ
41	Z	PEAK
42	Z	SPEC 4 HZ
43	Z	SPEC 8 HZ
44	Z	SPEC 16 HZ

STRUCTURAL ACCELERATION RESPONSES

RESPONSE NUMBER	STRUCTURE	NODE	DIRECTION	ACCELERATION TYPE
65	STRUCT. 1	20	X	PEAK
66	STRUCT. 2	936	X	PEAK
67	STRUCT. 2	936	X	SPEC 4 HZ
68	STRUCT. 2	936	X	SPEC 8 HZ
69	STRUCT. 2	936	X	SPEC 16 HZ
70	STRUCT. 2	1412	X	SPEC 4 HZ
71	STRUCT. 2	1418	X	SPEC 4 HZ
72	STRUCT. 2	1462	X	PEAK
73	STRUCT. 2	1462	X	SPEC 4 HZ
74	STRUCT. 2	1462	X	SPEC 8 HZ
75	STRUCT. 2	1462	X	SPEC 16 HZ
76	STRUCT. 3	21	X	PEAK
77	STRUCT. 3	21	X	SPEC 4 HZ
78	STRUCT. 3	21	X	SPEC 8 HZ
79	STRUCT. 3	21	X	SPEC 16 HZ
80	STRUCT. 3	530	X	PEAK
81	STRUCT. 3	530	X	SPEC 4 HZ
82	STRUCT. 3	530	X	SPEC 8 HZ

83	STRUCT. 3	530	X	SPEC 16 HZ
84	STRUCT. 3	1543	X	PEAK
85	STRUCT. 3	1543	X	SPEC 4 HZ
86	STRUCT. 3	1543	X	SPEC 8 HZ
87	STRUCT. 3	1543	X	SPEC 16 HZ
88	STRUCT. 3	2012	X	PEAK
89	STRUCT. 3	2012	X	SPEC 4 HZ
90	STRUCT. 3	2012	X	SPEC 8 HZ
91	STRUCT. 3	2012	X	SPEC 16 HZ
92	STRUCT. 3	3005	X	PEAK
93	STRUCT. 3	3005	X	SPEC 4 HZ
94	STRUCT. 3	3005	X	SPEC 8 HZ
95	STRUCT. 3	3005	X	SPEC 16 HZ
96	STRUCT. 1	20	Y	PEAK
97	STRUCT. 2	936	Y	PEAK
98	STRUCT. 2	936	Y	SPEC 4 HZ
99	STRUCT. 2	936	Y	SPEC 8 HZ
100	STRUCT. 2	936	Y	SPEC 16 HZ
101	STRUCT. 2	1412	Y	SPEC 4 HZ
102	STRUCT. 2	1418	Y	SPEC 4 HZ
103	STRUCT. 2	1462	Y	PEAK
104	STRUCT. 2	1462	Y	SPEC 4 HZ
105	STRUCT. 2	1462	Y	SPEC 8 HZ
106	STRUCT. 2	1462	Y	SPEC 16 HZ
107	STRUCT. 3	13	Y	PEAK
108	STRUCT. 3	13	Y	SPEC 4 HZ
109	STRUCT. 3	13	Y	SPEC 8 HZ
110	STRUCT. 3	13	Y	SPEC 16 HZ
111	STRUCT. 3	505	Y	PEAK
112	STRUCT. 3	505	Y	SPEC 4 HZ
113	STRUCT. 3	505	Y	SPEC 8 HZ
114	STRUCT. 3	505	Y	SPEC 16 HZ
115	STRUCT. 3	544	Y	PEAK
116	STRUCT. 3	544	Y	SPEC 4 HZ
117	STRUCT. 3	544	Y	SPEC 8 HZ
118	STRUCT. 3	544	Y	SPEC 16 HZ
119	STRUCT. 3	1511	Y	PEAK
120	STRUCT. 3	1511	Y	SPEC 4 HZ
121	STRUCT. 3	1511	Y	SPEC 8 HZ
122	STRUCT. 3	1511	Y	SPEC 16 HZ
123	STRUCT. 3	1530	Y	PEAK
124	STRUCT. 3	1530	Y	SPEC 4 HZ
125	STRUCT. 3	1530	Y	SPEC 8 HZ
126	STRUCT. 3	1530	Y	SPEC 16 HZ
127	STRUCT. 3	1537	Y	PEAK
128	STRUCT. 3	1537	Y	SPEC 4 HZ
129	STRUCT. 3	1537	Y	SPEC 8 HZ
130	STRUCT. 3	1537	Y	SPEC 16 HZ
131	STRUCT. 3	1562	Y	PEAK
132	STRUCT. 3	1562	Y	SPEC 4 HZ
133	STRUCT. 3	1562	Y	SPEC 8 HZ
134	STRUCT. 3	1562	Y	SPEC 16 HZ
135	STRUCT. 3	2012	Y	PEAK
136	STRUCT. 3	2012	Y	SPEC 4 HZ
137	STRUCT. 3	2012	Y	SPEC 8 HZ
138	STRUCT. 3	2012	Y	SPEC 16 HZ
139	STRUCT. 3	3005	Y	PEAK
140	STRUCT. 3	3005	Y	SPEC 4 HZ
141	STRUCT. 3	3005	Y	SPEC 8 HZ
142	STRUCT. 3	3005	Y	SPEC 16 HZ
143	STRUCT. 3	3006	Y	PEAK
144	STRUCT. 3	3006	Y	SPEC 4 HZ
145	STRUCT. 3	3006	Y	SPEC 8 HZ

146	STRUCT. 3	3006	Y	SPEC 16 HZ
147	STRUCT. 1	20	Z	PEAK
148	STRUCT. 2	936	Z	PEAK
149	STRUCT. 2	936	Z	SPEC 4 HZ
150	STRUCT. 2	936	Z	SPEC 8 HZ
151	STRUCT. 2	936	Z	SPEC 16 HZ
152	STRUCT. 2	1463	Z	PEAK
153	STRUCT. 2	1463	Z	SPEC 4 HZ
154	STRUCT. 2	1463	Z	SPEC 8 HZ
155	STRUCT. 2	1463	Z	SPEC 16 HZ
156	STRUCT. 3	13	Z	PEAK
157	STRUCT. 3	13	Z	SPEC 4 HZ
158	STRUCT. 3	13	Z	SPEC 8 HZ
159	STRUCT. 3	13	Z	SPEC 16 HZ
160	STRUCT. 3	505	Z	PEAK
161	STRUCT. 3	505	Z	SPEC 4 HZ
162	STRUCT. 3	505	Z	SPEC 8 HZ
163	STRUCT. 3	505	Z	SPEC 16 HZ
164	STRUCT. 3	544	Z	PEAK
165	STRUCT. 3	544	Z	SPEC 4 HZ
166	STRUCT. 3	544	Z	SPEC 8 HZ
167	STRUCT. 3	544	Z	SPEC 16 HZ
168	STRUCT. 3	1511	Z	PEAK
169	STRUCT. 3	1511	Z	SPEC 4 HZ
170	STRUCT. 3	1511	Z	SPEC 8 HZ
171	STRUCT. 3	1511	Z	SPEC 16 HZ
172	STRUCT. 3	1530	Z	PEAK
173	STRUCT. 3	1530	Z	SPEC 4 HZ
174	STRUCT. 3	1530	Z	SPEC 8 HZ
175	STRUCT. 3	1530	Z	SPEC 16 HZ
176	STRUCT. 3	1537	Z	PEAK
177	STRUCT. 3	1537	Z	SPEC 4 HZ
178	STRUCT. 3	1537	Z	SPEC 8 HZ
179	STRUCT. 3	1537	Z	SPEC 16 HZ
180	STRUCT. 3	1562	Z	PEAK
181	STRUCT. 3	1562	Z	SPEC 4 HZ
182	STRUCT. 3	1562	Z	SPEC 8 HZ
183	STRUCT. 3	1562	Z	SPEC 16 HZ
184	STRUCT. 3	2012	Z	PEAK
185	STRUCT. 3	2012	Z	SPEC 4 HZ
186	STRUCT. 3	2012	Z	SPEC 8 HZ
187	STRUCT. 3	2012	Z	SPEC 16 HZ
188	STRUCT. 3	3005	Z	PEAK
189	STRUCT. 3	3005	Z	SPEC 4 HZ
190	STRUCT. 3	3005	Z	SPEC 8 HZ
191	STRUCT. 3	3005	Z	SPEC 16 HZ
192	STRUCT. 3	3006	Z	PEAK
193	STRUCT. 3	3006	Z	SPEC 4 HZ
194	STRUCT. 3	3006	Z	SPEC 8 HZ
195	STRUCT. 3	3006	Z	SPEC 16 HZ

SUBSYSTEM ACCELERATION RESPONSES

RESPONSE NUMBER	SUBSYSTEM	NODE	DIRECTION	ACCELERATION TYPE
216	SUBSYS. 1	13		RESULTANT
217	SUBSYS. 1	15		RESULTANT
218	SUBSYS. 1	18		RESULTANT
219	SUBSYS. 1	80		RESULTANT
220	SUBSYS. 1	83		RESULTANT
221	SUBSYS. 1	154		RESULTANT

222	SUBSYS.	1	163	RESULTANT
223	SUBSYS.	1	176	RESULTANT
224	SUBSYS.	1	178	RESULTANT
225	SUBSYS.	1	181	RESULTANT
226	SUBSYS.	1	186	RESULTANT
227	SUBSYS.	1	193	RESULTANT
228	SUBSYS.	1	202	RESULTANT
229	SUBSYS.	1	243	RESULTANT
230	SUBSYS.	1	249	RESULTANT
231	SUBSYS.	1	261	RESULTANT
232	SUBSYS.	1	326	RESULTANT
233	SUBSYS.	1	331	RESULTANT
234	SUBSYS.	2	12	RESULTANT
235	SUBSYS.	2	18	RESULTANT
236	SUBSYS.	2	34	RESULTANT
237	SUBSYS.	2	41	RESULTANT
238	SUBSYS.	2	64	RESULTANT
239	SUBSYS.	2	89	RESULTANT
240	SUBSYS.	2	168	RESULTANT
241	SUBSYS.	3	110	RESULTANT
242	SUBSYS.	4	5	RESULTANT
243	SUBSYS.	4	8	RESULTANT
244	SUBSYS.	4	32	RESULTANT
245	SUBSYS.	4	35	RESULTANT
246	SUBSYS.	4	41	RESULTANT
247	SUBSYS.	4	106	RESULTANT
248	SUBSYS.	4	109	RESULTANT
249	SUBSYS.	4	119	RESULTANT
250	SUBSYS.	4	124	RESULTANT
251	SUBSYS.	4	161	RESULTANT
252	SUBSYS.	4	163	RESULTANT
253	SUBSYS.	4	191	RESULTANT
254	SUBSYS.	4	193	RESULTANT
255	SUBSYS.	4	226	RESULTANT
256	SUBSYS.	4	228	RESULTANT
257	SUBSYS.	4	240	RESULTANT
258	SUBSYS.	4	248	RESULTANT
259	SUBSYS.	4	292	RESULTANT
260	SUBSYS.	4	294	RESULTANT
261	SUBSYS.	4	306	RESULTANT
262	SUBSYS.	4	308	RESULTANT
263	SUBSYS.	4	376	RESULTANT
264	SUBSYS.	4	378	RESULTANT
265	SUBSYS.	4	384	RESULTANT
266	SUBSYS.	4	404	RESULTANT
267	SUBSYS.	5	7	RESULTANT
268	SUBSYS.	5	10	RESULTANT
269	SUBSYS.	5	20	RESULTANT
270	SUBSYS.	5	31	RESULTANT
271	SUBSYS.	5	34	RESULTANT
272	SUBSYS.	5	47	RESULTANT
273	SUBSYS.	5	60	RESULTANT
274	SUBSYS.	5	63	RESULTANT
275	SUBSYS.	6	8	RESULTANT
276	SUBSYS.	6	24	RESULTANT
277	SUBSYS.	6	48	RESULTANT
278	SUBSYS.	6	52	RESULTANT
279	SUBSYS.	6	70	RESULTANT
280	SUBSYS.	6	87	RESULTANT
281	SUBSYS.	7	186	RESULTANT
282	SUBSYS.	7	215	RESULTANT
283	SUBSYS.	7	240	RESULTANT
284	SUBSYS.	7	243	RESULTANT

285	SUBSYS.	7	262	RESULTANT
286	SUBSYS.	7	268	RESULTANT
287	SUBSYS.	7	275	RESULTANT
288	SUBSYS.	7	279	RESULTANT
289	SUBSYS.	7	335	RESULTANT
290	SUBSYS.	7	342	RESULTANT
291	SUBSYS.	7	377	RESULTANT
292	SUBSYS.	7	391	RESULTANT
293	SUBSYS.	7	400	RESULTANT
294	SUBSYS.	8	11	RESULTANT
295	SUBSYS.	8	22	RESULTANT
296	SUBSYS.	8	26	RESULTANT
297	SUBSYS.	8	42	RESULTANT
298	SUBSYS.	8	53	RESULTANT
299	SUBSYS.	8	63	RESULTANT
300	SUBSYS.	8	68	RESULTANT
301	SUBSYS.	8	80	RESULTANT
302	SUBSYS.	8	95	RESULTANT
303	SUBSYS.	9	6	RESULTANT
304	SUBSYS.	9	48	RESULTANT
305	SUBSYS.	9	50	RESULTANT
306	SUBSYS.	9	55	RESULTANT
307	SUBSYS.	9	73	RESULTANT
308	SUBSYS.	9	101	RESULTANT
309	SUBSYS.	9	120	RESULTANT
310	SUBSYS.	9	151	RESULTANT
311	SUBSYS.	10	16	RESULTANT
312	SUBSYS.	10	59	RESULTANT
313	SUBSYS.	11	10	RESULTANT
314	SUBSYS.	11	17	RESULTANT
315	SUBSYS.	11	51	RESULTANT
316	SUBSYS.	11	70	RESULTANT
317	SUBSYS.	11	78	RESULTANT
318	SUBSYS.	11	85	RESULTANT
319	SUBSYS.	11	97	RESULTANT
320	SUBSYS.	11	102	RESULTANT
321	SUBSYS.	11	108	RESULTANT
322	SUBSYS.	11	140	RESULTANT
323	SUBSYS.	11	147	RESULTANT
324	SUBSYS.	11	175	RESULTANT
325	SUBSYS.	11	178	RESULTANT
326	SUBSYS.	11	209	RESULTANT
327	SUBSYS.	11	229	RESULTANT
328	SUBSYS.	11	261	RESULTANT
329	SUBSYS.	11	324	RESULTANT
330	SUBSYS.	11	334	RESULTANT
331	SUBSYS.	11	398	RESULTANT
332	SUBSYS.	11	438	RESULTANT
333	SUBSYS.	11	473	RESULTANT
334	SUBSYS.	12	27	RESULTANT
335	SUBSYS.	12	36	RESULTANT
336	SUBSYS.	13	6	RESULTANT
337	SUBSYS.	13	49	RESULTANT
338	SUBSYS.	13	106	RESULTANT
339	SUBSYS.	13	149	RESULTANT
340	SUBSYS.	13	206	RESULTANT
341	SUBSYS.	13	249	RESULTANT
342	SUBSYS.	13	306	RESULTANT
343	SUBSYS.	13	349	RESULTANT
344	SUBSYS.	13	438	RESULTANT
345	SUBSYS.	13	506	RESULTANT
346	SUBSYS.	13	560	RESULTANT
347	SUBSYS.	13	612	RESULTANT

348	SUBSYS.	13	618	RESULTANT
349	SUBSYS.	13	622	RESULTANT
350	SUBSYS.	13	726	RESULTANT
351	SUBSYS.	13	733	RESULTANT
352	SUBSYS.	13	737	RESULTANT
353	SUBSYS.	15	91	RESULTANT
354	SUBSYS.	16	110	RESULTANT
355	SUBSYS.	17	87	RESULTANT
356	SUBSYS.	19	8	RESULTANT
357	SUBSYS.	19	11	RESULTANT
358	SUBSYS.	20	10	RESULTANT
359	SUBSYS.	20	78	RESULTANT
360	SUBSYS.	21	85	RESULTANT
361	SUBSYS.	21	91	RESULTANT
362	SUBSYS.	21	184	RESULTANT
363	SUBSYS.	21	192	RESULTANT

SUBSYSTEM MOMENT RESPONSES

RESPONSE NUMBER	SUBSYSTEM	ELEMENT	DIRECTION	MOMENT TYPE
384	SUBSYS. 1	1		RESULTANT
385	SUBSYS. 1	3		RESULTANT
386	SUBSYS. 1	6		RESULTANT
387	SUBSYS. 1	7		RESULTANT
388	SUBSYS. 1	8		RESULTANT
389	SUBSYS. 1	17		RESULTANT
390	SUBSYS. 1	18		RESULTANT
391	SUBSYS. 1	19		RESULTANT
392	SUBSYS. 1	20		RESULTANT
393	SUBSYS. 1	24		RESULTANT
394	SUBSYS. 1	25		RESULTANT
395	SUBSYS. 1	26		RESULTANT
396	SUBSYS. 1	33		RESULTANT
397	SUBSYS. 1	36		RESULTANT
398	SUBSYS. 1	39		RESULTANT
399	SUBSYS. 1	40		RESULTANT
400	SUBSYS. 1	43		RESULTANT
401	SUBSYS. 1	46		RESULTANT
402	SUBSYS. 1	48		RESULTANT
403	SUBSYS. 1	51		RESULTANT
404	SUBSYS. 1	54		RESULTANT
405	SUBSYS. 1	58		RESULTANT
406	SUBSYS. 1	64		RESULTANT
407	SUBSYS. 1	67		RESULTANT
408	SUBSYS. 1	87		RESULTANT
409	SUBSYS. 1	88		RESULTANT
410	SUBSYS. 1	90		RESULTANT
411	SUBSYS. 1	93		RESULTANT
412	SUBSYS. 1	94		RESULTANT
413	SUBSYS. 1	95		RESULTANT
414	SUBSYS. 1	97		RESULTANT
415	SUBSYS. 1	101		RESULTANT
416	SUBSYS. 1	103		RESULTANT
417	SUBSYS. 1	110		RESULTANT
418	SUBSYS. 1	117		RESULTANT
419	SUBSYS. 1	118		RESULTANT
420	SUBSYS. 1	122		RESULTANT
421	SUBSYS. 1	125		RESULTANT
422	SUBSYS. 1	135		RESULTANT
423	SUBSYS. 1	137		RESULTANT

424	SUBSYS.	1	139	RESULTANT
425	SUBSYS.	1	140	RESULTANT
426	SUBSYS.	1	143	RESULTANT
427	SUBSYS.	1	150	RESULTANT
428	SUBSYS.	1	153	RESULTANT
429	SUBSYS.	1	156	RESULTANT
430	SUBSYS.	1	160	RESULTANT
431	SUBSYS.	1	161	RESULTANT
432	SUBSYS.	1	162	RESULTANT
433	SUBSYS.	1	165	RESULTANT
434	SUBSYS.	1	174	RESULTANT
435	SUBSYS.	1	175	RESULTANT
436	SUBSYS.	1	179	RESULTANT
437	SUBSYS.	1	181	RESULTANT
438	SUBSYS.	1	182	RESULTANT
439	SUBSYS.	1	183	RESULTANT
440	SUBSYS.	1	186	RESULTANT
441	SUBSYS.	1	187	RESULTANT
442	SUBSYS.	1	188	RESULTANT
443	SUBSYS.	1	192	RESULTANT
444	SUBSYS.	1	194	RESULTANT
445	SUBSYS.	1	199	RESULTANT
446	SUBSYS.	1	201	RESULTANT
447	SUBSYS.	1	209	RESULTANT
448	SUBSYS.	1	210	RESULTANT
449	SUBSYS.	1	214	RESULTANT
450	SUBSYS.	1	216	RESULTANT
451	SUBSYS.	1	218	RESULTANT
452	SUBSYS.	1	219	RESULTANT
453	SUBSYS.	1	222	RESULTANT
454	SUBSYS.	1	223	RESULTANT
455	SUBSYS.	1	224	RESULTANT
456	SUBSYS.	1	229	RESULTANT
457	SUBSYS.	1	231	RESULTANT
458	SUBSYS.	1	235	RESULTANT
459	SUBSYS.	1	236	RESULTANT
460	SUBSYS.	1	237	RESULTANT
461	SUBSYS.	1	240	RESULTANT
462	SUBSYS.	1	241	RESULTANT
463	SUBSYS.	1	243	RESULTANT
464	SUBSYS.	1	246	RESULTANT
465	SUBSYS.	1	251	RESULTANT
466	SUBSYS.	1	252	RESULTANT
467	SUBSYS.	1	253	RESULTANT
468	SUBSYS.	1	254	RESULTANT
469	SUBSYS.	1	259	RESULTANT
470	SUBSYS.	1	260	RESULTANT
471	SUBSYS.	1	263	RESULTANT
472	SUBSYS.	1	265	RESULTANT
473	SUBSYS.	1	267	RESULTANT
474	SUBSYS.	1	288	RESULTANT
475	SUBSYS.	1	292	RESULTANT
476	SUBSYS.	1	295	RESULTANT
477	SUBSYS.	1	297	RESULTANT
478	SUBSYS.	1	303	RESULTANT
479	SUBSYS.	1	305	RESULTANT
480	SUBSYS.	1	311	RESULTANT
481	SUBSYS.	1	312	RESULTANT
482	SUBSYS.	1	315	RESULTANT
483	SUBSYS.	1	316	RESULTANT
484	SUBSYS.	1	317	RESULTANT
485	SUBSYS.	1	320	RESULTANT
486	SUBSYS.	1	322	RESULTANT

487	SUBSYS.	1	323	RESULTANT
488	SUBSYS.	1	324	RESULTANT
489	SUBSYS.	1	326	RESULTANT
490	SUBSYS.	1	327	RESULTANT
491	SUBSYS.	2	1	RESULTANT
492	SUBSYS.	2	4	RESULTANT
493	SUBSYS.	2	5	RESULTANT
494	SUBSYS.	2	6	RESULTANT
495	SUBSYS.	2	7	RESULTANT
496	SUBSYS.	2	11	RESULTANT
497	SUBSYS.	2	29	RESULTANT
498	SUBSYS.	2	34	RESULTANT
499	SUBSYS.	2	64	RESULTANT
500	SUBSYS.	2	66	RESULTANT
501	SUBSYS.	2	69	RESULTANT
502	SUBSYS.	2	72	RESULTANT
503	SUBSYS.	2	74	RESULTANT
504	SUBSYS.	2	86	RESULTANT
505	SUBSYS.	2	88	RESULTANT
506	SUBSYS.	2	91	RESULTANT
507	SUBSYS.	2	94	RESULTANT
508	SUBSYS.	2	97	RESULTANT
509	SUBSYS.	2	98	RESULTANT
510	SUBSYS.	2	159	RESULTANT
511	SUBSYS.	2	161	RESULTANT
512	SUBSYS.	2	164	RESULTANT
513	SUBSYS.	2	166	RESULTANT
514	SUBSYS.	2	169	RESULTANT
515	SUBSYS.	2	172	RESULTANT
516	SUBSYS.	2	173	RESULTANT
517	SUBSYS.	3	10	RESULTANT
518	SUBSYS.	3	14	RESULTANT
519	SUBSYS.	3	18	RESULTANT
520	SUBSYS.	3	23	RESULTANT
521	SUBSYS.	3	34	RESULTANT
522	SUBSYS.	3	44	RESULTANT
523	SUBSYS.	3	52	RESULTANT
524	SUBSYS.	3	62	RESULTANT
525	SUBSYS.	3	71	RESULTANT
526	SUBSYS.	3	76	RESULTANT
527	SUBSYS.	3	82	RESULTANT
528	SUBSYS.	3	86	RESULTANT
529	SUBSYS.	3	93	RESULTANT
530	SUBSYS.	3	98	RESULTANT
531	SUBSYS.	3	101	RESULTANT
532	SUBSYS.	3	108	RESULTANT
533	SUBSYS.	3	110	RESULTANT
534	SUBSYS.	3	121	RESULTANT
535	SUBSYS.	3	132	RESULTANT
536	SUBSYS.	3	133	RESULTANT
537	SUBSYS.	3	134	RESULTANT
538	SUBSYS.	3	157	RESULTANT
539	SUBSYS.	3	158	RESULTANT
540	SUBSYS.	4	1	RESULTANT
541	SUBSYS.	4	2	RESULTANT
542	SUBSYS.	4	5	RESULTANT
543	SUBSYS.	4	7	RESULTANT
544	SUBSYS.	4	12	RESULTANT
545	SUBSYS.	4	15	RESULTANT
546	SUBSYS.	4	18	RESULTANT
547	SUBSYS.	4	20	RESULTANT
548	SUBSYS.	4	24	RESULTANT
549	SUBSYS.	4	25	RESULTANT

550	SUBSYS.	4	27	RESULTANT
551	SUBSYS.	4	29	RESULTANT
552	SUBSYS.	4	37	RESULTANT
553	SUBSYS.	4	39	RESULTANT
554	SUBSYS.	4	40	RESULTANT
555	SUBSYS.	4	44	RESULTANT
556	SUBSYS.	4	45	RESULTANT
557	SUBSYS.	4	46	RESULTANT
558	SUBSYS.	4	68	RESULTANT
559	SUBSYS.	4	71	RESULTANT
560	SUBSYS.	4	73	RESULTANT
561	SUBSYS.	4	74	RESULTANT
562	SUBSYS.	4	76	RESULTANT
563	SUBSYS.	4	77	RESULTANT
564	SUBSYS.	4	80	RESULTANT
565	SUBSYS.	4	81	RESULTANT
566	SUBSYS.	4	83	RESULTANT
567	SUBSYS.	4	85	RESULTANT
568	SUBSYS.	4	87	RESULTANT
569	SUBSYS.	4	90	RESULTANT
570	SUBSYS.	4	92	RESULTANT
571	SUBSYS.	4	102	RESULTANT
572	SUBSYS.	4	107	RESULTANT
573	SUBSYS.	4	110	RESULTANT
574	SUBSYS.	4	113	RESULTANT
575	SUBSYS.	4	114	RESULTANT
576	SUBSYS.	4	116	RESULTANT
577	SUBSYS.	4	117	RESULTANT
578	SUBSYS.	4	122	RESULTANT
579	SUBSYS.	4	127	RESULTANT
580	SUBSYS.	4	137	RESULTANT
581	SUBSYS.	4	140	RESULTANT
582	SUBSYS.	4	144	RESULTANT
583	SUBSYS.	4	146	RESULTANT
584	SUBSYS.	4	152	RESULTANT
585	SUBSYS.	4	155	RESULTANT
586	SUBSYS.	4	159	RESULTANT
587	SUBSYS.	4	166	RESULTANT
588	SUBSYS.	4	167	RESULTANT
589	SUBSYS.	4	170	RESULTANT
590	SUBSYS.	4	176	RESULTANT
591	SUBSYS.	4	178	RESULTANT
592	SUBSYS.	4	180	RESULTANT
593	SUBSYS.	4	181	RESULTANT
594	SUBSYS.	4	184	RESULTANT
595	SUBSYS.	4	185	RESULTANT
596	SUBSYS.	4	196	RESULTANT
597	SUBSYS.	4	197	RESULTANT
598	SUBSYS.	4	199	RESULTANT
599	SUBSYS.	4	201	RESULTANT
600	SUBSYS.	4	203	RESULTANT
601	SUBSYS.	4	214	RESULTANT
602	SUBSYS.	4	217	RESULTANT
603	SUBSYS.	4	225	RESULTANT
604	SUBSYS.	4	231	RESULTANT
605	SUBSYS.	4	232	RESULTANT
606	SUBSYS.	4	235	RESULTANT
607	SUBSYS.	4	237	RESULTANT
608	SUBSYS.	4	238	RESULTANT
609	SUBSYS.	4	239	RESULTANT
610	SUBSYS.	4	245	RESULTANT
611	SUBSYS.	4	247	RESULTANT
612	SUBSYS.	4	251	RESULTANT

613	SUBSYS.	4	254	RESULTANT
614	SUBSYS.	4	261	RESULTANT
615	SUBSYS.	4	263	RESULTANT
616	SUBSYS.	4	266	RESULTANT
617	SUBSYS.	4	266	RESULTANT
618	SUBSYS.	4	267	RESULTANT
619	SUBSYS.	4	272	RESULTANT
620	SUBSYS.	4	273	RESULTANT
621	SUBSYS.	4	275	RESULTANT
622	SUBSYS.	4	277	RESULTANT
623	SUBSYS.	4	285	RESULTANT
624	SUBSYS.	4	286	RESULTANT
625	SUBSYS.	4	292	RESULTANT
626	SUBSYS.	4	297	RESULTANT
627	SUBSYS.	4	298	RESULTANT
628	SUBSYS.	4	299	RESULTANT
629	SUBSYS.	4	301	RESULTANT
630	SUBSYS.	4	302	RESULTANT
631	SUBSYS.	4	305	RESULTANT
632	SUBSYS.	4	311	RESULTANT
633	SUBSYS.	4	315	RESULTANT
634	SUBSYS.	4	318	RESULTANT
635	SUBSYS.	4	323	RESULTANT
636	SUBSYS.	4	325	RESULTANT
637	SUBSYS.	4	328	RESULTANT
638	SUBSYS.	4	330	RESULTANT
639	SUBSYS.	4	331	RESULTANT
640	SUBSYS.	4	334	RESULTANT
641	SUBSYS.	4	356	RESULTANT
642	SUBSYS.	4	360	RESULTANT
643	SUBSYS.	4	363	RESULTANT
644	SUBSYS.	4	367	RESULTANT
645	SUBSYS.	4	371	RESULTANT
646	SUBSYS.	4	374	RESULTANT
647	SUBSYS.	4	375	RESULTANT
648	SUBSYS.	4	376	RESULTANT
649	SUBSYS.	4	377	RESULTANT
650	SUBSYS.	4	383	RESULTANT
651	SUBSYS.	4	384	RESULTANT
652	SUBSYS.	4	385	RESULTANT
653	SUBSYS.	4	391	RESULTANT
654	SUBSYS.	4	400	RESULTANT
655	SUBSYS.	4	408	RESULTANT
656	SUBSYS.	5	1	RESULTANT
657	SUBSYS.	5	2	RESULTANT
658	SUBSYS.	5	8	RESULTANT
659	SUBSYS.	5	11	RESULTANT
660	SUBSYS.	5	12	RESULTANT
661	SUBSYS.	5	13	RESULTANT
662	SUBSYS.	5	14	RESULTANT
663	SUBSYS.	5	19	RESULTANT
664	SUBSYS.	5	20	RESULTANT
665	SUBSYS.	5	21	RESULTANT
666	SUBSYS.	5	22	RESULTANT
667	SUBSYS.	5	23	RESULTANT
668	SUBSYS.	5	29	RESULTANT
669	SUBSYS.	5	30	RESULTANT
670	SUBSYS.	5	31	RESULTANT
671	SUBSYS.	5	33	RESULTANT
672	SUBSYS.	5	34	RESULTANT
673	SUBSYS.	5	35	RESULTANT
674	SUBSYS.	5	40	RESULTANT
675	SUBSYS.	5	41	RESULTANT

676	SUBSYS.	5	42	RESULTANT
677	SUBSYS.	5	45	RESULTANT
678	SUBSYS.	5	46	RESULTANT
679	SUBSYS.	5	52	RESULTANT
680	SUBSYS.	5	53	RESULTANT
681	SUBSYS.	5	54	RESULTANT
682	SUBSYS.	6	1	RESULTANT
683	SUBSYS.	6	2	RESULTANT
684	SUBSYS.	6	8	RESULTANT
685	SUBSYS.	6	9	RESULTANT
686	SUBSYS.	6	11	RESULTANT
687	SUBSYS.	6	15	RESULTANT
688	SUBSYS.	6	16	RESULTANT
689	SUBSYS.	6	17	RESULTANT
690	SUBSYS.	6	23	RESULTANT
691	SUBSYS.	6	24	RESULTANT
692	SUBSYS.	6	25	RESULTANT
693	SUBSYS.	6	30	RESULTANT
694	SUBSYS.	6	31	RESULTANT
695	SUBSYS.	6	36	RESULTANT
696	SUBSYS.	6	37	RESULTANT
697	SUBSYS.	6	44	RESULTANT
698	SUBSYS.	6	45	RESULTANT
699	SUBSYS.	6	50	RESULTANT
700	SUBSYS.	6	51	RESULTANT
701	SUBSYS.	6	53	RESULTANT
702	SUBSYS.	6	54	RESULTANT
703	SUBSYS.	6	60	RESULTANT
704	SUBSYS.	6	61	RESULTANT
705	SUBSYS.	6	62	RESULTANT
706	SUBSYS.	6	63	RESULTANT
707	SUBSYS.	6	67	RESULTANT
708	SUBSYS.	6	68	RESULTANT
709	SUBSYS.	6	74	RESULTANT
710	SUBSYS.	6	75	RESULTANT
711	SUBSYS.	6	76	RESULTANT
712	SUBSYS.	7	1	RESULTANT
713	SUBSYS.	7	2	RESULTANT
714	SUBSYS.	7	6	RESULTANT
715	SUBSYS.	7	9	RESULTANT
716	SUBSYS.	7	29	RESULTANT
717	SUBSYS.	7	30	RESULTANT
718	SUBSYS.	7	31	RESULTANT
719	SUBSYS.	7	34	RESULTANT
720	SUBSYS.	7	35	RESULTANT
721	SUBSYS.	7	41	RESULTANT
722	SUBSYS.	7	44	RESULTANT
723	SUBSYS.	7	47	RESULTANT
724	SUBSYS.	7	51	RESULTANT
725	SUBSYS.	7	53	RESULTANT
726	SUBSYS.	7	54	RESULTANT
727	SUBSYS.	7	56	RESULTANT
728	SUBSYS.	7	59	RESULTANT
729	SUBSYS.	7	65	RESULTANT
730	SUBSYS.	7	68	RESULTANT
731	SUBSYS.	7	73	RESULTANT
732	SUBSYS.	7	74	RESULTANT
733	SUBSYS.	7	79	RESULTANT
734	SUBSYS.	7	80	RESULTANT
735	SUBSYS.	7	83	RESULTANT
736	SUBSYS.	7	88	RESULTANT
737	SUBSYS.	7	90	RESULTANT
738	SUBSYS.	7	91	RESULTANT

739	SUBSYS.	7	94	RESULTANT
740	SUBSYS.	7	95	RESULTANT
741	SUBSYS.	7	96	RESULTANT
742	SUBSYS.	7	100	RESULTANT
743	SUBSYS.	7	103	RESULTANT
744	SUBSYS.	7	104	RESULTANT
745	SUBSYS.	7	105	RESULTANT
746	SUBSYS.	7	111	RESULTANT
747	SUBSYS.	7	112	RESULTANT
748	SUBSYS.	7	113	RESULTANT
749	SUBSYS.	7	114	RESULTANT
750	SUBSYS.	7	116	RESULTANT
751	SUBSYS.	7	117	RESULTANT
752	SUBSYS.	7	118	RESULTANT
753	SUBSYS.	7	121	RESULTANT
754	SUBSYS.	7	122	RESULTANT
755	SUBSYS.	7	123	RESULTANT
756	SUBSYS.	7	125	RESULTANT
757	SUBSYS.	7	127	RESULTANT
758	SUBSYS.	7	129	RESULTANT
759	SUBSYS.	7	130	RESULTANT
760	SUBSYS.	7	131	RESULTANT
761	SUBSYS.	7	133	RESULTANT
762	SUBSYS.	7	134	RESULTANT
763	SUBSYS.	7	137	RESULTANT
764	SUBSYS.	7	140	RESULTANT
765	SUBSYS.	7	143	RESULTANT
766	SUBSYS.	7	145	RESULTANT
767	SUBSYS.	7	146	RESULTANT
768	SUBSYS.	7	147	RESULTANT
769	SUBSYS.	7	148	RESULTANT
770	SUBSYS.	7	149	RESULTANT
771	SUBSYS.	7	155	RESULTANT
772	SUBSYS.	7	156	RESULTANT
773	SUBSYS.	7	157	RESULTANT
774	SUBSYS.	7	160	RESULTANT
775	SUBSYS.	7	160	RESULTANT
776	SUBSYS.	7	161	RESULTANT
777	SUBSYS.	7	162	RESULTANT
778	SUBSYS.	7	165	RESULTANT
779	SUBSYS.	7	171	RESULTANT
780	SUBSYS.	7	178	RESULTANT
781	SUBSYS.	7	181	RESULTANT
782	SUBSYS.	7	182	RESULTANT
783	SUBSYS.	7	184	RESULTANT
784	SUBSYS.	7	185	RESULTANT
785	SUBSYS.	7	191	RESULTANT
786	SUBSYS.	7	192	RESULTANT
787	SUBSYS.	7	193	RESULTANT
788	SUBSYS.	7	194	RESULTANT
789	SUBSYS.	7	195	RESULTANT
790	SUBSYS.	7	196	RESULTANT
791	SUBSYS.	7	197	RESULTANT
792	SUBSYS.	7	199	RESULTANT
793	SUBSYS.	7	200	RESULTANT
794	SUBSYS.	7	203	RESULTANT
795	SUBSYS.	7	213	RESULTANT
796	SUBSYS.	7	214	RESULTANT
797	SUBSYS.	7	222	RESULTANT
798	SUBSYS.	7	223	RESULTANT
799	SUBSYS.	7	224	RESULTANT
800	SUBSYS.	7	225	RESULTANT
801	SUBSYS.	7	226	RESULTANT

802	SUBSYS.	7	230	RESULTANT
803	SUBSYS.	7	233	RESULTANT
804	SUBSYS.	7	234	RESULTANT
805	SUBSYS.	7	235	RESULTANT
806	SUBSYS.	7	238	RESULTANT
807	SUBSYS.	7	246	RESULTANT
808	SUBSYS.	7	249	RESULTANT
809	SUBSYS.	7	252	RESULTANT
810	SUBSYS.	7	255	RESULTANT
811	SUBSYS.	7	259	RESULTANT
812	SUBSYS.	7	260	RESULTANT
813	SUBSYS.	7	264	RESULTANT
814	SUBSYS.	7	265	RESULTANT
815	SUBSYS.	7	266	RESULTANT
816	SUBSYS.	7	267	RESULTANT
817	SUBSYS.	7	271	RESULTANT
818	SUBSYS.	7	272	RESULTANT
819	SUBSYS.	7	273	RESULTANT
820	SUBSYS.	7	279	RESULTANT
821	SUBSYS.	7	280	RESULTANT
822	SUBSYS.	7	281	RESULTANT
823	SUBSYS.	7	282	RESULTANT
824	SUBSYS.	7	287	RESULTANT
825	SUBSYS.	7	288	RESULTANT
826	SUBSYS.	7	289	RESULTANT
827	SUBSYS.	7	290	RESULTANT
828	SUBSYS.	7	292	RESULTANT
829	SUBSYS.	7	295	RESULTANT
830	SUBSYS.	7	299	RESULTANT
831	SUBSYS.	7	301	RESULTANT
832	SUBSYS.	7	302	RESULTANT
833	SUBSYS.	7	302	RESULTANT
834	SUBSYS.	7	303	RESULTANT
835	SUBSYS.	7	304	RESULTANT
836	SUBSYS.	7	305	RESULTANT
837	SUBSYS.	7	306	RESULTANT
838	SUBSYS.	7	310	RESULTANT
839	SUBSYS.	7	313	RESULTANT
840	SUBSYS.	7	317	RESULTANT
841	SUBSYS.	7	318	RESULTANT
842	SUBSYS.	7	319	RESULTANT
843	SUBSYS.	7	320	RESULTANT
844	SUBSYS.	8	1	RESULTANT
845	SUBSYS.	8	2	RESULTANT
846	SUBSYS.	8	3	RESULTANT
847	SUBSYS.	8	6	RESULTANT
848	SUBSYS.	8	11	RESULTANT
849	SUBSYS.	8	14	RESULTANT
850	SUBSYS.	8	20	RESULTANT
851	SUBSYS.	8	21	RESULTANT
852	SUBSYS.	8	27	RESULTANT
853	SUBSYS.	8	28	RESULTANT
854	SUBSYS.	8	29	RESULTANT
855	SUBSYS.	8	30	RESULTANT
856	SUBSYS.	8	32	RESULTANT
857	SUBSYS.	8	37	RESULTANT
858	SUBSYS.	8	40	RESULTANT
859	SUBSYS.	8	41	RESULTANT
860	SUBSYS.	8	42	RESULTANT
861	SUBSYS.	8	44	RESULTANT
862	SUBSYS.	8	47	RESULTANT
863	SUBSYS.	8	48	RESULTANT
864	SUBSYS.	8	49	RESULTANT

865	SUBSYS.	8	52	RESULTANT
866	SUBSYS.	8	55	RESULTANT
867	SUBSYS.	8	56	RESULTANT
868	SUBSYS.	8	57	RESULTANT
869	SUBSYS.	8	63	RESULTANT
870	SUBSYS.	8	64	RESULTANT
871	SUBSYS.	8	65	RESULTANT
872	SUBSYS.	8	66	RESULTANT
873	SUBSYS.	8	73	RESULTANT
874	SUBSYS.	8	77	RESULTANT
875	SUBSYS.	8	80	RESULTANT
876	SUBSYS.	8	84	RESULTANT
877	SUBSYS.	8	88	RESULTANT
878	SUBSYS.	9	1	RESULTANT
879	SUBSYS.	9	5	RESULTANT
880	SUBSYS.	9	8	RESULTANT
881	SUBSYS.	9	14	RESULTANT
882	SUBSYS.	9	18	RESULTANT
883	SUBSYS.	9	22	RESULTANT
884	SUBSYS.	9	25	RESULTANT
885	SUBSYS.	9	28	RESULTANT
886	SUBSYS.	9	31	RESULTANT
887	SUBSYS.	9	38	RESULTANT
888	SUBSYS.	9	39	RESULTANT
889	SUBSYS.	9	40	RESULTANT
890	SUBSYS.	9	43	RESULTANT
891	SUBSYS.	9	53	RESULTANT
892	SUBSYS.	9	54	RESULTANT
893	SUBSYS.	9	56	RESULTANT
894	SUBSYS.	9	57	RESULTANT
895	SUBSYS.	9	58	RESULTANT
896	SUBSYS.	9	61	RESULTANT
897	SUBSYS.	9	64	RESULTANT
898	SUBSYS.	9	68	RESULTANT
899	SUBSYS.	9	69	RESULTANT
900	SUBSYS.	9	70	RESULTANT
901	SUBSYS.	9	71	RESULTANT
902	SUBSYS.	9	74	RESULTANT
903	SUBSYS.	9	75	RESULTANT
904	SUBSYS.	9	77	RESULTANT
905	SUBSYS.	9	78	RESULTANT
906	SUBSYS.	9	81	RESULTANT
907	SUBSYS.	9	85	RESULTANT
908	SUBSYS.	9	89	RESULTANT
909	SUBSYS.	9	94	RESULTANT
910	SUBSYS.	9	95	RESULTANT
911	SUBSYS.	9	98	RESULTANT
912	SUBSYS.	9	99	RESULTANT
913	SUBSYS.	9	102	RESULTANT
914	SUBSYS.	9	105	RESULTANT
915	SUBSYS.	9	109	RESULTANT
916	SUBSYS.	9	110	RESULTANT
917	SUBSYS.	9	111	RESULTANT
918	SUBSYS.	9	112	RESULTANT
919	SUBSYS.	9	115	RESULTANT
920	SUBSYS.	9	116	RESULTANT
921	SUBSYS.	9	117	RESULTANT
922	SUBSYS.	9	119	RESULTANT
923	SUBSYS.	9	122	RESULTANT
924	SUBSYS.	9	125	RESULTANT
925	SUBSYS.	9	129	RESULTANT
926	SUBSYS.	9	133	RESULTANT
927	SUBSYS.	9	137	RESULTANT

928	SUBSYS. 10	1	RESULTANT
929	SUBSYS. 10	2	RESULTANT
930	SUBSYS. 10	3	RESULTANT
931	SUBSYS. 10	6	RESULTANT
932	SUBSYS. 10	9	RESULTANT
933	SUBSYS. 10	16	RESULTANT
934	SUBSYS. 10	19	RESULTANT
935	SUBSYS. 10	20	RESULTANT
936	SUBSYS. 10	21	RESULTANT
937	SUBSYS. 10	22	RESULTANT
938	SUBSYS. 10	32	RESULTANT
939	SUBSYS. 10	33	RESULTANT
940	SUBSYS. 10	36	RESULTANT
941	SUBSYS. 10	39	RESULTANT
942	SUBSYS. 10	42	RESULTANT
943	SUBSYS. 10	47	RESULTANT
944	SUBSYS. 10	54	RESULTANT
945	SUBSYS. 10	59	RESULTANT
946	SUBSYS. 10	60	RESULTANT
947	SUBSYS. 10	61	RESULTANT
948	SUBSYS. 10	62	RESULTANT
949	SUBSYS. 10	70	RESULTANT
950	SUBSYS. 11	1	RESULTANT
951	SUBSYS. 11	2	RESULTANT
952	SUBSYS. 11	3	RESULTANT
953	SUBSYS. 11	5	RESULTANT
954	SUBSYS. 11	8	RESULTANT
955	SUBSYS. 11	10	RESULTANT
956	SUBSYS. 11	11	RESULTANT
957	SUBSYS. 11	12	RESULTANT
958	SUBSYS. 11	14	RESULTANT
959	SUBSYS. 11	15	RESULTANT
960	SUBSYS. 11	16	RESULTANT
961	SUBSYS. 11	17	RESULTANT
962	SUBSYS. 11	19	RESULTANT
963	SUBSYS. 11	22	RESULTANT
964	SUBSYS. 11	23	RESULTANT
965	SUBSYS. 11	24	RESULTANT
966	SUBSYS. 11	25	RESULTANT
967	SUBSYS. 11	26	RESULTANT
968	SUBSYS. 11	32	RESULTANT
969	SUBSYS. 11	33	RESULTANT
970	SUBSYS. 11	34	RESULTANT
971	SUBSYS. 11	37	RESULTANT
972	SUBSYS. 11	40	RESULTANT
973	SUBSYS. 11	46	RESULTANT
974	SUBSYS. 11	50	RESULTANT
975	SUBSYS. 11	53	RESULTANT
976	SUBSYS. 11	54	RESULTANT
977	SUBSYS. 11	55	RESULTANT
978	SUBSYS. 11	56	RESULTANT
979	SUBSYS. 11	58	RESULTANT
980	SUBSYS. 11	59	RESULTANT
981	SUBSYS. 11	63	RESULTANT
982	SUBSYS. 11	65	RESULTANT
983	SUBSYS. 11	66	RESULTANT
984	SUBSYS. 11	70	RESULTANT
985	SUBSYS. 11	71	RESULTANT
986	SUBSYS. 11	72	RESULTANT
987	SUBSYS. 11	73	RESULTANT
988	SUBSYS. 11	77	RESULTANT
989	SUBSYS. 11	78	RESULTANT
990	SUBSYS. 11	79	RESULTANT

991	SUBSYS. 11	80	RESULTANT
992	SUBSYS. 11	81	RESULTANT
993	SUBSYS. 11	84	RESULTANT
994	SUBSYS. 11	87	RESULTANT
995	SUBSYS. 11	88	RESULTANT
996	SUBSYS. 11	92	RESULTANT
997	SUBSYS. 11	93	RESULTANT
998	SUBSYS. 11	94	RESULTANT
999	SUBSYS. 11	98	RESULTANT
1000	SUBSYS. 11	99	RESULTANT
1001	SUBSYS. 11	100	RESULTANT
1002	SUBSYS. 11	101	RESULTANT
1003	SUBSYS. 11	104	RESULTANT
1004	SUBSYS. 11	107	RESULTANT
1005	SUBSYS. 11	108	RESULTANT
1006	SUBSYS. 11	109	RESULTANT
1007	SUBSYS. 11	112	RESULTANT
1008	SUBSYS. 11	115	RESULTANT
1009	SUBSYS. 11	118	RESULTANT
1010	SUBSYS. 11	121	RESULTANT
1011	SUBSYS. 11	123	RESULTANT
1012	SUBSYS. 11	124	RESULTANT
1013	SUBSYS. 11	125	RESULTANT
1014	SUBSYS. 11	128	RESULTANT
1015	SUBSYS. 11	129	RESULTANT
1016	SUBSYS. 11	130	RESULTANT
1017	SUBSYS. 11	131	RESULTANT
1018	SUBSYS. 11	135	RESULTANT
1019	SUBSYS. 11	136	RESULTANT
1020	SUBSYS. 11	137	RESULTANT
1021	SUBSYS. 11	138	RESULTANT
1022	SUBSYS. 11	141	RESULTANT
1023	SUBSYS. 11	144	RESULTANT
1024	SUBSYS. 11	147	RESULTANT
1025	SUBSYS. 11	150	RESULTANT
1026	SUBSYS. 11	152	RESULTANT
1027	SUBSYS. 11	153	RESULTANT
1028	SUBSYS. 11	154	RESULTANT
1029	SUBSYS. 11	156	RESULTANT
1030	SUBSYS. 11	157	RESULTANT
1031	SUBSYS. 11	160	RESULTANT
1032	SUBSYS. 11	163	RESULTANT
1033	SUBSYS. 11	166	RESULTANT
1034	SUBSYS. 11	167	RESULTANT
1035	SUBSYS. 11	168	RESULTANT
1036	SUBSYS. 11	169	RESULTANT
1037	SUBSYS. 11	170	RESULTANT
1038	SUBSYS. 11	173	RESULTANT
1039	SUBSYS. 11	176	RESULTANT
1040	SUBSYS. 11	180	RESULTANT
1041	SUBSYS. 11	184	RESULTANT
1042	SUBSYS. 11	191	RESULTANT
1043	SUBSYS. 11	193	RESULTANT
1044	SUBSYS. 11	196	RESULTANT
1045	SUBSYS. 11	199	RESULTANT
1046	SUBSYS. 11	200	RESULTANT
1047	SUBSYS. 11	201	RESULTANT
1048	SUBSYS. 11	202	RESULTANT
1049	SUBSYS. 11	205	RESULTANT
1050	SUBSYS. 11	208	RESULTANT
1051	SUBSYS. 11	213	RESULTANT
1052	SUBSYS. 11	214	RESULTANT
1053	SUBSYS. 11	215	RESULTANT

1054	SUBSYS. 11	222	RESULTANT
1055	SUBSYS. 11	223	RESULTANT
1056	SUBSYS. 11	224	RESULTANT
1057	SUBSYS. 11	225	RESULTANT
1058	SUBSYS. 11	226	RESULTANT
1059	SUBSYS. 11	227	RESULTANT
1060	SUBSYS. 11	228	RESULTANT
1061	SUBSYS. 11	232	RESULTANT
1062	SUBSYS. 11	233	RESULTANT
1063	SUBSYS. 11	234	RESULTANT
1064	SUBSYS. 11	236	RESULTANT
1065	SUBSYS. 11	237	RESULTANT
1066	SUBSYS. 11	240	RESULTANT
1067	SUBSYS. 11	243	RESULTANT
1068	SUBSYS. 11	247	RESULTANT
1069	SUBSYS. 11	250	RESULTANT
1070	SUBSYS. 11	252	RESULTANT
1071	SUBSYS. 11	253	RESULTANT
1072	SUBSYS. 11	254	RESULTANT
1073	SUBSYS. 11	257	RESULTANT
1074	SUBSYS. 11	260	RESULTANT
1075	SUBSYS. 11	261	RESULTANT
1076	SUBSYS. 11	271	RESULTANT
1077	SUBSYS. 11	274	RESULTANT
1078	SUBSYS. 11	277	RESULTANT
1079	SUBSYS. 11	280	RESULTANT
1080	SUBSYS. 11	284	RESULTANT
1081	SUBSYS. 11	292	RESULTANT
1082	SUBSYS. 11	302	RESULTANT
1083	SUBSYS. 11	304	RESULTANT
1084	SUBSYS. 11	305	RESULTANT
1085	SUBSYS. 11	314	RESULTANT
1086	SUBSYS. 11	315	RESULTANT
1087	SUBSYS. 11	321	RESULTANT
1088	SUBSYS. 11	324	RESULTANT
1089	SUBSYS. 11	325	RESULTANT
1090	SUBSYS. 11	337	RESULTANT
1091	SUBSYS. 11	340	RESULTANT
1092	SUBSYS. 11	343	RESULTANT
1093	SUBSYS. 11	347	RESULTANT
1094	SUBSYS. 11	350	RESULTANT
1095	SUBSYS. 11	352	RESULTANT
1096	SUBSYS. 11	360	RESULTANT
1097	SUBSYS. 11	369	RESULTANT
1098	SUBSYS. 11	370	RESULTANT
1099	SUBSYS. 11	371	RESULTANT
1100	SUBSYS. 11	388	RESULTANT
1101	SUBSYS. 11	389	RESULTANT
1102	SUBSYS. 11	390	RESULTANT
1103	SUBSYS. 11	398	RESULTANT
1104	SUBSYS. 11	402	RESULTANT
1105	SUBSYS. 11	407	RESULTANT
1106	SUBSYS. 11	411	RESULTANT
1107	SUBSYS. 11	414	RESULTANT
1108	SUBSYS. 11	415	RESULTANT
1109	SUBSYS. 11	416	RESULTANT
1110	SUBSYS. 11	417	RESULTANT
1111	SUBSYS. 11	420	RESULTANT
1112	SUBSYS. 11	423	RESULTANT
1113	SUBSYS. 11	430	RESULTANT
1114	SUBSYS. 11	434	RESULTANT
1115	SUBSYS. 11	440	RESULTANT
1116	SUBSYS. 11	443	RESULTANT

1117	SUBSYS. 11	446	RESULTANT
1118	SUBSYS. 11	447	RESULTANT
1119	SUBSYS. 12	1	RESULTANT
1120	SUBSYS. 12	2	RESULTANT
1121	SUBSYS. 12	3	RESULTANT
1122	SUBSYS. 12	5	RESULTANT
1123	SUBSYS. 12	17	RESULTANT
1124	SUBSYS. 12	19	RESULTANT
1125	SUBSYS. 12	20	RESULTANT
1126	SUBSYS. 12	21	RESULTANT
1127	SUBSYS. 12	22	RESULTANT
1128	SUBSYS. 12	25	RESULTANT
1129	SUBSYS. 12	26	RESULTANT
1130	SUBSYS. 12	27	RESULTANT
1131	SUBSYS. 12	28	RESULTANT
1132	SUBSYS. 12	31	RESULTANT
1133	SUBSYS. 12	32	RESULTANT
1134	SUBSYS. 13	1	RESULTANT
1135	SUBSYS. 13	3	RESULTANT
1136	SUBSYS. 13	4	RESULTANT
1137	SUBSYS. 13	7	RESULTANT
1138	SUBSYS. 13	8	RESULTANT
1139	SUBSYS. 13	21	RESULTANT
1140	SUBSYS. 13	23	RESULTANT
1141	SUBSYS. 13	24	RESULTANT
1142	SUBSYS. 13	25	RESULTANT
1143	SUBSYS. 13	30	RESULTANT
1144	SUBSYS. 13	31	RESULTANT
1145	SUBSYS. 13	40	RESULTANT
1146	SUBSYS. 13	50	RESULTANT
1147	SUBSYS. 13	51	RESULTANT
1148	SUBSYS. 13	53	RESULTANT
1149	SUBSYS. 13	54	RESULTANT
1150	SUBSYS. 13	57	RESULTANT
1151	SUBSYS. 13	58	RESULTANT
1152	SUBSYS. 13	71	RESULTANT
1153	SUBSYS. 13	73	RESULTANT
1154	SUBSYS. 13	74	RESULTANT
1155	SUBSYS. 13	75	RESULTANT
1156	SUBSYS. 13	80	RESULTANT
1157	SUBSYS. 13	81	RESULTANT
1158	SUBSYS. 13	90	RESULTANT
1159	SUBSYS. 13	100	RESULTANT
1160	SUBSYS. 13	101	RESULTANT
1161	SUBSYS. 13	107	RESULTANT
1162	SUBSYS. 13	108	RESULTANT
1163	SUBSYS. 13	121	RESULTANT
1164	SUBSYS. 13	123	RESULTANT
1165	SUBSYS. 13	124	RESULTANT
1166	SUBSYS. 13	125	RESULTANT
1167	SUBSYS. 13	130	RESULTANT
1168	SUBSYS. 13	131	RESULTANT
1169	SUBSYS. 13	261	RESULTANT
1170	SUBSYS. 13	263	RESULTANT
1171	SUBSYS. 13	264	RESULTANT
1172	SUBSYS. 13	290	RESULTANT
1173	SUBSYS. 13	291	RESULTANT
1174	SUBSYS. 13	293	RESULTANT
1175	SUBSYS. 13	295	RESULTANT
1176	SUBSYS. 13	298	RESULTANT
1177	SUBSYS. 13	301	RESULTANT
1178	SUBSYS. 13	303	RESULTANT
1179	SUBSYS. 13	308	RESULTANT

1180	SUBSYS. 13	310	RESULTANT
1181	SUBSYS. 13	312	RESULTANT
1182	SUBSYS. 13	315	RESULTANT
1183	SUBSYS. 13	316	RESULTANT
1184	SUBSYS. 13	318	RESULTANT
1185	SUBSYS. 14	140	RESULTANT
1186	SUBSYS. 14	144	RESULTANT
1187	SUBSYS. 14	145	RESULTANT
1188	SUBSYS. 14	150	RESULTANT
1189	SUBSYS. 14	151	RESULTANT
1190	SUBSYS. 14	153	RESULTANT
1191	SUBSYS. 14	154	RESULTANT
1192	SUBSYS. 14	157	RESULTANT
1193	SUBSYS. 14	158	RESULTANT
1194	SUBSYS. 14	171	RESULTANT
1195	SUBSYS. 14	173	RESULTANT
1196	SUBSYS. 14	174	RESULTANT
1197	SUBSYS. 14	175	RESULTANT
1198	SUBSYS. 14	180	RESULTANT
1199	SUBSYS. 14	181	RESULTANT
1200	SUBSYS. 14	190	RESULTANT
1201	SUBSYS. 14	194	RESULTANT
1202	SUBSYS. 14	195	RESULTANT
1203	SUBSYS. 14	200	RESULTANT
1204	SUBSYS. 14	201	RESULTANT
1205	SUBSYS. 14	204	RESULTANT
1206	SUBSYS. 14	205	RESULTANT
1207	SUBSYS. 14	212	RESULTANT
1208	SUBSYS. 14	213	RESULTANT
1209	SUBSYS. 14	214	RESULTANT
1210	SUBSYS. 14	223	RESULTANT
1211	SUBSYS. 14	224	RESULTANT
1212	SUBSYS. 14	225	RESULTANT
1213	SUBSYS. 14	227	RESULTANT
1214	SUBSYS. 14	228	RESULTANT
1215	SUBSYS. 14	230	RESULTANT
1216	SUBSYS. 14	342	RESULTANT
1217	SUBSYS. 14	344	RESULTANT
1218	SUBSYS. 14	352	RESULTANT
1219	SUBSYS. 14	354	RESULTANT
1220	SUBSYS. 14	356	RESULTANT
1221	SUBSYS. 14	361	RESULTANT
1222	SUBSYS. 14	365	RESULTANT
1223	SUBSYS. 14	367	RESULTANT
1224	SUBSYS. 14	377	RESULTANT
1225	SUBSYS. 14	381	RESULTANT
1226	SUBSYS. 14	384	RESULTANT
1227	SUBSYS. 14	391	RESULTANT
1228	SUBSYS. 14	400	RESULTANT
1229	SUBSYS. 14	405	RESULTANT
1230	SUBSYS. 14	409	RESULTANT
1231	SUBSYS. 14	410	RESULTANT
1232	SUBSYS. 14	413	RESULTANT
1233	SUBSYS. 14	419	RESULTANT
1234	SUBSYS. 14	420	RESULTANT
1235	SUBSYS. 14	421	RESULTANT
1236	SUBSYS. 14	425	RESULTANT
1237	SUBSYS. 14	429	RESULTANT
1238	SUBSYS. 14	434	RESULTANT
1239	SUBSYS. 14	437	RESULTANT
1240	SUBSYS. 14	438	RESULTANT
1241	SUBSYS. 14	439	RESULTANT
1242	SUBSYS. 14	444	RESULTANT

1243	SUBSYS. 14	451	RESULTANT
1244	SUBSYS. 14	454	RESULTANT
1245	SUBSYS. 14	458	RESULTANT
1246	SUBSYS. 14	476	RESULTANT
1247	SUBSYS. 14	477	RESULTANT
1248	SUBSYS. 14	480	RESULTANT
1249	SUBSYS. 14	490	RESULTANT
1250	SUBSYS. 14	492	RESULTANT
1251	SUBSYS. 14	494	RESULTANT
1252	SUBSYS. 15	1	RESULTANT
1253	SUBSYS. 15	5	RESULTANT
1254	SUBSYS. 15	8	RESULTANT
1255	SUBSYS. 15	13	RESULTANT
1256	SUBSYS. 15	17	RESULTANT
1257	SUBSYS. 15	24	RESULTANT
1258	SUBSYS. 15	27	RESULTANT
1259	SUBSYS. 15	33	RESULTANT
1260	SUBSYS. 15	37	RESULTANT
1261	SUBSYS. 15	42	RESULTANT
1262	SUBSYS. 15	49	RESULTANT
1263	SUBSYS. 15	58	RESULTANT
1264	SUBSYS. 15	67	RESULTANT
1265	SUBSYS. 15	77	RESULTANT
1266	SUBSYS. 15	89	RESULTANT
1267	SUBSYS. 15	92	RESULTANT
1268	SUBSYS. 15	96	RESULTANT
1269	SUBSYS. 15	101	RESULTANT
1270	SUBSYS. 15	107	RESULTANT
1271	SUBSYS. 15	113	RESULTANT
1272	SUBSYS. 15	115	RESULTANT
1273	SUBSYS. 15	116	RESULTANT
1274	SUBSYS. 15	133	RESULTANT
1275	SUBSYS. 15	142	RESULTANT
1276	SUBSYS. 15	147	RESULTANT
1277	SUBSYS. 15	148	RESULTANT
1278	SUBSYS. 15	148	RESULTANT
1279	SUBSYS. 16	1	RESULTANT
1280	SUBSYS. 16	3	RESULTANT
1281	SUBSYS. 16	17	RESULTANT
1282	SUBSYS. 16	30	RESULTANT
1283	SUBSYS. 16	34	RESULTANT
1284	SUBSYS. 16	38	RESULTANT
1285	SUBSYS. 16	53	RESULTANT
1286	SUBSYS. 16	62	RESULTANT
1287	SUBSYS. 16	64	RESULTANT
1288	SUBSYS. 16	77	RESULTANT
1289	SUBSYS. 16	81	RESULTANT
1290	SUBSYS. 16	90	RESULTANT
1291	SUBSYS. 16	97	RESULTANT
1292	SUBSYS. 16	102	RESULTANT
1293	SUBSYS. 16	112	RESULTANT
1294	SUBSYS. 16	129	RESULTANT
1295	SUBSYS. 16	139	RESULTANT
1296	SUBSYS. 16	149	RESULTANT
1297	SUBSYS. 16	163	RESULTANT
1298	SUBSYS. 16	169	RESULTANT
1299	SUBSYS. 16	171	RESULTANT
1300	SUBSYS. 16	185	RESULTANT
1301	SUBSYS. 16	187	RESULTANT
1302	SUBSYS. 16	198	RESULTANT
1303	SUBSYS. 16	201	RESULTANT
1304	SUBSYS. 16	203	RESULTANT
1305	SUBSYS. 16	206	RESULTANT

1306	SUBSYS. 16	212	RESULTANT
1307	SUBSYS. 17	1	RESULTANT
1308	SUBSYS. 17	4	RESULTANT
1309	SUBSYS. 17	12	RESULTANT
1310	SUBSYS. 17	27	RESULTANT
1311	SUBSYS. 17	32	RESULTANT
1312	SUBSYS. 17	44	RESULTANT
1313	SUBSYS. 17	48	RESULTANT
1314	SUBSYS. 17	55	RESULTANT
1315	SUBSYS. 17	58	RESULTANT
1316	SUBSYS. 17	64	RESULTANT
1317	SUBSYS. 17	74	RESULTANT
1318	SUBSYS. 17	77	RESULTANT
1319	SUBSYS. 17	82	RESULTANT
1320	SUBSYS. 17	91	RESULTANT
1321	SUBSYS. 17	101	RESULTANT
1322	SUBSYS. 17	110	RESULTANT
1323	SUBSYS. 17	125	RESULTANT
1324	SUBSYS. 17	131	RESULTANT
1325	SUBSYS. 17	134	RESULTANT
1326	SUBSYS. 17	137	RESULTANT
1327	SUBSYS. 17	144	RESULTANT
1328	SUBSYS. 17	147	RESULTANT
1329	SUBSYS. 17	152	RESULTANT
1330	SUBSYS. 17	162	RESULTANT
1331	SUBSYS. 17	165	RESULTANT
1332	SUBSYS. 17	168	RESULTANT
1333	SUBSYS. 17	172	RESULTANT
1334	SUBSYS. 18	1	RESULTANT
1335	SUBSYS. 18	4	RESULTANT
1336	SUBSYS. 18	9	RESULTANT
1337	SUBSYS. 18	10	RESULTANT
1338	SUBSYS. 18	12	RESULTANT
1339	SUBSYS. 18	17	RESULTANT
1340	SUBSYS. 18	24	RESULTANT
1341	SUBSYS. 18	28	RESULTANT
1342	SUBSYS. 19	1	RESULTANT
1343	SUBSYS. 19	2	RESULTANT
1344	SUBSYS. 19	3	RESULTANT
1345	SUBSYS. 19	11	RESULTANT
1346	SUBSYS. 19	14	RESULTANT
1347	SUBSYS. 19	22	RESULTANT
1348	SUBSYS. 19	32	RESULTANT
1349	SUBSYS. 19	43	RESULTANT
1350	SUBSYS. 19	49	RESULTANT
1351	SUBSYS. 19	51	RESULTANT
1352	SUBSYS. 19	58	RESULTANT
1353	SUBSYS. 19	59	RESULTANT
1354	SUBSYS. 20	1	RESULTANT
1355	SUBSYS. 20	4	RESULTANT
1356	SUBSYS. 20	16	RESULTANT
1357	SUBSYS. 20	19	RESULTANT
1358	SUBSYS. 20	22	RESULTANT
1359	SUBSYS. 20	25	RESULTANT
1360	SUBSYS. 20	30	RESULTANT
1361	SUBSYS. 20	65	RESULTANT
1362	SUBSYS. 20	68	RESULTANT
1363	SUBSYS. 20	71	RESULTANT
1364	SUBSYS. 20	73	RESULTANT
1365	SUBSYS. 20	77	RESULTANT
1366	SUBSYS. 21	1	RESULTANT
1367	SUBSYS. 21	4	RESULTANT
1368	SUBSYS. 21	5	RESULTANT

1369	SUBSYS. 21	6	RESULTANT
1370	SUBSYS. 21	7	RESULTANT
1371	SUBSYS. 21	10	RESULTANT
1372	SUBSYS. 21	15	RESULTANT
1373	SUBSYS. 21	19	RESULTANT
1374	SUBSYS. 21	23	RESULTANT
1375	SUBSYS. 21	28	RESULTANT
1376	SUBSYS. 21	31	RESULTANT
1377	SUBSYS. 21	34	RESULTANT
1378	SUBSYS. 21	39	RESULTANT
1379	SUBSYS. 21	43	RESULTANT
1380	SUBSYS. 21	46	RESULTANT
1381	SUBSYS. 21	49	RESULTANT
1382	SUBSYS. 21	52	RESULTANT
1383	SUBSYS. 21	55	RESULTANT
1384	SUBSYS. 21	59	RESULTANT
1385	SUBSYS. 21	62	RESULTANT
1386	SUBSYS. 21	65	RESULTANT
1387	SUBSYS. 21	70	RESULTANT
1388	SUBSYS. 21	73	RESULTANT
1389	SUBSYS. 21	77	RESULTANT
1390	SUBSYS. 21	80	RESULTANT
1391	SUBSYS. 21	91	RESULTANT
1392	SUBSYS. 21	94	RESULTANT
1393	SUBSYS. 21	97	RESULTANT
1394	SUBSYS. 21	100	RESULTANT
1395	SUBSYS. 21	101	RESULTANT
1396	SUBSYS. 21	102	RESULTANT
1397	SUBSYS. 21	104	RESULTANT
1398	SUBSYS. 21	107	RESULTANT
1399	SUBSYS. 21	110	RESULTANT
1400	SUBSYS. 21	133	RESULTANT
1401	SUBSYS. 21	136	RESULTANT
1402	SUBSYS. 21	139	RESULTANT
1403	SUBSYS. 21	143	RESULTANT
1404	SUBSYS. 21	148	RESULTANT
1405	SUBSYS. 21	156	RESULTANT
1406	SUBSYS. 21	160	RESULTANT
1407	SUBSYS. 21	163	RESULTANT
1408	SUBSYS. 21	166	RESULTANT
1409	SUBSYS. 21	169	RESULTANT
1410	SUBSYS. 21	172	RESULTANT
1411	SUBSYS. 21	175	RESULTANT
1412	SUBSYS. 21	189	RESULTANT
1413	SUBSYS. 21	192	RESULTANT
1414	SUBSYS. 21	195	RESULTANT
1415	SUBSYS. 21	196	RESULTANT
1416	SUBSYS. 21	198	RESULTANT
1417	SUBSYS. 21	199	RESULTANT